Dissertation

Submitted to the

Combined Faculties for the Natural Sciences and for Mathematics

of the Ruperto-Carola University of Heidelberg, Germany

for the Degree of Doctor of Natural Sciences

Presented by

Michael Delacher (M.Sc.)

Born in Ulm, Germany

Oral Examination: April 7th, 2016

Transcriptional Control of Regulatory T cells

Referees

Dr. Markus Feuerer

Prof. Dr. Viktor Umansky

This dissertation was performed and written during the period from July 2012 to December 2015 at the German Cancer Research Center (DKFZ) and the Weizmann Institute of Science (WIS) under the supervision of Prof. Dr. Viktor Umansky and joint direct supervision of both Dr. Markus Feuerer (DKFZ) and Dr. Jakub Abramson (WIS). The dissertation was submitted to the Combined Faculties for the Natural Sciences and for Mathematics of the Ruperto-Carola University of Heidelberg, Germany in January 2016.

German Cancer Research Center (DKFZ)
Tumor Immunology Program
Research Group Immune Tolerance (D100)
Im Neuenheimer Feld 280
69120 Heidelberg
Germany

Weizmann Institute of Science (WIS)
Faculty of Biology
Department of Immunology
Laboratory of Dr. Jakub Abramson
Hertzl 234 Street
76100 Rehovot
Israel

Declaration

I herewith declare that I performed and wrote this dissertation independently under supervision and used no other sources and aids than those indicated. Furthermore, I declare that I have not submitted this thesis for a degree to any other academic or similar institution. No parts of this dissertation were published prior to the submission to the Combined Faculties for the Natural Sciences and for Mathematics of the Ruperto-Carola University of Heidelberg. Parts of the experiments in this dissertation were performed in collaboration with other research groups as follows:

- CG methylation analysis with the 454 pyrosequencing technology:
  Division of Epigenetics, DKFZ, Heidelberg
  Dr. Achim Breiling & Prof. Dr. Frank Lyko
- Sample preparation and allocation of Dnmt1-hypomorphic mice:
  Laboratory of Molecular Stem Cell Biology, Münster University, Münster
  Melinda Czeh & Prof. Dr. Frank Rosenbauer
- Proteomics on EL4 T cells with inverted ChIP technology:
  Genome Biology Unit, EMBL, Heidelberg
  Dr. Katrin Eichelbaum & Dr. Jeroen Krijgsveld
- Generation of viral constructs for T cell transduction and luciferase measurements:
  Department of Immunology, Weizmann Institute of Science, Rehovot, Israel
  Yonatan Herzig & Dr. Jakub Abramson
- Preparation of H&E staining and pathological evaluation:
  Division of Cellular and Molecular Pathology, DKFZ, Heidelberg
  Dr. Guiseppina Federico & Prof. Dr. Hermann-Josef Gröne
- Tagmentation-based whole genome sequencing of tissue-resident T cells:
  Department of Epigenomics and Cancer Risk Factors, DKFZ, Heidelberg
  Dr. Dieter Weichenhan & Prof. Dr. Christoph Plass
- Bioinformatic computation of next-generation sequencing data:
  Division of Applied Bioinformatics, DKFZ, Heidelberg
  Charles Imbusch & Prof. Dr. Benedikt Brors

_____ _____

(Place/Date) (Signature)

Table of Contents

Table of Figures

1 Summary

Regulatory T cells (Treg cells) are crucial mediators of peripheral self-tolerance, and their specific ablation causes catastrophic autoimmunity. The protein Foxp3 has been described as the key transcription factor delineating cells of this lineage. In this thesis, we investigate different levels of transcriptional control in Foxp3-expressing Treg cells:

At first, we identified CpG rich regions along the *Foxp3* gene and investigated them for their epigenetic profile. We were able to validate already-described Treg-specific demethylated regions, but we also identified new Treg-specific demethylation patterns along the *Foxp3* gene. These patterns are initiated during thymic Treg development and persist in circulation, and remain intact also in DNA-methyltransferase deficient mice. Next, we explored the epigenetic control of Treg cells on a broader scale. We isolated tissue-resident Treg cells from fat, skin, liver, and lymph nodes and subjected them to whole-genome tagmentation-based methylation analysis in correlation with RNA expression profiling. This enables us to investigate tissue-specific epigenetic patterns that drive and manifest Treg cell adaption to local tissues. Additionally, we observed that the *Foxp3* core promoter is completely demethylated also in Foxp3 non-expressing cell types. Therefore, we identified binding partners to the *Foxp3* gene promoter in a novel procedure called inverted Chromatin IP. We validated the suppressive nature of these target proteins via luciferase-based screens, tested their differential expression profile in different cell types, and investigated the effect of their virus-mediated overexpression on *in-vitro* Treg cell induction.

Finally, we investigated the role of one specific transcriptional regulator in Treg cells: Rbpj, commonly known as an important co-factor of Notch signaling. While we did not find evidence that Notch signaling was active in bona fide Treg cells, we still measured an upregulation of Rbpj mRNA in Treg cells compared to their conventional T-cell (Tconv) counterparts in many different tissues. Upon Treg-specific *Rbpj* gene deletion, we observed a steady increase in Treg frequency and number in several anatomical locations, finally leading to autoimmune pathology despite the presence of otherwise functionally-intact Treg cells. We identified the IL7-receptor, an important growth-promoting cytokine receptor, to be specifically upregulated in Rbpj-deficient Treg cells, whereas Dtx-1, a paramount anergy-promoting factor, was strongly downregulated. Furthermore, gene expression profiling and antibody staining revealed that both Treg and Tconv cells gained T_H subset lineage profiles, indicating an inability of Treg cells to control (auto) immune responses *in-vivo*. Our data suggest a novel, Notch-independent function of Rbpj to specifically regulate Treg cell proliferation and functionality.

2 Zusammenfassung

Regulatorische T-Zellen sind wichtige Bausteine für die periphere Immun-Selbsttoleranz, und ihre Abwesenheit führt zu schweren Autoimmunerkrankungen. Das Foxp3-Protein wurde als Hauptfaktor für die Entstehung dieser Zellen beschrieben. In dieser Arbeit untersuchen wir mehrere Ebenen der molekularen Kontrolle dieses Zelltyps sowie seines Hauptgens *Foxp3*:
Zuerst identifizierten wir Regionen im *Foxp3*-Gen, die sich durch eine hohe Dichte an CG-Dinukleotiden auszeichnen. Diese wurden epigenetisch untersucht, wodurch wir bereits bekannte regulatorische T-Zell-spezifische Regionen validieren konnten, aber auch neue differenziell-methylierte Regionen identifizierten. Diese Methylierungsmuster werden im Thymus angelegt, bleiben während der Zirkulation dieser Zellen erhalten und bestehen ebenfalls in DNA-Methyltransferase-defizienten Mäusen. Des Weiteren haben wir die epigenetischen Merkmale von regulatorischen T-Zellen über das Gesamtgenom bestimmt. Hierzu haben wir Zellen aus Fett, Haut, Leber, und Lymphknoten isoliert und über Ganzgenomsequenzierung in Korrelation mit Genexpressionbestimmungen analysiert. Mit diesem Datensatz können wir gewebespezifische Anpassungsmuster von regulatorischen T-Zellen identifizieren. In unseren epigenetischen Studien haben wir auch den zentralen *Foxp3* Promoter untersucht und festgestellt, dass dieser in Foxp3-negativen Zelltypen demethyliert ist. Daher haben wir diesen Promoter mit einer invertierten Chromatin-Immunopräzipitation nach Bindefaktoren untersucht. Die gensuppressive Natur der in dieser Methode identifizierten Kandidaten wurde über Luziferase-Messungen getestet, und ihr differenzielles Expressionprofil über eine Vielzahl von Zelltypen bestimmt. Schlußendlich wurden die Faktoren in induzierten regulatorischen T-Zellen überexprimiert, um ihren Einfluß auf die Expression des *Foxp3* Gens zu untersuchen.
In einem weiteren Projekt haben wir uns mit dem Rbpj Protein, einem wichtigen Faktor im Notch-Signalweg, und seiner Rolle in regulatorischen T-Zellen beschäftigt. Das Rbpj Protein ist in diesem Zelltyp überexprimiert, obwohl keine Notch-Aktivität nachzuweisen ist. Daher haben wir dieses Protein in regulatorischen T-Zellen deletiert, was zu einer systemweiten Zunahme dieser Zellen und der Entstehung einer Autoimmunerkrankung führte. Rbpj-defiziente regulatorische T-Zellen zeigten eine charakteristische Überexpression des wachstumsstimulierenden IL7-Oberflächenrezeptors sowie eine starke Herunterregulierung von Dtx-1, einem Anergie-fördernden Transkriptionsfaktor. Genexpressionsanalysen deuten auf eine Differenzierung der regulatorischen T-Zellen sowie der Effektor T-Zellen in T_H-Subpopulationen hin. Unsere Daten lassen auf eine bisher unbeschriebene, Notch-unabhängige Rolle von Rbpj für die Regulation von Proliferation und Funktion regulatorischer T-Zellen im Gleichgewichtszustand hin.

3 Acknowledgements

First and foremost, I want to acknowledge my parents Charlotte and Johann as well as my brother Stefan for emotional and strategic support during the challenging and unsettling task of working towards a PhD degree. Next, I want to appreciate my joint PhD supervisors, Markus and Kobi, for their help and support during my time at the DKFZ and Weizmann Institute of Sciences; it was a pleasure to work with you guys.
Furthermore, I was supported by my lab members in Heidelberg: Melanie, Jan, David, Kristin, Elke, Ann-Cathrin, Alexander, Ulrike, Sabine, Danny, and Marina; and by my lab members in Israel: Yonatan, Noam, Ben, Netta, Mirika, Anna, and Yael. Special thanks go to Fabian for helpful discussions and scientific advice (plus “Glaswecken”).
Furthermore, I want to thank members of my Thesis Advisory Committee Dr. Jeroen Krijgsveld and Prof. Dr. Viktor Umansky, and members of my PhD Defense Committee Prof. Dr. Ana Martin-Villalba and Prof. Dr. Stefan Wiemann. In addition, I want to appreciate the support by the FACS Core Facility and Imaging Facility with Stefan, Áine, Claudia, Klaus, Tobias, Damir, and Felix. Finally, the DKFZ Animal Core Facility was exemplary in handling and taking care of our animals.
I want to thank the Helmholtz International Graduate Research School office, with Lindsay, Evelyn and Heike, for their open-door policy and flexibility in the organization of the Israel exchange lab visits and for generous funding.
“Last but not least”, I want to acknowledge my good friends from Ringingen and my soccer team (SV Ringingen), my friends from Heidelberg, from Ulm, from Munich, and from abroad.

4 Background

4.1 T cells originate from hematopoietic stem cells

In adults, immune cells originate from hematopoietic stem cells (HSCs) in the bone marrow. Already there, a distinct lineage-decision is made: whereas common lymphoid progenitors (CLPs) give rise to B-, T-, and NK cells, common myeloid progenitors (CMP) can differentiate into lineages of granulocyte/macrophage cells (GMP) or megakaryocytes/erythrocytes (MEP). Each progenitor will end-differentiate into a specific subset, as shown in **Figure 1**. But not all cell lineages end-differentiate in the bone marrow – T cells are trained and specialized in the thymus, an organ situated at the base of the heart in the upper thorax. T-cell progenitors travel to this organ via the blood stream and give rise to thymocytes, which undergo highly controlled selection and quality control measures while they mature into $CD4^{pos}$ or $CD8^{pos}$ T cells. Afterwards, they re-enter the blood stream to take on effector functions [1].

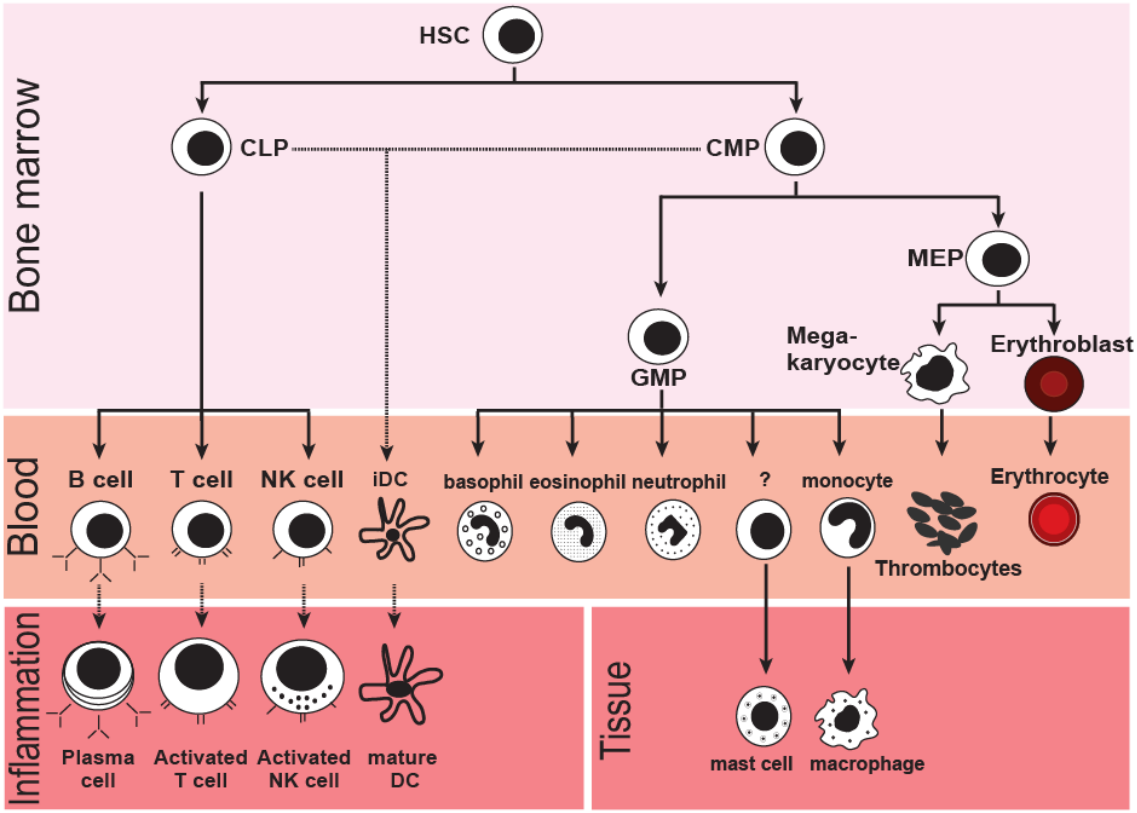

Figure 1: The origin of immune cells in the hematopoietic system.
This graph depicts the development of lymphoid and myeloid cells from the hematopoietic stem cell (HSC). CLP = common lymphoid progenitor; CMP = common myeloid progenitor; GMP = granulocyte/macrophage progenitor; MEP = megakaryocyte/erythrocyte progenitor; DC = Dendritic cell; NK cell = Natural Killer cell.

4.2 Central tolerance is mediated by thymus-resident TEC

Our body requires a portfolio of protective systems to prevent harmful immune responses towards self-peptides and harmless environmental antigens. This tolerance relies on both central and peripheral mechanisms. Negative selection of self-reactive lymphocytes during their development in thymus (T cells) or bone marrow (B cells) is part of the central tolerance mechanism, and is supplemented by self-antigen binding causing anergy, lack of APC-derived co-stimulation against self-peptides, and expression of inhibitory receptors [2]. In addition, regulatory T cells (Tregs) are important mediators of peripheral tolerance in tissues and circulation. But what happens if the thymus, and its tolerance-inducing mechanism, is absent? When newborn mice have their thymus removed (thymectomy) very early after birth (between day 2 and day 4), immediate adverse events such as autoimmune disease are followed by long-term immunodeficiency, increased tumor incidence and overall increased mortality. These findings lead to the appreciation of the thymus as central organ for the proper development of functionally intact $CD4^{pos}$ and $CD8^{pos}$ T cells (reviewed in [3]).
Looking at thymic T cell development in more detail, while thymocytes differentiate, they migrate through two different anatomical parts of the thymus, the medulla and the cortex. The cortex contains more immature thymocytes alongside of macrophages and cortical epithelial cells (cTECs). The medulla, including its Hassall's corpuscles as sites of massive cell death, contain more mature thymocytes accompanied by dendritic cells (DCs) and medullary TECs (mTEC). Early precursor thymocytes enter the thymic cortex via the corticomedullary junction and engage TECs. At this stage, active Notch-ligand expression on mTECs commits early precursor thymocytes to the lymphoid lineage. This close interaction with the stroma and stroma-resident APCs accompanies thymocytes along their way through the thymus. First, thymocytes enter the double negative 1 (DN1) stage where they express Kit and CD44, but TCR-α and β chains remain in germline configuration. They then travel to the cortex where they closely interact with cTECs. There, they re-arrange the β chain and express CD25 to become DN2 thymocytes. Once V-D-J rearrangement of the TCR β-chain is complete, it is paired with an unarranged α-chain to form the pre-T-cell receptor, which is the hallmark of DN3 stage thymocytes. Cells with incorrectly rearranged β-chains die at this stage. Finally, once CD25 expression is lost, DN4 cells start to express both CD4 and CD8 and become double-positive (DP) thymocytes. They proliferate heavily, and account for

the vast majority of thymoyctes at any given time. They soon start with α-chain rearrangement and stop extensive proliferation to undergo first quality control measures of central tolerance: only clones with intact αβ-TCR complexes survive interactions with cTECs and become small-resting double-positive thymocytes. Now, the lineage decision into CD8 ^{pos} T cell or CD4 ^{pos} T cell is made and negative selection, mediated by TECs, APCs and macrophages, ensures that strongly self-reactive clones are eliminated. Clones with an intermediate-range self-reactivity can become Treg cells, with the special mandate to downmodulate autoimmune reactions in the periphery [1].
In summary, mTECs play an essential role to maintain tolerance towards self. They are involved in the negative selection of self-reactive T-cells as well as the development of thymus-generated Treg cells [4, 5]. They have the ability to express essentially all of the body's self antigens (so-called tissue-restricted antigens) and display them to maturing T cells. Once maturing T cells recognize and strongly bind to self peptide: MHC complexes on TECs, they are deleted [6]. Expression of these antigens on thymus-resident epithelial cells depends on the expression of the Aire protein, and a deficiency of this factor causes autoimmune disease in both mice and humans[7, 8]. Therefore, one can conclude that T-cell birth and education in the thymus is central for the development of a functional immune system, being able to determine friend from foe. But protection is not complete - potentially self-reactive T cells still escape the thymus and travel the periphery. Here, a second mechanisms of immune tolerance comes into place – regulatory T cells, either born and educated in the thymus (tTreg) or induced in the periphery (pTreg), keep these potentially very harmful clones under control.

4.3 Peripheral tolerance is mediated by regulatory T cells

As mentioned in the earlier paragraph, postnatal thymectomy of newborn mice between day 2 and day 4 of age causes severe autoimmune disease, with lymphocyte infiltration into peripheral organs and the presence of autoantibodies. Interestingly, the adoptive transfer of immune cells from adult euthymic mice can prevent the onset of autoimmune disease, which was indicative of a transferable cellular mediator protecting against autoimmunity [9]. This cellular "mediator" of peripheral tolerance was later identified as an IL-2 receptor α-chain (CD25) overexpressing T cell, and the adoptive transfer of this specific cell type alone can rescue the autoimmune phenotype caused by postnatal thymectomy. More detailed studies showed that this cell type can also prevent

autoimmune events caused by the injection of CD25-depleted $CD4^{pos}$ T-cell suspensions into *nu/nu* recipient mice, inhibit transplant rejection events, but also promote the escape of tumors from immunological surveillance[10, 11, 12, 13]. Later, the transcription factor Foxp3 was identified as key driver of regulatory T-cell phenotype and function. Once Foxp3 was retrovirally transduced into naive T-cells, they acquired a regulatory phenotype. When the gene was deleted, autoimmune syndromes reminiscent of early-life thymectomy arose [14, 15, 16]. As with central tolerance and AIRE, mutations in the forkhead box domain of the *Foxp3* gene have been linked to severe autoimmune disease in mouse and man. In humans, a selective defect in the *Foxp3* gene causes IPEX (immune dysregulation, polyendocrinopathy, enteropathy, X-linked syndrome), which is accompanied by severe autoimmune syndromes to the gastro-intestinal tract, the epidermis, the pancreas (inducing insulin-dependent diabetes), and other organs in a varying intensity. Children diagnosed with IPEX, if untreated, die early in their childhood[17]. This disease can be mirrored in scurfy mice, where male mice with a mutation in the *Foxp3* gene ("scurfin") display skin adenopathies, infections, gastroenetrophy, and ultimately die within four weeks after birth [18]. In addition to this, later studies using a selective depletion of Foxp3-positive Treg cells in newborn mice resulted in autoimmune pathologies, which finally validated the molecular link between $CD4^{pos}CD25^{pos}Foxp3^{pos}$ regulatory T cells and their function to protect against autoimmune disease in a peripheral manner [19].

Since not all Treg cells are generated in the thymus, the Treg population has been classified and denominated based on their origin or birthplace: thymus-born Treg cells (tTreg); peripherally-induced Treg cells (pTreg); *in-vitro* induced Treg cells (iTreg) [20]. We will shortly review all three subsets in the following paragraph.

4.4 tTreg cells are born in the thymus, whereas pTreg cells are induced locally

Treg cells can, just like $CD4^{pos}$ conventional T cells (Tconv) or $CD8^{pos}$ cytotoxic T lymphocytes (CTL), leave the blood or lymph circulation and extravasate into tissues. There, they built a strong tissue compartment even in the absence of pro-inflammatory stimuli and take on tissue-protective functions. But are all Treg cell populations in tissues derived from the thymus, or can they also be induced locally?

To define the developmental origin of Treg cells, Fontenot and colleagues analyzed the development of Foxp3 ^{GFP}-positive Treg cells in the thymus using a transgenic mouse model where the *Foxp3* promoter sequence, followed by a GFP reporter, was added to the genome. They observed that CD25-positive cells arise early in the CD4 single-positive fraction, whereas Foxp3^{GFP}CD25 double-positive cells slowly increased over the first 3 weeks of life to a final plateau of ~4% of CD4 single-positive thymocytes [21]. In the thymus, high-affinity TCR binding to self-antigen presented on thymic APCs [22, 23, 24] alongside a special cytokine environment [25] and an overall low frequency of antigen-specific Treg cell clones [24, 26, 27] is pivotal for the generation of tTreg cells. First, Treg cells are primed by TCR- and APC-promoted signals (early Treg precursor cells, $CD4^{pos}TCR\beta^{pos}CD69^{pos}CD25^{neg}Foxp3^{neg}$), followed by expression of CD25, causing the transformation into late Treg precursor cells ($CD4^{pos}TCR\beta^{pos}CD69^{neg}CD25^{pos}Foxp3^{neg}$)**.** Once late Treg precursor cells are stimulated by IL-2 and IL-15, *Foxp3* gene expression is induced to generate tTreg cells ($CD4^{pos}TCR\beta^{pos}CD69^{neg}CD25^{pos}Foxp3^{pos}$) [28, 29]**.** Another study by Yang S et al. in 2015 investigated the perinatal generation of Treg cells [30]. They claim that a first wave of Treg cells, important for the prevention of early-onset autoimmune disease against specific targets, is induced by Aire-expressing thymic stromal cells and persists throughout life, supplementing the pool of Treg cells continuously produced by thymic output after birth. Therefore, Treg cell generation must be distinguished in a temporal manner (perinatal vs. aged) as well as a spatial/origin-specific (thymus vs. periphery) manner. Based on origin, two anatomical locations of Treg induction have been described so far: Treg cell induction in the thymus, as described above, is supplemented by peripheral conversion of $CD4^{pos}CD25^{neg}Foxp3^{neg}$ Tconv cells into $CD4^{pos}CD25^{pos}Foxp3^{pos}$ pTreg cells. This occurs predominantly in the colon and gut where a high load of food antigens and commensal bacteria requires a special tolerogenic environment [25, 31, 32, 33]. It has been proposed that pTregs and tTregs can be distinguished via the cell surface receptor Nrp-1 and the intracellular protein Helios, further discussed in paragraph 4.6.

If $CD4^{pos}CD25^{neg}Foxp3^{neg}$ Tconv cells are stimulated by CD3/28 microbeads together with IL-2 and TGF-β *in-vitro*, Foxp3 expression can be induced to generate *in-vitro* induced Treg cells (iTreg). Although they express Foxp3 protein at high levels, their expression pattern is not as stable as *ex-vivo* isolated Treg cells, probably due to missing demethylation of the Treg-specific demethylated region in the *Foxp3* gene [34, 35, 36].

4.5 Treg cells suppress pro-inflammatory effector cells

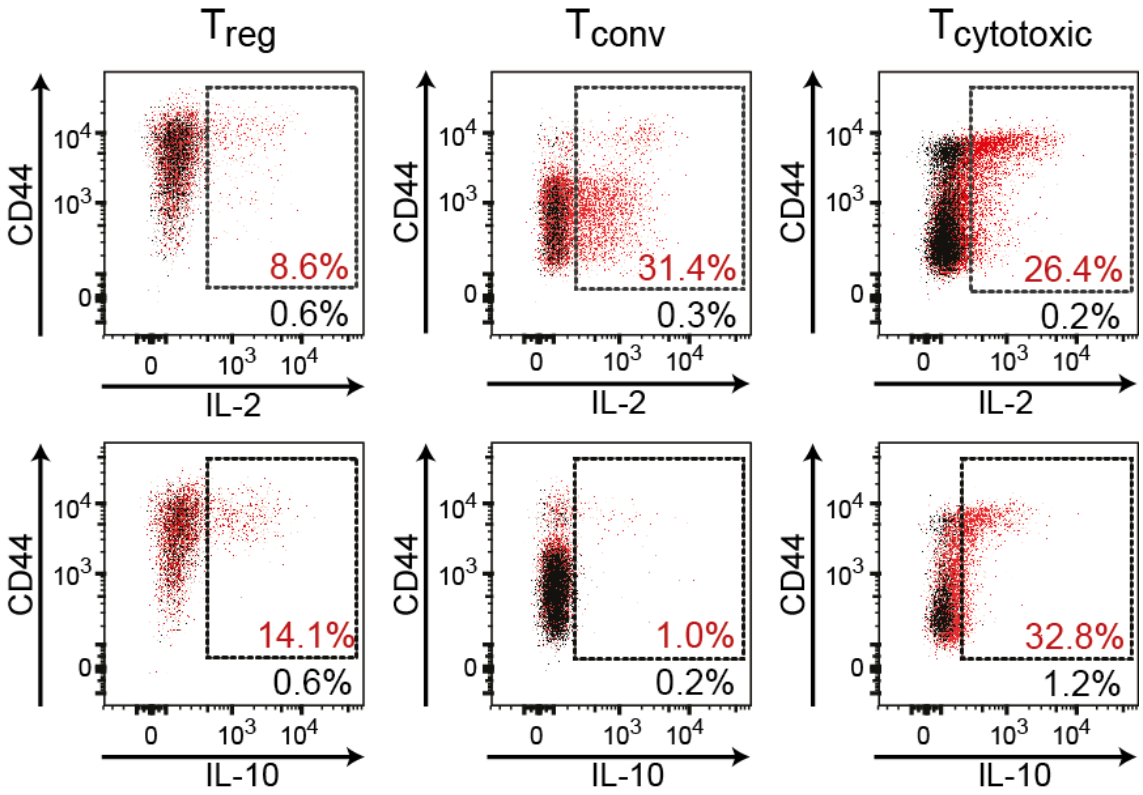

Figure 2: T cell cytokine expression profile.
Treg, Tconv and CD8 ^{pos} T cells were FACS-isolated and treated with PMA/Ionomycin or left unstimulated for eight hours at 37°C in the presence of transport inhibitors. Afterwards, cells were stained intracellularly for the presence of IL-2 and IL-10. The dot plots indicate that Treg cells make less IL-2 than Tconv or CD8 ^{pos} CTL, but more IL-10 than Tconv. Furthermore, Treg cells have a clear correlation between cytokine production and CD44 expression, indicating the antigen-experienced Treg cells are more readily induced to secrete cytokines. Red dots represent T cells treated with PMA/Ionomycin and transport inhibitors, black dots are transport inhibitor only treated T cells serving as unstimulated controls.

Thymus-derived tTreg cells, peripherally induced pTreg cells, and *in-vitro* induced iTreg cells all share conserved mechanisms to exert their immunosuppressive functions, reviewed in [37]. They can secrete immunosuppressive cytokines such as IL-10 and IL-35 to create an anti-inflammatory local milieu. The cytokine profile of Treg cells versus Foxp3-negative Tconv cells and CD8^{pos} T cells is exemplified in **Figure 2,** where a CD44-based stratification allows the discrimination between naive (CD44 low) and antigen-experienced (CD44 high) cell types. Besides the very low endogenous IL-2 production of Treg cells, they can also starve effector T-cells of locally available IL-2 via the high expression of the IL2 receptor α-chain (CD25) and binding of local IL-2 to the surface of Treg cells. Via the release of granzyme B or the expression of galectin-1,

they can either actively lyse target cells or induce apoptosis in those. Treg cells can also suppress the inflammation-inducing effects of APCs by forced downmodulation of CD80 and CD86 co-stimulatory proteins on dendritic cells or prevention of their maturation. Finally, they can just occupy binding sites at DCs, making them sterically inaccessible to effector cells [37]. A consequence of these anti-inflammatory effects is the potential to suppress TCR-stimulated effector T cells in an *in-vitro* suppression assay, as exemplified in **Figure 3**.

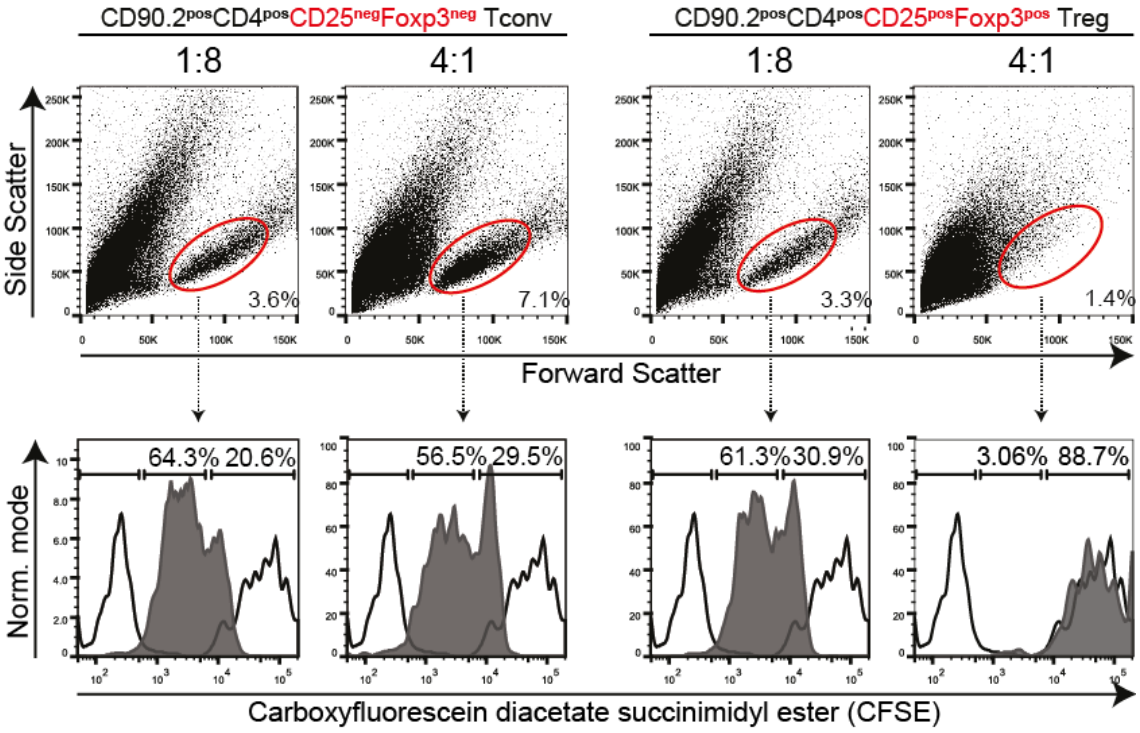

Figure 3: Classical *in-vitro* Treg suppression assay.
A classical Treg suppression assay was performed with CFSE-labeled T-responder cells and MHCII-positive APCs incubated with soluble anti-CD3 mAb for six days at 37°C. One can appreciate that the addition of increasing numbers of Tconv cells does not hinder CFSE-dilution in T-responder cells: in both low (1:8) and high (4:1) relative presence of Tconv cells, active CFSE-dilution is still between 64.3% and 56.5%, indicating proper APC-CD3-stimulated cell division. On the other hand, escalating numbers of Treg cells increasingly disturb T-responder cell proliferation and thereby prevent CFSE dilution: a 1:8 Treg dilution does not affect cell proliferation (61.3% CFSE-diluting cells), whereas a high 4:1 relative Treg frequency effectively prevents T-responder cell proliferation (only 3.1% CFSE-diluting cells). White histograms indicate unstimulated controls (no CFSE dilution due to missing stimulation, CFSE signal $>2x10^4$ fluorescence units) or CFSE non-treated T-responder cells (CFSE signal $<5.0x10^2$ fluorescence units).

4.6 Treg cells express key lineage proteins related to their function

First, we want to take a look at key Treg-specific protein expression as shown in **Figure 4.** The Treg lineage-defining marker is Foxp3, but it only induces part of the Treg-specific gene signature. Forced Foxp3 expression alone is not sufficient to induce the full Treg phenotype, since it is also expressed in activated Tconv cells in mouse and human without inducing a regulatory phenotype [38, 39, 40] Therefore, Foxp3 regulates only a fraction of Treg-specific genes, and is mostly important for consolidation and stability of Treg lineage once initiated [41, 42, 43].

Many other proteins are involved to generate the full Treg signature[44]. Some of the most paramount ones, such as Helios, Neuropillin-1, GITR, and CTLA-4, are reviewed in the following paragraph.

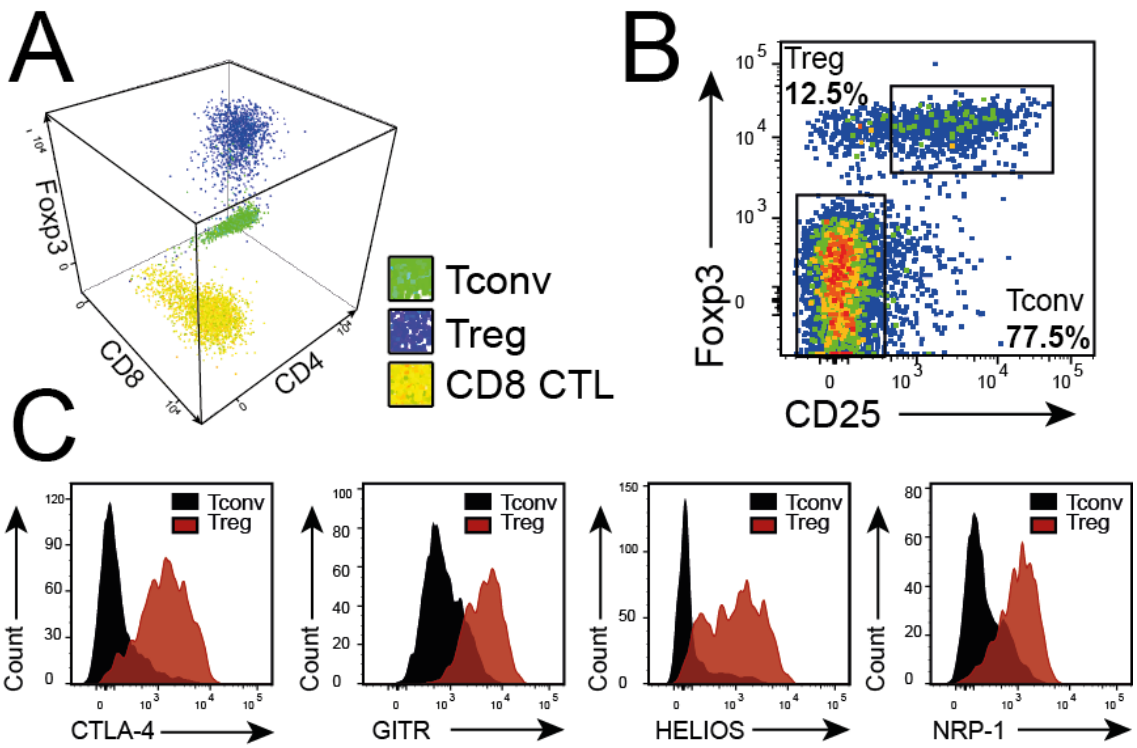

Figure 4: Overview of Treg lineage-specific protein expression.
What makes a Treg a Treg? In A, a three-dimensional dot plot displays three key T-cell populations and their specific surface and intracellular protein expression profile: $CD8^{pos}CD4^{neg}Foxp3^{neg}$ cytotoxic T cells, $CD8^{neg}CD4^{pos}Foxp3^{neg}$ conventional T cells and $CD8^{neg}CD4^{pos}Foxp3^{pos}$ regulatory T cells. A typical gating strategy for Treg cells from spleen is also shown in B, where they constitute about 10%-15% of all CD4 T cells. In C, expression patterns of key Treg proteins such as CTLA-4, GITR, Helios, or Nrp-1 are shown.

One such characteristic protein, Helios, is a member of the Ikaros family of transcription factors. It is expressed pre-dominantly in Treg cells. It is dispensable for their suppressive function or the cytokine profile of Treg cells, but forced expression in iTreg cells enhanced suppressive function [45]. It is thought to be a marker for thymic-derived Treg cells due to its absence on pTreg and iTreg in human samples. Therefore, Helios enhances iTreg function in cooperation with Foxp3, but might be a dispensable co-factor/enhancer for tTreg function [46].

Another marker specifically expressed on thymus-derived Treg cells is Neuropillin-1 (CD304), a cell surface transmembrane glycoprotein. Its ligands are semaphorin 3A and VEGF, and it plays roles in vascular and neuronal development [47]. Identified by comparative gene expression analysis in mice, it was shown to be expressed independently of activation status as a surface marker for Treg cells[48], with higher expression on tTreg than on pTreg or iTreg [49, 50]. In the human system, Nrp-1 is induced on activated human T-lymphocytes [51], what has also been described for Foxp3 and CD25.

Tumor necrosis factor receptor superfamily member 18 (TNFRSF18) or glucocorticoid-induced TNFR-related protein (GITR, CD357) is expressed highly on Treg cells under steady-state conditions. It is involved in TCR-mediated activation of T cells and protects from apoptotic cell death [52]. Its ligands are expressed on APCs, and blocking of the ligand-GITR interaction causes autoimmune disease, highlighting its role to maintain self-tolerance [53]. Since it is dispensable for Treg suppressive capacity *in-vitro* [54], its role has been defined as driver of Treg cell expansion via NFκB signaling in healthy mice and inducer of apoptosis under inflammatory conditions [55, 56].

Finally, cytotoxic T-lymphocyte-associated protein 4 (CTLA-4, CD152), which is expressed on activated T lymphocytes [57] and highly expressed on Treg cells, participates in DC-Treg binding to B7-1 and B7-2 ligands and in the regulation of tryptophan catabolism leading to suppression of effector T cells. It was also shown to be important for TCR hyposignaling, suppressive function and anergy. Interestingly, in Treg cells, it is retained in submembrane vesicles that recycle to and from cell surface rapidly upon activation, whereas Tconv cells have CTLA-4 retained in the Golgi aparatus [58]. It was shown to promote the expression of Foxp3 *in-vitro* and might also be involved in the induction of pTreg in the intestine [59].

4.7 Treg cells are distributed throughout the body and take on tissue-specific protective functions

In the previous paragraphs, we described the cellular origin of Treg cells, their capacity to suppress inflammatory reactions, and their specific protein expression profile. Now we will summarize their tissue-specific distribution and their importance to promote local immune homeostasis (reviewed in [60]). In **Figure 5**, the tissue distribution and selected functions of Treg cells can be appreciated.

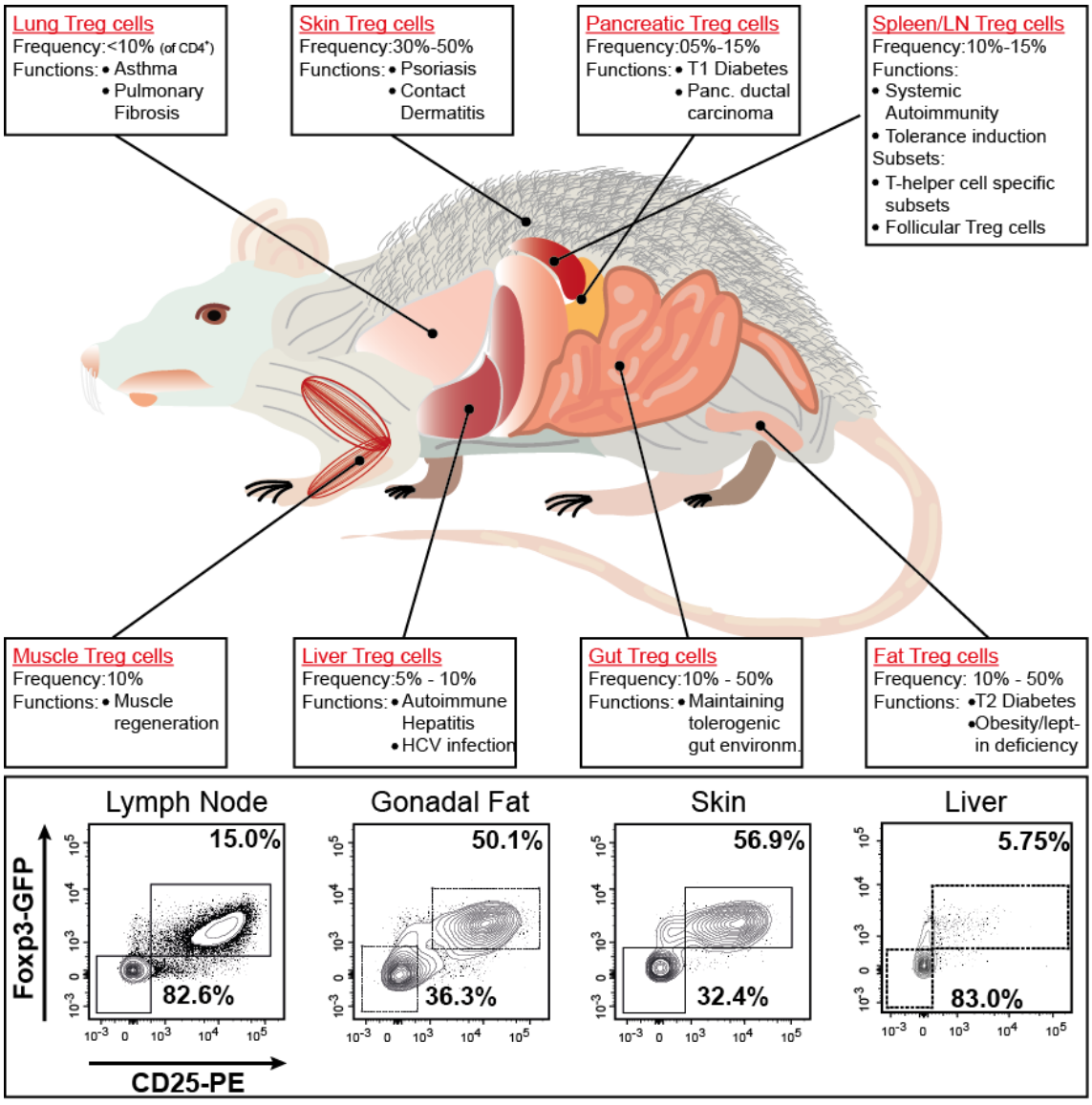

Figure 5: Treg cells and their distribution in various tissues.
Anatomical details of a mouse with relations to their Treg cell compartments. Each compartment has a distinct frequency of Treg cells, and they take over tissue-specific functions in many cases. The dot plots in the lower part of the graphs are representative examples of the presence of $CD25^{pos}Foxp3^{GFPpos}$ Treg cells in tissues like lymph node, fat, skin and liver.

Several studies addressed the function of tissue-specific Treg cells. For example, Treg cells from visceral adipose tissue (VAT) were shown to display a dynamic frequency: they increase in number from an age of 5 weeks to 25 weeks to about 50% of all CD4 ^{pos} T cells, followed by a decline to about 10% in 40 week old animals, unlike Treg cells in lymphoid organs such as the spleen [61, 62]. Also, they carry distinct gene expression and protein signatures compared to lymphoid Treg cells, but remain positive for key proteins such as CD25, GITR, CTLA-4, or Foxp3[63]. Fat-resident Treg cells express peroxisome proliferator-activated receptor-γ (PPAR-γ) as key driver of VAT Treg cell accumulation, function and phenotype, and have an important role to modulate obesity-induced insulin resistance in fat tissue [64]. Treg cells also protect against insulin resistance and diabetes induction in other organs. In the pancreatic duct, specific loss of Treg cells causes Type 2 diabetes [17, 65, 66], whereas increased Treg infiltrations have been identified in pancreatic ductal carcinoma patients and correlated with worse disease prognosis [67]. In the skin, Treg cells can account for 40 to 90 percent of all CD4^{pos} T cells in mouse [68] and human [69]. Relative Treg frequencies and/ or their suppressive capacity is modulated in psoriasis and other dermatological diseases, indicating a Treg-specific role to prevent autoimmune disease of the skin[70, 71]. Treg cells are also implicated in common lung diseases such as pulmonary fibrosis and asthma [72], where patients have either reduced numbers of Treg cells in the bronchoalveolar fluid [73] or impaired Treg suppressive capacity [74].The murine liver has 5-10% of Treg cells [68, 75]. In autoimmune hepatitis, a reduction of Treg frequency has been noted [76, 77]. This contrasts the increase of tumor-resident Treg cells in hepatic cancer lesions [78, 79]. In the healthy muscle, 10% of all CD4^{pos} T cells are Foxp3-expressing Treg cells. They have a specific function to repair muscle damage via the release of amphiregulin [80]. Finally, the gastro-intestinal tract contains an increased number of locally induced pTreg cells, which are important to maintain the intestinal barrier and homeostasis in the presence of harmless commensal bacteria and food antigens [81].

We can summarize that Treg cells take on specific functions in many peripheral tissues, thereby protecting against autoimmune disease and tissue damage. Often, a dysregulation of the balance between Treg and Tconv cells in these tissues can cause a loss of tissue function and pathological effects: a depletion of Treg cells can cause autoimmune disease and infiltration of effector cells into the specific tissue, whereas enrichment of Treg cells in tumor tissues can dampen anti-tumor immunity and lead to

enhanced tumor growth. Therefore, careful therapeutic adjustment of the Treg-/Tconv balance would be an attractive treatment opportunity, from autoimmune disease to cancer.

4.8 Treg cell depletion as cancer therapy

Treg cells with their unique immunosuppressive capacities have been targeted for novel treatment approaches to fight cancer. In this disease, immunological self-tolerance promoted by intra-tumoral Treg cells dampens a favorable anti-tumor immune response. Tumor immunity is in part overlapping with autoimmunity, since tumors are derived from self-tissues and often display self-antigens.

In patients suffering from tumors of head and neck, breast, lung, liver, pancreas, the gastro-intestinal tract, the ovaries and the skin (melanoma), high Treg frequencies in tumors and the draining lymph nodes have been described [82]. Furthermore, a decreased ratio of $CD8^{pos}$ T cells to Treg cells can be a negative prognostic marker in breast, gastric and ovarian cancer. In contrast to this, infiltrating $Foxp3^{pos}$ T cells improve prognosis for colon, head/neck cancer and Hodgkin's lymphoma patients, but studies indicate that these Foxp3-positive cell populations are non-regulatory and secrete pro-inflammatory cytokines [83]. Taken together, these studies indicate the presence of various $Foxp3^{pos}$ T-cell populations in tumors, some of which exert different functions. This needs to be addressed in more details and reliable surface and intracellular markers have to be defined to detect specific subtypes of tumor-resident Treg cells.

Where do these tumor-resident Treg cells come from? Studies indicate that some tumors display CCL22, which attracts CCR4-expressing Treg cells from the circulation. In addition, since Treg cells have a higher avidity towards self-peptide and a generally heightened antigen-primed state, peripheral conversion *in-situ* into pTreg cells is also very likely [82].

The obvious next question – whether Treg cell ablation can then induce anti-tumor immunity – has been addressed in many pre-clinical studies. A first study in 1999 used injections of anti-CD25 mAb (PC61) before tumor inoculation. The Treg-depleting effect leads to an eradication of syngeneic tumors, but did not show efficacy if the antibody was administered later than day 2 after tumor inoculation[84]. Another study combined the removal of Treg cells with CTLA-4 blockade. This improved the function of a tumor cell-based vaccine against melanoma, leading to tumor rejection [85].

Additionally, a third study showed that the transfer to Treg-depleted $CD4^{pos}$ cells, together with the administration of tumor or self-reactive CD8 T cells, augmented the anti-tumor responses in a melanoma model [86]. Two studies addressed the use of low-dose cyclophosphamide for Treg cell depletion. The authors observed decreased Treg cell number and functionality alongside a downmodulation of GITR and Foxp3 expression [87]. Vaccination of cyclophosphamide-treated animals with HER-2/neu targeting vaccines raised strong CD8 T cell responses and protected from a HER2/neu expressing tumor challenge [88]. Finally, in a gain-of-function experiment, it has been shown that the transfer of Treg cells from immunized mice enhanced metastatic spread and tumor growth and development [89].

Two studies in human cancer patients also addressed the issue of Treg-promoted tolerance towards tumors: Treg cells actively prevent immune responses against NY-ESO-1 (human cancer/testis antigen expressed in many tumors) and tyrosinase (expressed in melanoma), and once peripheral blood lymphocytes had been depleted of Treg cells, $CD4^{pos}$ T cells could be re-activated by tumor-based peptide *in-vitro* [82].

Taken together, these pre-clinical studies illustrate that intra-tumoral Treg cells downmodulate anti-tumor immune responses through the specific suppression of tumor-resident CD4 T cells, CD8 cytotoxic T cells, NK cells, and NK-T cells. In addition, the selective eradication of Treg cells can ameliorate tumor burden and re-activate tumor- and self-reactive T cells – especially in combination with immune system-boosting vaccine regimens [82].

In order to harness the potential of the immune system to destroy tumor cells, a treatment strategy for the selective depletion of Treg cells, ideally only tumor-resident ones, is urgently needed. Several strategies are investigated, some of which already led to FDA-approved drugs.

A first approach is the use of chemotherapeutic drugs at certain dosage. It has been shown that treatment of patients with cyclophosphamide or fludarabine preferentially depletes Treg cells due to their higher proliferation rate, and that the combination of chemotherapy with multiple peptide vaccines increased the survival of renal cancer patients while decreasing their Treg cell number [90].

Another approach is the antibody-based depletion of Treg cells via their specific surface marker expression. In the human setting, CD25-depleting regimens cannot be used since activated T cells, also in the tumor, express CD25. In rodents, a selective depletion is functional (as described earlier). Clinical studies indirectly tested the depletion of Treg

cells with denileukin detox, a fusion protein of IL-2 and diphtheria toxin. A first study in 2005 identified no specific decrease in Treg cell numbers and their *in-vitro* suppressive capacity, causing no relevant regression in patients with advanced metastatic melanoma [91], while another study combined denileukin detox treatment with RNA-transfected dendritic cell vaccination. The authors could show significant Treg depletion from PBMCs, no acute toxicity, and abrogated Treg suppressive capacity *in-vivo*, leading to improved tumor-specific responses. Progression-free survival has not been evaluated [92]. Finally, a third study used daclizumab, a mAb directed against CD25, followed by DC vaccination: as expected, all CD25-highly expressing cells were depleted, actually leading to decreased vaccine-specific effector T cell presence in circulation. This translated into no changes in overall progression-free survival [93]. These studies clearly indicate that targeting CD25 has rather negative effects for therapeutic treatment of patients. Using toxin-conjugated recombinant IL-2 can induce clinical benefits in the right context, but care must be taken since tumor-attacking effector T cells also rely on IL-2.

Other surface molecules overexpressed on Treg cells have also been targeted for treatment. One of those is CCR4, specifically expressed by antigen-experienced Treg cells, but not naive Treg cells or effector T cells. Treatment with a CCR4-antibody was shown to improve CD4 T cells response to peptide *in-vitro*, comparable to an *in-vitro* Treg depletion, and clinical testing is under way. Another such target molecule is the Toll-like receptor. It has been shown that LPS or CpG can block Treg-suppressive mechanisms and increase IL-2 secretion by effector T cells, and trials using vaccination with TLR-stimulating viral or bacterial vectors are being conducted. This treatment is expected to break tolerance of effector T cells to tumor antigen. Additionally, OX40, overexpressed on Treg cells, has been targeted with anti-OX40 monoclonal antibodies. This regimen has shown to dampen Treg suppressive capacity, and intratumoral injection of the mAb can inhibit tumor growth while activating effector T cells in pre-clinical studies. Finally, GITR, as described earlier, can be targeted with anti-GITR mAb or GITR ligand. This was shown to inhibit Treg suppressive capacity and thereby increase anti-tumor CD4 and CD8 T-cell responses (all reviewed in [82, 94]).

A very exiting new strategy was the development of so-called immune checkpoint inhibitors, leading to the treatment of patients with blocking antibodies against CTLA-4 or PD-1. Blockade of CTLA-4 on Treg cells impairs suppressive function of Treg cells in tumor sites and breaks tolerance, while also augmenting effector T-cell activity. First

studies with ipilimumab ®, a humanized anti-CTLA-4 mAb, evaluated this antibody in combination with glycoprotein peptide vaccines in stage III or IV melanoma patients. Increased overall survival of patients was reported, along with grade 3-4 immune-related adverse events in 10-15% of patients [95]. Based on clinical efficacy and due to available therapeutic options to manage immune-related adverse events, ipilimumab® was approved for treatment of malignant melanoma by the FDA. It was shown to also work in combination with chemotherapy [96]. Its mode of action is more likely the selective Treg depletion rather than activation of effector T cells. It was shown that FC-γ expressing macrophages delete tumor lesion-resident Treg cells [97], and decreased Treg numbers in tumor tissue following treatment correlates with better prognosis.

Another immune-checkpoint inhibitor is PD-1. Antibodies have been engineered to block the PD-1 receptor (pidilizumab® and nivolumab®) or its ligand, PD-L1 (BMS-936559/MDX-1105® and MPDL3280A ®). PD-1 is an inhibitory receptor expressed on T cells, B cells, monocytes, NK cells and, in general, on tumor-infiltrating lymphocytes as well as tumor-infiltrating Treg cells. Some tumors highly express PD-ligand 1, often leading to more aggressive growth and poor prognosis. PD-L1 binding to PD-1 inhibits T-cell proliferation, cytokine production and cell adhesion [98]. A thorough clinical study with PD-1 immune checkpoint inhibitors reported grade 3-4 adverse events in 14% of patients diagnosed with melanoma, lung cancer, prostate cancer and colorectal cancer. Importantly, objective anti-tumor responses were observed in one in four/five patients. Response to treatment is probably linked to the level of PD-1 ligand expression on tumor cells [99]. Currently, more than 50 Phase 1, 2 and 3 trials are under way to evaluate PD-1 based treatments in many different solid and hematological malignancies [98]. Some patients already show durable responses in a variety of cancers, even long after treatment was completed.

4.9 Treg cell adoptive transfer to combat autoimmune disease

In contrast to cancer, where the presence of tolerance-mediating Treg cells is unwanted, patients suffering from autoimmune disease could benefit from increased numbers of Treg cells. Studies have already addressed the functionality and frequency of Treg cells in various autoimmune diseases (reviewed in [100]). In type-1 diabetes (T1D), patients and healthy donors have similar numbers of Treg cells. But it was shown that Treg cells from T1D-patients have a generally decreased suppressive activity together with a heightened resistance of pro-inflammatory T cells to Treg-mediated suppressive effects. Importantly, *ex-vivo* cultivation of Treg cells can revert their defects in suppressive potential.

Similar results have been obtained for patients suffering from systemic lupus erythematosus (SLE): Circulating Treg cells in the blood of these patients are less suppressive, more susceptible to apoptosis and therefore also decreased in overall frequency. *In-vitro* expansion normalizes Treg cell function and phenotype.

In contrast to this, patients suffering from Sjörgen's syndrome, an autoimmune disease affecting salivary and lacrimal glands, have functionally intact Treg cells, but significantly reduced numbers in both peripheral blood and target organs.

In multiple sclerosis patients, Tregs with diminished suppressive capacity have been described, but it is yet to be investigated whether Treg function can be restored by *in-vitro* cultivation and expansion protocols.

Finally, patients suffering from autoimmune rheumatic disease have Treg cell populations with limited ability to suppress cytokine production in autoimmune T-effector cells. Furthermore, Treg cells have defects in CTLA-4 expression, and they are unable to control IL-6 and TNF-induced inflammation.

Taken together, all these studies report either defects in Treg suppressive capacity or their cellular frequency in patients of various autoimmune diseases. Interestingly, it is often possible to revert these defects by *in-vitro* cultivation and expansion of Treg cells.

One possible therapeutic treatment method could be the *ex-vivo* expansion and re-infusion of functionally-corrected and frequency-increased Treg cells into patients (adoptive Treg cell therapy) to correct for the defects in Treg-mediated suppression.

Pre-clinical testing of adoptive Treg cell therapy has already shown promise. In experimental autoimmune encephalitis, a mouse model of SLE, Treg infusion can prevent disease when injected before disease initiation, but efficacy is nearly lost when

Treg cells are infused once the disease is already established. In mouse models of collagen-induced arthritis, total body irradiation followed by infusion with expanded Treg cells significantly slows disease progression. In a model of proteoglycan-induced arthritis, peptide-induced Treg cells were able to suppress arthritis in a LAG3 (lymphocyte activation gene 3 protein) positive manner with only a few thousand cells required for transfer [94]. Another very prominent autoimmune scenario, graft-versus host disease (GvHD) following hematopoietic stem cell transplantation, has also been addressed in murine studies. Myeloablative chemoradiotherapeutic conditioning for hematopoietic stem cell transplantation induces a systemic inflammatory environment despite multi-agent immunosuppressive drugs. If immune tolerance is protected in this time window, long-lasting tolerance without further immunosuppression might be possible. Infusion of isolated or *ex-vivo* expanded Treg cells was shown to be highly effective to prevent acute and/or chronic GVHD, and activated donor or host Treg cells (expressing CD103) were able to prevent ongoing chronic GVHD [101].

But what are the challenges for adoptive Treg cell therapy for human patients? First, there is the absence of unique cell surface markers on human Treg cells, causing a very likely contamination of clinical products with CD4 ^{pos}CD25^{pos} activated effector T cells. Acceptable levels of "contamination" with Foxp3-negative cells upon expansion have to be defined, and precise parameters to measure Treg-suppressive capacity or potency are still amiss. To prevent conversion of Treg cells into Tconv cells before and after infusion, different protocols using rapamycin or retinoic acid (stabilizes Treg cell expansion), demethylating agents (stabilization of TSDR demethylation) or HDACs (chromatin remodeling) for expansion protocols are being tested. Second, there is a limited availability of GMP-compatible expansion procedures, especially for large doses required for adoptive Treg transfer. Finally, system-wide treatment with high doses of Treg cells might enhance global immunosuppression, leading to diminished responses to infectious agents or tumor cells ([100] and [94]).

Besides these challenges, different Treg expansion protocols are in development and being tested in first clinical trials –using Treg cells expanded from peripheral blood, umbilical cord blood or HLA-matched third party blood. It has already been shown that *in-vivo* expansion by low-dose IL-2 with or without rapamycin showed some clinical benefits in human GVHD and T1D patients - now adoptive therapy with *ex-vivo* expansion and activation of allogeneic or autologous Treg cells has to prove its validity.

4.10 Scope of this thesis

In the previous paragraphs, we reviewed current knowledge about Treg cells: origin, molecular control, and tissue-specific distribution and function. We furthermore provided details about the potential use of Treg cells to modulate autoimmune disease and cancer. In this thesis, we now describe three projects investigating the molecular makeup of regulatory T cells: First, we performed an epigenetic analysis of the *Foxp3* gene, combined with an identification of transcription factors residing at the proximal *Foxp3* promoter. Second, we widened this approach to a whole-genome based CG-dinucleotide methylation analysis of fat, skin, liver and lymph node Treg cells. And third, we investigated the importance of Rbpj, an important cellular transcription factor, for the homeostasis and function of Treg cells. It was our ultimate goal to gain more insight into the molecular control of Treg cells and Treg-specific modes of action, which could lead to new strategies for the therapeutic modulation of the Treg/Tconv balance. This would allow the fine-adjustment of peripheral tolerance to combat autoimmunity or cancer.

5 Introduction

5.1 Epigenetic control of the *Foxp3* gene in Treg cells

Epigenetics is the study of DNA methylation and histone/nucleosome modifications

Epigenetics is the study of heritable changes in the genome. In one organism, all somatic cells have the same genetic code, but tissue-resident cells still express different parts of the genome - causing a variety of cell types and tissues. The study of epigenetics provides key mechanisms to explain the interaction between DNA and proteins (transcription-inducing factors, factors of the translational machinery, and so on), causing a regulation of gene and microRNA expression on the molecular level. These changes in global gene expression translate into cellular differentiation, ultimately leading to their specific tissue adaptation. Already in embryogenesis, epigenetic events influence proper development from fertilized egg to blastocyst. In adults, epigenetic silencing is an important means of inactivating the second maternal X-chromosome in female mammals, and methylation of one in two alleles is responsible for the mono-allelic expression of genes. On the chromosomal level, hypermethylation of repetitive elements stabilizes chromosomal structure and integrity. Furthermore, varying epigenetic patterns can re-organize the nuclear framework and promote special chromosomal territories. Finally, genomic imprinting is an important means of transporting parental epigenetic modification patterns to the offspring [102].

Epigenetics comprises three distinct categories: DNA methylation, histone modification and nucleosome positioning. DNA methylation, also the focus of this paper, occurs almost exclusively at CpG dinucleotides (**C**ytosine-**p**hosphate-**G**uanine). It describes the addition of a methyl group to the 5' position of the cytosine pyrimidine ring, and was already identified in 1951 [103]. Histone modification describes the composition of nucleosomes with regulatory subunits. An assembly of H2.A-H2.B dimers, a H3-H4 tetramer, and a H1 monomer forms nucleosomes. Nucleosome-resident histones can undergo post-translational modifications, like acetylation, methylation, phosphorylation, and many others. These mechanisms influence transcriptional activity, DNA-repair mechanisms, DNA replication and splicing, as well as chromatin condensation. In fact, euchromatin is composed of high levels of acetylated and trimethylated histones H3K4, H3K36 and H3K79, allowing efficient transcription and translation. Heterochromatin,

on the other hand, is transcriptionally inert and shows low levels of acetylation in concert with specific methylation of H3K9, H3K27 and H4K20 [104]. Besides DNA methylation and histone modifications, nucleosome positioning is a third means of epigenetic control. The precise positioning of the nucleosomes can pose a barrier for transcription factor and polymerase access to DNA, especially at the transcription start site (TSS). Four families of chromatin remodeling complexes can move, eject or re-structure nucleosomes to modify gene expression patterns (all reviewed in [102]).

Methylation of cytosine residues in CpG islands can control gene expression

Generally, mammalian DNA is hypermethylated at most of its CG sites, to a degree between 60% and 90%[105]. In particular, gene bodies or repeat sequences are highly methylated, and loss of gene methylation is linked to genomic instability of these regions [106]. But how does methylation affect the regulation of single genes?

So-called "CpG islands" are areas of high CG density. They are generally underrepresented in vertebrate DNA since they occur only in about one-fifth of the expected frequency in DNA [107, 108]. But when they occur, they are often located in promoter and first exons of genes, where they regulate gene expression. They are defined as regions of 200 bp or more, with a high GC content and on observed/expected ratio of CpG occurrence of more than 0.6 [109]. In the mammalian genome, approx. 20 000 CpG islands can be detected, which incorporate about 5% of all CGs and about 1% of all nucleotides of the genome. 95% of the remaining CG dinucleotide in non-CpG islands are methylated [110].

Promoters can be classified according to their load of CG dinucleotides. CpG-rich promoters tend to be unmethylated and mostly regulate housekeeping genes, which are ubiquitously expressed and important for essential cellular functions. Here, demethylation often allows for efficient gene expression, and increases genetic stability and integrity. Demethylation can directly affect transcription factor binding efficiencies to the promoter, allowing more efficient recruiting of co-factors and RNA polymerase II [111, 112]. Intermediate-density promoters can vary in methylation and, depending on the environment, regulate tissue-specific functions via selective methylation or demethylation. Low-CG-density promoters are mostly methylated in somatic cells, but still induce gene expression via the binding of special methylation-favoring transcription factors [113], although they are genetically rather unstable.

In conclusion, high or low density CpG areas are regulatory elements where specific methylation or demethylation can induce or repress gene expression based on the local environment. Therefore, treatment of cell lines with 5-Aza-2′-Deoxycytidine (5-aza), a globally demethylating agent, does not only induce gene expression through the release of methylation-based expression blockade, but can also induce gene repression by demethylation – this is based on the nature of the promoter or enhancer which controls the target gene [114].

Sodium bisulfite sequencing and other methods to investigate DNA methylation

First global CG methylation data were based on methylation-sensitive restriction enzyme digestions of ribosomal DNA – these studies identified a generally high methylation level in somatic cells, while some sites were specifically unmethylated [105]. Furthermore, they discovered that in highly methylated genomes, as seen in vertebrates, methylated CG dinucleotide can undergo deamination to TG (tyrosine-guanine) dinucleotides, which does not happen with unmethylated CGs.

These findings lead to the development of the bisulfite conversion method in 1992 [115]. First, genomic DNA is purified and digested. Linearized DNA is incubated with sodium bisulfite and hydroquinone. Following the *in-vitro* deamination of unmethylated cytosine to tyrosine, several dialysis steps remove unreacted sodium bisulfite. Bisulfite-converted DNA can now be used to generate PCR amplicons with specific primer pairs, which can ultimately be cloned into vectors for Sanger sequencing or analyzed via next-generation sequencing. In this paper, we use sodium-bisulfite conversion via a commercial kit, followed by 454-pyrosequencing of PCR amplicons (see **Figure 8**).

A first method for the genome-wide investigation of methylation events at CG dinculeotides was based on bisulfite padlock probing technology (BSPPs) [116]. The authors used 100 nucleotide-long DNA probes, which specifically hybridize to target DNA in a horseshoe manner: 3’ and 5’ end of the probe bind DNA, and the remaining nucleotide DNA forms a circle. The “gap” between 3’ and 5’ end of the probe is closed by PCR and the linearized vector is then analyzed by DNA sequencing. This technology allows the sequence-specific analysis of methylation hotspots and requires the design of probes with barcodes and sequencing adaptors. In another approach published in the same study, the methyl sensitive cut counting assay (MSCC) was introduced [116]. It uses the methylation sensitive *HpaII* restriction enzyme on DNA to cut only unmethylated

CCGG palindromic sequences. The digested sequences are ligated to first and second adapter sequences followed by amplification and high-throughput sequencing. With this approach, no probe design was necessary, but efficiency of restriction enzyme digestion and the limitation to CCGG palindromic sequences restricted potential applications. In 2005, a paper introduced methylated DNA immunoprecipitation-sequencing (MeDIP-seq) [117]. In this approach, antibodies directed against methylated cytosine are used to precipitate methylated DNA, followed by next-generation sequencing and mapping to the whole genome. The technology offers a resolution of 150bp to 200 bp, but areas of very low CG density may not be recovered by the chromatin IP. In contrast to this, whole-genome bisulfite sequencing, which requires bisulfite-conversion of DNA followed by the ligation of adapter sequences via PCR and next-generation sequencing [118], allows for the precise detection and evaluation of every single CG dinucleotide in the whole genome. One limitation, the relatively large amount of genomic input DNA required for this method, was overcome with the introduction of tagmentation-based whole genome bisulfite sequencing [119]. In this method, transposase-fragmented DNA is linked to a sequencing adapter, followed by oligonucleotide replacement and gap repair events. Following a final PCR amplification, NGS reveals the methylation profile of the genome. Relatively low amounts of genomic DNA (less than 30 ng) can be analyzed for their methylational footprint. We use this method, with an even more advanced protocol, in Chapter 8 – there, we study the differential methylation of tissue-resident Treg cells, with a total input of less than 20,000 cells. Finally, some commercial suppliers now offer bead chips for the analysis of methylation "hotspots" in a standardized procedure.

Zygotes become demethylated and require DNA-methyltransferase to regain epigenetic control

The above-described methods can be used to gain genome-wide information about CG methylation and have been used in various contexts. Several studies analyzed the genome of the "first cell", the fused sperm and oocyte, and traced its methylation pattern. Fused sperm and oocyte initially carry highly methylated genomes. But then, right after the fertilization of the egg, the paternal genome becomes completely demethylated – this also erases the paternal epigenetic imprinting. After a first replication cycle, the maternal genome becomes demethylated as well, but imprinted

epigenetic marks are conserved. In the blastocyst stage, DNA methyl transferase 3 (Dnmt3) restores the methylation level to the one of a pluripotent stem cell, right around the time of blastocyst implantation. When Dnmt activity is lost, so are pluripotency and differentiation potential of the growing embryo ([110] and [120]).

In this context, DNA-methyl transferases have been studied extensively for their role to establish and maintain methylation at CG dinculeotides. They have an important function to maintain pluripotency, to conserve genomic imprinting and genome stability, and to inactivate one X chromosome in females. There are three classes of methyl transferases with catalytic activity: Dnmt1, Dnmt3A, and Dnmt3B. Dnmt3A and B mediate, as described above, the *de novo* methylation during embryonic development. They selectively methylate CG dincleotides based on a proper target sequence and presence of special co-factors. In contrast to this, Dnmt1 serves as a maintenance methyl transferase preserving the methylation pattern during cell replication. It can bind the replication fork in the S phase of cell division and detect hemi-methylated CG dinucleotides on the template strand. It catalyzes the methylation of the respective palindromic CG dinucleotide on the newly synthesized strand as well and thereby promotes genomic stability (reviewed in [121]).

Epigenetics and disease

Global epigenetic changes have been observed in many forms of human disease. In one particular case, the malignant transformation of cells causing cancer, global changes in DNA methylation occur. In general, a specific loss of DNA methylation (20%-60%) has been noted for highly repetitive sequences in the genome of cancer cells. This causes chromosomal instability, thereby inducing translocation events, disrupting the gene architecture and even re-activating endoparasitic sequences. Demethylation events have also been described for specific promoters encoding for oncogenes, unleashing the expression of those. In contrast to this, promoters and gene-controlling elements of DNA repair enzymes, cell cycle control proteins and apoptosis-regulating factors can become hypermethylated and thereby transcriptionally inactivated. Changes also occur on the level of histone modifications and chromatin remodeling factors, all in favor of more proliferative capacity and less cell cycle control in tumor cells.

Epigenetic changes have also been observed for neurological disorders, such as Rett syndrome. Here, an enzyme recruiting histone deacetylase (HDAC) to methylated DNA (MeCP2) is specifically up-or downregulated via epigenetic marks, causing pathological symptoms associated with the disease. Involvement of epigenetic changes has also been identified for fragile X syndrome, Parkinson's disease, Multiple Sclerosis, and Prader-Willi and Angelman Syndrome. Furthermore, autoimmune syndromes such as Rheumatoid Arthritis, Systemic Lupus Erythematosus (SLE) and ICF syndrome (Immunodeficiency, centromeric instability and facial anomalies) have been linked to epigenetic changes. This highlights the central role of epigenetics to modulate gene expression and chromosomal stability, and demonstrates the consequences of disregulated epigenetic control (all reviewed in [102]).

Methylation analysis of the *Foxp3* gene reveals the Treg-specific demethylated region (TSDR)

When sequence-comparing mouse and human *Foxp3* genetic code, several highly conserved non-coding sequences can be identified (**Figure 11**). These are important binding sites for transcription factors, as reviewed in the next chapter. In terms of epigenetic control, a histogram depicting areas of high CG density in the *Foxp3* gene can identify CG hotspots (also in **Figure 11**).

First studies identified the importance of methylation for the *Foxp3* gene promoter in an indirect way. When NK cells were treated with 5-aza, IL-2 dependent *Foxp3* induction in NK cells was restored. This was a first hint that methylation of CG nucleotides might be involved in *Foxp3* gene expression regulation [122]. Next, a 2007 study identified an area in the first *Foxp3* gene intron, CNS2, which contains both a TCR-responsive element, with a cyclic-AMP response element binding protein (CREB)/activating transcription factor (ATF) binding site, and an area of high CG density meeting the criteria of a CpG island. Again, using 5-aza or a knockdown of Dnmt1, the authors showed that methylation of the CNS 2 locus inversely correlates with *Foxp3* gene expression, probably by downmodulating CREB binding to this region and thereby reducing *Foxp3* gene expression [123]. Since this study was based entirely on 5-aza treatments or Dnmt1 knockdown followed by *Foxp3* expression analysis, sequencing-based proof was still amiss. Therefore, another 2007 study used amplicon-based sequencing to validate that CNS2 is demethylated in human Treg cells. Furthermore, no

demethylation was observed in activated human Tconv cells, which only express *Foxp3* upon TCR stimulation, or in TGFβ-treated *in-vitro* induced Treg cells. Based on this finding, the authors conducted a genome-wide analysis of differentially methylated sites in Treg versus Tconv cells, and they determined CNS2 to be the best marker to discriminate Treg cells from *in-vitro* induced iTreg cells or activated Tconv in the human system [124]. Based on these data, the CNS2 area was designated Treg-specific demethylated region (TSDR). Since all studies mentioned above used human material, a third 2007 study evaluated the methylation status of the TSDR in mice. The authors showed, again, the differential methylation of this area between Treg and Tconv, along with the identification of a TSDR-resident response element induced by PMA/Ionomycin treatment. They showed that, in Tconv cells, the TSDR is packed with condense, more inaccessible chromatin structures via histone acetylation and trimethylation events, adding to the gene-expression inhibiting effects of CG methylation at this spot[125]. In summary, the *Foxp3* TSDR has been investigated and identified as a methylation-sensitive element regulating *Foxp3* gene expression. Its demethylation is essential to promote stable *Foxp3* gene expression and Treg lineage commitment, and it cannot be induced in macrophages, B cells or iTreg cells. Therefore, *Foxp3* expression stability is tightly linked to TSDR demethylation [36, 126, 127].

Aim of this subproject

Is the TSDR the only demethylation-sensitive element in the *Foxp3* gene? The highly conserved *Foxp3* promoter or other *Foxp3*-resident CG-rich regions have not been carefully evaluated for their CG methylation status. This motivated us to study all CG-rich regions of the *Foxp3* gene promoter in more detail. We want to answer the following questions: Is the TSDR the only region with a specific demethylation pattern in the *Foxp3* gene? Are there other regions with the same pattern? What is the methylation status of the promoter and exons in the *Foxp3* gene? When during Treg development in the thymus is *Foxp3* gene demethylation established? And, finally, is the specific TSDR methylation also present in Foxp3-negative T cells from DNA-methyltransferase hypomorphic mice?

5.2 Transcriptional and epigenetic control of tissue-specific Treg cells

Previously, we discussed the role of the Treg-specific demethylated region (TSDR) in Treg cells. Specific demethylation at this site is a pre-requisite for stable and long-lasting *Foxp3* expression, and deletion causes Treg instability and reversion to a non-regulatory phenotype over time. One specific question was to determine whether the methylation pattern seen at the TSDR is one of only few specific methylation events, or whether there is a unique Treg-specific epigenetic signature independent of Foxp3-regulated mechanisms. Some observations would point into the direction of a Foxp3-independent epigenetic signature: The retroviral overexpression of *Foxp3* in Tconv cells promoted a suppressive phenotype, but microarray-based gene expression analysis revealed substantial differences between tTreg and *Foxp3*-transduced Tconv cells. Furthermore, mostly in the human system, Tconv cells transiently express *Foxp3* upon TCR stimulation without becoming a stable regulatory lineage. In addition to this, Treg cells may lose *Foxp3* expression under certain inflammatory conditions while they still remain lineage-committed. Therefore, one can assume that expression of Foxp3 protein alone is not sufficient to induce the Treg phenotype, but other heritable marks could supplement the effects of this transcription factor [128]. Since DNA methylation is a heritable and stable means of cell subset definition, and Treg cells proliferate actively *in-vivo*, several studies addressed the epigenetic regulation of Treg cells.

Global H3K4me3 and H3K27me3 study in Treg cells

A pilot study investigated the H3K4me3 and H3K27me3 trimethylation in T_H subsets and Treg cells, where H3K4me3 promotes gene-repressive state and H3K27me3 promotes gene induction, respectively. Interestingly, not many genes were different between Treg and Tconv cells or other T_H subsets. Some genes, such as *Foxp3*, *Il2ra*, *Ifng*, *Il4*, *Il17*, and *Rorc* were differentially modified between Treg and Tconv cells, but these changes are probably mediated by Foxp3 downstream regulation (most of the above mentioned genes are directly regulated by Foxp3) and not by an independent regulatory complex [129].

Global MeDIP-Seq of Treg cells reveals 300 Treg-specific demethylated regions

A landmark study in 2012 investigated the genome-wide CG methylation profile of Treg vs. Tconv cells in mice via methylated DNA immunoprecipitation-sequencing [44, 128, 130]. The authors identified 160,000 methylation regions, 300 of which were specifically demethylated in Treg cells (about 0.19% of all methylation sites). 50% of those sites were located in gene bodies (coding regions and introns) and comprised 10 or more CpG residues. Most promoter regions of genes were shown to be hypomethylated in both Tconv and Treg – which is true for the *Foxp3* gene promoter as well. From the 150 differentially methylated regions, gene annotations revealed that demethylation-sensitive regions were located in areas related to *Foxp3*, *Ctla4*, *Il2ra*, *Tnfrsf18* (GITR), *lkzf2* (Helios), and *lkzf4* (Eos). The demethylation pattern of these genes is specific for thymus-derived Treg cells and peripherally induced Treg cells, but not *in-vitro* induced Treg cells, *Foxp3*-retrovirally transduced Tconv cells, activated Tconv cells, or other T_H subsets. Furthermore, these regions are stably induced in *Foxp3-IRES-GFP* knock-in reporter mice and mice of various genetic backgrounds. Importantly, the regions are also induced in *Foxp3*-scurfy mice (carrying a *Foxp3*-promoter GFP reporter, but no functional Foxp3 protein) or Foxp3-null mice despite the absence of Foxp3 protein. This indicates that the epigenetic framework is established independent of Foxp3 protein expression during thymic Treg cell generation. Indeed, Foxp3 protein consensus binding sites (2800) have no overlap with Treg-specific demethylated gene areas except the *Foxp3* TSDR. Therefore, one can infer that the epigenetic pattern induced in Treg cells provides a stable and functional framework, whereas Foxp3 is required to induce the suppressive phenotype of these cells. This can be illustrated by the epigenetic-based induction of genes such as *Ctla4* and *Il2ra*, which code for CTLA-4 protein and CD25 cell surface receptor, hallmarks of Treg cells. Foxp3, on the other hand, represses expression of pro-inflammatory genes encoding for IL-2 or IFN-γ, thereby promoting the anti-inflammatory phenotype of this cell lineage. This also illustrates that, while epigenetic modifications in Treg cells often release gene expression via selective demethylation, Foxp3 acts more as a repressor of gene transcription.

Another 2013 study investigated the methylation of human Treg vs. Tconv cells with an Illumina Infinium Human Methylation 450K array. The authors isolated human naive resting T cells ($CD45RA^{pos}CD25^{pos}$) and Tconv cells from male donors. Out of 450,000 probes, 2315 single CG dinucleotides were differential between resting Treg and Tconv

cells (0.5% of total). 70% of those were associated with genes, and of those, 33% were located in gene promoter regions and 40% in gene bodies. Interestingly, the CG dinucleotides showed an even distribution of hypo – and hypermethylation at those sites, strongly contrasting the results presented in the murine cell-based study discussed previously. Furthermore, the authors identified an overlap between differentially methylated genes and Foxp3 protein bound genes, leading to the conclusion that methylation events might allow the specific binding of Foxp3 protein to its target genes. Furthermore, in this study, both Treg and Tconv cells were activated for six days with CD3/28 stimulation in the presence of IL-2 to study effects of TCR stimulation on the epigenetic profile. After six days, 85% of Treg cells and 30% of activated Tconv cells expressed Foxp3. The methylational profile of Treg cells was not affected by activation, but Tconv cells were, indicating plasticity of DNA methylation only in Tconv cells. But from where do the obvious differences, compared to the previously mentioned study with mouse cells, originate? First, in the human system, there are no reliable markers for the isolation of Treg cells with high purity. Therefore, a certain level of contamination of Treg cells with activated Tconv cells is likely. Furthermore, the 450K Methylation Array only scans certain CG sites of the genome, but the vast majority of sites is not probed. Finally, system differences between human and mouse epigenetic marks might cause different conclusions from these studies.

Aim of this subproject

We use a novel tagmentation-based whole genome bisulfite sequencing method to study the epigenetic profile of infrequent tissue-resident Treg cells from different anatomical locations (skin, fat, liver and lymph node). This protocol had already been used to study hematopoietic stem cells and four multipotent progenitor populations in a pilot study [119, 131, 132]. The authors identified 15,000 differentially methylated regions, and correlated their methylation data with RNA-sequencing and proteomics data. The study revealed specific expression clusters to operate in HSCs, and showed a dynamic modulation of loss – and gain of methylation during differentiation of HSCs. Therefore, this analysis provided a detailed overview of epigenetic changes during HSC differentiation, linking it to the gene expression changes and proteomics signature description.

The aim of our work was to identify tissue-specific epigenetic patterns, which show that Treg cells have the potential to adapt to local tissue environments both on a

transcriptional and on an epigenetic level. For example, fat-resident Treg cells overexpress PPAR-γ, which mediates its function to suppress the development of type-2 diabetes [64]. We are now interested in linking the differential gene expression profile of Treg cells in fat tissue with epigenetic modifications. Already, some of our preliminary data suggest that the whole-genome methylation levels are very different in Treg cells from fat, liver, or skin, compared to their lymph node counterparts (see Chapter 7). Interestingly, the methylation levels between Treg and Tconv in the lymph nodes are almost equal. Since we know that only about 300 regions or 0.19% of all CG sites are differentially methylated (in the MeDIP-Seq studies mentioned before), this is not surprising. But the relatively high difference in overall CG methylation between tissue-resident Treg cells might already implicate a tissue-specific adaption based on epigenetics. Furthermore, in correlation with gene expression data, we want to identify landmark tissue-specific transcription factors, as exemplified with PPAR-γ for fat Treg cells.

5.3 Transcription-factor based control of the *Foxp3* gene

In the previous paragraphs, we reviewed current literature about the epigenetic regulation of Treg cells and the *Foxp3* gene. In this section, it was also mentioned that gene promoters are often demethylated, allowing the binding of the transcription factor machinery to these loci. Motivated by this, we investigated the *Foxp3* promoter more closely and identified it to be completely demethylated in both Foxp3-expressing Treg cells and Foxp3-negative Tconv cells. Therefore, we concluded that there might be additional mechanisms of *Foxp3* gene repression in Tconv cells and investigated this hypothesis with a novel method called inverted Chromatin-IP. First, we summarize already-published signaling pathways at the *Foxp3* locus, followed by a more detailed literature review of specific highly conserved TF binding sites along the *Foxp3* gene.

Gene conservation studies reveal highly conserved non-coding sequences (CNS)

The *Foxp3* gene is located on the X-chromosome (Xp 11.23). It contains 14 exons, three of which are not translated (-2a, -2b and -1). Just upstream of the transcription start site (TSS), the promoter with TATA box, GC box, and CAAT box is located. When comparing the sequence homology between mouse and human *Foxp3* genetic code (as already described in **Chapter 5**), a high degree of conservation can be appreciated for the coding exons, three regions in non-coding introns, and the promoter itself, as shown in **Figure 6** below [18, 133].

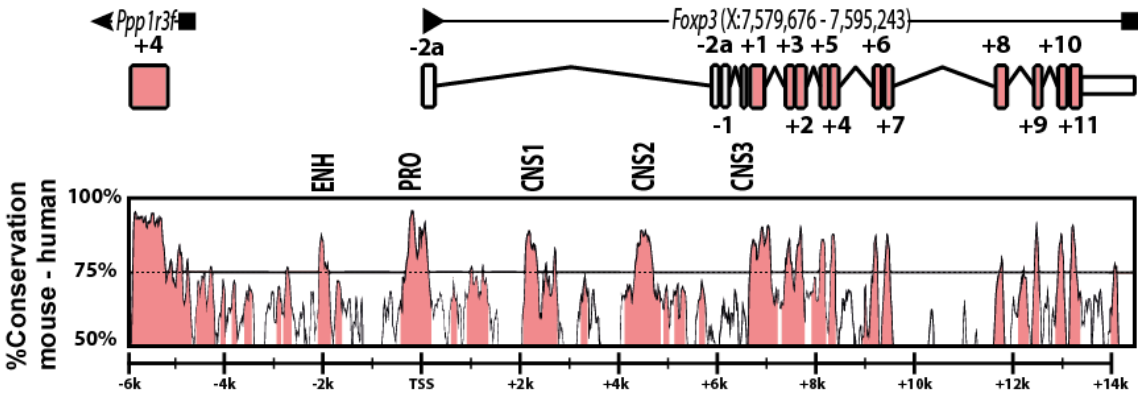

Figure 6: Conversation of the murine *Foxp3* gene and identification of CNS1-2-3.

As depicted in the graph, there are three distinct conserved regions within the non-coding intronic sequences of the *Foxp3* gene. These were determined conserved non-coding sequences 1, 2, and 3 (**CNS1-3**). Each CNS region has a distinct function in the

initiation or stabilization of *Foxp3* gene expression, just like the core *Foxp3* promoter (**PRO**). A putative enhancer can be detected 2000 bp upstream of the TSS (**ENH**), but no functional evaluation of this region has been performed to date. In the following paragraphs, we will review literature about the specific role of the promoter and each CNS region for the induction and maintained expression of the *Foxp3* gene in Treg cells.

Signaling Pathways involved in the regulation of *Foxp3* gene expression

Treg precursor cells in the thymus receive various signals during their maturation. First, Treg lineage fate decision depends on signals received by the T-cell receptor through the binding of self-ligands. Proper TCR: self-peptide signaling strength together with CD28 co-stimulation and cytokines promotes Treg cell development in a two-stage model: First, TCR signals prime Treg cells. Then, common γ-chain cytokines such as IL-2, IL-7 and IL-15 induce *Foxp3* gene expression via STAT5 signaling cascades. If all three cytokines are absent in the thymus, Treg cells cannot be induced [134].

In contrast to these *Foxp3*-promoting signaling pathways, the PI3K-Akt-mTOR pathway acts as a repressor of *Foxp3* gene induction. It is triggered by TCR/CD28 signaling events, by common γ -chain cytokines such as IL-2, by specific complement factors, or by Programmed Death-1 (PD-1) receptor ligation. Binding to these receptors mediates the selective phosphorylation of Foxo proteins, in turn inhibiting *Foxp3* gene induction. Overexpression of pathway components, such as Akt, impairs *Foxp3* induction, and inhibition of pathway components by small molecules, in turn, induces *Foxp3* gene expression – as observed with Rapamycin, an inhibitor of mTOR, which can be used to expand Treg cells *in-vitro* and *in-vivo* [135]. The suppressive function of the PI3K-Akt-mTOR pathway seems to contradict the need of TCR-stimulation required for *Foxp3* induction in the two-stage model proposed above. But the duration of the Treg-precursor cell priming by thymic epithelial cells is short, and no more TCR signals are required to complete the Treg differentiation program afterwards. Additionally, this fail-safe mechanism prevents the induction of Treg cells from pro-inflammatory T helper cells in the periphery once they detect their cognate antigen (e.g. foreign antigen or virus-infected cells). To prime Treg cells in the periphery, TGF-β can promote *Foxp3* gene expression via NFAT and SMAD signaling, as discussed later.

Another important signaling pathway involved in Treg cell induction is the classical NFκB signaling pathway. When Active Inhibitor of NFκB (iKκB) is overexpressed in T cells, leading to the degradation of NFκB signaling inhibitors, *Foxp3* expression is induced. If NFκB signaling components are deleted, *Foxp3* expression is impaired (pathways reviewed in [136] and [60]).

The *Foxp3* promoter can bind several TF to induce *Foxp3* gene transcription

The precise location of the *Foxp3* promoter and the true TSS were identified by rapid amplification of 5' ends (RACE): mRNA transcription starts at the TSS, as expected, indicating that the core promoter is indeed the area where polymerase and expression-promoting TF bind to initiate DNA-dependent RNA transcription of *Foxp3* pre-mRNA. In the same study, Foxp3 protein expression was induced in EL4 T cells by TCR stimulation and cytokine treatment with TGF-β. Interestingly, the *Foxp3* promoter, more precisely the region of -1702 to +174 (relative to the TSS), showed no luciferase reporter activity in Foxp3-induced EL4 T cells compared to non-induced Foxp3-negative EL4 cells [137]. This indicates that the *Foxp3* gene promoter does not translate TGF-β-signals to induce *Foxp3* gene expression. Eventually, other studies identified a TGF-β response element at the conserved non-coding 1 (CNS1) region, as discussed in the next paragraph.

Tone and co-workers also identified NFAT (Nuclear Factor of Activated T cells) binding to the *Foxp3* promoter via electromobility shift assays (EMSA). The *Foxp3* promoter contains six NFAT and AP-1 (Activator protein 1) binding sites, which translate T-cell receptor signals into promoter activity. Mutations in the binding sites disrupt its activity. Also, treatment with cyclosporine A disrupts NFAT activity: it blocks NFAT translocation to the cell nucleus and thereby inhibits *Foxp3* promoter activation by this TF. Furthermore, if mice are deficient of STIM1/2 calcium sensors, NFAT cannot enter the nucleus and *Foxp3* expression is impaired ([138] and [139]). Together, these studies indicate that the promoter can respond to T-cell receptor signals, but not to the TGF-β mediated pathway, for *Foxp3* induction.

As mentioned earlier, Foxo proteins bind the *Foxp3* promoter as part of the PI3K-Akt-mTOR pathway. Specific deletion of Foxo1 and Foxo3a causes multifocal inflammatory disorder. Also, Treg conversion via TGF-β is diminished in T cells devoid of Foxo transcription factors [140, 141].

Another factor mentioned previously, STAT5, has also been detected at the *Foxp3* gene promoter. Cytokine-derived signals promote STAT5 activation and Treg cell differentiation, and its selective deletion prevents Treg cell development. It has been hypothesized that STAT5 can bind to the promoter only when the CNS2 regions is demethylated, indicating an indirect regulation of promoter activity by epigenetic events elsewhere [142, 143].

Another interesting example of direct *Foxp3* promoter regulation by epigenetic events is the study of Nr4a family members. Mice devoid of all three family members (Nr4a1, Nr4a2, Nr4a3) cannot produce Treg cells and die of systemic autoimmunity, but single knockouts have no effects, probably due to compensatory mechanisms. It has been shown that Nr4a factors are induced by TCR binding to self peptides in Treg cells, and that all members bind to the *Foxp3* promoter in different affinities to induce Foxp3 protein expression. It is proposed that Nr4a2, which can recruit histone modification enzymes, can open the *Foxp3* promoter epigenetically and thereby allow the binding of the RNA translation machinery [144, 145].

In 2009, Ruan and co-workers identified a complex, the c-Rel enhanceosome, at the *Foxp3* promoter. Interestingly, this complex is first initiated by binding of Smad to Creb (cAMP response element-binding protein) at *Foxp3* enhancer sites, and afterward moves to the *Foxp3* promoter to link with c-Rel, p65, and NFAT. Once c-Rel is deleted, the enhanceosome cannot form anymore and the Treg cell number decreases by about 90% [146].

One more complex has been described by three studies in 2009. They identified Runt-related transcription factor (Runx) proteins, induced by TGF-β, to bind the *Foxp3* promoter at the Runx binding sites. Their binding is co-operatively increased by their co-factor Core-binding factor subunit β (Cbf-β). Inhibition of both the co-factor Cbf-β or Runx1/3 reduces *Foxp3* expression or silences the *Foxp3* gene promoter completely, leading to impaired suppressive capacity *in-vitro* and *in-vivo* as well as higher IL-4 expression. The complex also binds the *Foxp3* gene at its regulatory regions CNS2 and CNS3, making it important for not only the induction, but also the maintenance of *Foxp3* gene expression [147, 148].

Finally, the E2A-Id3 signaling axis has been identified as a negative regulator of T_H2 differentiation in Treg cells. First, TGF-β signaling can induce Id3 protein. Id3 then enriches for E2A, which in turn binds the *Foxp3* promoter at specific E-boxes and induces *Foxp3* transcription. When Id3 was deleted, Treg cell generation was defective.

Besides promoting *Foxp3* promoter gene activity, E2A can actively replace trans-acting T-cell-specific transcription factor GATA-3 at the *Foxp3* promoter [149]. GATA-3 is, once expressed, an important lineage-defining factor of T_H2 cells, but also a repressor of *Foxp3* gene transcription at the *Foxp3* promoter [150]. Two studies in 2011 further investigated the impact of GATA-3 in Treg cells. Once it was specifically deleted, inflammatory disorder was induced. GATA-deficient Treg cells could not promote peripheral homeostasis and lost suppressive function, and they gained a T_H17 pro-inflammatory phenotype. As mentioned earlier, GATA-3 binding to the promoter has rather *Foxp3*-suppressive effects – but its binding to the *Foxp3* CNS2, induced by TCR and IL-2 cytokine stimulation, and to other cis-acting elements in the *Foxp3* gene is important for proper Foxp3 protein expression [151, 152].

Taken together, we here summarized various binding partners to the *Foxp3* promoter. They modulate their downstream functions via direct binding to the promoter and initiation of transcription, via the recruitment of co-activators, by the selective displacement of repressive TFs, or by epigenetic modulation of the promoter. But some of these factors are not expressed differentially in bona fide Treg vs. Tconv cells, and it is believed that many factors operate in a context-dependent manner in a multiprotein network occupying the *Foxp3* promoter. It was therefore our rationale to gain more insight into the *Foxp3* core promoter and to identify binding partners in an unbiased way by the inverted Chromatin IP, as described later.

The CNS1 region is important for peripheral, but not thymic, induction of Treg cells

The conserved non-coding sequence 1 region (CNS1) has been defined to be precisely between +2079 and +2198 bp downstream of the TSS (**Figure 6**). Probing the *Foxp3* promoter with 400-1200 bp long luciferase reporter fragments identified this specific area. Besides the transcription-inducing activity, this region is highly conserved between species. It contains a CD3 response element, promoting TCR signal transduction to the *Foxp3* gene. Furthermore, it contains a TGF-β response element, which is important for the peripheral conversion into pTreg cells: The CNS1 region becomes strongly activated upon treatment with TGF-β in concert with TCR-stimulation by CD3 and CD28 ligation. Otherwise, the region has only weak activity in non-stimulated T cells.

Importantly, the region contains selected NFAT and Smad3 binding sites – these promote deacetylation of the CNS1 region and thereby maintain *Foxp3* expression. The binding sites of NFAT and Smad3 are highly conserved not only between human and mouse, but also chimpanzee, elephant, horse, goat, rat, and guinea pig [137].
A complete CNS1 knockout showed that CNS1 is dispensable for the thymic generation of Treg cells, but is important for the induction of peripherally induced Treg cells via TGF-β. CNS1-deficient mice have a normal thymic Treg output, but decreased frequency of Treg cells in the mesenteric lymph nodes, indicating decreased peripheral conversion rates. No immune-mediated lesions in the gastro-intestinal tract have been reported under steady state-conditions upon CNS1 deletion [153, 154].
In summary, CNS1 is an important TGF-β -sensitive enhancer region for the induction of pTreg and iTreg, but not relevant for thymic Treg cell generation.

The CNS2 stabilizes *Foxp3* gene expression by selective CG demethylation

In contrast to the previously mentioned region CNS1, the conserved non-coding sequence 2 (CNS2) has no function for *Foxp3* gene induction. It is located approx. 4000 bp downstream of the TSS (**Figure 6**) and contains a high degree of CpG sites – in fact, the regions just fits the definition of a CpG island. As mentioned in **Chapter 5**, it becomes demethylated upon *Foxp3* expression and has an important function to stabilize this expression in tTreg and pTreg [125]. When the region was deleted, no differences were observed in young mice. In more aged mice, Treg cell frequencies decrease, probably by peripheral conversion of tTreg cells into Tconv cells. This also happened once Treg cells from CNS2 KO mice were transferred into another host – a certain fraction of congenically labeled Treg cells lost Foxp3 expression after the transfer. Therefore, one can conclude that the CNS2 module is responsible for strengthening heritable *Foxp3* expression in dividing cells [155].
Besides epigenetic regulation, the CNS2 region also contains TF binding sites. In 2007, binding of CREB (cyclic-AMP response element binding protein) to the demethylated CNS2 regions has been described: it is thought to actively keep CNS2 in its demethylated state, thereby preventing conversion of Treg into Tconv cells [123]. Furthermore, it was identified that CNS2 has two binding sites for ETS-1 (Avian Erythroblastosiosis Virus E26 Oncogene Homolog-1). It is believed that this transcription factor is required to maintain its demethylation, just as CREB. Once the

ETS-1 TF was deleted, methylation at CNS2 increased and Treg cells showed reduced Foxp3 protein and transcript levels, finally leading to systemic autoimmune disease [156]. In summary, we can conclude that the CNS2 or TSDR has an important role to stabilize *Foxp3* gene expression. Furthermore, some factors specifically bind this region to stabilize the demethylated phenotype.

CNS3 is a pioneer element required for efficient induction of *Foxp3* transcription

The last one of the intronic regulatory regions, the conserved non-coding sequence 3, is about 7000 bp downstream of the TSS. Its specific deletion caused an approx. 5 fold decrease in thymic Treg output, indicating its importance as a pioneer element used in early *Foxp3* induction. Mice with a CNS3 knockout evade autoimmune disease by compensating for the loss of thymic Treg output by increased Treg cell proliferation. It seems that CNS3 is only important for the induction of *Foxp3*, but not its maintained expression.

Two studies identified binding partners to the CNS3. To initiate *Foxp3* gene expression, c-Rel can bind to CNS3 once triggered by CD3 and CD28 stimulation [155]. Furthermore, the CNS3 region contains a binding site of the atypical inhibitor of NFκB (iKκB): iKκB deficiency reduces Treg cell numbers, but not their stability. Finally, Treg cells from iKκB deficient mice have a reduced ability to induce *Foxp3 in-vitro*, again indicating the role of CNS3 to increase the probability of *Foxp3* gene expression [157].

Aim of this subproject

We described the to-date published regulatory elements at the *Foxp3* promoter and the conserved non-coding sequences. We were now interested to identify the complex at the *Foxp3* promoter in an unbiased manner with a new technology (inverted Chromatin IP). In this study, we used Foxp3 non-expressing EL4 T cells and isolated nuclear protein, followed by *in-vitro* binding reactions to *Foxp3* promoter fragments. Afterwards, these binding partners were identified by mass spectrometry and cloned into eukaryotic expression vectors. The proteins were then evaluated for their gene function at the *Foxp3* promoter, their expression pattern in T cells, and for their effects once overexpressed in primary T cells.

5.4 Rbpj and its function for Treg cell homeostasis

That far, we discussed the epigenetic and transcription factor-based control of Treg cells and the *Foxp3* gene in particular. Now, we are selecting only one specific transcription factor, Rbpj, to study its role for the homeostasis and function of Treg cells. First, we will summarize current literature about Rbpj and Notch signaling, followed by the specific implications of this pathway for T cell subset differentiation.

The Notch Signaling Pathway

The Notch Signaling Pathway is a highly conserved system for cell-cell communication. It was first discovered in 1914: Notch heterozygous mutants showed a pronounced "notch" in the drosophila melanogaster wing. Later research identified four different Notch receptors in mammals: Notch 1, 2, 3, and 4. They are synthesized as single-transmembrane proteins in the endoplasmatic reticulum and afterwards transported to the Golgi apparatus (see **Figure 7**). There, they undergo S1 cleavage and become heterodimeric receptors, consisting of a large extracellular domain and a small intracellular domain, to be transported to the cell surface [158]. All four receptors share the Notch extracellular domain (NECD) consisting of EGF-like and Lin-Notch repeat sequences. The Notch transmembrane and intracellular domain (NTMIC) is connected to the NECD via their heterodimerization domain, linking them non-covalently [159]. Once the Notch receptor binds its cognate ligands, single-pass transmembrane proteins of the DSL (Delta/Serrate/LAG-2) family, the heterodimeric receptor is separated via mechanotransduction (S2 cleavage): the extracellular domain is degraded, and the remaining Notch extracellular truncated domain (NEXT) remains attached to the membrane. NEXT then undergoes cleavage by ADAM metalloproteases and γ-secretases (S3 cleavage), which liberate the Notch intracellular domain (NICD). This potent transcription factor is composed of several domains, amongst which the RAM (Rbp-associated molecule domain), TAD (transactivation domain) and NLS (nuclear localization signal) domains take part in the downstream effector functions [159]. Once the NICD is liberated from the cell membrane, its nuclear localization signal mediates the import into the cell core. There, it can displace co-repressors at target genes and bind co-activators such as Rbpj (CSL/CBF-1/suppressor of hairless/Lag-1) and Mastermind. Upon establishment of the NICD-RBPJ complex, it can induce target gene transcription, for example at *Hes1*, *Hey1* and *Dtx1* gene loci [158].

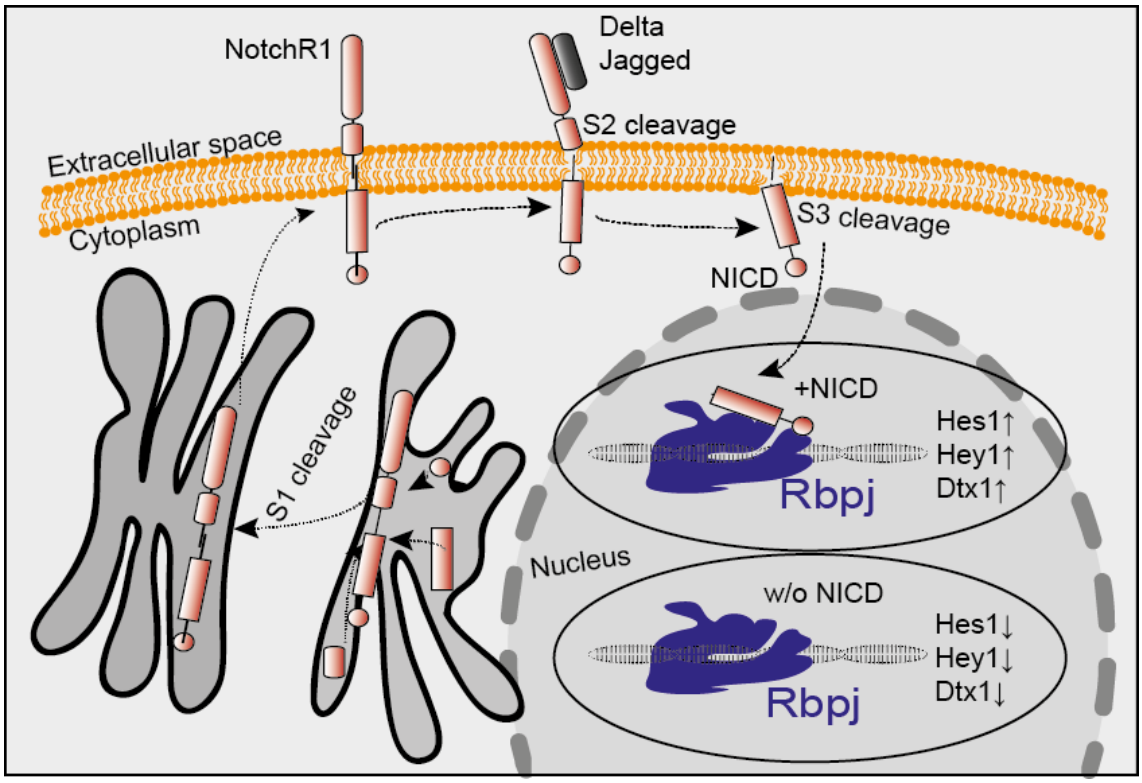

Figure 7: Simplified illustration of the Notch / Rbpj signaling pathway.
The Notch receptor is assembled in the Golgi apparatus and transported to the cell membrane. Upon ligand binding and cleavage, the NICD translocates to the nucleus and binds Rbpj to induce or repress target gene transcription. We show the NICD-Rbpj dependent effects on three target genes *Hes1*, *Hey1*, and *Dtx1*.

Notch ligands induce Notch signaling to regulate many aspects of mammalian life

In mammals, there are five canonical Notch ligands. They are type 1 transmembrane proteins of the Serrate family (Jagged 1: Jag1 and Jagged 2: Jag2) and of the Delta family (Delta-like 1: Dll1; Dll3; Dll4). They all contain DSL (Delta/Serrate/LAG-2, DOS (Delta and OSM-11-like proteins) and EGF motifs. Both DSL and DOS domains take part in Notch receptor binding. Non-canonical Notch ligands lack DSL and DOS motifs and work in a secreted form or as GPI-anchored proteins, although their physiological functions remain elusive [159]. Notch signaling is involved in the homeostasis of multiple organs and tissues, for example in neuronal development and function, angiogenesis, embryonic development, generation and expansion of hematopoietic stem cells, cardiac valve homeostasis, cell-fate decisions in mammary glands and the gut, and T-cell lineage commitment. The dysregulation of Notch pathway components has been implicated in many diseases. Mutations in the Dll3 gene can cause Spondylocostal dysostosis, a skeleton segmentation disorder, and patients

with Jag1 mutations show a diverse phenotype with bile duct paucity, cardiac defects, spine defects and deafness (Alagille syndrome). Mutations in Notch1 have been implicated in the development of T-cell acute lymphoblastic leukemia and aortic valve disease. Dysfunctions in essentially every member of the Notch pathway cause clinical pathology, highlighting the importance of this conserved mechanisms for development and homeostasis [158].

Notch signaling in hematopoietic stem cell development and cell fate decision

The hematopoietic system is generated in three waves during embryonic development: a primitive, a transient definitive, and a definitive wave.

The primitive wave consists of maturing primitive erythrocytes forming blood islands and is generated in the murine yolk sac around embryonic development day 7.5 (E7.5). It contains some macrophages, megakaryocytes, and mast cells, but no hematopoietic stem cells (HSCs). Notch signaling is of no relevance for this wave, since Notch1 or Rbpj mutants display a normal number of primitive erythrocytes.

The transient definitive wave, emerging from yolk sac cells around E9, consists of erythromyeloid progenitors, neutrophils, and definitive erythrocytes. Progenitor cells can colonize the blood stream and fetal liver, but Notch signaling has, again, no importance during this second wave.

The definitive wave, initiated at E11.5, is not produced in the yolk sac, but the Aorta-Gonad-Mesenephros (AGM), an embryonic mesodermal region. It contains HSCs, which then migrate to the fetal liver and later colonize the bone marrow niche. Notch1, Rbpj or Dll4 mutants cannot establish the arterial program and therefore cannot produce HSCs. This indicates that Notch signaling is a pre-requisite for the proper development of the blood-forming system outside the yolk sac. It is believed that Notch signaling is important not only for HSC differentiation, but also to maintain stemness of the developing HSCs in the AGM. Once HSCs leave the AGM and travel to the fetal liver, no more Notch-based signals are required for their amplification. Once they enter the BM niche and colonize it to form the blood system, Notch signaling is again implicated in cell fate decisions at this stage: high Notch dosage induces T-lymphocyte differentiation, whereas low Notch levels cause myeloid-lineage commitment [160].

Notch signaling controls thymic T-cell development

Previously, we reviewed the importance of Notch signaling for the generation of HSCs and the lymphoid/myeloid fate decision process in the bone marrow. Once the T-lymphocyte differentiation program has been initiated, the BM-derived lymphomyeloid progenitor cells enter the thymus via the corticomedullary junction. They are then denominated as early T-lineage progenitors or double-negative 1 cells and interact closely with thymus-resident TECs. Expression of Notch-ligands in adult thymic cTECs is restricted to the Dll4 ligand, the most relevant ligand for T-cell development in the thymus. Other ligands, such as Dll1, Jag1, and Jag2 are expressed in the E16 thymus, and to a certain extent also in adult thymi. When deleting Dll4, T-cell development was interrupted and B cells suddenly emerged in the thymus. Dll1 deletion had no such consequences. Interestingly, mice with modifications in Jag1 and Jag2 display normal T-cell development, but have a reduced commitment to the γδ T-cell lineage. Studies indicate that FoxN1, a pivotal transcription factor required for proper TEC differentiation, regulates Notch ligand expression in the thymus [161].

In order to receive signals via Notch ligands expressed on thymic epithelial cells, thymocytes need to express Notch receptors. Indeed, expression of Notch receptor 1, 2, and 3 on developing thymocytes has been identified. Notch 1 and 2 are highly expressed in DN 1 and 2 thymocytes and steadily decrease after the DN4 stage during further maturation. In contrast to this, γδ T cells retain their high Notch 1 and Notch 2 expression. Notch 3 is expressed mostly at the DN3 stage.

But what does TEC-thymocyte signaling via Notch promote? First, Notch signaling strengthens the T-cell commitment of the developing thymocyte. It then progresses through the DN2 and DN3 stage, expresses the IL7R and starts to proliferate, triggered by TEC-provided local IL7. Notch signaling actually induces IL7R expression, as discussed in the following paragraph. IL7R-expressing thymocytes proliferate extensively and mature their T-cell receptor to undergo positive and negative selection by thymic APCs, as summarized in **Chapter 4**. Selected cells then exit the thymus through the cotricomedullary junction.

Therefore, we can summarize that Notch signals determine the T-cell fate in the thymus and bone marrow. Furthermore, they are required for T-cell survival, proliferation and further differentiation. Notch signaling is also involved in VDJ recombination and the β-selection checkpoint control. Finally, this pathway regulates αβ or γδ T-cell lineage commitment [160, 161].

The IL7R is induced by Notch/Rbpj and promotes T-cell expansion and survival

Following the ETP to DN2 transition, developing thymocytes undergo massive cellular expansion, which is dependent on their concomitant expression of the IL7R. This marks the first Notch-promoted checkpoint in thymic T-cell development, followed by gene rearrangement and αβ or γδ lineage decision. The IL7R is composed of the IL7Rα chain and the common γ chain receptor. When ETPs in transition to DN2 upregulate the IL7Rα chain, IL7 produced by thymic epithelium can cross-link IL7Rα and γ chain to form an actively signaling heterodimer: this promotes T-cell survival and proliferation. In the bone marrow, stroma cells also secrete IL7 and promote survival and expansion of B cells. In transgenic mice with IL7R deficiency, T-cell development is blocked at an early stage, and B-cell development is severely impaired [162]. In human patients with X-linked severe combined immunodeficiency, deficiencies in IL7R expression have been linked to severe T-cell paucity, but had no impact on B-cell or NK-cell development [163]. Typical target genes of IL7R signaling are Bcl-2 family members, cycline D1, SOCS, and c-myc. Therefore, the constitutive expression of Bcl-2 in IL7R or IL7 KO mice can rescue T-cell development, indicating that this pathway is important to promote survival. Once DN2 thymocytes use IL7R stimulation to expand and proceed to DN3 stage, no more IL7R signaling is required at this point. Therefore, IL7Rα expression is downregulated thereafter and completely terminated between β-selection and positive selection. Once positive selection is complete, IL7R expression is restored to provide the homeostatic proliferation potential of peripheral mature T cells.

But what induces IL7Rα expression in ETPs? Interestingly, the expression profile of Notch1 in early thymopoiesis closely mimics the IL7Ra expression profile. A 2009 study investigated this link carefully: in a loss-of-function experiment, the authors inhibited Notch signaling by the ectopic expression of a dominant negative form of mastermind-like 1 (dnMAML1), normally a co-activator of Notch signaling. Inhibiting Notch signaling resulted in impaired IL7Rα expression. In contrast to this, NICD-transduced T-cell progenitors upregulated IL7Rα expression, indicating that Notch1 is indeed involved in the regulation of the IL7R expression pathway. When transducing an IL7Rα promoter luciferase vector into cell lines, it was shown that co-transfection of NICD significantly increases luciferase activity, which was abrogated by co-transfection of dnMAML1. Since the NICD can promote target gene expression via Rbpj, and the IL7Ra gene has a putative Rbpj binding site in its promoter (consensus sequence *CTTGGGAA*, -936 bp upstream of TSS), it was proposed that Notch1

regulates IL7R gene expression via Rbpj. In fact, IL7R promoter luciferase studies in RBPJ-deficient or heterozygous cultures showed that Rbpj is required for Notch1-mediated IL7R induction. Site-directed mutagenesis of the putative binding site impaired IL7R expression upon ectopic NICD expression. Furthermore, Chromatin-IP studies indicated that Notch1 indeed binds the Rbpj binding site at the IL7R promoter. In conclusion, the above-mentioned study clearly states that Notch 1 in combination with Rbpj induces IL7Rα expression in T cells [160, 164].

Peripheral T cells express Notch receptors upon activation

T cells upregulate Notch1 receptor 4 hours after TCR-stimulation, and express it until 48 hours post activation. Also, Notch2 is upregulated upon anti-CD3 stimulation in T cells, but expression levels peak at 24 hours and already returns to basal expression 48 hours post TCR engagement. Interestingly, Notch receptors co-localize with CD4 upon T-cell activation. T cells binding Notch ligands become activated even without additional TCR stimulation, with Dll4-based activation reminiscent of anti-CD3 stimulation, and Dll1 and Jag1 less potent to promote T-cell activation. Ongoing Notch signaling in activated T cells is then involved in the regulation of IFN-γ and IL-2 production as well as IL2Rα (CD25) expression. Activated T cells can bind Notch ligands, which in turn determines their differentiation potential (in combination with other factors such as antigen presentation and cytokine milieu): Dll family members drive T_H1 responses, and Jagged ligands promote differentiation into T_H2 lineage. Notch signaling is also implicated in T_H17 and Treg lineage maturation[165]. We will discuss the Notch-driven T_H subset differentiation program in the following paragraphs.

Dll ligands can induce T_H1 differentiation of peripheral T cells

First insights into T_H differentiation bias by Notch signaling were based on co-transfection studies. When T-cells were transfected with Notch3-ICD (N3ICD), they secreted more IFN-γ and less IL-4, reminiscent of a T_H1 phenotype. Furthermore, they expressed Tbx21/Tbet, the master TF of T_H1 cells. Transfection of Notch1-ICD also resulted in increased IFN-γ secretion and upregulation of Tbx21/Tbet. Treatment with γ-secretase inhibitors (GSI) reduced T_H1 polarization *in-vitro*, indicating that Notch signaling is important to drive T_H subset differentiation. In contrast to this, *in-vitro* genetic loss-of-function studies with Rbpj or Notch1/2 deficient T cells showed no

skewing of T_H subset generation. To fully address this question, *in-vivo* studies with Notch1, Notch2, or Notch1/2 double-knockout T cells were conducted. Single knockouts of Notch 1 or 2 had no effect, pointing to a redundant role of both receptors in this system. But a double Notch 1/2 knockout had decreased numbers of IFN-γ secreting T_H1 cells, leading to the inability to clear an experimental bacterial infection [166]. A 2004 study by Tanigaki and co-workers addressed the need of Notch signaling for T-cell subset development with a conditional T-cell Rbpj-deficient mouse. Once they crossed their Rbpj-floxed mouse with Lck ^{Cre} (expressed early in thymic development), the block in Notch signaling caused enhanced γδ T-cell production, while αβ T-cell differentiation arrested at the DN3 stage. These data are in accordance with the notion that DN3 cells require Notch signaling to pass the β-selection checkpoint in thymic T cell development. The same paper also crossed CD4 ^{Cre} mice with Rbpj floxed animals. Interestingly, these mice had normal numbers of $CD4^{pos}$ and $CD8^{pos}$ T cells in the periphery. In general, a reduced proliferation capacity of peripheral CD4 ^{pos} T cells in the presence of APCs was noted, but no (auto)immune pathology evolved from this. Upon analysis of the T-cell differentiation potential, a bias towards T_H1 specialization *in-vitro* and *in-vivo* was observed. Furthermore, peripheral blood serum contained decreased IgG1 and IgE immunoglobulin levels, also indicating a T_H1 response. Finally, expression levels of GATA-3, an inhibitor of T_H1 differentiation, were reduced by 50% in Rbpj-deficient T cells, paving the road towards a T_H1 bias [167]. Another 2014 study investigated the effects of Rbpj deletion in $CD4^{pos}$ T cells upon challenge with experimental autoimmune uveoretinitis (EAU). Rbpj deficiency in T cells decreased EAU disease severity due to decreased IL-22 secretion. GSI-treatment had beneficial effects on EAU clinical scores, indicating that Notch pathway components also regulate IL-22 signaling [168].

Jagged ligands promote T_H2 subset differentiation

In contrast to T_H1 promoting Dll ligands, Jagged ligands expressed on APCs predominantly induce a T_H2 phenotype in T cells. Immature dendritic cells express Jagged 1, which in turn induces GATA-3 and IL-4 expression in T cells, key markers for a T_H2 phenotype. When these immature DCs undergo TLR ligation, Jagged-1 expression is reduced and Dll4 expression is upregulated, switching the T-cell response to a T_H1 bias. *In-vitro* co-cultivation experiments with Jagged-ligand expressing DCs induce IL-4 and

IL-5 secretion, what can be inhibited by GSI treatment, again indicating that Notch signals drive this phenotype. *In-vivo* studies with Jagged1-Fc fusion proteins showed that these ligands drive T_H2 immune responses in animal models of EAE and lung asthma. A Notch pathway interruption via T-cell specific Rbpj deletion interrupted T_H2 differentiation upon SEA or antigen immunization in mice. Furthermore, Notch1 or Notch2 deficiency in T cells impaired their IL-4 secretion and T_H2 differentiation *in-vivo*. In addition to this, dominant expression of the Notch inhibitor dnMAML1 or treatment with GSI prevented T_H2 induction in response to infection. Again, *in-vitro* studies did not substantiate that Notch1 or Notch2 are required for T_H2 differentiation, similar to *in-vitro* studies for T_H1 bias. To explain the T_H2-inducing role of Notch signaling on a molecular basis, inverted Chromatin IP studies have been performed with Rbpj and Notch1 antibodies. These studies revealed that both Rbpj and Notch1 bind the *IL4* promoter, and Rbpj consensus binding sequences have been detected at the 3' enhancer of *IL4*. No IL-4 response was possible once Rbpj was deleted in T cells. Luciferase studies indicate that the *IL-4* promoter responds to Notch signals via *IL-4* resident Rbpj [169, 170]. Furthermore, Notch1 has been reported to bind the *GATA-3* promoter together with Rbpj, regulating its transcription [166].

Dll4 ligand drives T_H17 subset differentiation

The overexpression of Dll4 ligands on dendritic cells has been shown to increase IL-17 secretion by T cells, whereas Dll4 neutralization reverted this effect. *In-vivo* studies with an anti-Dll4 mAb followed by challenge with mycobacteria infection lead to increased granulomas and a decreased IL-17 secretion by T cells. Furthermore, treatment of EAE-induced mice with GSI reduced IL-17 secretion levels, and also affected the T_H1/T_H2 balance, as described previously. A deletion of Notch had no consequences in terms of T_H17 differentiation, but influenced IL-17 cytokine secretion levels – therefore, it is hypothesized that Rbpj can bind the *Il17* promoter and regulate cytokine expression in concert with Notch signals [166]. The precise role of Notch signals for the development of Treg cells will be reviewed in the discussion part of this thesis and linked to data generated with our experiments presented in the following chapters.

Aim of this subproject

Until now, we summarized the role of Notch signaling for the generation of T cells and for their differentiation into T-cell subpopulations. It was now our aim to study another aspect of the Notch signaling axis: Rbpj and its Notch-independent functions. We observed that Rbpj is upregulated in bona fide Treg cells from many tissues (**Figure 30**), while studies with our Notch^{GFP} reporter mouse clearly indicated that Treg cells under steady-state conditions do not signal via the Notch axis (**Figure 31**). What is the function or Rbpj in this context? Is there a Treg-specific, Notch-independent role of this protein? When we deleted Rbpj in Treg cells, mice develop severe lymphoproliferative disease despite strongly increased numbers of Treg cells. Is there a function of Rbpj to control Treg cell homeostasis? Or does it mediate the potential to suppress a specific T_H1, T_H2, or other T-cell subpopulation, or even all of them? These questions will be addressed in the following thesis.

6 Materials and Methods

6.1 Epigenetic control of the *Foxp3* gene in Treg cells

Mice

Animals were housed under specific pathogen-free conditions at the DKFZ, and the governmental committee for animal experimentation approved all experiments. We used either wild type B/6 mice, Foxp3GFP, DTR, CD90.1 B/6 mice 171 or Dntm1chip mice 172. Dntm1chip mice were housed at the university clinics Münster, and splenocyte preparations were transported to our laboratories for experimental testing. Because the *Foxp3* gene is located on the X chromosome, we only used male animals for methylation analyses. More detailed information about mouse strains is provided in the appendix section.

Cell isolation and cell sorting

Lymphoid tissues such as spleen and lymph nodes were isolated and single-cell suspensions established. Red blood cells were lysed with ammonium-chloride potassium bicarbonate (ACK) lysis buffer. Cells were pre-enriched for CD4, CD8 or CD25 via staining with the respective biotinylated antibodies followed by anti-biotin microbead (Miltenyi Biotec) labeling and magnetic separation in an automated carrier (AutoMACS, Miltenyi Biotec). Upon enrichment, cells were stained with fluorescent antibodies and incubated for at least 20 minutes at 4°C. Cell subpopulations were then sorted on an FACS ARIA II or III cell sorters (BD Biosciences). For analysis, cell populations were acquired on LSR II, LSR Fortessa or Canto II flow cytometers. For intracellular staining, cells were first stained with surface antibodies followed by fixation / permeabilization (Foxp3 Fix/perm buffer set, eBiosciences) and intracellular staining. Antibodies used in these experiments are listed in the appendix section (10.1 List of antibodies used for flow cytometry and FACS).

Isolation of RNA and reverse transcription followed by qPCR

Sorted cell populations were lysed and RNA was isolated using the RNeasy Mini Kit (Quiagen). Synthesis of cDNA was performed with SuperScript Reverse Transcriptase

II and oligo(dT) primers (both Life Technologies) according to manufacturer's instructions. Real-time PCR was performed using a ViiA7 instrument (Life Technologies) and Power SYBR green master mix or Taqman master mix (both Applied Biosystems). Gene expression values were normalized to housekeeping genes (Hprt or Gapdh). Both SYBR primer sequences and Taqman order numbers are listed in the appendix section.

Purification and bisulfite conversion of genomic DNA

Sorted cell populations were resuspended in PBS and genomic DNA was purified according to manufacturers guidelines using the DNEasy Blood and Tissue kit (Quiagen). DNA purity and concentration was measured with a NanoDrop® photometer. DNA concentration was adjusted to 2000 ng DNA, if applicable. Bisulfite-conversion was performed using the EpiTect Bisulfite Conversion Kit (Quiagen) and converted DNA (BS-DNA) was used immediately after purification or stored at -20°C.

Computation and testing of BS-DNA primers

Foxp3 genomic DNA was *in-silico* bisulfite-converted using the Bisulfite Primer Seeker software (http://www.zymoresearch.com/tools/bisulfite-primer-seeker). Primer sequences were calculated based on manufacturers recommendations. Primer pairs were tested on BS-converted genomic DNA to determine optimal annealing temperature range and cycle number for each specific reaction. Once parameters were optimized, adaptor sequences for 454 sequencing and barcodes to distinguish individual reactions were attached to each primer pair sequence and re-synthesized. Based on optimal annealing temperature and PCR cycle number, primers were used to generate PCR amplicons from bisulfite-converted DNA for each cell type tested. An overview of primers used for our sequencing experiments is listed in the appendix (10.3 List of bisuflite primers used for 454 pyrosequencing).

BS-DNA PCR and 454 pyrosequencing

The complete workflow for the epigenetic analysis of selected regions is illustrated in **Figure 8**. Once genomic DNA had been bisulfite-converted, PCR reactions with BS-specific primers were performed. PCR amplicons were separated from primer dimers on

1%-2% agarose gels and visualized using ethidium bromide. Specific bands were excised under UV light exposure and DNA amplicons were purified using a Quick Gel Extraction Kit (Life Technologies). Equimolar amounts of amplicons were combined and processed on a GS Junior Sequencer (Roche). Sequence reads were aligned to the BS-converted mouse genome and methylation levels were visualized in heat maps.

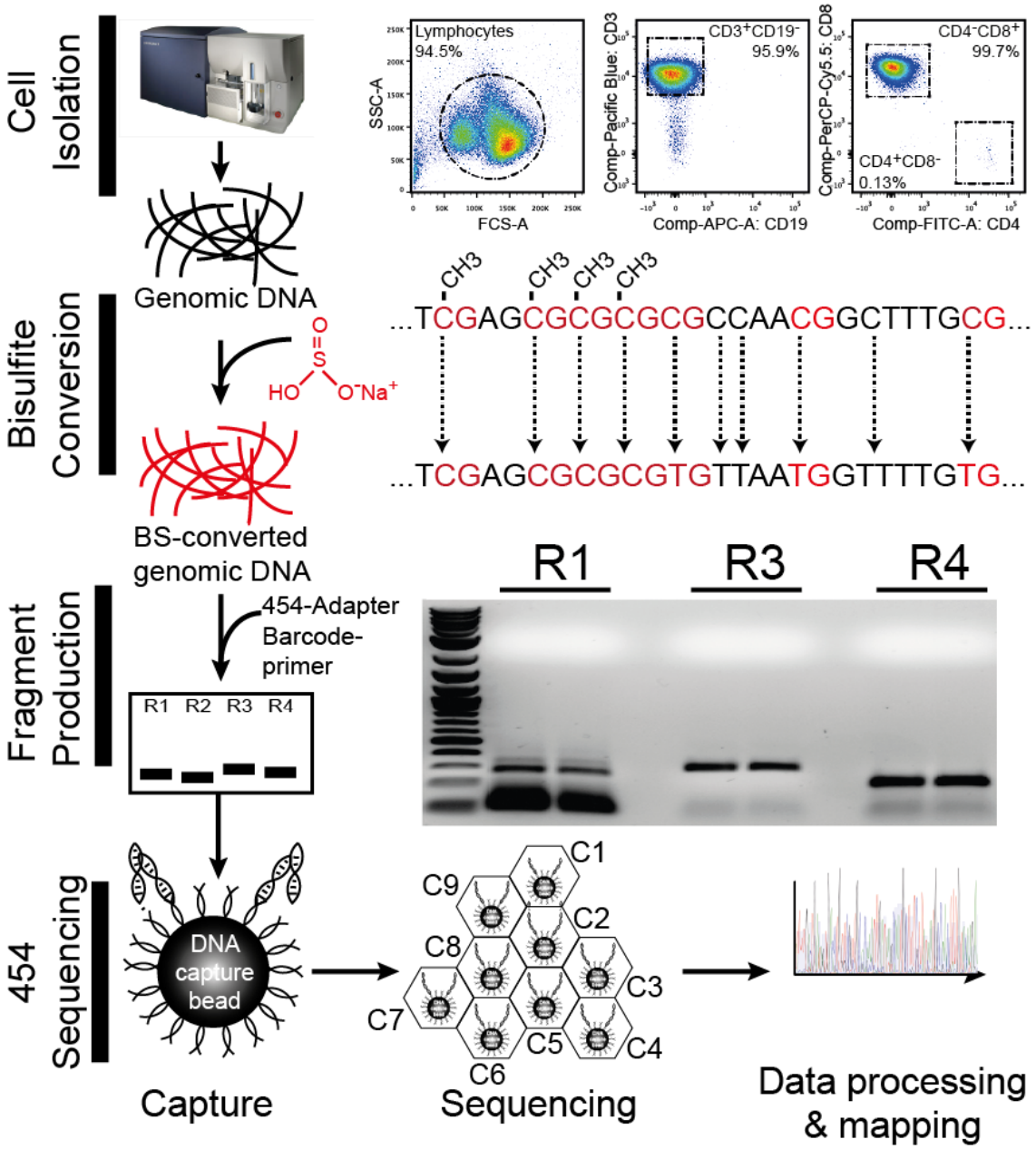

Figure 8: Workflow for the epigenetic analysis of selected CG-rich regions in cells. First, primary cells are isolated using FACS and genomic DNA (gDNA) is extracted. Then, gDNA is converted via the sodium bisulfite reaction, where methylated CG dinculeotides are protected and unmethylated cysteine residues are converted into thymidine. Once conversion is complete, a PCR reaction with bisulfite-DNA specific primers containing barcodes and adapter sequences is performed. PCR amplicons are extracted and purified for 454 pyrosequencing. Data are mapped against the *in-silico* bisulfite-converted mouse genome and CG methylation status is calculated.

6.2 Transcriptional and epigenetic control of tissue-specific Treg cells

Mice

Animals were housed under specific pathogen-free conditions at the DKFZ, and the governmental committee for animal experimentation approved all animal experiments. In these experiments, we used wild type B/6 mice or Foxp3 $^{GFP, DTR, CD90.1}$, Foxp3$^{GFP, DTR, CD45.1}$ B/6 mice or Foxp3$^{YFP, Cre}$ B/6 mice. All animals were male.

Isolation of T cells from various tissues

We isolated T cells from gonadal fat, skin, liver, and inguinal lymph nodes. For lymph nodes, single-cell suspensions were established and red blood cells were lysed. Cells were stained with antibodies for FACS-based purification. Gonadal fat tissue was mechanically dissected following a digestion with buffers containing collagenase II (1 mg/mL), BSA (20 mg/mL) and DNAse (20 µg / mL). Skin tissue was digested using a buffer containing collagenase IV (4 mg/mL), FCS (2% vol/vol), and DNAse (10 µg / mL). Liver tissue cells were isolated with a collagenase II (1 mg/mL), BSA (5 mg/mL), and DNAse (20 µg/mL) containing digestion buffer followed by a Ficoll/hypaque gradient centrifugation step. Digestions were performed at 37°C in a slow-shaking water bath for 30 minutes to 45 minutes. Afterwards, cells were filtered and stained for FACS-based isolation of target cells. Antibodies and reagent suppliers are listed in the appendix section.

Fluorescence-activated cell sorting and gDNA / RNA isolation

Stained cells were pre-sorted with moderate purity settings on an ARIA II or III cell-sorting machine (4-way sort, “enrich mode”) into FACS buffer. Then, cells were re-acquired and sorted again with high purity settings (4-way sort, “4-way purity mode”) directly into lysis buffer. Aliquots were sorted into FACS buffer for post-sort purity controls. Genomic DNA was isolated using a gDNA Microprep Kit (Zymo Research) and concentrations were measured with a Qubit® fluorometer. Average DNA concentration was 39.5 ng per sample. RNA was isolated with the RNEasy mini kit (Quiagen) and concentration was determined with a 2100 Bioanalyzer instrument

(Agilent technologies). The average RNA integrity number was 8.5, and the average RNA concentration per sample was 3.1 ng.

Tagmentation-based whole genome bisulfite sequencing (TWGBS)

We used a protocol adapted from [173], based on the original tagmentation protocol described in [119] with top oligo 1 Tn5mC-Apt1 (TcGTcGGcAGcGTcAGATGTGTATAAGAGAcAG), top oligo 2 Tn5mC-Apt2 (GTcTcGTGGGcTcGGAGATGTGTATAAGAGAcAG), and complementary oligo Tn5mErev (5'-[phos] CTGTCTCTTATACACATCT-3'). Next, oligonucleotides were pre-annealed in a final volume of 40µL and 50µM concentration with a PCR (95°C 3min, 70°C 3 min, 70°C – 26°C 30sec, 45 cycles). Load adapters were then diluted to 10 µM in glycerol-H_2O. Transposome assembly was performed with 12 µL of load adapters and 10 µL Ez-Tn5 transposase (Epicentre EZI011RK) for 30 minutes at RT. Then, 10 ng of genomic DNA were combined with Tris-MgAc-DMF buffer and 5pg unmethylated λ DNA, followed by heat treatment (55°C for 8 min). After that, DNA was purified with AmPure bead system (Agilent technologies) followed by gap repair with Bst DNA polymerase (NEB M0275S) and 5mC-dNTP mix (Zymo D1030) for 20 min at 65°C. After gap repair, samples were again purified with the AmPure bead system. Samples were bisulfite-converted with the EZ DNA methylation kit (Zymo D5001) according to manufacturer's instructions. Following complete conversion, PCRs were performed to attach barcodes and adapters for high throughput sequencing with bisulfite-converted DNA, Kapa 2G Robust HotStart ReadyMix (Kapa Biosystems KK5515), SYBRGreen® reagent (Life Technologies), a Tn5mCP1 primer (AATGATACGGCGACCACCGAGATCTACACTCGTCGGCAGCGTC) and barcoded Tn5mC reverse primer (CAAGCAGAAGACGGCATACGAGAT (-BARCODE-) GTCTCGTGGGCTCGG) with barcodes eitherGACTGATA , AGGCAGAA, GCTACGCT, CGAGGCTG to assemble four libraries. PCR was stopped at six or more fluorescence units, followed by purification of PCR products with the AmPure bead system. Sample DNA concentration and size distribution was measured, where DNA concentrations and molarity were similar between different replicates of one cell type and different cell types and size distributions were homogenously between 270bp and 700bp, with a peak at 350bp-380bp. We prepared equimolar library pools of 10nM concentration and 30µL volume for sequencing. Sequencing was performed with Illumina HiSeq 2000 v3 Paired End 100bp runs according to manufacturer's recommendations for bisulfite sequencing.

RNA-Sequencing

cDNA was generated and amplified using 0.8 ng of total RNA and SMARTer Ultra Low Input RNA for Illumina Sequencing - HV (Clontech Laboratories, Inc.) according to the manufacturer's protocol. Then, sequencing libraries were prepared using the NEBNEXT ChIP-Seq Library Prep Master Mix Set for Illumina (New England Biolabs E6240) according to the manufacturer's instructions with the following modifications: The adapter-ligated double-stranded cDNA (10µl) was amplified using NEBNext Multiplex Oligos for Illumina (New England Biolabs E7335 and E7500, 25 µM primers), NEBNext High-Fidelity 2x PCR Master Mix (New England Biolabs M0541) and 15 cycles of PCR. The final libraries were validated using Agilent 2100 Bioanalyzer (Agilent Technologies) and Qubit flourometer (Invitrogen), normalized and pooled in equimolar ratios. 50bp single-read sequencing was performed on the Illumina HiSeq 2000 v4 according to the manufacturer's protocol.

Mapping of whole-genome bisulfite sequencing data

The TWGBS data were processed as described in [119]: The hg19 reference genome (37d5) was transformed *in silico* for both the top strand (C to T) and bottom strand (G to A) using MethylCtools [174]. Before alignment, adaptor sequences were trimmed using SeqPrep (https://github.com/jstjohn/SeqPrep). The first read in each read pair was then C-to-T converted and the 2nd read in the pair was G-to-A converted. The converted reads were aligned to a combined reference of the transformed top (C to T) and bottom (G to A) strands using BWA (bwa-0.6.2-tpx) with default parameters, yet, disabling the quality threshold for read trimming (-q) of 20 and the Smith-Waterman for the unmapped mate (-s). After alignment, reads were converted back to the original states, and reads mapped to the antisense strand of the respective reference were removed. Duplicate reads were removed, and the complexity determined using Picard MarkDuplicates (http://picard.sourceforge.net/). Reads with alignment scores less than 1 were filtered before subsequent analysis. Total genome coverage was calculated using the total number of bases aligned from uniquely mapped reads over the total number of mappable bases in the genome.

Methylation calling

At each cytosine position, reads that maintain the cytosine status were considered methylated, and the reads that have cytosine converted to thymine were considered unmethylated. Only bases with Phred-scaled quality score of ≥20 were considered. In addition, the 5 bp at the two ends of the reads were excluded from methylation calling according to M-bias plot quality control. For TWGBS libraries, the first 9 bp of the second read and the last 9 bp before the adaptor of the first read were excluded from methylation calling.

6.3 Transcription-factor based control of the *Foxp3* gene

Mice / cell lines

Animals were housed under specific pathogen-free conditions at the DKFZ, and the governmental committee for animal experimentation approved all animal experiments. In these experiments, we used wild type B/6 mice or Foxp3 $^{GFP, DTR, CD45.1}$ B/6 mice [171]. For cell lines, we used a human embryonic kidney cell line (ATCC® CRL-1573™), a murine EL4 T-cell line (ATCC® TIB-39™), and a human Jurkat JE6.1 T-cell line (ATCC® TIB-152™). Cells were incubated at standard TC conditions (37°C, 5% CO2) in complete medium and were regularly tested for mycoplasma infection and contamination with other cell types.

Isolation of nuclear protein

Nuclear protein was isolated from EL4 T cells with the NXtract isolation kit (Sigma), and protein concentration was measured using a BCA kit (Thermo). Upon isolation of nuclear protein, a selective enrichment of nuclear protein of 5.5 fold compared to the cytosolic fraction was achieved (data not shown). Furthermore, we observed a good enrichment for nucleus-associated proteins based on gene ontology of detected peptides (**Figure 9**C). About 40 mg of nuclear protein were used for each replicate.

Preparation of *Foxp3* Fra1, Fra2, and Fra3 probes

Short *Foxp3*-promoter fragments were produced from a Full *Foxp3* promoter vector with a biotinylated forward primer and standard reverse primers. PCR conditions for the production of biotinylated PCR primers were optimized to reduce a contamination with unbound biotinylated PCR primers (see **Figure 9**). PCR products were purified using a quick PCR purification kit (Life Technologies). To measure successful biotinylation of the probe, the PCR product and its individual primers were plotted onto a PVDF membrane and UV cross-linked. Biotinylation was detected with an anti-biotin HRP and chromogenic detection substrate in a Western-Blot visualization unit.

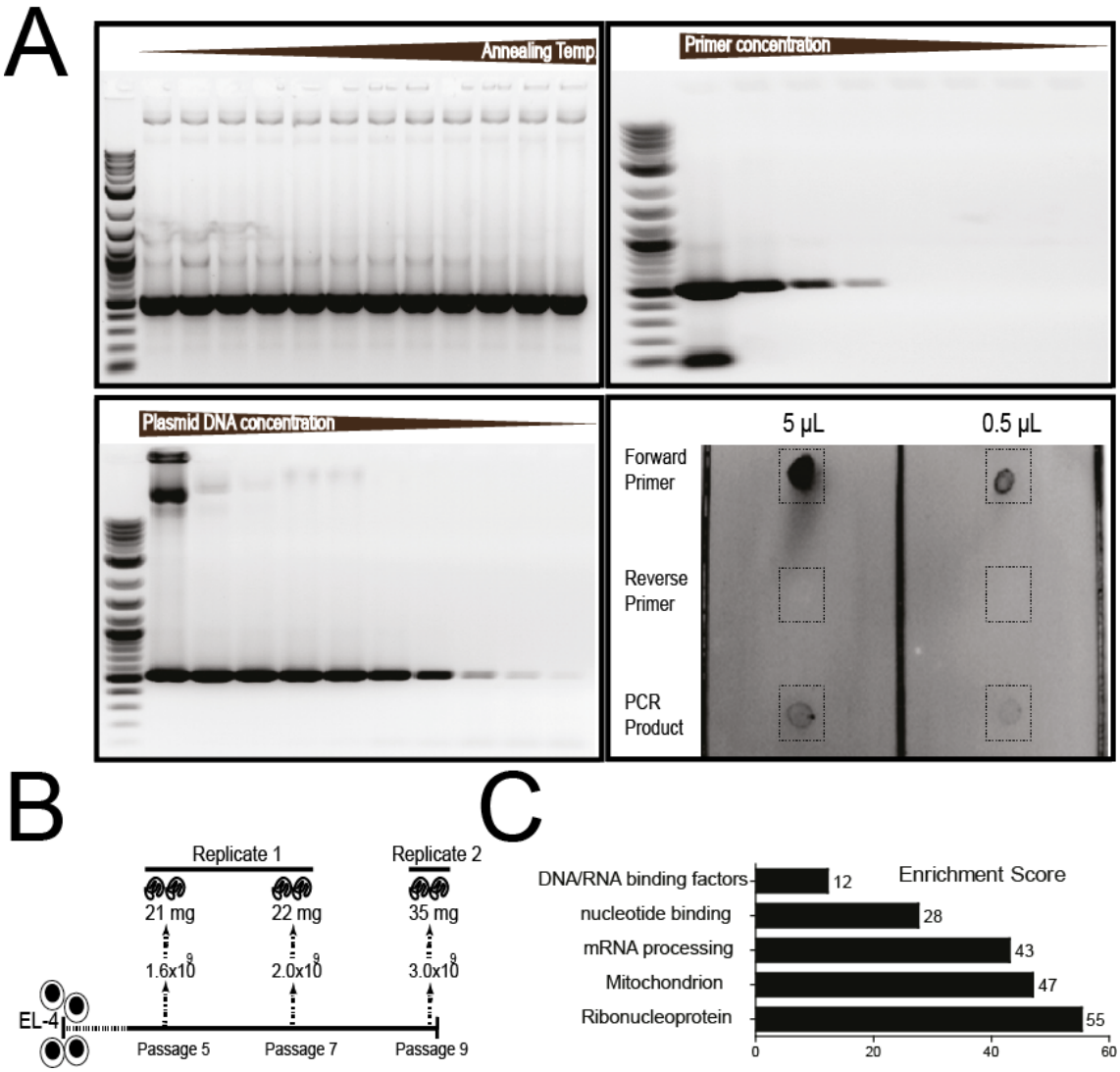

Figure 9: Preparation of probes and nuclear protein for the inverted ChIP.
We determined optimal annealing temperature and concentration of template plasmid DNA and primers for the generation of 500 bp oligonucleotide probes (A). We used the same parameters for the generation of all three probes (*Foxp3*-**Fra1**, *Foxp3*-**Fra2**, *Foxp3*-**Fra3**). The membrane in the lower right quadrant shows the selective biotinylation of the forward primer as well as the biotinylation of the final PCR product. In B, we show the purification of several milligrams of nuclear protein from the EL4 T cell line, which is highly enriched for DNA binding factors and RNA processing factors as well as RNA-Protein complexes, as shown in C.

Inverted Chromatin IP

The inverted Chromatin IP procedure is visualized in **Figure 10**. First, carefully washed streptavidin beads were linked individually to *Foxp3*-Fra1 probes, *Foxp3*-Fra 2 probes, or *Foxp3*-Fra 3 probes for 3 hours at RT. Then, free bead binding sites were blocked and beads were washed again. Nuclear protein was pre-incubated with unlabeled beads to remove non-specific bead-binding proteins. The cleared nuclear protein was then added to each probe-labeled bead and incubated on a rotating wheel for 3 hours at 4°C.

After incubation, beads were washed to remove unbound protein and bead-bound sequence-specific proteins were eluted. Protein was trypsin-digested and peptides were labeled with stable isotopes by dimethylation of N-termini and lysines. Samples were then combined and reduced by isoelectric focusing. Finally, samples were subjected to nanoLN-MS/MS analysis, which allows the quantitative detection of peptides that were originally bound to specific probe-labeled beads.

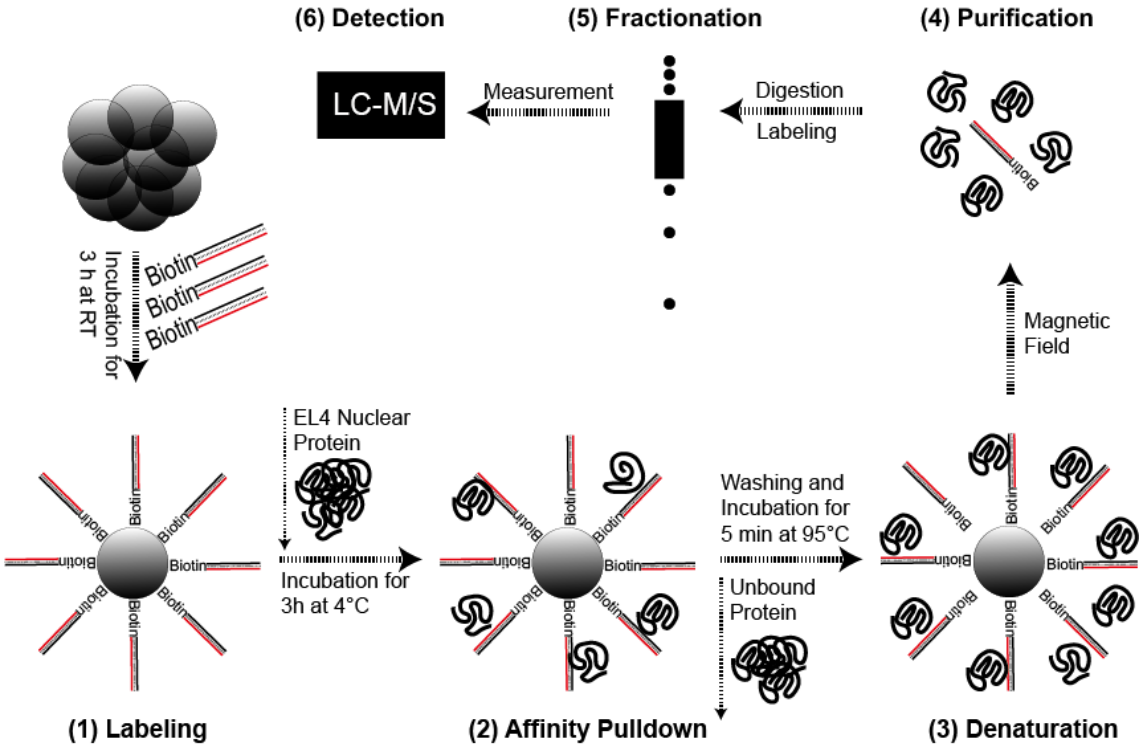

Figure 10: Overview of inverted ChIP procedure.

First, beads are labeled with the respective biotinylated oligonucleotide probes. Then, nuclear protein from murine EL4 T cells is added for a three-hour *in-vitro* binding reaction. Next, beads are purified via magnetic enrichment and unbound protein is washed off. Finally, protein is released from the beads, purified and fractionated for mass spectrometry-based analysis.

Real-time PCR to check expression levels of candidate proteins

First, we synthesized and tested Sybr primers for both mouse and human candidate proteins with the aid of a public database (http://pga.mgh.harvard.edu/primerbank/). Primer efficiency and melting curve characteristics were analyzed, with efficiencies between 80% and 120% and single melting curves as criteria. We then isolated RNA from cell lines, FACS-sorted primary Treg and Tconv cells or plasmid-transfected 293 cells with the RNeasy mini kit. RNA was concentration-adjusted and reversely transcribed using Reverse Transcriptase II and oligo(dT) primers (Life Technologies)

according to manufacturers standards. Real-time PCR was performed with Sybr Master Mix (Applied Biosystems) and Sybr primers. Sybr primer sequences are listed in the appendix.

Cloning of candidate genes and evaluation of proper expression for downstream reporter assays

First, we generated PCR products containing intron-free coding DNA for each candidate protein, either from mouse splenic cDNA or commercially available vector clones. PCR products were ligated into pENTR/D-TOPO ® vectors (Life Technologies) and sequenced for proper gene orientation and exclusion of mutations. Once complete, pENTR® vectors were used to shuttle coding DNA into destination vectors such as pDEST26® for eukaryotic overexpression and pMSCV-CD90.1 ® for viral transduction of T cells with LR clonase II enzyme (Life Technologies). Again, vectors were sequence-verified to exclude mutations. To exclude vector mix-ups and demonstrate eukaryotic expression, we transfected HEK 293 cells with each pDEST® eukaryotic production vector and isolated RNA 48hrs post transfection followed by reverse transcription and Real-time PCR. To check for protein expression, we re-shuttled some pENTR®-based genes into FLAG ®-tagged pDEST® eukaryotic production vectors and performed Western-Blot based detection of FLAG ®-tagged protein with an anti-FLAG® antibody. Size and band intensity was used to identify the transgene of interest. Finally, we validated vector DNA integrity on agarose gels to ensure vector stability and concentration for downstream analyses.

Molecular cloning of short *Foxp3* promoter luciferase vectors

We used a full *Foxp3* promoter luciferase vector as a template to create short *Foxp3* promoter Fragment 1, Fragment 2 and Fragment 3 PCR products with gene-specific primers including restriction-enzyme binding sites: *Foxp3* Fra 1 (ForP with *Xho*I CTAGCTCGAGACTGCTAGAGGGGGATCAGC and RevP with *Sbf*1 GATCCCTGCAGGGCAGGCTTCAGATCCCTTCT), *Foxp3* Fra 2 (ForP with *Xho*I CTAGCTCGAGCTGCCATGTGAATGGGAAG and RevP with *Sbf*1 GATCCCTGCAGGCCTGGGCCGCTATGTGTAT) and *Foxp3* Fra 3 (ForP with *Xho*I CTAGCTCGAGCCAGGGTCCTAGTCCTGTCA and RevP with *Sbf*1 GATCCCTGCAGGGTTGGCTTCAGGAAAACTGG). The Full *Foxp3* promoter vector was

then digested with *Xho*I and *Sbf*1 restriction enzymes to remove the *Foxp3* promoter sequence, size-separated and isolated from an agarose gel, and treated with phosphatase to prevent re-ligation. Next, the individual small fragments 1,2, or 3 were ligated into the empty vector. The *Foxp3* Fra1, Fra2, and Fra3-pGL3 vectors were sequenced to confirm proper orientation of the small *Foxp3* fragments into the luciferase reporter vector pGL3.

Luciferase-based reporter assays in HEK 293 cells

First, we optimized the dual luciferase reporter system for cell seeding numbers, incubation time, linearity of the luciferase system, and transfection efficiencies. In our optimized protocol, we seeded 50,000 HEK 293 cells into a 96-well flat bottom plate on day 1. After overnight cell attachment, we added 125 ng each of three vectors: first, the β-galactosidase (β-gal) transfection normalization vector; second, a luciferase reporter vector, either the Full, Fra1, Fra2, or Fra3 *Foxp3* promoter vector; third, we added the transgene of interested in an eukaryotic production vector. A total of 375 ng of plasmid DNA were transfected into each well. For transfection, we used the Lipofectamine® transfection system (Life Technologies) according to manufacturer's recommendation. In short, the DNA-water mix containing all three vectors was mixed with a Lipofectamine®-medium suspension and incubated for 5 minutes at RT for liposome formation. Then, the liposomal mix was added to the cell culture and incubated for 24 hours. 50% of medium was exchanged followed by an additional 24 hours of incubation. 48 hours after transfection, cell culture medium was aspirated and cells were lysed with respective lysis buffer from a Dual Light luciferase kit (Thermo Fisher). 75 µL of supernatant were transferred to a black 96-well plate and 12.5 µL of buffer A was added. We then automatically injected 50 µL of Buffer B plus X-GAL substrate and measured luciferase signals for the pGL3 luciferase vector on a luminometer (Berthold). After sixty minutes, another 50 µL of Accelerator-II solution were injected and the b-galactosidase signal was measured.

Normalization of luciferase values

To check for transfection efficiency differences, we averaged β-gal light intensity values across all transfected wells of a 96-well plate. We then divided the β-gal readings of each individual well by the average β-gal intensity to determine a relative

transfection efficiency reading. The measured luciferase values were then corrected for transfection differences by normalization with the respective β-gal ratio for each individual well.

$$\textbf{Transfection efficiency A1} = \frac{\text{Individual read (β-gal) A1}}{\text{Average (β-gal) across 96w plate}}$$

$$\textbf{Normalized luciferase A1} = \frac{\text{Individual read (luciferase) A1}}{\text{Transfection efficiency A1}}$$

Calculation of specific binding

To test for unspecific binding effects to elements on the pGL3 luciferase vector other than the integrated *Foxp3* promoter, we measured all our candidate proteins against a control-pGL3 vector, which does not contain any relevant promoter sequence before the luciferase ORF. We then cross-compared the normalized luciferase values for the Full *Foxp3* promoter vector as well as Fra1, Fra2 and Fra3 *Foxp3* promoter vectors against the control pGL3 vector to determine sequence-specific up-or downregulation of gene expression. These values are depicted in graphs in **Figure 27**. To now check whether any of our candidate proteins significantly up-or downregulate *Foxp3* promoter activity, we compared normalized luciferase expression values between cells co-transfected with GFP, a non-nuclear protein without transcription factor activity, and cells co-transfected with a candidate *Foxp3*-promoter binding protein.

$$\textbf{Sequence-specific binding} = \frac{\text{Norm. luciferase value for Foxp3-luciferase vector A2}}{\text{Norm. luciferase value for control-luciferase vector A1}}$$

Significance level for protein X = T.Test (Specific binding GF P vs. Specific binding X)

Luciferase-based reporter assays in TCR-stimulated Jurkat cells

Analogously to the screenings described above, we used a three-vector system to check the effects of our candidate proteins in Jurkat T cells: The first vector was a luciferase reporter vector containing the Full *Foxp3* promoter sequence (5000 ng per test); the second vector was a eukaryotic production vector carrying the candidate gene (5000 ng per test); third, we used a Renilla-based normalization vector (500 ng per test). Before electroporation, Jurkat T cells were counted and adjusted to $2x10^6$ cells per electroporation. Cells were washed with OptiMEM medium and a mix of all three plasmids was added to each Jurkat cell preparation. Cells were transferred to electroporation cuvettes (Biorad) and electroporated with 125 V of electric current and

Mammalian 11 – Jurkat settings with a Biorad electroporation machine. Afterwards, cells were transferred into pre-warmed six-well plates with 1500 µL of complete medium. 24 hours after incubation, electroporated cells were either stimulated with PMA (100 ng/µL) and Ionomycin (1000 ng/µL) or left untreated. 20 hours after stimulation, cells were washed and resuspended in 330 µL 1X lysis buffer (Promega) and lysed for 15 minutes at RT. Lysate was transferred to black 96-well plates, with 120 µL of luciferase measurements and 30 µL for Renilla measurements. Luciferase substrate and Renilla substrate were freshly prepared (details see Appendix) and 100 µL were injected followed by 10s reading time on a luminometer (Berthold).

Calculation of specific binding for the Jurkat T cell screening

Similar to our transfection efficiency calculation for the HEK293-cell based screenings, we first averaged the Renilla transfection control values across all Renilla-transfected and non-stimulated samples. We then divided the individual Renilla read per well by the average reading to yield a measure of electroporation efficiency for each well. It should be noted that we used electroporation efficiencies of unstimulated wells to normalize PMA/Ionomycin-treated samples, since PMA specifically induces activity on the Renilla vector and thereby causes false-positive results also in the luciferase channel.

$$\textbf{Electroporation efficiency A1} = \frac{\text{Individual read (Renilla) A1}}{\text{Average (Renilla) across experiment}}$$

$$\textbf{Normalized luciferase A1} = \frac{\text{Individual read (luciferase) A1}}{\text{Electroporation efficiency A1}}$$

Next, we calculated normalized luciferase values for wells carrying the Full *Foxp3* pGL3 luciferase vector plus a selected transgene and calculated the relative induction compared to non-stimulated controls. These values were combined across four independent experiments and used to check for significant downregulators in comparison to GFP controls.

$$\textbf{Rel. Induction (protein X)} = \frac{\text{Normalized luciferase of stimulated well protein X}}{\text{Normalized luciferase of unstimulated well protein X}}$$

Significance level for protein X = T.Test (Rel. Induction GF P vs. Rel. Induction X)

Viral transduction of candidate genes into primary induced Treg cells

Retrovirus in the pMSCV-CD90.1® system can be manufactured in PhxEco cells, a pCL-Eco (packaging plasmid) carrying variant of HEK 293 cells. Therefore, PhxEco cells were seeded on a gelatin matrix at 400,000 cells per well in a six well plate 24 hours before lipofection. To produce liposomal particles containing the viral transgene, we co-incubated 3000ng of vector DNA and 1000ng of additional pCL-Eco packaging plasmid with 7.5 µL of TransIT-293 ® transfection reagent (Mirus) for 15-30 minutes at RT. Liposomes were added to PhxEco-carrying six-well plates and incubated for an additional 48 hours. In parallel, T-cells were isolated from spleen and lymph nodes via AutoMACS-based negative selection (depletion of CD8, CD19, CD25, CD11b, CD11c, CD49b positive cells) and TCR-stimulated with plate-bound CD3 and CD28 monoclonal antibodies (CD3 @ 0.1 µg/mL and CD28 @ 1.0 µg/mL) on a 96-well flat bottom plate. We also added 50 ng/mL TGF-β to T-cell cultures to induce Foxp3 expression. Two days after cell seeding, we added viral supernatant carrying pMSCV ® retrovirus with the transgenes of interest. Viral supernatant was supplemented with IL-2 (20 U/mL), TGF-β (50 ng/mL) and polybrene (4 µL/mL). T cells were spun for 90 minutes at 32°C and 2000 rpm followed by five hours of incubation at 37°C. Afterwards, viral supernatant was removed and cells were incubated with fresh medium supplemented with IL-2 and TGF-β for another 72 hours. Then, cells were harvested and surface-stained with CD4, CD90.1 and a live/dead exclusion dye, followed by fixation and intracellular staining for Foxp3 protein expression. Cells were analyzed on a Canto II flow cytometer, and transduction efficiency was tested using GFP controls and overall CD90.1 transgene expression levels.

6.4 Rbpj and its function for Treg cell homeostasis

Mice / cell lines

Animals were housed under specific pathogen-free conditions at the DKFZ, and the governmental committee for animal experimentation approved all animal experiments. In these experiments, we used wild type B/6 mice or *Foxp3*$^{GFP\text{-}DTR\text{-}CD90.1}$ or *Foxp3*$^{GFP\text{-}DTR\text{-}CD45.1}$ B/6 mice [171]. *Rbpj*^{floxed} mice [175] were crossed to *Foxp3*^{YFPCre} mice to generate Treg-specific Rbpj knockout mice (*Foxp3*^{Cre}*Rbpj*$^{\Delta/\Delta}$). *NICD*^{LSL} mice were crossed to *Foxp3*^{YFPCre} mice to generate Treg-specific NICD knock-in mice (*Foxp3*^{Cre}*NICD*^{LSL}). *Notch*^{eGFP} reporter mice were housed at the Weizmann Institute of Science and described in [176].

Isolation of Treg cells from various tissues

We isolated Treg cells from fat, skin, colon, lung, liver, and different lymph nodes as well as spleen and thymus. For lymph nodes and spleen, single-cell suspensions were established and red blood cells were lysed. Cells were stained with antibodies and purified using FACS. For thymus samples, cells were first depleted of double-positive and CD8-single positive thymocytes by staining with CD8 biotinylated mAb and anti-biotin beads followed by AutoMACS-based depletion. Gonadal fat tissue was mechanically dissected following a digestion with buffers containing collagenase II (1 mg/mL), BSA (20 mg/mL) and DNAse (20 µg / mL). Skin and colon tissue was digested using a buffer containing collagenase IV (4 mg/mL), FCS (2% vol/vol), and DNAse (10 µg / mL). Liver tissue cells were isolated with collagenase II (1 mg/mL), BSA (5 mg/mL), and DNAse (20 µg/mL) containing digestion buffer followed by a Ficoll/hypaque gradient centrifugation step. Lung tissue was digested in a buffer containing collagenase IV (2 mg/mL), BSA (0.5% w/vol), and DNAse (20 µg / mL). Digestions were performed at 37°C in a slow-shaking waterbath for 30 minutes to 45 minutes. Afterwards, cells were filtered and stained for FACS-based isolation of target cells.

Flow cytometry, FACS and cell counting (plus Annexin-V and Caspase-3)

For flow cytometric evaluation of surface proteins or cell isolation via FACS, surface staining with monoclonal antibodies was performed at 4°C for 20 minutes followed by

immediate analysis. For intracellular staining, cells were first surface-stained for 20 minutes at 4°C followed by fixation, permeabilization and intracellular staining with the Foxp3 Fix/perm buffer set (eBiosciences) according to manufacturer's instructions. Annexin-V staining and active Caspase-3 staining was performed according to manufacturer's instructions (Biolegend, Abcam). Flow cytometric analysis was performed using BD LSRII, LSR Fortessa, or BD Canto II flow cytometers with AccuCheck® counting beads (Life Technologies). Cell sorting was performed using BD FACS ARIA II or III cell sorting machines (BD Biosciences).

Isolation of RNA and reverse transcription followed by qPCR

Sorted cell populations were lysed and RNA was isolated using the RNeasy mini kit (Quiagen). cDNA synthesis was performed with SuperScript reverse transcriptase (Life Technologies) and oligo(dT) primers according to manufacturer's instructions. qPCR analysis was performed using a ViiA7 instruments (Life Technologies) and either Power SYBR green master mix (Life Technologies) or Taqman master mix (Life Technologies). Gene expression values were normalized to housekeeping genes (Hprt or Gapdh). Both SYBR primer sequences and Taqman order numbers are listed in the appendix section.

Western Blot for Rbpj

We isolated 500,000 $CD4^{pos}CD25^{pos}Foxp3^{YFP\text{-}pos}$ Treg cells and 500,000 $CD4^{pos}CD25^{neg}Foxp3^{YFPneg}$ Tconv cells from *Foxp3*^{Cre}*Rbpj*$^{\Delta/\Delta}$ and *Foxp3*^{Cre} animals. Cells were lysed in RIPA buffer with protease inhibitors and supplemented with loading buffer for SDS-PAGE. 125,000 cells were separated on a gradient acrylamide gel (Biorad). Proteins were blotted onto a PVDF membrane and blocked with 5% milk-PBST for one hour at RT, followed by incubation with primary anti-Rbpj mAb (Cell signaling, clone D10A4) overnight at a 1:3000 dilution. After washing, the membrane was stained with an anti-rabbit HRP conjugated secondary mAb at 1:10000 for one hour at RT. Membrane was washed and specific binding was detected using a chromogenic substrate and a Western Blot detection unit.

***In-vitro* Treg suppression assay**

First, we isolated CD90.1-congenically labeled CD4-positive T-responder cells and MHCII-positive antigen-presenting cells from spleen and liver of *Foxp3*$^{GFP\text{-}DTR\text{-}CD90.1}$ animals. CD90.1^{pos} T-responder cells were labeled with CFSE (final concentration 1 µM, Life Technologies) for 15 minutes at RT followed by stringent washings steps. We incubated 100,000 MHCII-positive APCs with 50,000 CFSE-labeled T-responder cells in a 96-well U-bottom plate. To stimulate T-responder cell division, we added 2µg/mL soluble CD3 mAb to each well for TCR crosslinking through APCs. Next, we isolated CD4^{pos}CD25^{pos}Foxp3^{YFPpos} Treg cells and CD4 ^{pos}CD25^{neg}Foxp3^{YFPneg} Tconv cells from sick *Foxp3*^{Cre}*Rbpj*$^{\Delta/\Delta}$ and *Foxp3* ^{Cre} mice. Treg and Tconv cells were titrated and added to each well for a 4:1, 2:1, 1:1, 1:2, 1:4, 1:8, 1:16 and 1:0 Treg or Tconv to T-responder cell ratio. Cells were incubated for 5 days at 37°C (144 hours) followed by re-staining for flow cytometric analysis and measurement on a flow cytometer. T-responder cells were identified by CD90.1 expression, whereas *Foxp3* ^{Cre}*Rbpj*$^{\Delta/\Delta}$ and *Foxp3* ^{Cre} animals express CD90.2 and MHCII^{pos} APCs express neither. Cell division was identified by active CFSE dilution of CD90.1^{pos} T-responder cells.

Epigenetic analysis of the TSDR

To analyze specific demethylation of Treg-specific demethylated region, we isolated Treg and Tconv cells from sick *Foxp3* ^{Cre}*Rbpj*$^{\Delta/\Delta}$ and *Foxp3* ^{Cre} control mice via FACS. We purified genomic DNA with the DNA Blood and Tissue Kit (Quiagen) followed by sodium-bisulfite conversion (Epitect BS conversion kit) according to manufacturer's protocol. Barcode-labeled amplicons from BS-DNA were generated with TSDR-specific BS primers (see appendix). Equimolar amounts of amplicons were combined and processed on a GS junior sequencer (Roche). Sequence reads were aligned to a BS-converted mouse genome and methylation levels were visualized in heat maps.

TCR sequencing

We isolated spleen as well as inguinal, axial, brachial, and cervical LN from sick *Foxp3*^{Cre}*Rbpj*$^{\Delta/\Delta}$ and *Foxp3*^{Cre} animals. We pre-purified Treg cells via CD25-positive selection via magnetic bead enrichment (Miltenyi Biotec) and isolated CD4^{pos}CD25^{pos}Foxp3^{pos} Treg cells from via FACS. Genomic DNA was isolated with the DNEasy Blood and Tissue Kit followed by nanodrop $^{®}$-based gDNA concentration

adjustment. 500 ng of gDNA were submitted for immunoSEQ® TCR-β Survey Sequencing (Adaptive Biotechnologies) followed by bioinformatic analysis.

Intracellular cytokine secretion assay

Whole spleen was isolated from sick *Foxp3*^{Cre}*Rbpj*$^{\Delta/\Delta}$ and *Foxp3*^{Cre} animals and red blood cells were lysed. Splenocytes were resuspended in fresh complete medium and treated with 1X PMA/Ionomycin stimulation cocktail plus transport inhibitors or just transport inhibitors (eBiosciences). Cells were incubated for eight hours at 37°C, followed by surface antibody staining for 20 minutes at 4°C. Cells were then fixed, permeabilized, and stained intracellularly with the Foxp3 Fix/perm buffer set (eBiosciences) and anti-cytokine antibodies. Cells were analyzed on a LSR II flow cytometer.

Ig subtype ELISA

Peripheral blood serum was isolated from sick *Foxp3*^{Cre}*Rbpj*$^{\Delta/\Delta}$ and *Foxp3*^{Cre} control animals via intracardial puncture. Blood was allowed to clot for 30 minutes at RT, followed by centrifugation (20,000xg for 15 minutes) and removal of blood serum. Blood serum was titrated for Ig subtypes with an ELISA against mouse IgG1, IgG2a, IgG2b, IgG3, IgE and IgM.

Autoantibody screening with RAG2 KO organ protein via Western Blot

We isolated organs of the gastro-intestinal tract (stomach, small intestine, large intestine), lymphatic system (lymph nodes), endocrine system (pancreas), brain, eye, spleen, salivary gland, liver, heart, lung, and testis from a RAG2 $^{-/-}$ animal. Protein was extracted using ProteoJet lysis buffer with protease inhibitors for 10 minutes at RT and orbital shaking (1000 rpm). Lysate was cleared for 15 minutes at 16,000xg and supernatant was measured for protein content with BCA (Pierce). 20 µg of protein were loaded onto a gradient acrylamide gel (Biorad) and separated using SDS-PAGE. Proteins were transferred onto a PVDF membrane and blocked with 5% Milk-PBS-Tween. Membranes were cut into strips and incubated individually with peripheral blood serum in 5% Milk overnight (1:500 serum concentration). Membrane strips were washed and incubated with an HRP-conjugated donkey-anti mouse IgG mAb (1:3000 in

5% milk-PBST) for one hour at RT. Membrane strips were washed, re-assembled and measured with a chromogenic detection kit and a Western Blot detection unit.

Gene expression microarray

We isolated 50,000 $CD4^{pos}CD25^{pos}Foxp3^{YFPpos}$ Treg and 50,000 $CD4^{pos}CD25^{neg}Foxp3^{YFPneg}$ Tconv cells from sick *Foxp3* ^{Cre}*Rbpj*$^{\Delta/\Delta}$ and *Foxp3*^{Cre} animals using FACS ARIA II or III cell sorters. Furthermore, we isolated $CD4^{pos}CD25^{pos}$Foxp3-$NICD^{YFPpos}Foxp3^{GFPpos}$ Treg and 50,000 $CD4^{pos}CD25^{pos}$Foxp3-$NICD^{YFPneg}Foxp3^{GFPpos}$ Treg cells from *Foxp3* ^{Cre}*Notch*^{LSL} mice using FACS ARIA II or III cell sorters. RNA was extracted using the RNEasy Plus Micro Kit (Qiagen) followed by amplification and hybridization of material to the MouseWG-6 v2.0 Expression BeadChip (Illumina) through the DKFZ Genomics and Proteomics Core Facility. Microarray data will be deposited at the Gene Expression Omnibus (GEO).

Chromatin-IP with Rbpj

Chromatin-IP experiments were performed with an anti-Rbpj monoclonal antibody (Cell Signaling, clone D10A4, concentration 25 µg / mL) at a 1:50 dilution with the Magnify ChIP system (Lie Technologies). We used three to four biological replicates of $CD4^{pos}CD25^{pos}Foxp3^{YFPpos}$ Treg cells from *Foxp3*^{Cre} animals, $CD4^{pos}CD25^{pos}Foxp3^{YFPpos}$ Treg cells from *Foxp3*^{Cre}*Rbpj*$^{\Delta/\Delta}$ animals, and $CD4^{pos}CD25^{neg}Foxp3^{YFPneg}$ Tconv cells from *Foxp3* ^{Cre} animals. Chromatin IP was performed according to manufacturers recommendations. Bead-bound DNA was eluted in 100µL elution buffer and used for Real-time PCR based measurements with Sybr primers specific for *Hes1*, *Dtx1*, and *IL7R* putative RBPJ binding sites (see appendix). Real-time PCR measurements were performed using the Sybr Master Mix and a Viia 7 RT-PCR system (Life Technologies). Results were normalized to input controls, and Rbpj-specific binding at different loci was identified by calculation of binding in Rbpj-proficient Treg cells vs. binding in Rpbj-deficient Treg cells.

7 Results

7.1 Epigenetic control of the *Foxp3* gene in Treg cells

Identification of CG hotspots for analysis

First, we downloaded the mouse and human genetic code for the *Foxp3* gene and its promoter region from public databases (human: *FOXP3* CCDS14323, mouse: *Foxp3* CCDS29965). We then compared the conservation between both sequences on a nucleotide-per-nucleotide level and computed a histogram shown in **Figure 11** (http://genome.lbl.gov/vista/mvista/submit.shtml). Using this histogram, we overlaid mouse *Foxp3* intron and exon information and identified highly conserved regions such as the conserved non-coding sequences (CNS1-3), the promoter (PRO) and a putative upstream enhancer (ENH). Along this line, we used the mouse *Foxp3* genetic code and calculated the number of CG dinucleotides per 100 bases. We plotted the CG density in another histogram to identify 6 regions that are enriched for CG dinucleotides. Some of these regions also show a high degree of conservation (region 1, 2, 4, and 6). These six CG hotspots were used for a detailed downstream CG dinucleotide methylation analysis. Their specific location is described in **Table 1**.

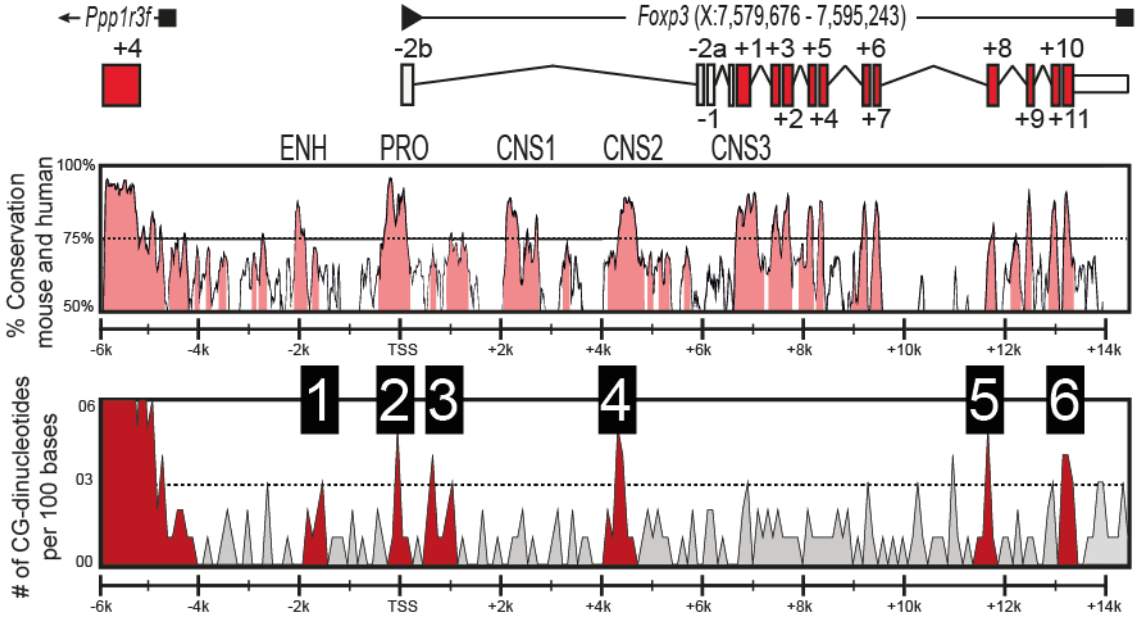

Figure 11: Conservation of the *Foxp3* gene and identification of CG hotspots.
The upper histogram shows the conservation between mouse and human genetic code for the *Foxp3* gene. Relative positions of *Foxp3* gene introns and exons are superimposed on top. The lower histogram depicts the average CG dinucleotide distribution across the whole *Foxp3* gene. Six distinct CG-rich regions can be identified and will be analyzed throughout this chapter.

R	Area	Start TSS	Start	Stop	Length	AUC
R1	Enhancer	-2000	7,577,676	7,578,176	500	800
R2	Promoter	-300	7,579,376	7,579,876	500	800
R3	Promoter/Intron	+400	7,580,076	7,580,776	700	1300
R4	TSDR	+4,000	7,583,676	7,584,376	700	1400
R5	Exon 8	+11,400	7,591,076	7,591,776	700	800
R6	Exon 11	+13,100	7,592,776	7,593,176	400	1100

Table 1: Precise description of *Foxp3* CG-rich regions, their location relative to TSS (7,579,676) or precise genomic location, specific length and area under the curve.

Epigenetic analysis reveals distinct methylation of several regions of the *Foxp3* promoter

Next, we prepared primers for each specific region 1-6 and synthesized them with specific barcodes and adaptor sequences. To identify the methylation pattern among Treg cells, Tconv cells and CD8 T cells, we FACS-purified each cell type from pre-enriched cell preparations and measured the methylation pattern (**Figure 12**). We observed that region 1, which is a potential upstream enhancer of the *Foxp3* gene, carries a partial demethylated phenotype only in Treg cells. Region 2, which is the core *Foxp3* promoter, was mostly demethylated in all cell types, indicating a rather transcription-factor based control of this gene area. In contrast to this, region 3, which is just downstream of the core promoter in the first intron, has a distinct demethylation phenotype. This phenotype is comparable to region 4, which is the already published TSDR. These results suggest a not yet appreciated, potentially regulatory region (R3) adjacent to the *Foxp3* gene promoter.

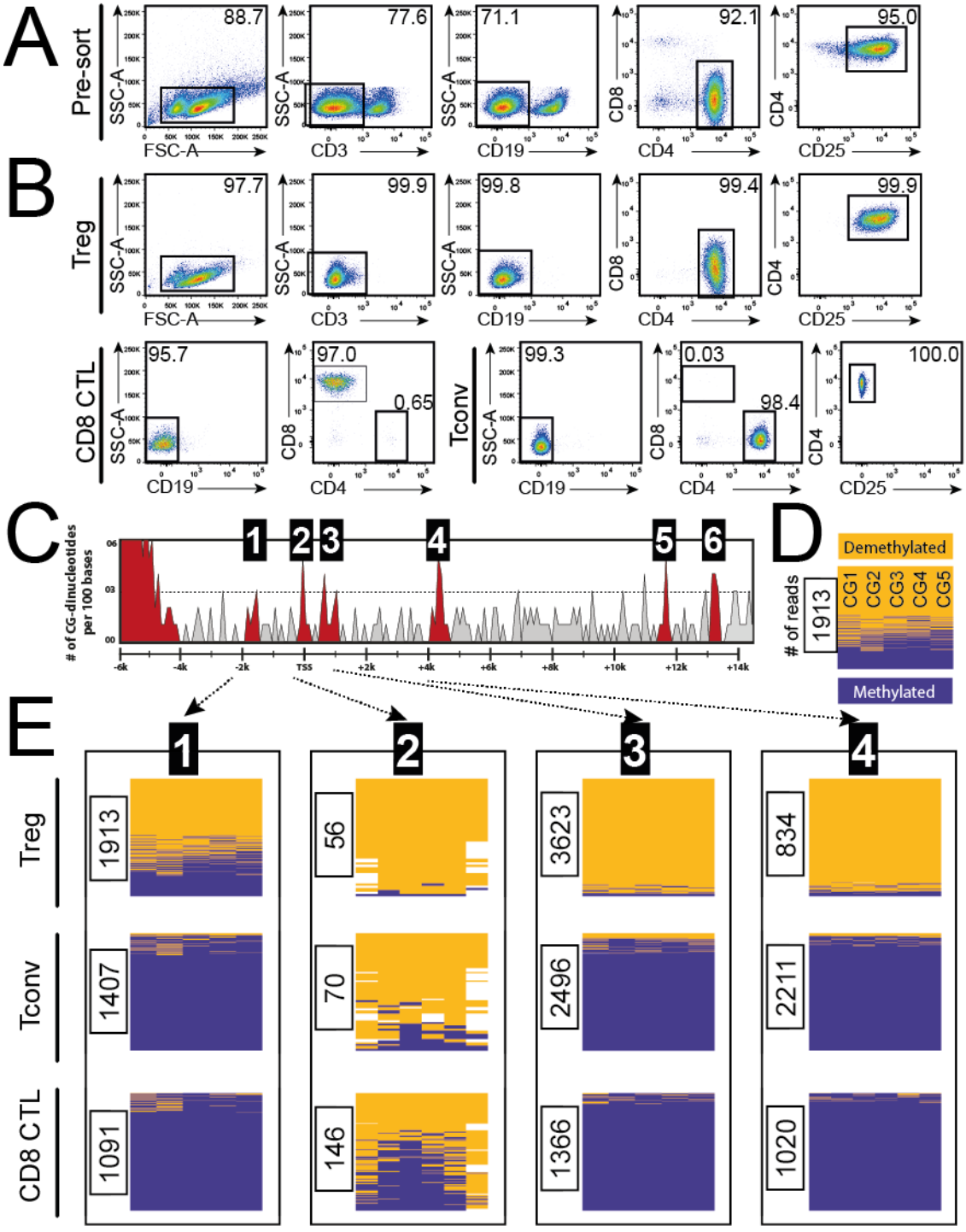

Figure 12: Analysis of *Foxp3* promoter R 1-4 in Treg, Tconv, and CD8 T cells.
The dot plots in A show the sorting strategy for CD25 pre-enriched samples from mouse spleen and lymph nodes. In B, we show post-sort quality control and purity measurements of Treg cells, CD8 T cells and Tconv cells. An overview of the CG-rich regions is shown in C. The plot in D guides along the interpretation for sequencing data: each column represents an individual CG dinucleotide, whereas each row represents an individual read. The total number of reads is written left-hand of the graph. A yellow color indicates unmethylated CG dinucleotides, whereas blue color shows methylation. In E, we show the differential methylation pattern of Treg, Tconv, and CD8 T cells for R1, R2, R3 and R4.

The epigenetic imprint of Treg cells is established during thymic development

To identify the precise developmental step at which *Foxp3* gene methylation at our target regions occurs, we isolated thymic T-cell precursors (double negative thymocytes), early Treg precursors cells (cytokine – and TCR-dependent Treg precursor cells), late Treg precursor cells (cytokine-dependent Treg precursor cells) as well as mature Foxp3^{GFP} positive thymic Treg cells as shown in **Figure 13** [29]. The epigenetic analysis revealed that region 1 is heavily methylated in all Treg precursor cells and becomes partially demethylated only in thymic Foxp3^{pos} Treg cells. The promoter-adjacent region 3 as well as the TSDR R4 is methylated just until Foxp3 is expressed in thymic Treg cells. Our results suggest that the demethylation on the *Foxp3* locus occurs immediately before *Foxp3* expression, and suggests a role of epigenetic imprinting in stabilizing and modulating the expression strength of *Foxp3*. Interestingly, the exonic regions R5 and R6 (situated in exon 8 and 11) conserve their highly methylated pattern, indicating that these regions have no impact on *Foxp3* gene expression or its strength, but rather promote genetic stability and integrity.

The Treg-specific methylation pattern is stable in circulating mature Treg cells

Since we already investigated the imprinting of the Treg-specific methylation pattern in thymic Treg cell induction, we now wanted to compare it to both circulating Treg cells and iTreg cells. To do so, we isolated either naive or antigen-experienced Treg and Tconv cells from spleen and lymph nodes from mice. Furthermore, we induced iTreg cells from Tconv cells via *in-vitro* activation and cytokine treatment. We investigated all cell types for their epigenetic phenotype and plotted the data in **Figure 14**. We could show that, first, *in-vitro* induced Treg cells, albeit Foxp3^{GFP} positive, carry no Treg-specific demethylation pattern at both R3 and R4 loci. The missing demethylation of R4-TSDR and its implications for the long-term stability of *in-vitro* induced Treg cells has been discussed already [126]. Importantly, the specific demethylation of R3 and R4 is stable in circulating Treg cells, independent of antigen experience. We also observed the partial demethylation of R1 only in Treg cells, but not in Tconv cells or induced Treg populations. The exonic regions R5 and R6 were again methylated in all cell types. Based on this dataset, we can draw the conclusion that region 3, which is established during thymic Treg development, remains demethylated once Treg cells leave their birthplace and travel the body. Antigen experience does not alter this epigenetic imprint.

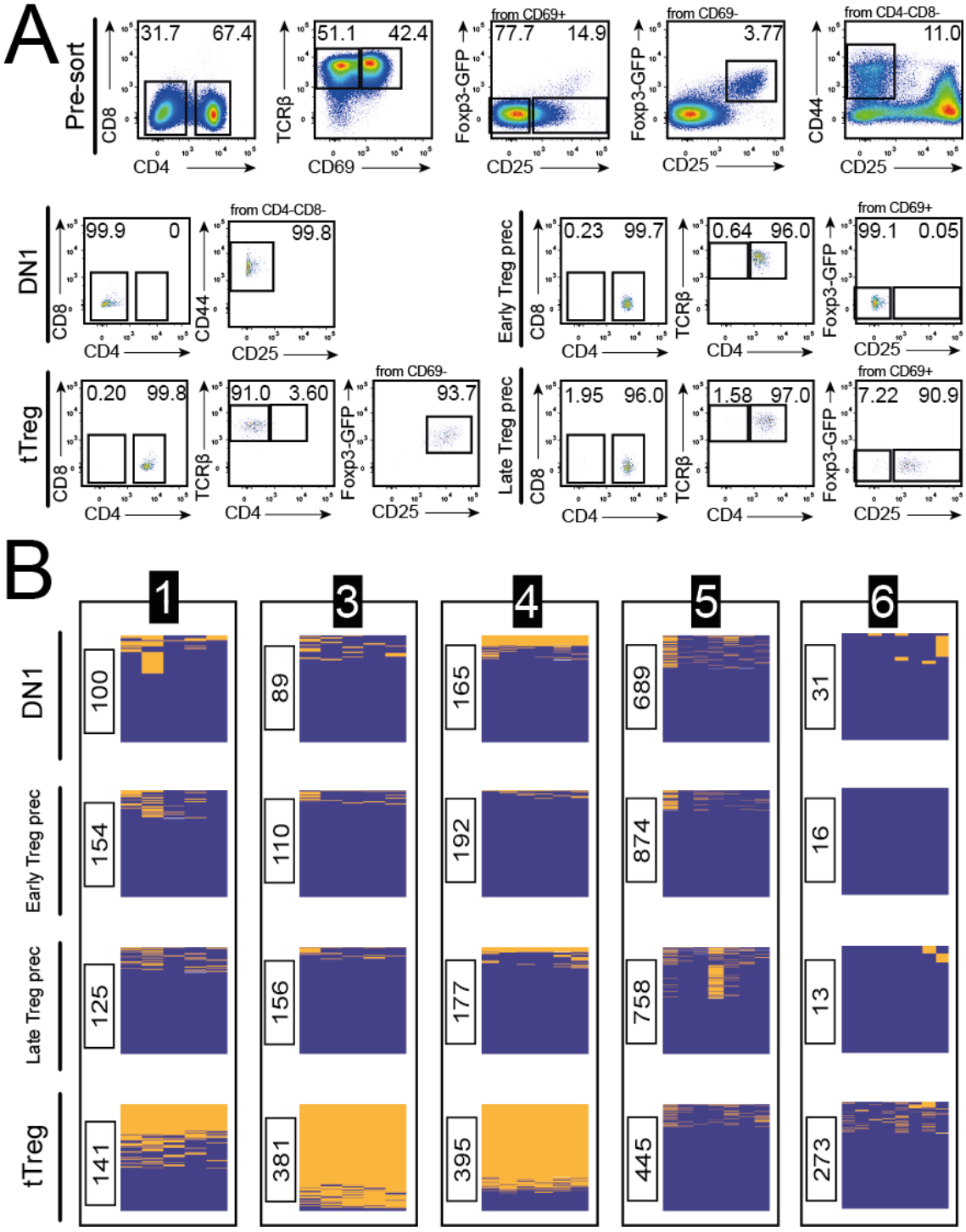

Figure 13: Investigation of *Foxp3* gene methylation in developing Treg cells.
We isolated T cell subpopulations from the thymus, and show the gating strategy in A. Post-sort controls show purity and surface phenotype of DN1 (CD4 ^{neg}CD8^{neg}CD25^{neg}CD44^{pos}), early Treg precursor cells (CD4 ^{pos}TCRβ^{pos}CD69^{pos}CD25^{neg}Foxp3^{GFPneg}), late Treg precursor cells (CD4^{pos}TCRβ^{pos}CD69^{neg}CD25^{pos}Foxp3^{GFPneg}), and mature thymic Treg cells (CD4^{pos}TCRβ^{pos}CD69^{neg}CD25^{pos}Foxp3^{GFPpos}). The methylation pattern is shown in B.

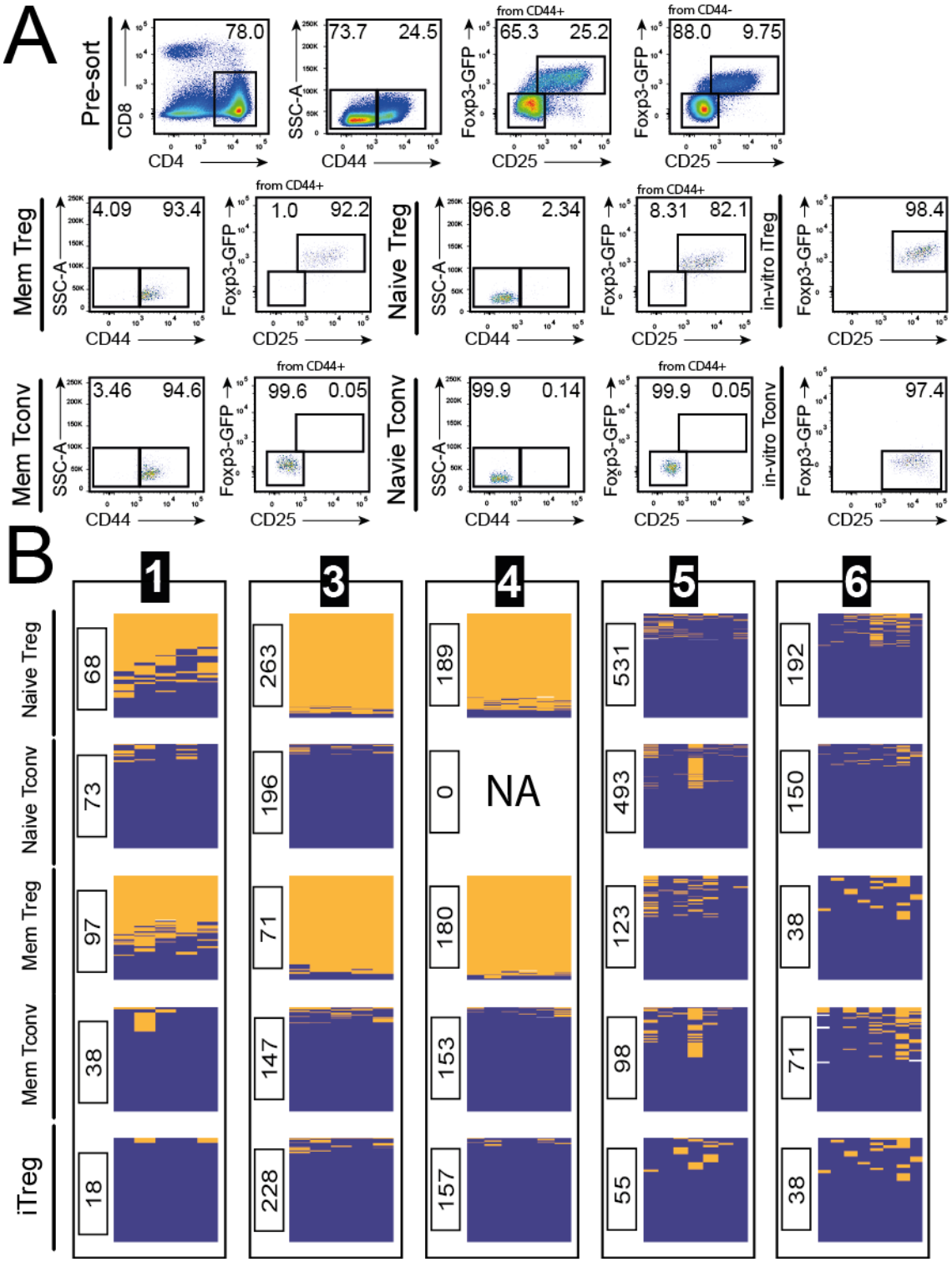

Figure 14: Investigation of *Foxp3* gene methylation in mature T cells.

Cells were isolated from spleen and lymph nodes. Cells were then separated into memory (antigen-experienced) and naive T cells based on their CD44 expression (A). The dot plots show the post-sort purity control for memory and naive Treg and Tconv as well as *in-vitro* induced Treg cells (iTreg). The methylation pattern of each group is shown in B.

The Treg-specific methylation pattern is independent of Foxp3 expression strength

Since selective CG methylation can not only modulate gene expression in a binary manner, but also level the gene expression strength, we isolated Foxp3 ^{GFP} high-, medium-, and low expressing Treg cells populations. Furthermore, we also isolated CD25-negative Foxp3-positive Treg cells as well as Tconv cells from spleen and lymph nodes (**Figure 15**). We compared Foxp3 ^{GFP} expression intensity with *Foxp3* and CD25 (*Il2ra*) mRNA levels and identified a positive correlation between Foxp3 ^{GFP} signals and *Foxp3* mRNA, and interestingly also for Foxp3 ^{GFP} signals and *Il2ra* mRNA. Zheng and co-workers have identified the molecular link between Foxp3 protein and CD25 expression as a Foxp3-dependent regulation of *Il2ra* levels, which fits our results [177]. Also, Foxp3^{pos}CD25^{neg} Treg cells had very low levels of *Foxp3* mRNA, albeit still higher than Tconv cells. If we now compare the specific methylation signature of all five cell types, we can observe that region 1, which is a potential upstream enhancer, is methylated in Tconv cells and partially demethylated in high – medium – and low-Foxp3 expressing Treg cells. This rules out a possible function of this region in manipulating *Foxp3* expression strength. Interestingly, it shows higher methylation in Foxp3^{pos}CD25-negative Treg cells, indicating that it might be involved in or regulated by IL-2 cytokine signaling pathways. We also compared region 3, a new Treg-specific demethylation region, amongst all cell types. To increase resolution, we probed the region with two amplicons and analyzed it separately. Our data indicate that region 3 clearly follows the pattern of region 4, again demonstrating its Treg-specific epigenetic imprint. Interestingly, both region 3 and 4 show the same demethylation pattern in high-medium- and low- Foxp3 expressing Treg cells. One can infer from this dataset that TSDR methylation does not regulate *Foxp3* expression strength, but only stabilizes its expression in a binary (on/off) manner. Furthermore, it is independent of signals derived from the IL-2 receptor (CD25), at least once Treg cells have matured in the thymus.

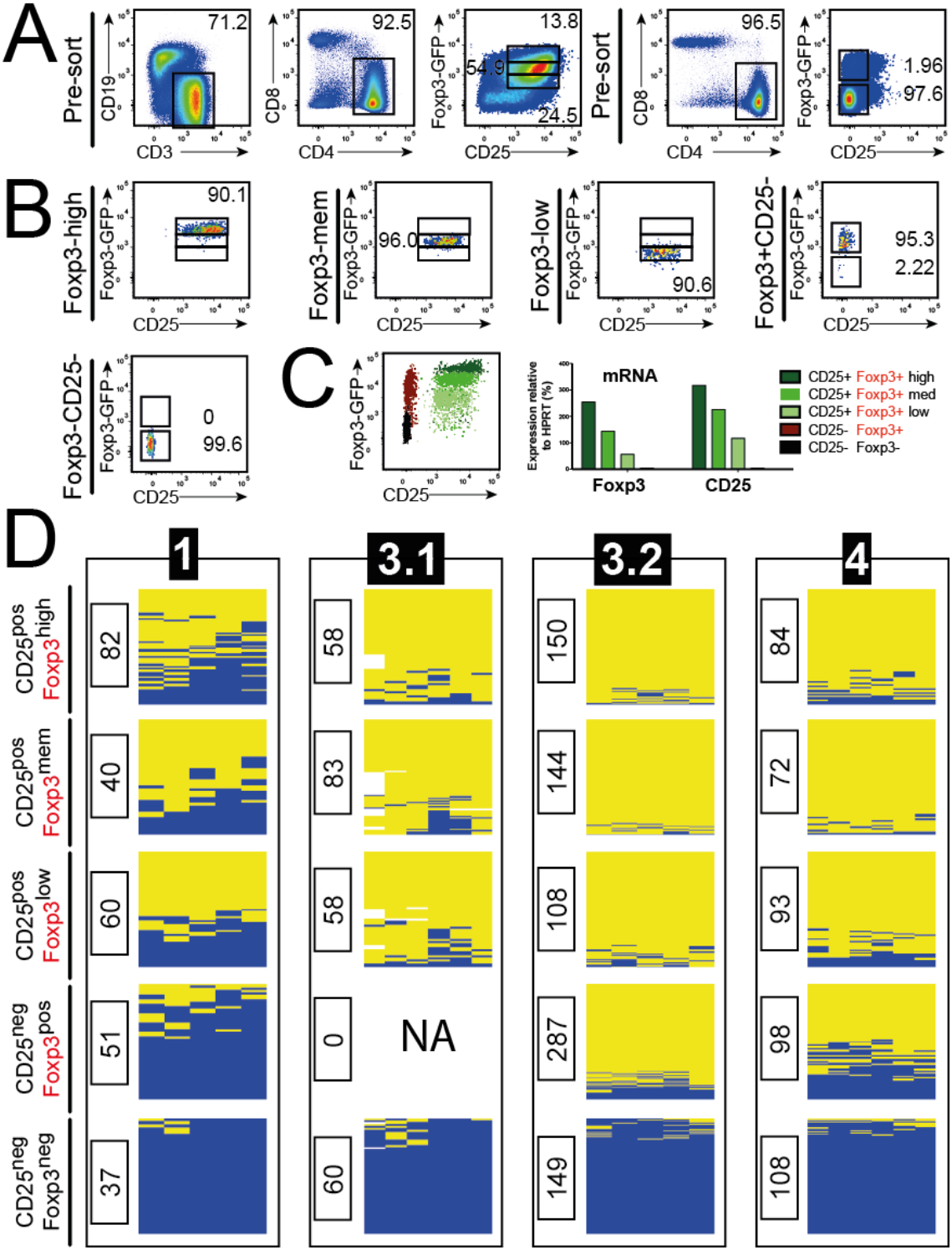

Figure 15: Influence of *Foxp3* gene methylation on Foxp3 protein expression.
Cells were isolated from spleen and lymph nodes and sorted based on their expression strength of Foxp3 (A). We isolated CD4 ^{pos}CD25^{pos}Foxp3^{GFPhigh}, CD4^{pos}CD25^{pos}Foxp3^{GFPmedium}, and CD4^{pos}CD25^{pos}Foxp3^{GFPlow} Treg cells. Furthermore, we sorted CD4 ^{pos}CD25^{neg}Foxp3^{GFPpos} Treg cells as well as CD4 ^{pos}CD25^{neg}Foxp3^{GFPneg} Tconv cells. Post sort purity is shown in B, with a correlation between sort purity and *Foxp3* and *Il2ra* mRNA expression shown in C. The methylation results are shown in D.

DNA-methyltransferase hypomorphic mice have phenotypically intact Treg cells

In order to analyze the importance of our Treg methylation patterns at the *Foxp3* promoter, we took advantage of a mouse carrying only the most basic methylation pattern due to is near-complete loss of the DNA-methyl transferase enzyme 1 (Dnmt1). Since a complete knockdown of this important maintenance and *de-novo* methyl transferase in mouse and human cells is embryonically lethal, a Dnmt1 hypomorphic allele (*Dnmt1*^{chip}) has been used to create a Dnmt1-hypomorphic mouse strain [172]. We analyzed the T-cell compartment in splenocyte preparations from these mice (**Figure 16**). We identified CD4 and CD8 T cells in the periphery, although at a lower frequency than in wild type controls. Foxp3^{pos} Treg cell percentage in the CD4 T cell populations was reduced to about 50% of normal (30% in WT vs. 15% in Dnmt1 hypomorphic mouse spleens). This also translates into a decrease in absolute Treg cell numbers in the spleen. In contrast to this, Tconv cell numbers were not drastically reduced, especially in comparison with the heavily constricted B cell compartment in the spleen. In addition to cell frequencies, we also measured lineage-defining protein expression in Treg cells from WT controls and *Dnmt1*^{chip} mice. We could not detect any abnormalities in the expression of CTLA-4, Nrp1, Helios or GITR, as well as Foxp3 protein. Since it has not been reported that *Dnmt1* ^{chip} mice develop autoimmune disease, protective function of the Treg lineage can be inferred since potentially self-reactive Tconv cells should be present in normal frequency. Last, we were also interested in the methylation levels of Treg vs. Tconv cells in this particular mouse. Therefore, we isolated both cell types from splenic preparations and measured the methylation phenotype as shown in **Figure 17**. Interestingly, the methylation patterns of region 3 and 4 are conserved also in animals with hypomorphic DNA methyltransferase 1 activity. One can appreciate the gradual loss of methylation for region 5 and 6, which in turn should not affect *Foxp3* gene expression. Also, the putative enhancer region 1 retains the differential methylation pattern. Taken together, these data indicate that methylation of Region 3 and 4 is necessary for Tconv cells to prevent an epigenetic opening of the *Foxp3* locus, and its differential methylation is maintained even in a Dnmt1 hypomorphic situation.

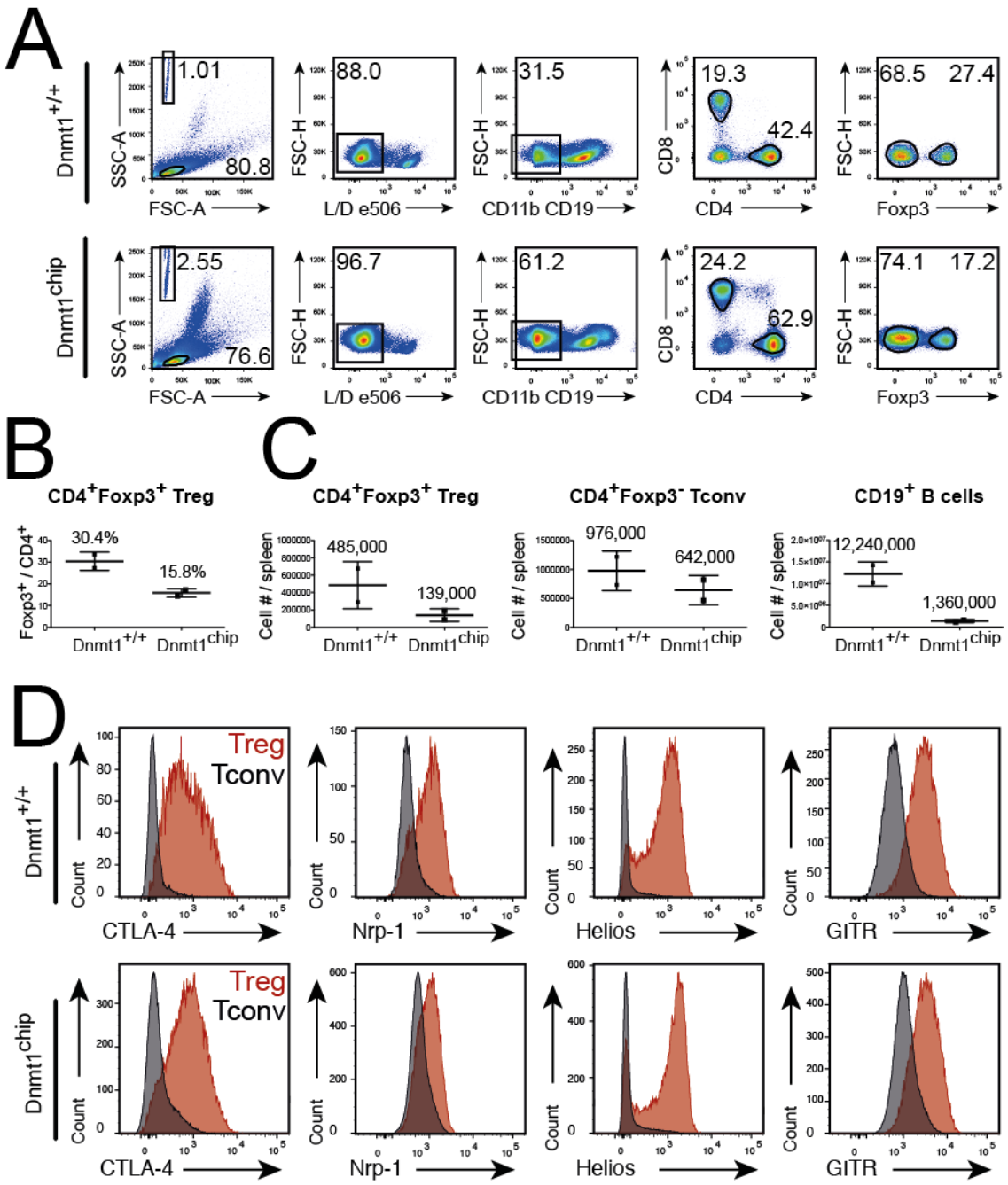

Figure 16: Analysis of the Treg cell compartment in Dnmt1-hypomorphic mice.
First, we investigated splenocytes from Dnmt1-hypomorphic mice for the presence of any Treg cell species. Representative gates are shown in A, with a quantification of Treg percentages (B) and absolute numbers (C). In D, we compared the expression of key Treg lineage proteins via flow cytometry. The histograms are representative of duplicate experiments from individually shipped cell samples.

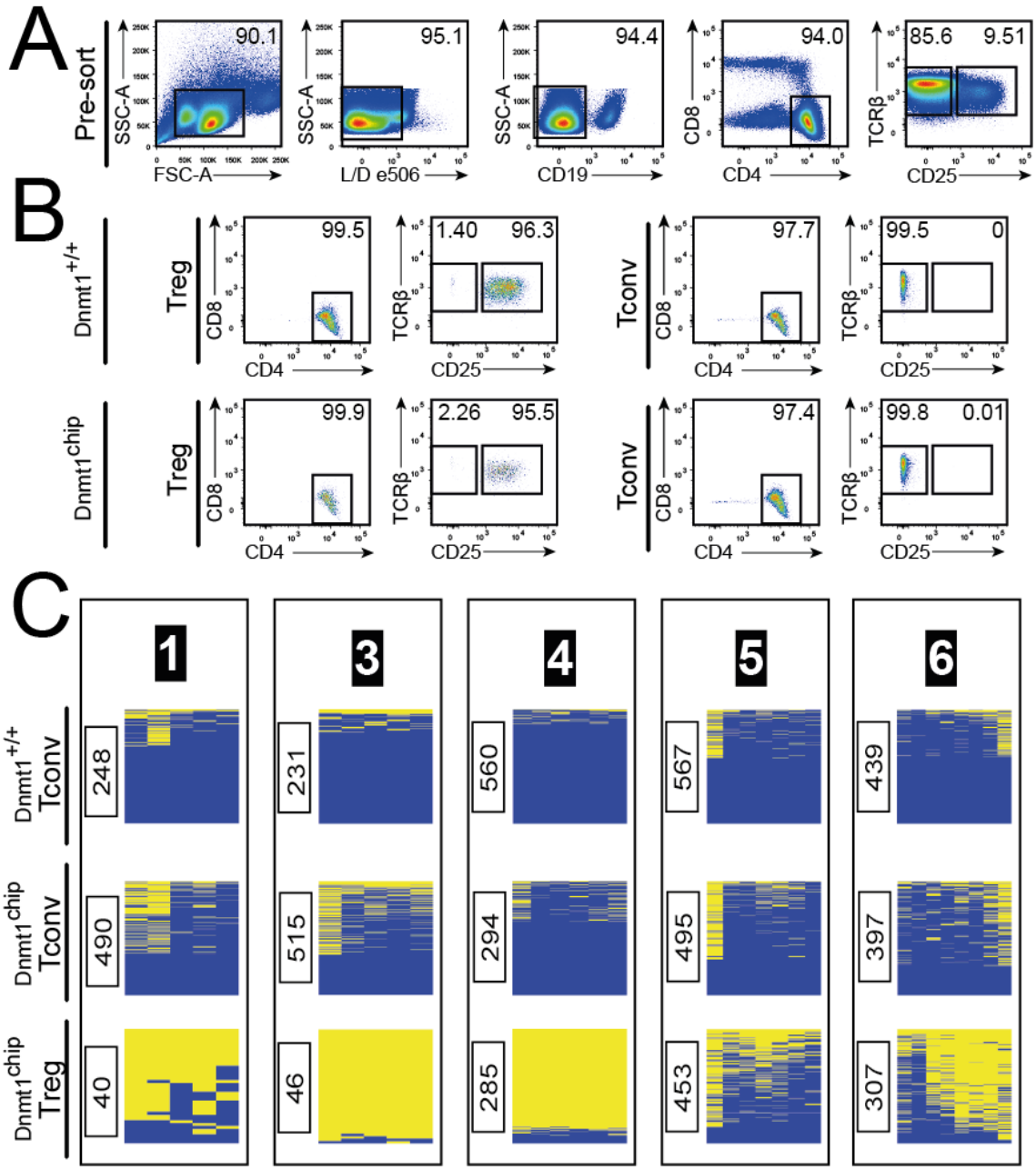

Figure 17: *Foxp3* gene methylation in Dnmt1-hypomorphic mice.

We isolated Treg and Tconv cells from the spleens of Dnmt1 hypomorphic mice (A). No purity-based differences have been observed between T cell populations isolated from wild type or Dnmt1-hypomorphic mice (B). Since we had no Foxp3 ^{GFP} marker in these animals, we used the surface marker CD25 to stratify Treg and Tconv cells. The methylation pattern for WT Tconv cells and Treg / Tconv cells from *Dnmt1* ^{chip} mice is shown in C.

The differential methylation of the *Foxp3* gene by whole-genome sequencing

In the following section, we describe the whole-genome sequencing based methylation analysis of Treg and Tconv cells from lymph nodes along with tissue-isolated Treg cells from fat, skin and liver. To obtain these data, we collaborated with the division of Epigenetics and Cancer Risk Factors at the DKFZ Heidelberg. Quality aspects of our dataset in terms of CG dinucleotide coverage across the whole genome, homogeneity amongst samples, and mapping efficiencies are described in the following section. We used this dataset to analyze the *Foxp3* gene and its CG-rich regions, as shown in **Figure 18**. We were able to confirm our amplicon-based data, showing that regions 3 and 4 are Treg-specific demethlated regions. Furthermore, we also confirmed the hypermethylated state of regions 5 and 6. We also observed the partially demethylated phenotype of region 1, which remains conserved also in tissue-specific Treg cells. Finally, region 2, which is the core *Foxp3* promoter, is demethylated in all cell types tested, which was shown already with amplicon-based methylation analysis.

Furthermore, we plotted the whole *Foxp3* gene along with its preceding gene *Ppp1r3f* (Protein Phosphatase1, Regulatory Subunit 3F) in 3' and the untranslated region (UTR) of the *Foxp3* 5' end (**Figure 19**). The *Ppp1r3f* gene, coding for the glycogen-binding protein R3F, which in turn binds the glycogen target protein phosphatase 1 (PP1), is involved in the regulation of glycogen metabolism. It can modulate the activity of glycogen synthase and glycogen phosphorylase, key enzymes in glucose metabolism [178]. It can be assumed that this gene is expressed in many different cells, and not regulated in a tissue-specific manner. Interestingly, the complete promoter and Exon 1 of the *Ppp1r3f* gene are demethylated in all cell types. Since this gene is located on the reverse strand, its promoter and the *Foxp3* promoter are linked. If we move further towards the extended *Foxp3* promoter, a differential methylation pattern between Treg cells and Tconv cells can be appreciated – this probably marks the end of the *Ppp1r3f* gene promoter. As mentioned earlier, the core *Foxp3* promoter with 9 CG dinucleotides is completely demethylated in all cell types, just like the promoter of the *Ppp1r3f* gene. Once we move across the transcription start site, the intronic region containing CNS1 and CNS2 regions is, again, differentially methylated between Tconv and Treg cells of all tissues. Importantly, this Treg-specific demethylated regions covers the whole *Foxp3* first intron, and not just the areas of high CG density such as Region 3 or Region 4 (TSDR/CNS2). In contrast to this, the differential methylation pattern is complete gone after exon 1, showing a fully demethylated phenotype for about 10 CG dinucleotides

(like at the promoter). Importantly, this is also the approximate location of the CNS3 region. Once this short demethylated stretch is passed, the remaining exons and the 5' UTR are highly methylated in all cell types.

In summary, we detect a Treg-specific demethylation only at the first intron, covering our regions 3 and 4, and at an upstream enhancer of the *Foxp3* promoter, our region 1. The promoter itself and *Foxp3* exons are unanimously methylated or de-methylated, independent of *Foxp3* expression activity.

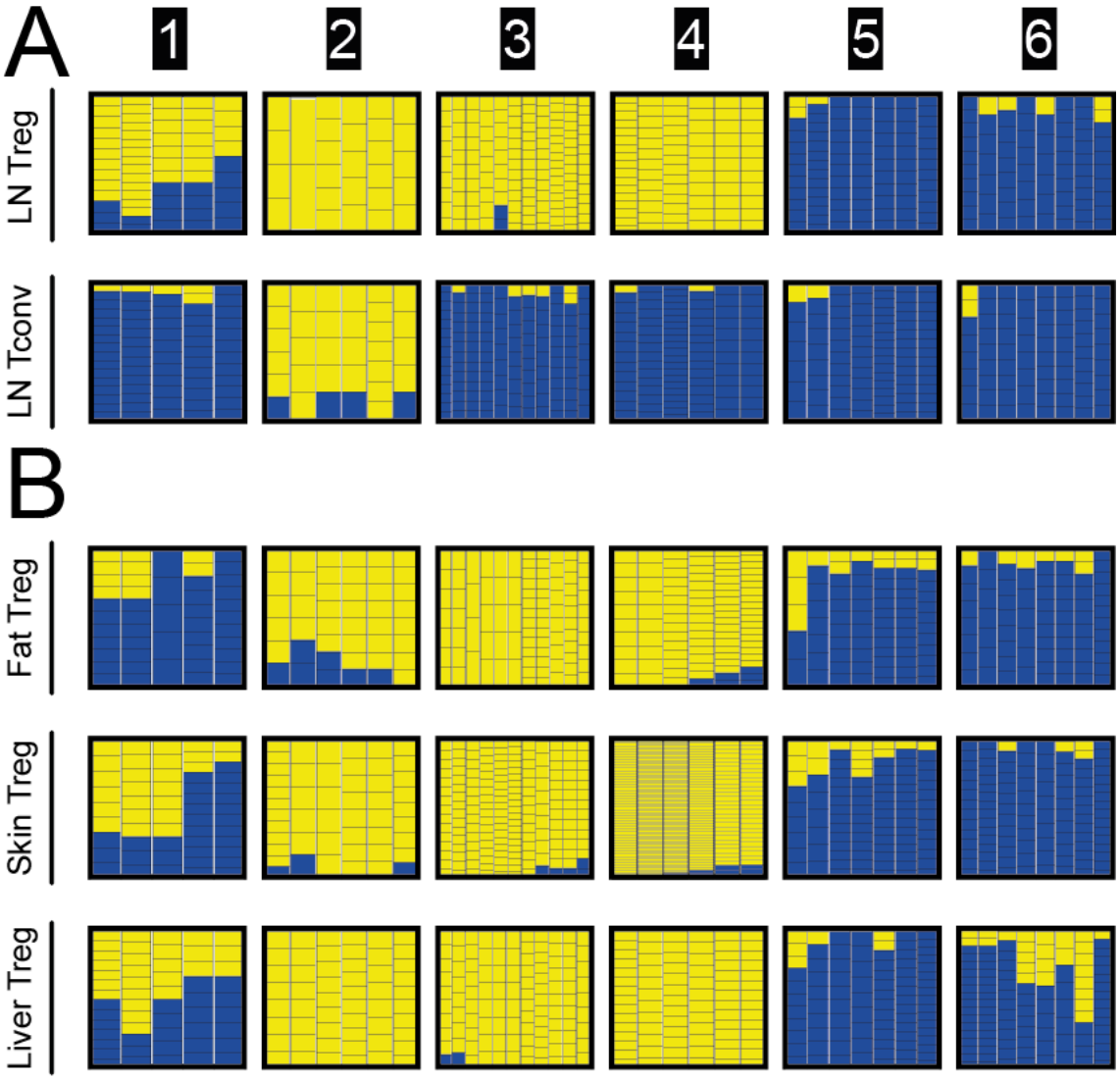

Figure 18: *Foxp3* gene methylation in tissue-resident Treg cells.
We isolated Treg and Tconv cells from lymph nodes, along with Treg cells from fat, liver, and skin. Genomic DNA was bisulfite-converted and analyzed with tagmentation-based next-generation sequencing, as described previously. Yellow color indicates demethylation, and blue color indicates methylated CG dinucleotides.

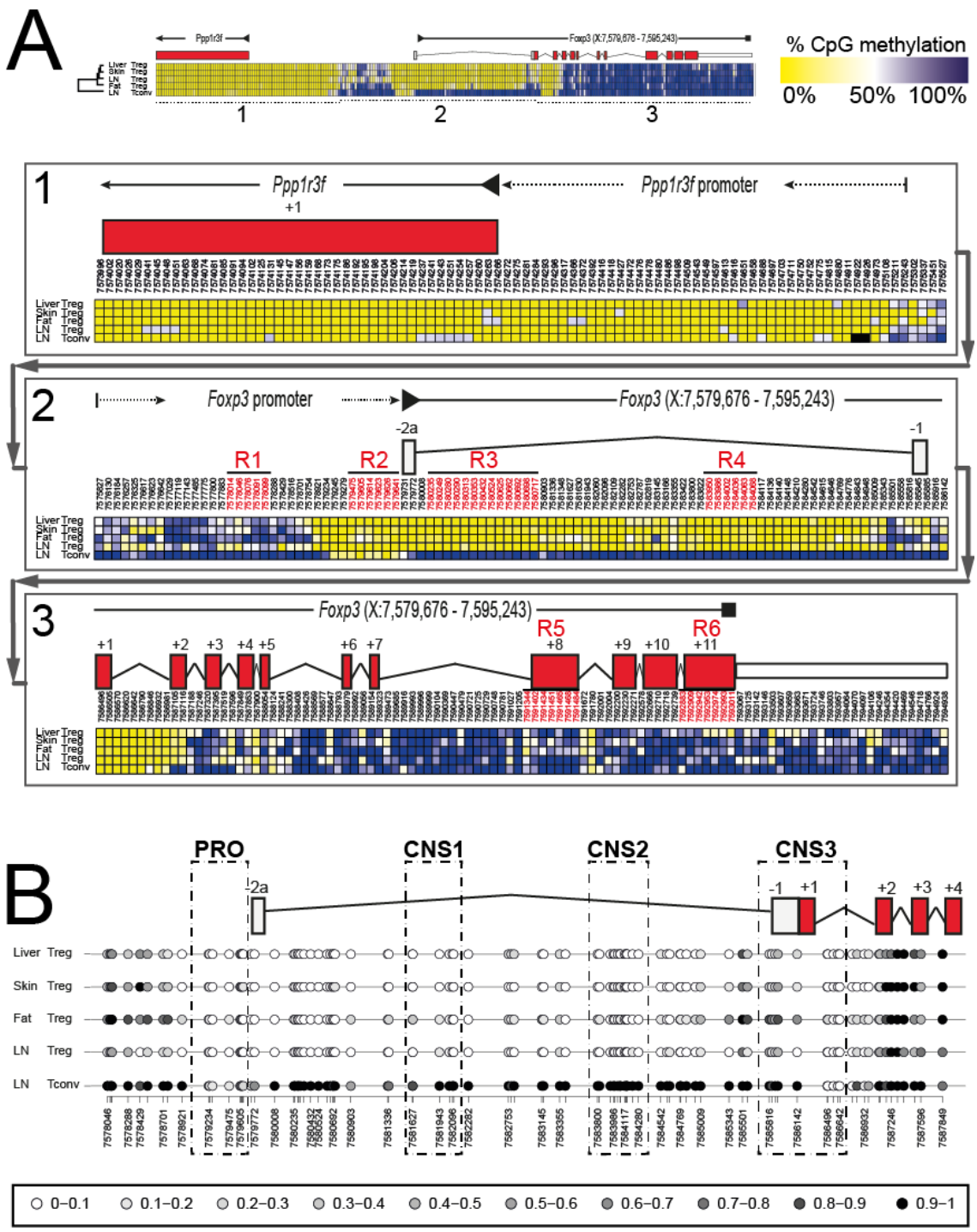

Figure 19: Overview of whole *Foxp3* gene methylation on single-nucleotide level.
Plotted are single-CpG nucleotide methylation data for Tconv and Treg cells from different tissues. The uppermost heatmap shows the CG methylation status for the whole *Foxp3* gene plus its 5' neighboring gene *Ppp1r3f* and the *Foxp3* 3' UTR (created with Gene Pattern Software). To be able to decipher the methylation status in more detail, we split the gene into three regions, shown separately below (1, 2, 3). The *Foxp3* gene intron and exons are annotated on top of the heatmaps, and the numbers indicate the genomic position of the CG dinculeotides. In B, we plot the *Foxp3* promoter and the first 4 exons of the *Foxp3* gene with methylation plotter software ([179]), and we overlaid the approximate localizations for the CNS 1-2-3 regions and the core *Foxp3* promoter. Colors or grey values indicate percent methylation as shown in the legends.

7.2 Transcriptional and epigenetic control of tissue-specific Treg cells

FACS-sorting of populations with high purity

First, we validated protocols to isolate tissue-resident T cells meeting our standards for viability and post-sort purity. Therefore, we tested and optimized different collagenase-based treatments of tissues to liberate intact immune cells. Afterwards, cells were pre-filtered and pre-enriched via FACS, followed by a second high-purity sort (polishing step). Pre-sort tissue T-cell numbers and post-sort quality control are exemplified in **Figure 20**. As appreciated in literature and discussed in the introduction to this thesis, Treg cells from different tissues also account for a different percentage of T cells. In our case, Treg cells accounted for more than 30% of $CD4^{pos}$ T cells in fat and skin, and about 13% in lymph nodes. In liver tissue, Treg cells account for only 3.9% of all $CD4^{pos}$ T cells on average. After double sorting, we obtained post-sort purities of 90% or more for all tissues. Since collagenase-treated T cells lose their expression of sort-relevant markers such as CD25 and CD4 over time during the sorting procedure, the end-gate purity without these shifting populations would be even higher. Taken together, one can conclude that we were able to isolate functionally intact, pure Treg and Tconv populations from the described target organs. Upon isolation of RNA and DNA, and measurement of the respective concentrations, we were able to determine a linear cell number – yield relationship for DNA, but not for RNA (**Figure 21**). Importantly, we observed high homogeneity between samples for methylomics run data (C) with almost equal total read numbers, GC content and duplication rate. For RNA-sequencing data, reads and duplication levels were also comparable between samples, highlighting the successful normalization of input genetic material before PCR-based amplification.

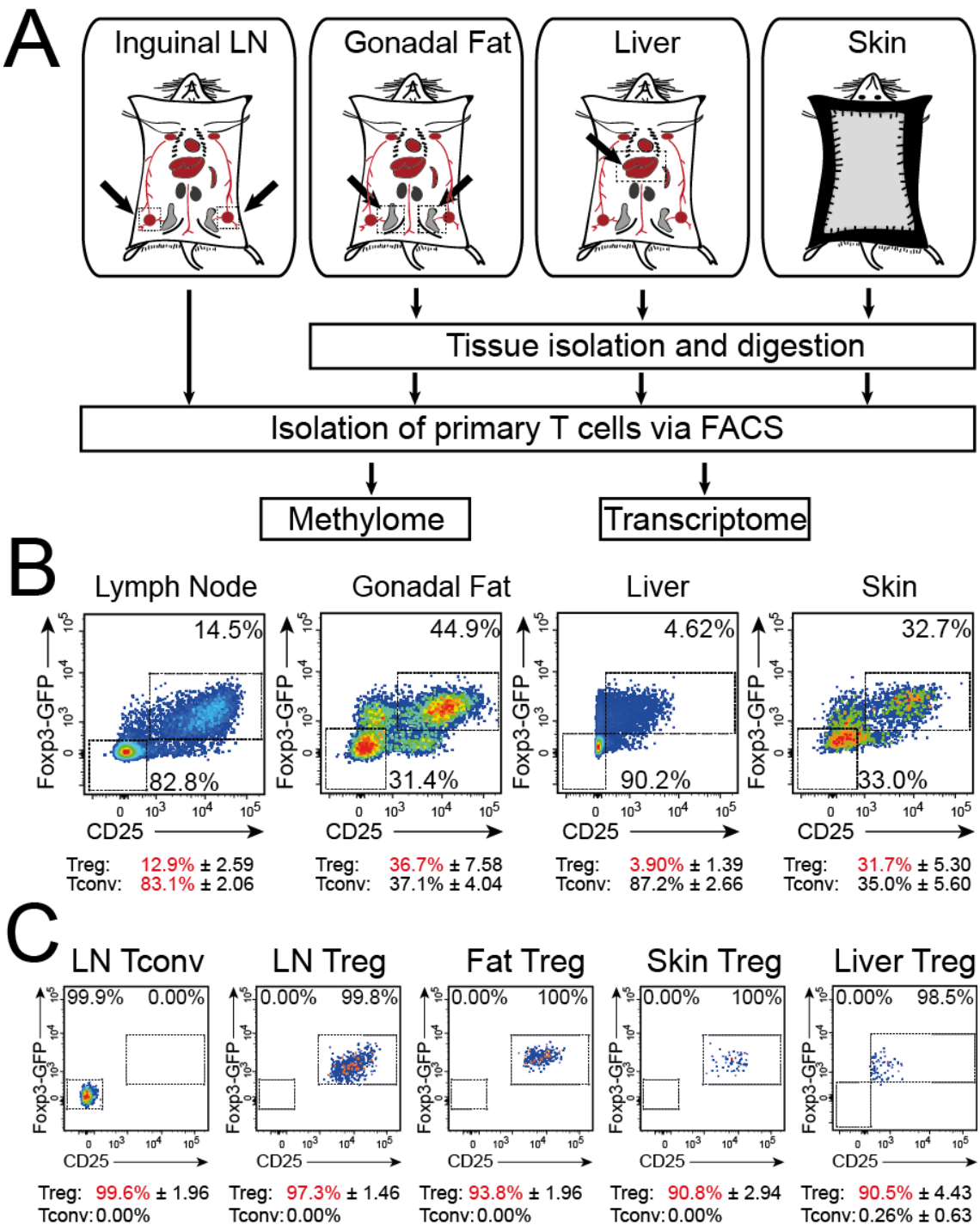

Figure 20: Isolation of tissue-specific T cell populations via FACS.

We isolated T cells from inguinal lymph nodes (LN), gonadal fat, liver, and skin. Anatomical details of tissue isolation are shown in Part A. Part B shows representative dot plots indicating $CD25^{pos}Foxp3^{GFPpos}$ Treg and $CD25^{neg}Foxp3^{GFPneg}$ Tconv frequency of intact $CD3^{pos}CD45^{pos}CD8^{neg}CD4^{pos}$ T cells. Percentages below the dot plots indicate average Treg and Tconv cell frequencies and standard deviation between different experiments. Part C highlights the post-sorting purity calculations with representative dot plots and average values across experiments.

A

Cell type	Cell#/R	gDNA/R
Fat Treg	20,000	38.0 ng
Skin Treg	15,000	35.3 ng
Liver Treg	15,000	39.5 ng
LN Treg	20,000	42.8 ng
LN Tconv	20,000	42.0 ng

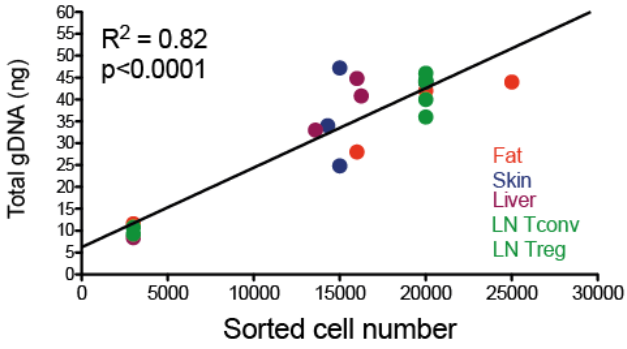

B

Cell type	Cell#/R	RNA/R
Fat Treg	12,500	2.2 ng
Skin Treg	12,000	5.0 ng
Liver Treg	12,500	3.4 ng
LN Treg	13,500	1.7 ng
LN Tconv	15,000	3.0 ng

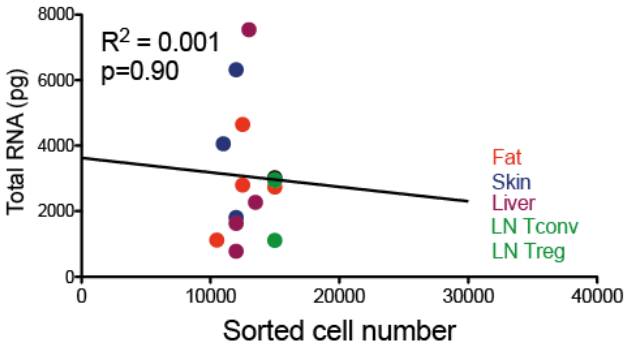

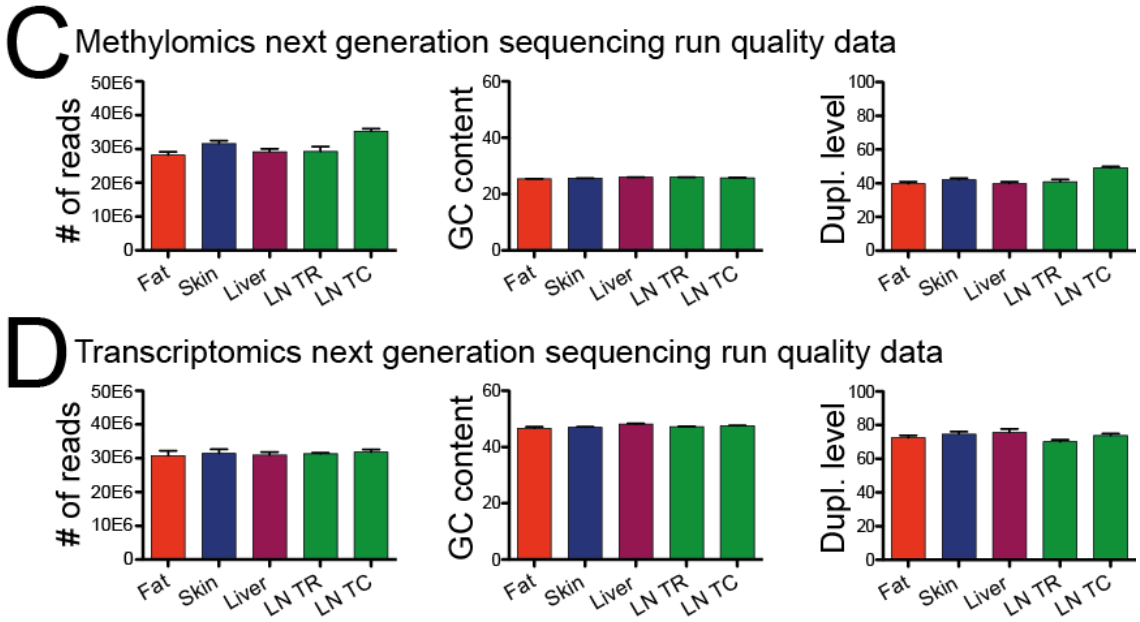

Figure 21: Quality control of DNA/RNA isolations and NGS run data.
The table in part A describes the total number of cells sorted for each cell type per biological replicate and the average genomic DNA (gDNA) concentration per replicate. This dataset is plotted again on the right hand side to highlight the linear relation between cell number and DNA yield. In parallel, we plotted average RNA concentration and cell numbers for our RNA isolation experiments in part B. Finally, we plot average read number, GC content and duplication rate for methylomics NGS data (part C) and transcriptomics NGS data (part D). Each group represents three biological replicates with several technical replicates.

Library complexity reveals the whole-genome coverage of methylation data

Reads recovered from whole-genome sequencing of bisulfite-converted DNA were mapped to a mouse reference genome. Based on mapping efficiency ("how many reads can be aligned to the genome") and pairing efficiency ("pairing of forward and reverse reads"), the overall library complexity was determined (**Figure 22**). It describes all reads that can finally be used to determine the methylation status of single CG dinucleotides over the whole genome. As already indicated by our next-generation sequencing run data, we achieved a homogenous complexity across all samples with only minor variations in read number. The read numbers eventually translate into coverage, which can be calculated for each individual chromosome, and describes how often individual reads cover every single nucleotide. Homogenously distributed over chromosome 1 through 19, we achieved about 3.5 reads per single CG dinucleotide per biological replicate. Since three replicates will be combined to determine differential methylation patterns, a median coverage of 10 or more is expected per group. The coverage of individual CG dinucleotide depends on the genomic context of its location and therefore varies for every single CG dinucleotide. Importantly, the coverage for the X allosome is only about half of the one for autosomes. Since we exclusively used male animals for this study, the reduction of coverage in the X chromosome was expected. Interestingly, the Y chromosome coverage is very poor (0.22 reads per CG dinucleotide). This problem is known to the field and based on the high content of repetitive DNA sequences, which translates into small, unmappable reads.

Tissue-resident Treg cells have lower whole-genome methylation levels

When comparing the methylation of all CGs on individual chromosomes, an interesting tissue-specific phenomenon can be appreciated. First, Treg and Tconv cells from lymph nodes do not differ in overall CG methylation levels, despite already-described Treg-specific methylation at Foxp3-Intron 1 and others (**Figure 19**). In contrast to this, Treg cells from liver, fat, and skin have different whole-genome methylation levels, indicating tissue-specific adaptation by epigenetic events. Importantly, control λ DNA and mitochondrial DNA do not display this tissue-specific methylation difference, ruling out PCR bias or input DNA variation as a source for this difference. Next, it will be interesting to analyze these differences on a per-gene basis with the aim to identify potential epigenetic hotspots of Treg tissue adaptation (work in progress).

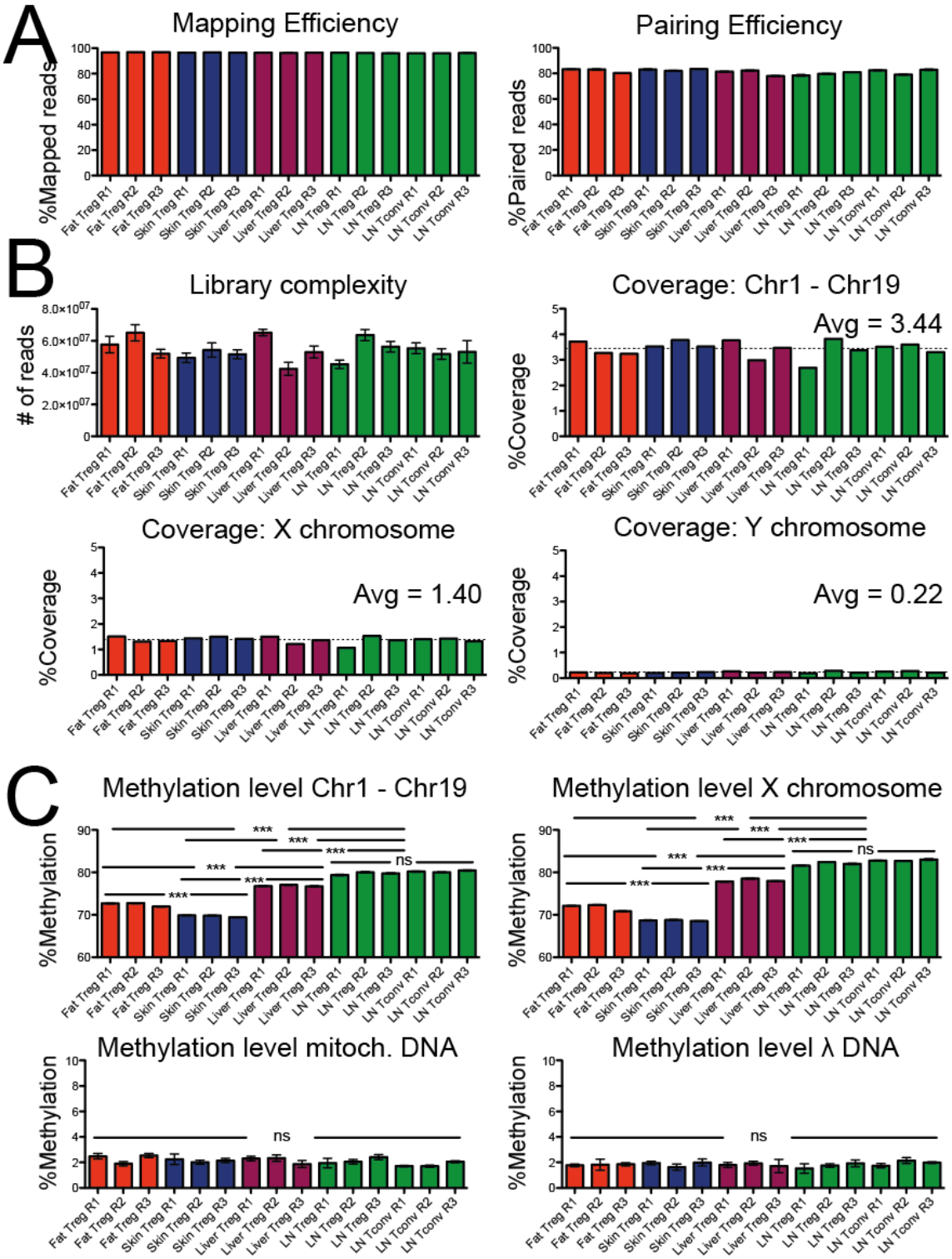

Figure 22: Mapping, coverage and whole-genome methylation status.
In A, we show mapping and pairing efficiency of adapter-trimmed reads to the hg19 mouse reference genome. Based on the mapped reads, the library complexity with all mappable reads can be determined (B). These reads were used to compute the coverage of every single CG nucleotide on a per-chromosome-basis for all four libraries in autosomes (Chromosome 1-19) and allosomes (X and Y chromosome). In C, we calculated the average CG methylation across all chromosomes and compared it to methylation level of mitochondrial DNA and λ DNA. Statistical evaluation was performed with two-way ANOVA (*** = $p<0.0001$, ns = $p>0.05$).

7.3 Transcription-factor based control of the *Foxp3* gene

The *Foxp3* promoter is highly conserved between species

In our epigenetic study of the *Foxp3* locus, we compared the conservation between mouse and human *Foxp3* genetic code. The histogram in **Figure 23** shows the conservation in percent with a superimposed *Foxp3* gene structure. We can interpret that the *Foxp3* gene promoter, at least in its very proximal 1000 bp, is highly conserved between mouse and human. This indicates transcription-factor binding sites to be present in this area, as already reviewed in the introduction. Furthermore, our epigenetic analysis summarized in **Chapter 5** showed that this particular part of the *Foxp3* gene is demethylated in regulatory and non-regulatory cell types, which could indicate that potential repressive factors occupy this area in Foxp3-negative cell types. To identify putative binding partners, we performed the inverted ChIP as described in **Figure 10** and the methods section.

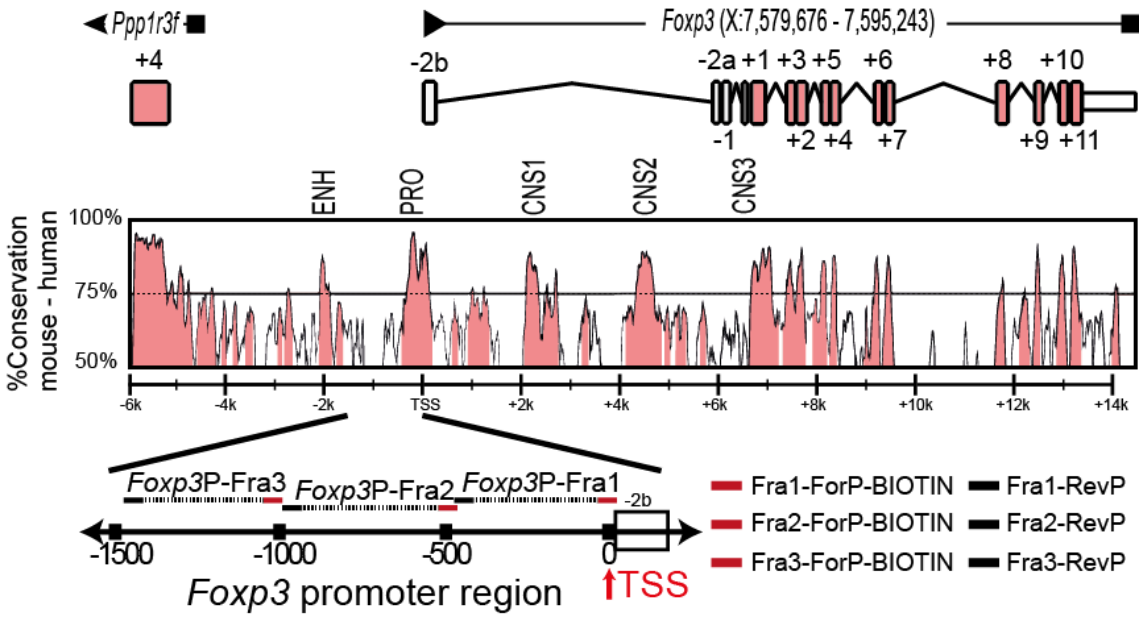

Figure 23: Overview of *Foxp3* species conservation and inverted ChIP procedure. The histogram in A highlights the conservation between mouse and human genetic code for the *Foxp3* gene. Highly conserved sequences are colored in red. The relative position of the *Foxp3* gene introns and exons are overlaid on top, and the specific probes used for the inverted ChIP are shown below.

A specific array of factors bind the *Foxp3* gene promoter

We performed the inverted ChIP and evaluated specific protein binding to each fragment (**Figure 24**). First, we cross-compared binding of each factor to each individual *Foxp3* probe: for example, the candidate factor Zinc finger protein 574

(Znf574) binds strongly to *Foxp3*-promoter fragment 2 since its relative binding to this fragment is much higher than its binding to Fra 1 (Fra2/1) or to Fra3 (Fra2/3). This can also be visualized in dot plots showing the relative binding or in a heatmap generated from selected candidate proteins and shown in **Figure 24**. In an effort to decrease the number of candidates, we applied filters based on published gene ontology (GO) terms for candidates identified in this experiment. First, we disregarded candidates with less than 3-fold differential binding between fragments. Next, we used a p-value threshold of $p<0.05$ to identify candidates with statistically sound binding patterns. Finally, we used the GO terms DNA-binding or RNA-binding to filter our candidate proteins, of which seven were reported transcription factors for the very proximal *Foxp3* promoter 1, five for the *Foxp3* promoter fragment 2, and three for the most distal probe *Foxp3* promoter fragment 3.

Candidate proteins are overexpressed in human, but not murine, Tconv cells

To evaluate differential gene expression of our candidate proteins, we cultivated several human and mouse cell lines. For the mouse system, we used EL4 (ATCC ® TIB-39™) and RMA cells that are commonly referred to as T-lymphoma cell lines[180]. Besides these, we also FACS-isolated primary Treg ($CD25^{pos}Foxp3^{GFPpos}$) and Tconv ($CD25^{neg}Foxp3^{GFPneg}$) cells from $Foxp3^{GFP}$ mice. In the human system, we also isolated primary Treg ($CD25^{pos}$) and Tconv ($CD25^{neg}$) cells from healthy human donors. For cell lines, we used Jurkat T cells (ATCC ® TIB-152™), an acute T leukemia cell line, as well as CCRF-CEM (ATCC ® CCL-119™) and BE-13 as additional leukemic cell lines [181]. We then isolated RNA and prepared cDNA libraries for each cell type. We tested the expression levels of our candidate proteins via qPCR, and plotted the results in **Figure 25**. We observed that many of our candidate factors are overexpressed in human Tconv cells compared to primary Treg cells and leukemic cell lines. In the mouse system, we observed that some factors are also overexpressed in Tconv cells, but most factors are upregulated in both Treg and Tconv cells compared to cell lines. Importantly, none of the factors are strongly upregulated in EL4 T cells - this makes non-physiological tumor cell-line based overexpression of proteins as a source for binding patterns in the inverted ChIP unlikely. If we now search for our candidate proteins in a differential mouse Treg / Tconv proteome (derived from[182]), we cannot identify any bias in the expression pattern between mouse Treg and Tconv, validating our qPCR data.

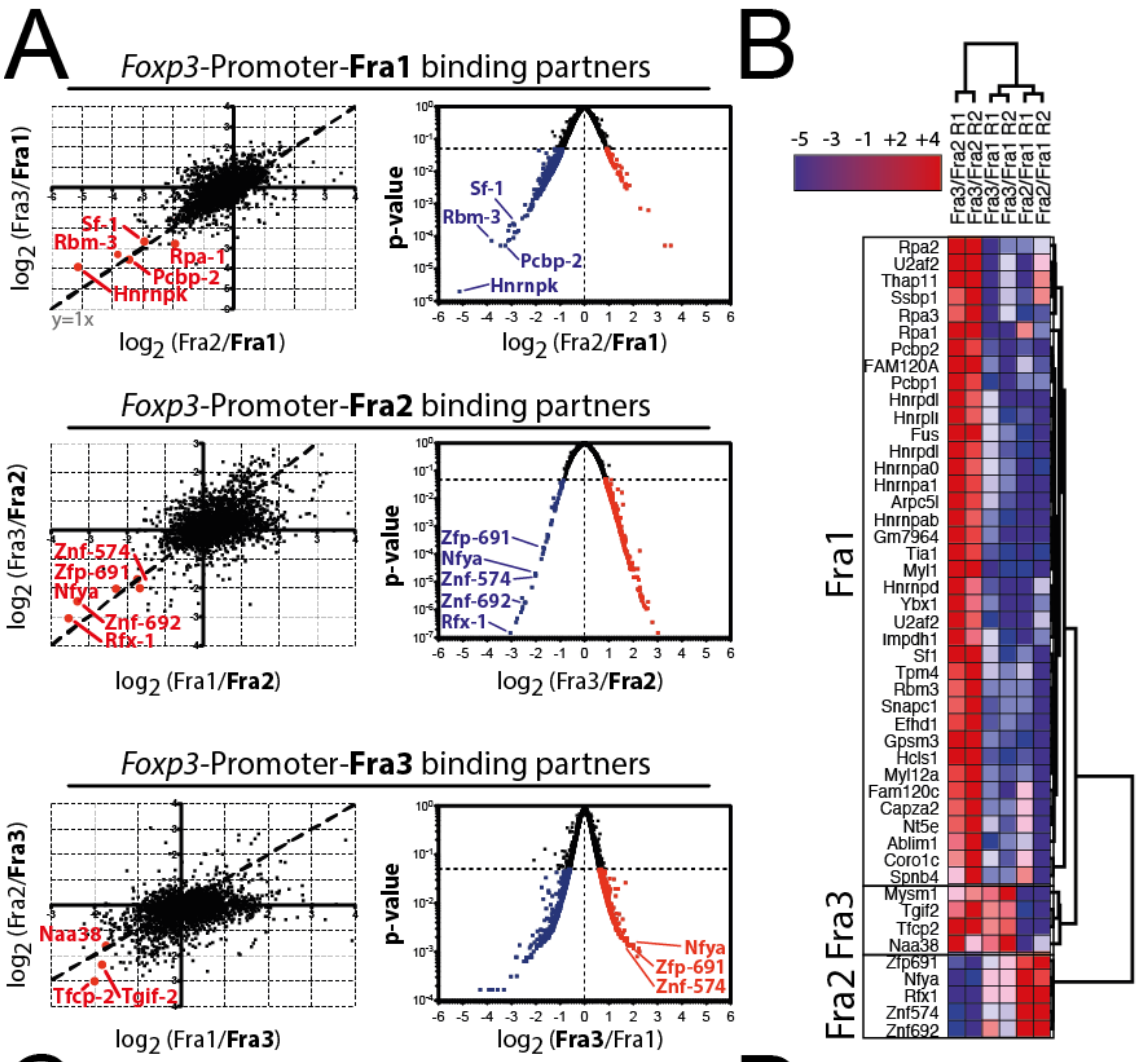

Foxp3-Promoter:	Fra1	Fra2	Fra3
Proteins Replicate 1	2658	2645	2648
Proteins Replicate 2	2723	2727	2727
Quantified Proteins	2349	2343	2348
FDR 1%, foldchange >3	106	97	93
p<0.05	38	5	4
Keyword: RNA-binding	16	0	1
Keyword: DNA-binding	11	5	3
Keyword: Transcript. Reg.	7	5	3

Figure 24: Results of the inverted ChIP with *Foxp3*-promoter Fra1, 2, 3 probes.
The left-hand dot plots in part A illustrate averaged relative binding of all detected proteins to Fra1, Fra2, or Fra3. Some selected candidates are highlighted. The p-value vs. relative binding plot on the right hand side adds the statistical evaluation of binding partners with a p-value calculation across all detected peptides from two replicates. To identify candidates, we filtered the candidate list with parameters shown in C. The heat map in B shows fragment-specific and significant binding partners via an unsupervised hierarchical clustering. Protein interaction analysis of several candidates in D shows an interrelated network of transcription factors.

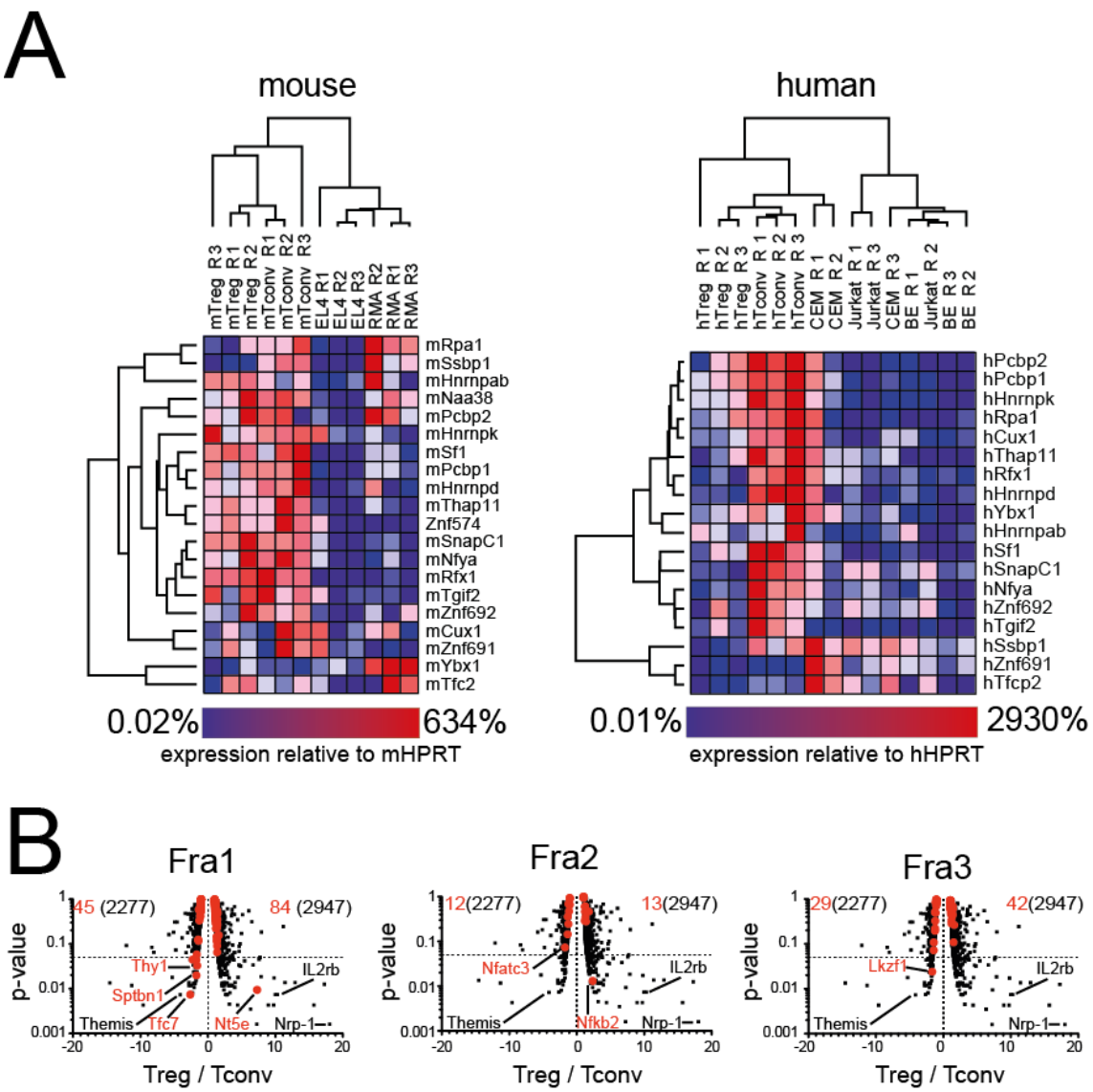

Figure 25: Gene expression analysis of target proteins in primary cells.

For our selected candidates, we tested their gene expression profile in primary Treg cells, primary Tconv cells and several cell lines in mouse and human background (A). To assess the differential expression profile of the *Foxp3*-binding candidates in murine Treg and Tconv cells on a protein level, we utilized the primary Treg/Tconv proteome data from M. Barra et al. [182] and mapped it to our dataset. We used candidate proteins with selective binding to only one fragment with a fold change of at least 2. Out of 153 proteins specifically binding to Fra1, we were able to map 129 to the Treg/Tconv proteome (Fra2: 25 out of 40, Fra3: 72 out of 98). We then overlaid the candidate proteins for each fragment onto the differential proteome in part B and highlighted some candidate proteins. On top of each graph, we indicate the total number of proteins up-or downregulated in Treg vs. Tconv cells, as well as the number of candidate proteins up-or downregulated in the Treg/Tconv proteome dataset.

Stable expression of our candidate proteins in cell culture systems

The table in **Figure 26** provides an overview of genes cloned into the pDEST26 ® and pMSCV-CD90.1® expression system. To avoid vector mix-ups and prove plasmid integrity, we transfected 293 cells with each plasmid, followed by RNA isolation, cDNA synthesis and gene expression measurement by qPCR. When we overexpressed a specific transgene, for example encoding the *Rpa1* gene, and analyzed the gene expression profile against all our candidate proteins, we only detected a high increase in mRNA for *Rpa1*, but not for others. This was the case for all genes observed except the *Ssbp1* transgene, which seems to also induce *Rfx1* mRNA. This could indicate cross-regulation of both proteins. Before performing extended *in-vitro* luciferase screens, we also tested transgene expression and protein production with FLAG ®-tagged expression vectors (**Figure 26C**). We were able to show that transgenes in pDEST26® and viral vectors are expressed and its protein products run at the specified molecular weight.

Most candidate proteins downregulate *Foxp3* gene expression or have no effect

We tested our candidate proteins in HEK 293 cells transfected with a full *Foxp3* promoter luciferase vector. We also cloned small *Foxp3* promoter luciferase vectors containing Fra1, Fra2 and Fra3 *Foxp3* promoter elements (**Figure 27A**). Then, we tested a positive control, the *Nr4a1* gene, and its effects on *Foxp3* expression (**Figure 27B**). As published, Nr4a1 specifically induces luciferase gene expression at the Full *Foxp3* promoter, but not at the basic (control) pGL3 vector or the Fra1-*Foxp3* promoter vector. Nr4a1 is reported to bind the *Foxp3* gene promoter, but probably not the most proximal promoter. Furthermore, we validated GFP as a control since it does not induce gene expression at any of our vectors. With these controls in place, we tested all our candidate proteins against the Full *Foxp3* promoter vector as well as each Fra1, Fra2, or Fra3 vector individually. The normalized data for the Full *Foxp3* promoter are shown in **Figure 27C**. We were able to show that some candidates specifically downmodulate *Foxp3* gene expression. When observing only one specific gene, Zinc finger protein 574, a sequence-specific regulatory behavior can be identified: whereas the protein downmodulates expression on the Full *Foxp3* promoter, it does not bind the *Foxp3* Fra1 promoter. Its weak binding to this region had also been predicted by our MS data. But since binding is predicted to Fra2, as well as to Fra3 with a lower intensity, we also see downregulation at these specific loci.

A

Gene	Destination Vector	Fragment binding	Vector size	Origin	pENTR cloning TA	Sequence verified
Hnrnpk	pDEST26	Fra1	7283 bp	cDNA	60°C	YES
Rpa1	pDEST26	Fra1	7703 bp	cDNA	60°C	YES
Naa38	pDEST26	Fra3	6122 bp	cDNA	60°C	YES
Tgif2	pDEST26	Fra3	6545 bp	cDNA	60°C	YES
Znf574	pDEST26	Fra2	8534 bp	6816316	56°C	YES
Thap11	Sport6	Fra1	6749 bp	cDNA	60°C	YES
Ybx1	pDEST26	Fra1	6000 bp	3481736	60°C	YES
Pcbp2	pDEST26	Fra1	6836 bp	cDNA	60°C	YES
Pcbp1	pDEST26	Fra1	6902 bp	3588737	66°C	YES
Ssbp1	pDEST26	Fra1	6290 bp	cDNA	60°C	YES
Nfya	pDEST26	Fra2	6872 bp	cDNA	60°C	YES
Snapc1	pDEST26	Fra1	7001 bp	cDNA	62°C	YES
Znf691	pDEST26	Fra2	6683 bp	cDNA	60°C	YES
Rfx1	pDEST26	Fra2	8723 bp	cDNA	67°C	YES
Sf1	pDEST26	Fra1	2389 bp	cDNA	67°C	YES
Znf692	pDEST26	Fra2	7798 bp	cDNA	56°C	YES
Tfcp2	pDEST26	Fra3	7511 bp	5098336	67°C	YES

B

Gene expression (%Gapdh)

Transfected pDEST plasmid — Top 1 or top 2 item (s) highlighted in red and bold

Sybr-Primer	Plasmid		Hnrnpk	Rpa1	Naa38	Tgif2	Znf574	Thap11	Ybx1	Pcbp2	Pcbp1	Ssbp1	Nfya	Snapc1	Znf691	Rfx1	Sf1	Znf692	Tfcp2
	Plasmid ID	H2O	252	248	244	242	255	257	258	251	253	246	243	247	254	250	249	256	245
	mHnrnpk	0,00	85,40	0,20	0,20	0,20	0,30	0,20	0,40	1,20	0,90	0,00	0,00	0,00	0,40	0,30	1,00	1,40	2,80
	mRpa1	0,00	0,00	174,50	0,00	0,00	0,00	0,00	0,00	0,00	0,00	0,00	0,00	0,00	0,00	0,00	0,00	0,00	0,00
	mNaa38	0,00	0,00	0,00	1043,20	0,00	0,00	0,00	0,00	0,00	0,00	0,00	0,00	0,00	0,00	0,00	0,00	0,00	0,00
	mTgif2	0,00	0,00	0,00	0,00	177,20	0,00	0,00	0,00	0,00	0,00	0,01	0,08	0,00	0,01	0,01	0,02	0,05	0,08
	mZnf574	0,00	0,00	0,00	0,00	0,00	8,60	0,00	0,00	0,00	0,00	0,00	0,00	0,00	0,00	0,00	0,00	0,00	0,00
	mThap11	0,00	0,10	0,10	0,10	0,00	0,10	97,70	0,10	0,00	0,10	0,11	0,09	0,00	0,10	0,06	0,07	0,06	0,07
	mYbx1	0,00	18,20	22,60	24,90	29,10	21,50	32,40	478,30	45,50	46,80	35,65	44,75	34,92	42,43	23,83	44,78	33,17	40,05
	mPcbp2	0,00	6,20	5,80	7,20	6,70	5,10	6,00	9,30	208,60	7,40	8,62	7,41	7,39	8,26	4,26	8,15	4,91	5,39
	mPcbp1	0,00	0,00	0,00	0,00	0,00	0,00	0,00	0,00	0,00	1008,40	0,01	0,01	0,01	0,01	0,00	0,01	0,01	0,02
	mSsbp1	0,00	0,00	0,00	0,00	0,00	0,00	0,00	0,10	0,10	0,10	28,50	0,01	0,01	0,01	0,01	0,01	0,01	0,02
	mNfya	0,00	0,00	0,00	0,00	0,00	0,00	0,00	0,10	0,10	0,10	0,04	201,67	0,04	0,07	0,03	0,06	0,04	0,05
	mSnapc1	0,00	0,00	0,00	0,00	0,00	0,00	0,00	0,00	0,00	0,00	0,00	0,00	281,28	0,00	0,00	0,00	0,00	0,00
	mZnf691	0,00	0,00	0,00	0,00	0,00	0,10	0,00	0,00	0,00	0,00	0,00	0,00	0,00	672,72	0,00	0,00	0,00	0,00
	mRfx1	0,00	0,00	0,00	0,00	0,00	0,00	0,00	0,00	0,00	0,00	42,69	0,00	0,00	0,00	0,64	0,00	0,00	0,00
	mSf1	0,00	0,00	0,00	0,00	0,00	0,00	0,00	0,00	0,00	0,00	0,01	0,01	0,03	0,01	0,00	153,58	0,01	0,00
	mZnf692	0,00	0,00	0,00	0,00	0,00	0,00	0,00	0,00	0,00	0,00	0,00	0,00	0,00	0,00	0,00	0,00	42,37	0,00
	mTfcp2	0,00	0,00	0,00	0,00	0,00	0,00	0,00	0,00	0,00	0,00	0,00	0,00	0,00	0,00	0,00	0,00	0,00	356,77

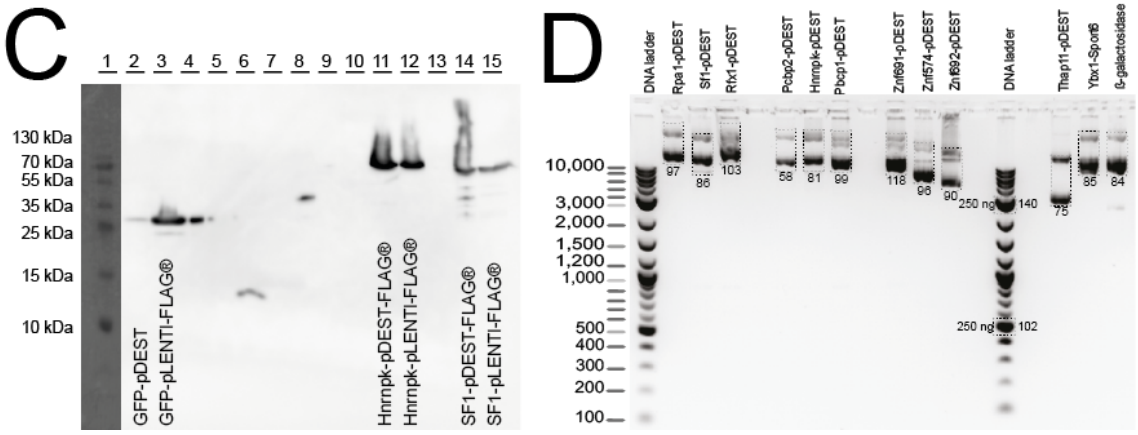

Figure 26: Molecular cloning of candidate genes and gene expression controls.
First, we cloned target gene cDNA into a pENTR® vector system. The annealing temperature (TA), origin of the PCR product (mouse cDNA or order from Thermo Open Biosystems), and size of the destination vector are shown in table A. In B, we compared the selective transgene expression in HEK293 cells that were transfected with the respective eukaryotic production vector. Afterwards, we isolated RNA and measured gene expression via qPCR. In C, we utilized FLAG®-tagged vectors and overexpressed our candidate genes in HEK293 cells. After lysis, proteins were separated via SDS-PAGE and blotted followed by staining with an anti-FLAG® antibody. We finally compared DNA integrity and concentration of each expression plasmid in graph D, where non-linearized intact vectors run at a higher DNA marker size than predicted.

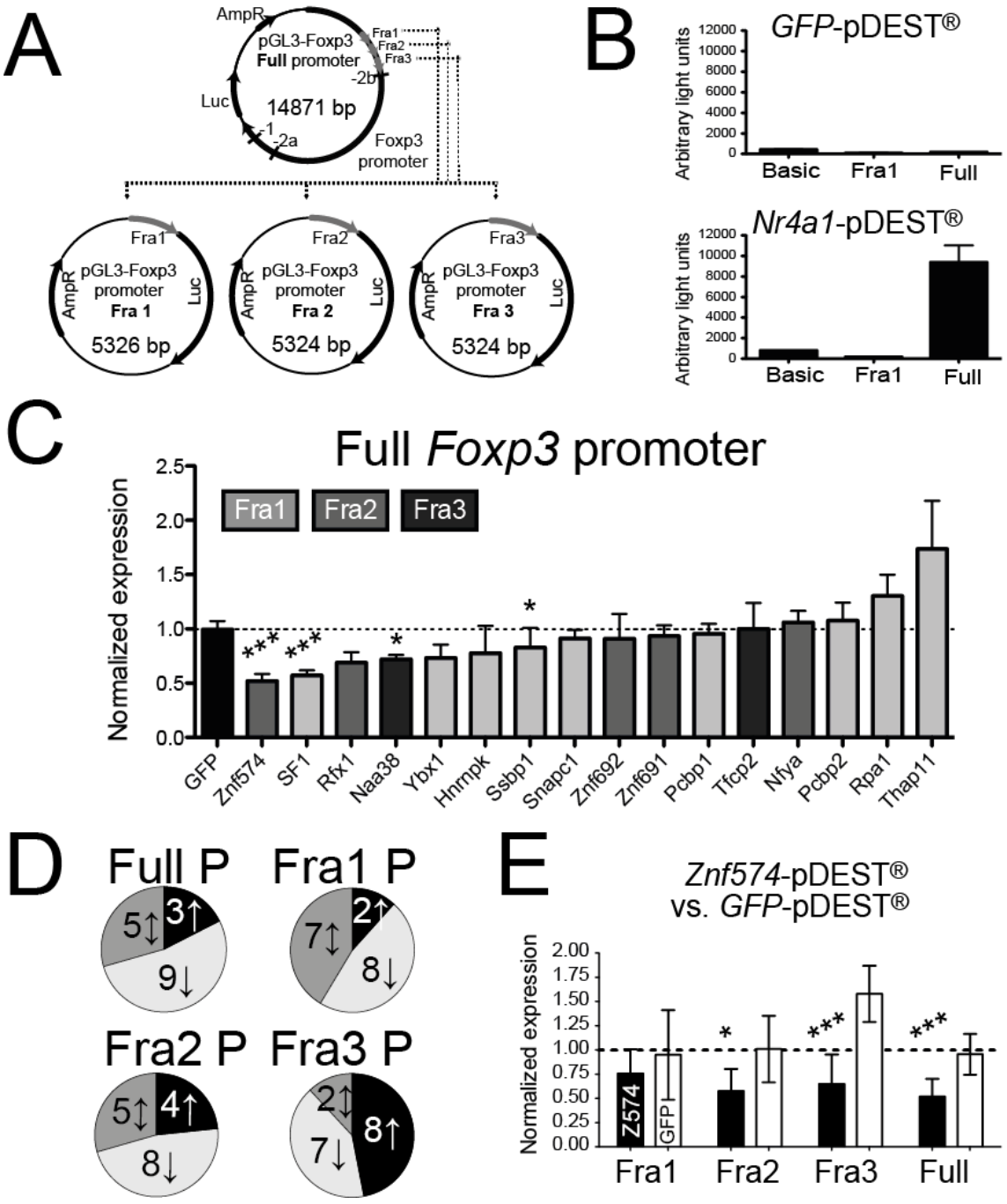

Figure 27: Luciferase-based evaluation of candidate proteins in HEK 293 cells.
We used a *Foxp3* promoter luciferase vector to clone small constructs containing the *Foxp3* promoter Fra1, Fra2, or Fra3 (A). As a positive control, we tested Nr4a1 against the Full *Foxp3* luciferase vector and the promotorless pGL3 luciferase basic vector (B). In C, we tested all candidate proteins against the Full *Foxp3* promoter vector. Data are representative of four or more independent experiments with two biological/technical replicates each. Statistical evaluation was performed using a two-tailed non-parametric Mann-Whitney t test against GFP controls. This experimental setup was utilized also for Fra1, Fra2 and Fra3 short luciferase vectors (D). If the average normalized luciferase expression was more than GFP, candidates were classified as upregulators. If the average luciferase expression was less than GFP, candidates were considered downregulators. In E, we show Zinc finger protein 574 and its normalized expression values across all four *Foxp3* luciferase fragments tested with this assay.

Some candidates downregulate T-cell receptor induced *Foxp3* promoter activity

Since we established that our candidates are mostly gene-repressing factors, we were interested in testing them in a T-cell line under TCR-stimulation conditions. Therefore, we introduced a system where Jurkat T cells were electroporated with the Full *Foxp3*-luciferase vector followed by T-cell receptor stimulation with PMA and Ionomycin (**Figure 28A, B**). We observed that TCR stimulation causes a 10-fold increase in luciferase activity of the *Foxp3* promoter as compared to TCR-stimulated Jurkat T cells tested with a promoterless luciferase plasmid. Next, we tested all our factors against the Full *Foxp3* luciferase vector to determine whether some of those can downmodulate TCR-induced *Foxp3* promoter gene activity (**Figure 28 D)**. Some candidates did indeed downregulate luciferase activity, and these effects were not seen with the control luciferase vector (**Figure 28 C)**. This dataset shows that some of our factors have the ability to downmodulate PMA/Ionomycin-stimulated *Foxp3* promoter activity.

Testing of candidate proteins in primary *in-vitro* induced Treg cells

Since our cell-culture derived testing methods showed promising *Foxp3* promoter inhibitory activity, we now wanted to test our factors in primary T cells. Therefore, we re-cloned all vectors into pMSCV-CD90.1 ® viral expression vectors and manufactured virus in PhxEco cells, a variant of HEK293 cells. Then, we isolated primary mouse Tconv cells and cultivated them under CD3/28 stimulation and TGF-β conditions to induce Foxp3 (iTreg cells). Then, we transduced these cells with retrovirus carrying the candidate genes and measured Foxp3 protein expression after 4 days (**Figure 29**). To evaluate our dataset, we compared Foxp3 expression in non-transduced T cells (CD90.1 negative) and candidate-gene transduced T cells (CD90.1-positive). When transducing a control vector (which does not carry any transgene), no differences in Foxp3 expression were observed, as expected. When transducing T-cells with *Foxp3*-pMSCV ®-CD90.1, retrovirally-transduced cells had almost twice as much Foxp3 expression compared to non-transduced cells in the same well. Once we tested all our candidate factors in this system, we could not detect any significant downmodulation of *Foxp3* gene expression, neither in percentage nor median fluorescence intensity (MFI) values. This could indicate that our factors operate in a TGF-β pathway-independent manner; especially, since *Foxp3* gene expression is initiated via binding of TGF-β response elements to the CNS1, but not to the *Foxp3* gene promoter.

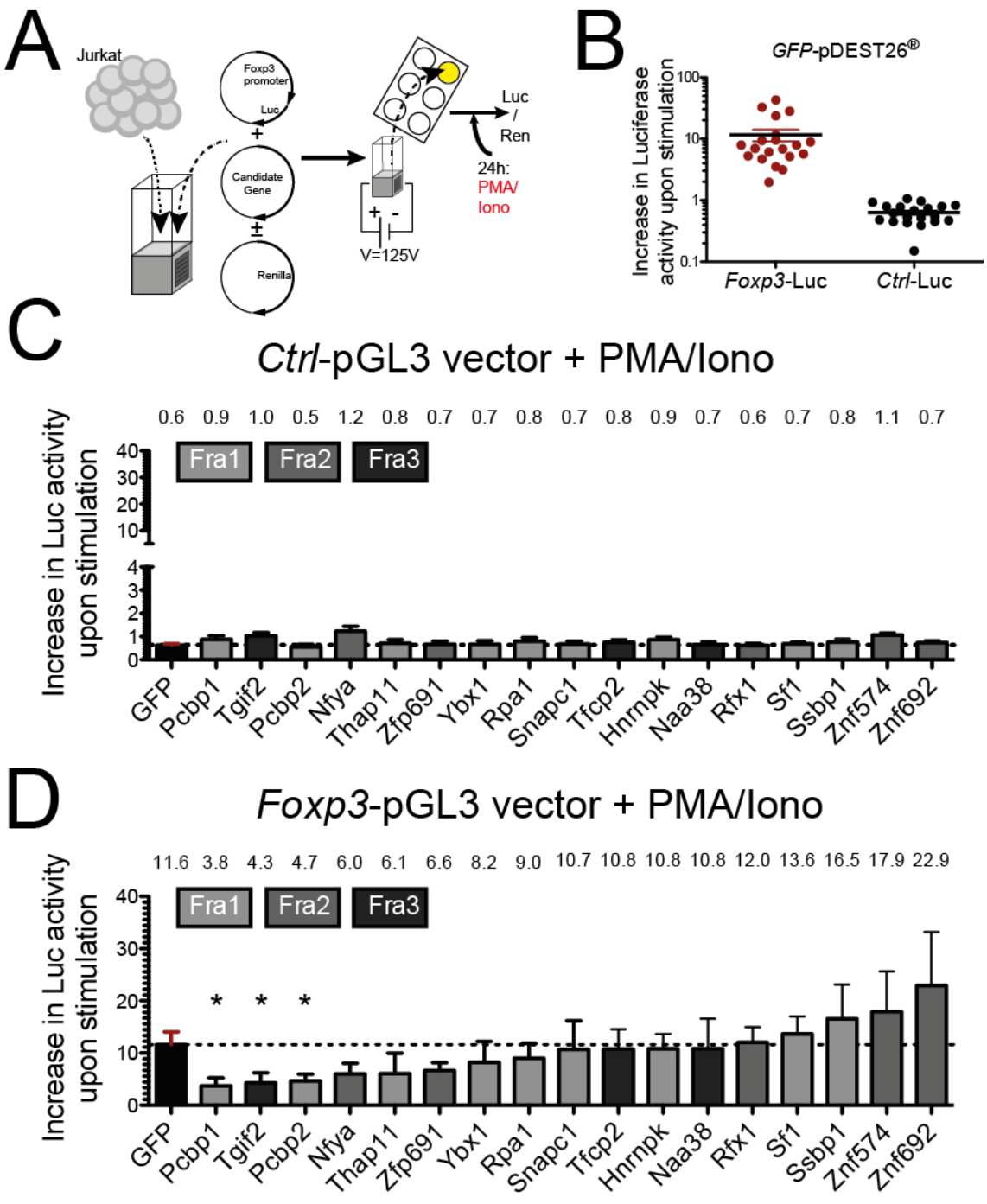

Figure 28: Luciferase-based testing of candidate proteins in Jurkat cells.

To test the effects of our candidate proteins on TCR-stimulated *Foxp3* gene induction, we used Jurkat T cells and electroporated them with a uciferase reporter plasmid, a candidate gene and a Renilla normalization vector. Cells were then either stimulated for 24h with PMA and Ionomycin or left unstimulated. Luciferase intensities were measured afterwards (schematic shown in A). The assay-specific increase in *Foxp3*-pGL3 luciferase activity is shown in B. In C, we show data across five independent experiments with the pGL3 basic vector. Once the basic vector is replaced with the Full *Foxp3* luciferase vector, down – or upregulation of *Foxp3* induction by electroporated vectors can be measured (D). Values above the bar graphs indicate average increase in Luc activity upon stimulation, compared to non-stimulated cells. Statistical analysis was performed using a non-parametric two-tailed Mann-Whitney t test against the GFP control.

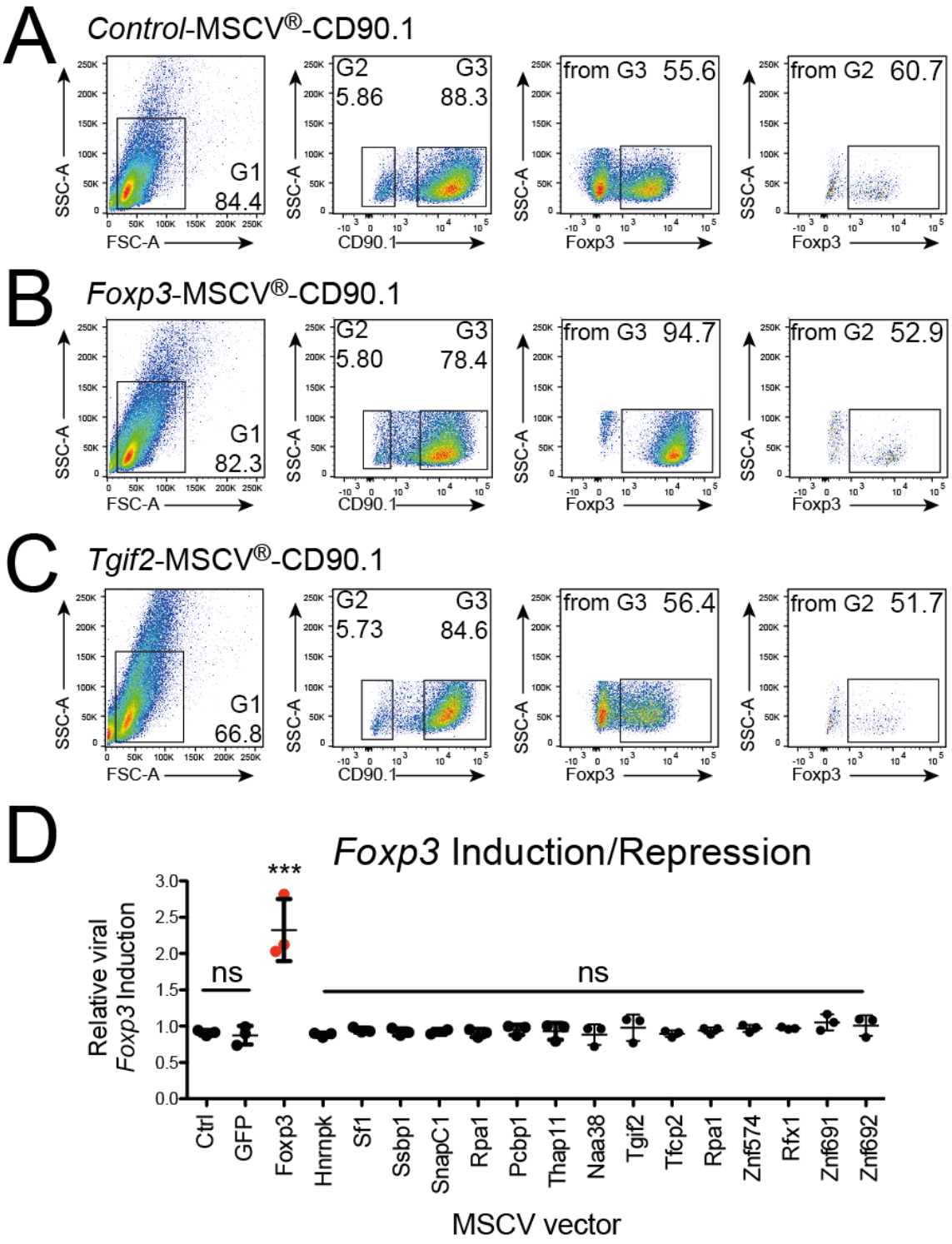

Figure 29: Viral overexpression of candidate proteins in induced Treg cells.
We transduced primary iTreg cells with murine stem cell virus (MSCV) produced in PhxEco cells. As controls, we used a control vector without transgene (A) or a *GFP*-pMSCV® vector. We gated on CD90.1-positive (virus-transduced) and CD90.1-negative (non-transduced) iTreg cells and quantified Foxp3 expression levels. As a positive control, we used a *Foxp3*-pMSCV®vector (B). With this experimental layout, we transduced all factors into iTreg cells (C, D) and quantified Foxp3 protein expression across four independent experiments. Data for relative viral Foxp3 induction are shown in the bar graph, with statistical evaluation performed by Mann-Whitney t testing.

7.4 Rbpj and its function for Treg cell homeostasis

Rbpj is upregulated in Treg cells on protein and RNA level

We analyzed the RNA expression of Rbpj in $CD4^{pos}CD25^{pos}Foxp3^{GFPpos}$ Treg cells versus $CD4^{pos}CD25^{neg}Foxp3^{GFPneg}$ Tconv cells from various tissues such as axial lymph node (LN), brachial LN, cervical LN, inguinal LN, mesenteric LN, spleen, thymus, colon, skin, fat, and liver from *Foxp3*^{GFP} animals (**Figure 30**). We observed an upregulation of Rbpj mRNA in Treg cells from most tissues. Furthermore, we also evaluated the expression of Rbpj in a proteomic dataset previously generated in our lab [182]. We identified RBPJ to be upregulated 1.5 fold in Treg cells with high confidence (p=0.056).

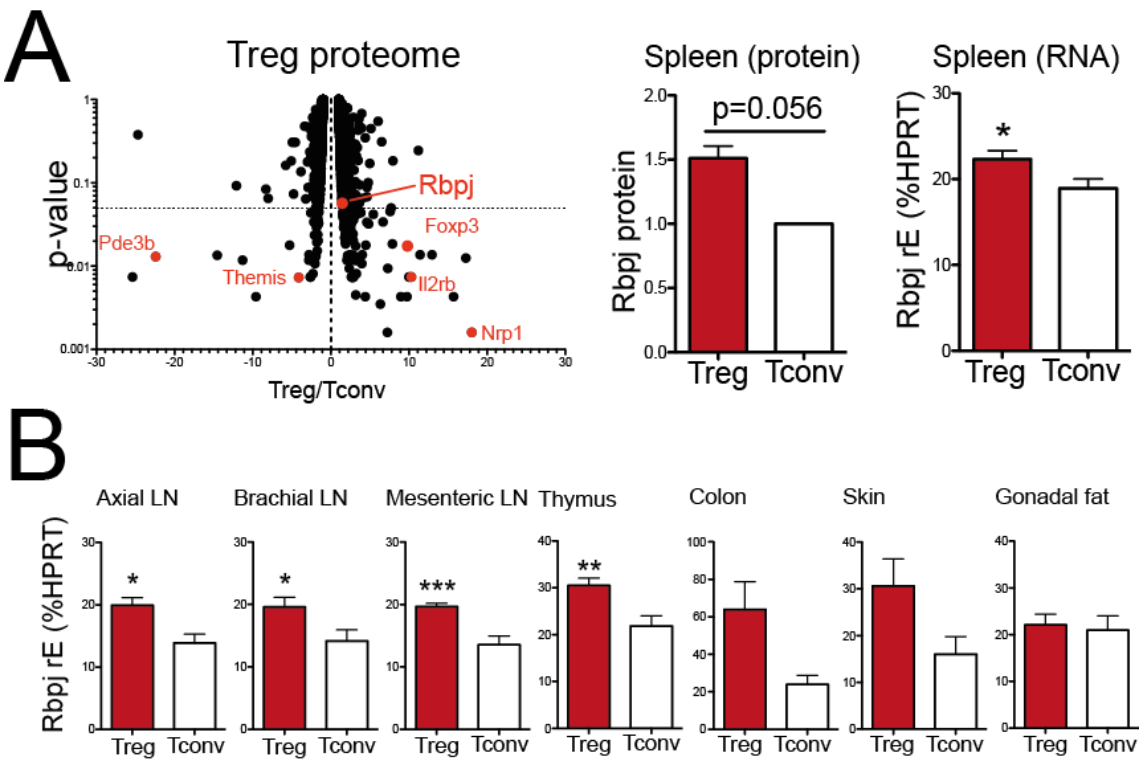

Figure 30: Rbpj expression levels in Treg and Tconv.

We investigated the expression strength of Rbpj in Treg vs. Tconv cells on protein and RNA level. The differential Treg/Tconv proteome dataset was derived from M. Barra et al. [182], whereas qPCR data were generated from FACS-isolated primary T cells. Part C shows the upregulation of Rbpj in Treg cells from various tissues. The data are representative of three or more biological replicates, and statistical significance was determined using the non-parametric Mann-Whitney t test with *p<0.05, **p<0.01, and ***p<0.001.

Notch Signaling is not active in steady state Treg cells

Following the observation that Rbpj is upregulated in Treg cells, we investigated the activity of the Notch signaling pathway in steady-state Treg cells from a *Notch*^{eGFP} reporter mouse in **Figure 31**. In this mouse, an Rbpj response element with four Rbpj binding sites and a minimal VS-40 promoter is linked to an eGFP reporter. As soon as Notch-receptor cross-linking releases the Notch intracellular domain, it can bind Rbpj at the reporter vector and induce GFP expression [176].

We stained peripheral Treg and Tconv cells from spleen and lymph nodes as well as thymic double-negative stage 1-4 thymocytes and measured eGFP intensities. In accordance with the literature, Notch signaling was induced following the DN1 stage, being highest at the DN2 and DN3 stages and declining again following the DN4 stage. In peripheral T cells, we detected virtually no *Notch* ^{eGFP} reporter activity in both Treg and Tconv cells. Furthermore, we stained for the expression of the Notch1 receptor. Again, only DN2 and DN3 thymocytes express high levels of Notch1, whereas mature Treg and Tconv cells did not express this receptor under steady-state conditions. The Notch1R flow cytometry data were supported by mRNA expression profiling for DN thymocytes and peripheral T cells.

Breeding of *Foxp3*^{Cre} mice with *Rbpj*^{floxed} mice specifically eliminates Rbpj in Tregs

Next, we wanted to investigate the effects of an Rbpj-specific deletion in Treg cells. Therefore, we crossed our *Foxp3* $^{YFP\text{-}Cre}$ mice with *Rbpj* ^{floxed} mice (see **Figure 32**). We expected a specific deletion between exon 6 and 7, making Rbpj functionally defective. In fact, we observed a clear deletion of *Rbpj* (Exon 6-7) on genomic DNA level from FACS-isolated Treg cells, but not Tconv cells, in *Foxp3*^{Cre}*Rbpj*$^{\Delta/\Delta}$ animals. We validated this Treg-specific deletion also on RNA level, where no differences were observed for Exon 1 *Rbpj* mRNA, but for Exon 6-7 *Rbpj* mRNA. Finally, we stained FACS-isolated Treg and Tconv cells from *Foxp3* ^{Cre}*Rbpj*$^{\Delta/\Delta}$ and *Foxp3* ^{Cre} animals with an anti-Rbpj mAb in a Western Blot (**Figure 32D**). It became obvious that Rbpj protein is specifically and exclusively deleted in *Foxp3* ^{Cre}*Rbpj*$^{\Delta/\Delta}$ Treg cells, but not in Tconv cells from these mice.

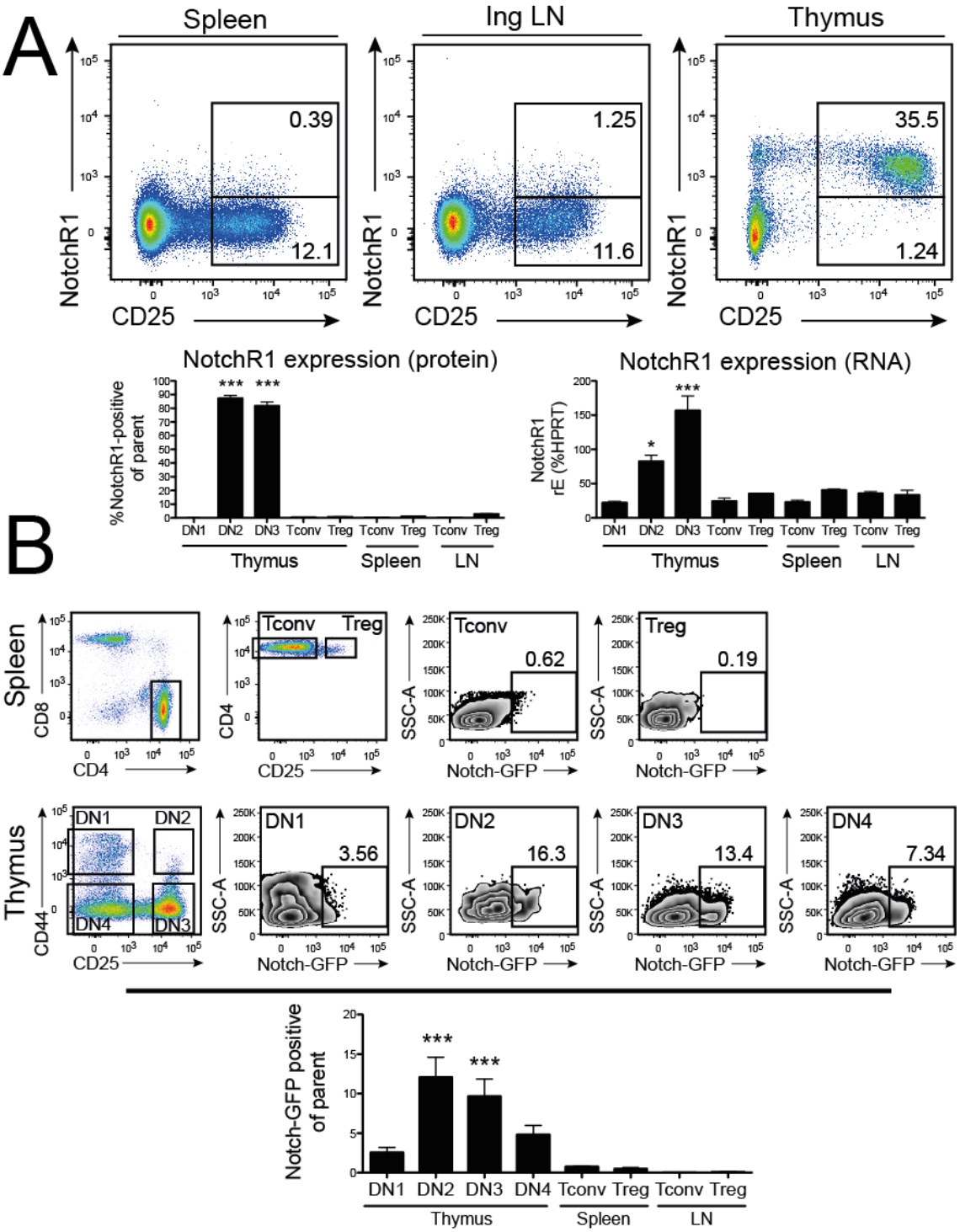

Figure 31: Notch receptor expression and Notch signaling in steady-state Tregs.
The dot plots in A show representative examples for Notch receptor 1 expression in Treg cells from spleen and lymph nodes as well as thymus-resident DN2/3 thymocytes. The bar graphs show average expression levels for at least four biological replicates on protein and RNA level. In part B, we investigated thymus-derived DN populations and splenic T cell populations for the activity of Notch-eGFP in a *Notch* ^{eGFP} reporter mouse. The dot plots show gating strategy and eGFP reporter signal intensity for each subpopulation. The bar graph is a representation of the analysis of four biological replicates. Statistical significance was determined using one-way ANOVA with Bonferroni post-test (*p<0.05, **p<0.01, and ***p<0.001).

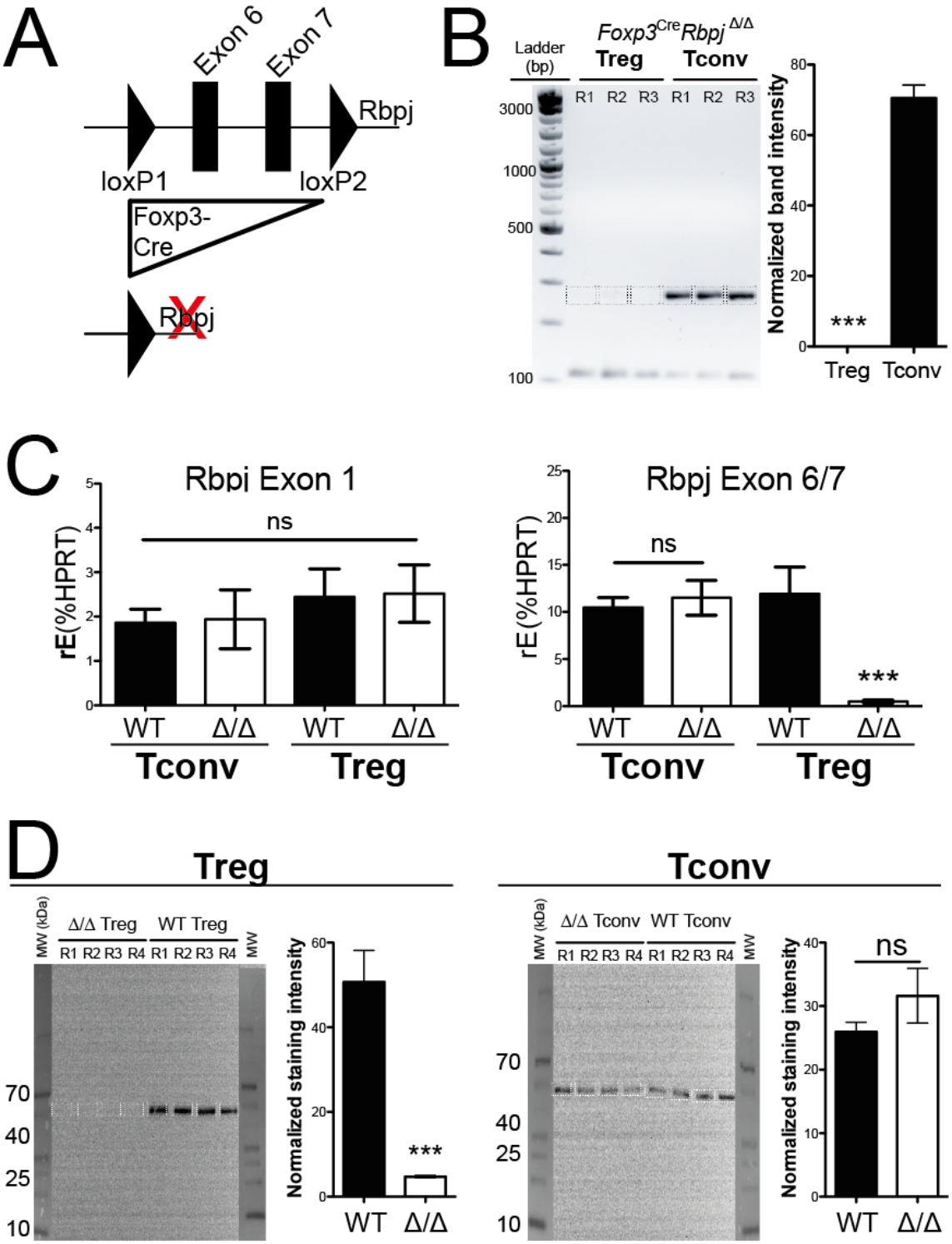

Figure 32: Treg-specific Rbpj deletion in *Foxp3*^{Cre}*Rbpj*$^{Δ/Δ}$ mice.

Part A illustrates the genomic location of *loxp* sites in the *Rbpj* gene. For graph B, we FACS-isolated Treg and Tconv from *Foxp3* ^{Cre}*Rbpj*$^{Δ/Δ}$ mice and measured the presence of exon 6-7 on genomic DNA level via PCR. In C, measured Rbpj RNA expression with exon 1 and exon 6-7 specific Taqman probes in Treg and Tconv cells via qPCR (C). Finally, we measured Rbpj protein in Treg and Tconv cells from *Foxp3* ^{Cre}*Rbpj*$^{Δ/Δ}$ and *Foxp3* ^{Cre} mice via Western Blot (part D). Bar graphs depict band intensity as measured via ImageJ software and normalized to background membrane/plot staining. Statistical significance was determined using unpaired t tests from three or four biological replicates (*p<0.05, **p<0.01, and ***p<0.001).

Some *Foxp3*^{Cre}*Rbpj*$^{\Delta/\Delta}$ mice spontaneously develop lymphadenopathies and inflammation

Upon careful investigation of our breeding, we detected signs of skin irritation in *Foxp3*^{Cre}*Rbpj*$^{\Delta/\Delta}$ mice. We observed skin abnormalities, indicating skin inflammation, as well as abnormalities on digits and tails reminiscent of psoriatic lesions. Some animals showed bloody lesions on ear and snout, probably due to extensive scratching. Once animals showed signs of skin irritation, we sacrificed them and analyzed them using gross pathology and flow cytometry. First, we observed lymphadenopathy of all easily accessible lymph nodes (axillary, brachial, cervical, inguinal) except mesenteric lymph nodes, which were protected from overt lymphadenopathy (**Figure 33**). Furthermore, an evident splenomegaly with more than twofold increase in organ weight (age-matched WT controls: spleen 111.4 ± 8.57 SEM vs. KO: spleen 278.0 ± 12.4 SEM, p-value <0.0001) as well as hepatomegaly with about 1.5 fold increase in weight (age-matched WT controls: liver 1263 ± 125.8 SEM vs. KO: spleen 1874 ± 31.72 SEM, p-value = 0.0026) was observed. No weight changes were observed for kidneys (WT: kidneys 382.0 ± 17.7 SEM vs. KO: kidneys 335.7 ± 24.2 SEM, p-value = 0.1864), heart (WT: heart 154.0 ± 19.6 SEM vs. KO: heart 148.6 ± 14.5 SEM, p-value = 0.8246) or overall mouse weight. Disease symptoms as described above presented from 5 weeks of age until 23 weeks of age, and breeding was usually discontinued beyond that time point. About 50% of *Foxp3*^{Cre}*Rbpj*$^{\Delta/\Delta}$ animals had no obvious disease at 23 weeks of age, this and the fact that we observed a widespread onset of disease (between 5-23 weeks of age) indicates that individual factors can modify the onset or progression.

Next, we studied Treg cell frequency and absolute Treg numbers in *Foxp3* ^{Cre}*Rbpj*$^{\Delta/\Delta}$ vs. *Foxp3*^{Cre} animals. We observed a strong increase in Treg frequency in spleen and lymph nodes, from about 15% of CD4 T cells in control animals to 30% and more in sick *Foxp3*^{Cre}*Rbpj*$^{\Delta/\Delta}$ animals (**Figure 33C**). Additionally, the absolute numbers of Treg cells increased about tenfold in individual tissues, as depicted in **Figure 33**D. We can conclude that the selective RPBJ knockout in Treg cells causes pathological disease symptoms reminiscent of autoimmune disease, with a strong increase in Treg cell frequency and absolute tissue numbers.

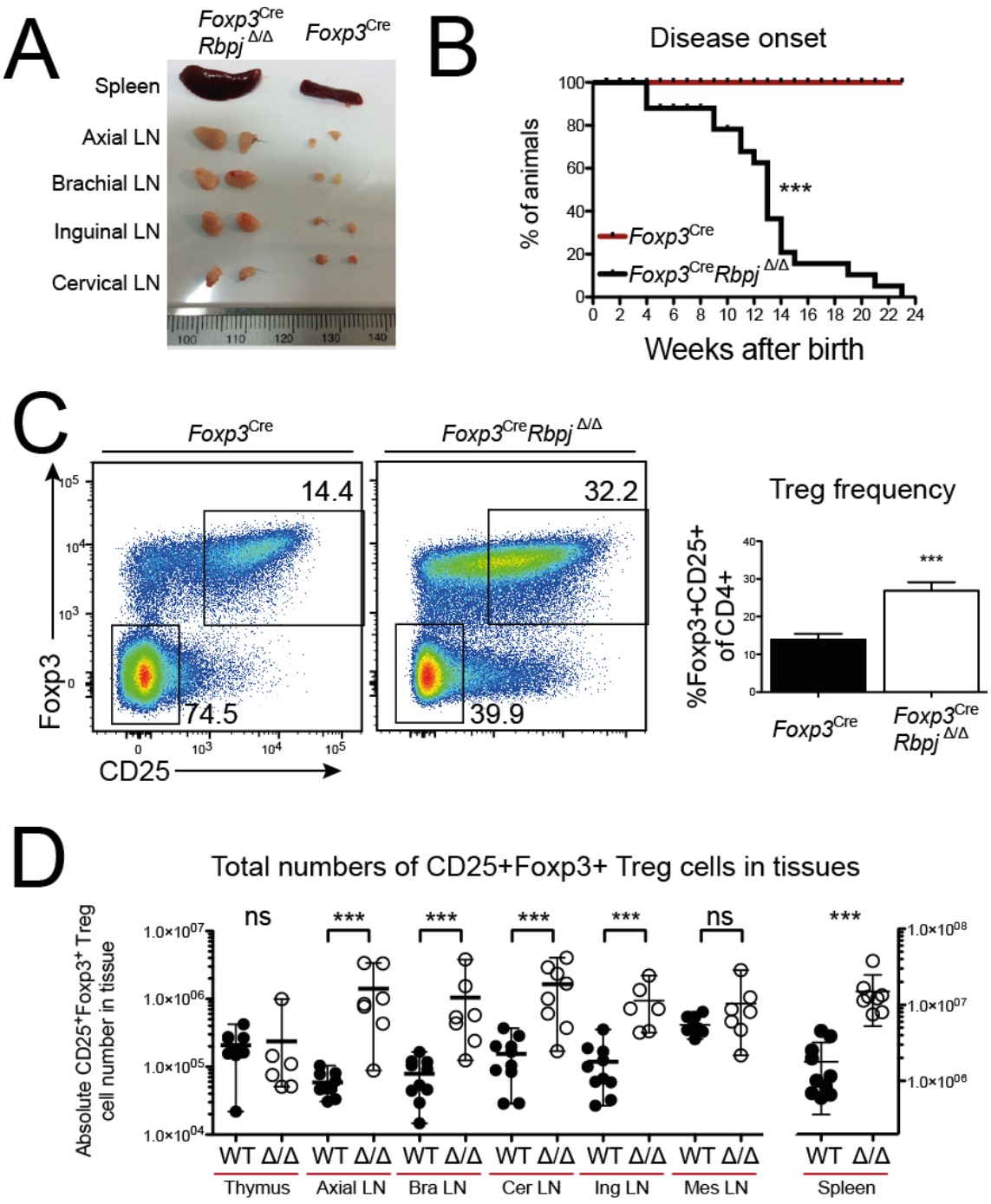

Figure 33: Consequences of Treg-specific Rbpj deletion in *Foxp3*^{Cre}*Rbpj*$^{Δ/Δ}$ mice.
The picture in A shows representative examples of splenomegaly and lymphadenopathy in *Foxp3*^{Cre} and sick *Foxp3*^{Cre}*Rbpj*$^{Δ/Δ}$ animals with evident pathological symptoms. These symptoms were observed in all sick *Foxp3* ^{Cre}*Rbpj*$^{Δ/Δ}$ animals shown throughout this paper. In B, we show the onset of disease of *Foxp3*^{Cre}*Rbpj*$^{Δ/Δ}$ and control animals for the duration of 23 weeks after animal birth. We do not show *Foxp3* ^{Cre}*Rbpj*$^{Δ/Δ}$ animals that did not develop disease until 23 weeks of age, which accounts to about 50% of all animals with Treg-specific Rbpj deficiency. Parts C and D show Treg cell frequency in sick *Foxp3*^{Cre}*Rbpj*$^{Δ/Δ}$ animals versus *Foxp3*^{Cre} controls. Each circle represents a single animal, and significance was determined using the Mann-Whitney t test (*p<0.05, **p<0.01, and ***p<0.001). Cell count measurements were performed in multiple experiments over an extended period of time.

Development of a 12-color flow cytometry panel to evaluate *Foxp3*^{Cre}*Rbpj*$^{\Delta/\Delta}$ mice

To investigate the systemic effects of Rbpj deletion in Treg cells, we established a 12-color/16-parameter flow cytometry panel as shown in **Figure 34**. It utilizes the fluorescent parameters GFP/YFP, PE, PE-Cy7, PerCP-Cy5.5, APC, APC-Cy7, BV 421, e506, BV 605, BV 711, BUV 395 and BUV 737 along with scatter parameters (FSC-H and FSC-W as well as SSC-H and SSC-W). We were able to evaluate the absolute number (with counting beads) and relative frequencies of CD4^{pos}CD25^{pos}Foxp3^{YFPpos} Treg cells, CD4 ^{pos}CD25^{neg}Foxp3^{YFPneg} Tconv cells, CD8 ^{pos} cytotoxic T cells, CD19 ^{pos} B-cells, NK1.1^{pos} NK cells, and CD11b ^{pos} and Ly6C ^{pos} subpopulations of myeloid cells in one staining. Furthermore, we included CD44 and CD62L as markers for memory phenotype on T and B cells.

Treg cells from *Foxp3*^{Cre}*Rbpj*$^{\Delta/\Delta}$ animals express Foxp3, Helios, GITR, CTLA-4, and Nrp-1

Since previous literature suggested that Treg cells deficient in Rbpj overexpress Treg-specific proteins such as Helios or Nrp-1, we were interested in the characterization of these Treg cells via flow cytometry. Therefore, we double-stained Treg cells and Tconv cells from various lymph nodes and spleen of sick *Foxp3* ^{Cre}*Rbpj*$^{\Delta/\Delta}$ and *Foxp3*^{Cre} animals for Foxp3 and other key Treg markers (**Figure 35**). First, we analyzed the expression of Helios, a marker of thymic-derived Treg cells, in Treg and Tconv populations. No significant differences in Rbpj-deficient Treg cells were observed. Next, we measured the expression of GITR. Interestingly, Tconv cells from sick *Foxp3*^{Cre}*Rbpj*$^{\Delta/\Delta}$ mice had slightly increased GITR levels, indicating active signaling via the TCR and heightened T-cell activation status [52]. Also, Rbpj-deficient Treg cells seem to have slightly elevated GITR levels. Staining for intracellular CTLA-4 revealed increased expression levels in Treg cells from axial and brachial lymph nodes in sick *Foxp3*^{Cre}*Rbpj*$^{\Delta/\Delta}$, but no other lymphoid tissues. Expression of Nrp-1 and CD86 was unaffected by the Treg-specific Rbpj deletion. Taken together, our data suggest that key proteins implicated in Treg suppressive capacity and Treg lineage identification are either expressed equally or increased in Treg cells from *Foxp3* ^{Cre}*Rbpj*$^{\Delta/\Delta}$ mice. The pro-inflammatory environment in sick *Foxp3*^{Cre}*Rbpj*$^{\Delta/\Delta}$ mice could cause some of those effects. In general, our data don't suggest that RBPJ-deficient Treg cells lose characteristic Treg markers, but maintain their Treg signature.

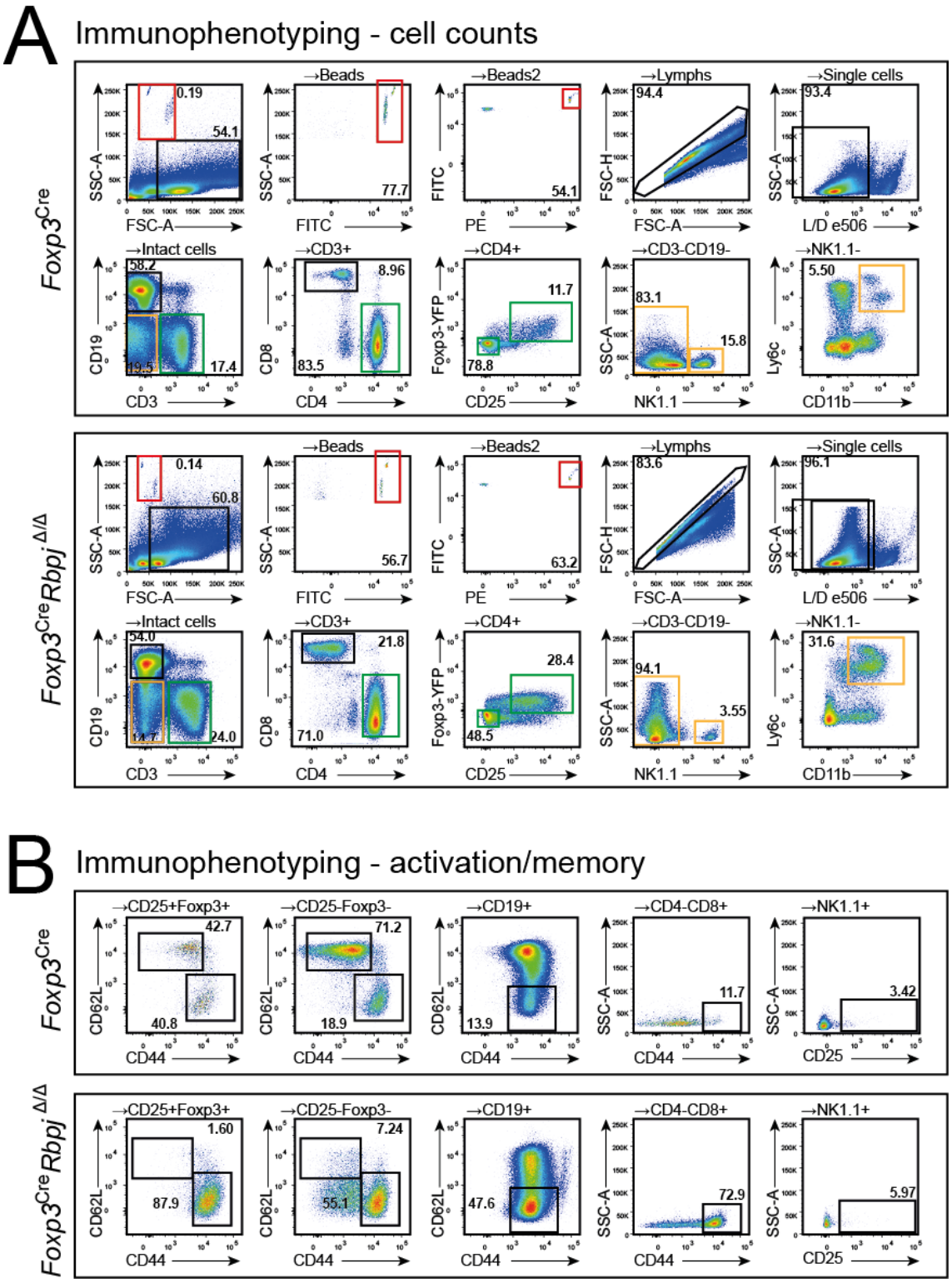

Figure 34: Overview of extended immunophenotyping panel and gating strategy.
We here show our 12-color/16-parameter flow cytometry panel used for the immunophenotypic evaluation in this study. Part A shows our gating strategy for cell counting of B cells, CD8 T cells, Treg cells, Tconv cells, NK cells, and myeloid-lineage cells. The upper rectangle is a representative example of a staining with wild type animal splenocytes followed by a staining with splenocytes from a sick *Foxp3* ^{Cre}*Rbpj*$^{\Delta/\Delta}$ animal with apparent signs of pathology. In section B, we show the expression of memory markers / activation markers on Treg cells, Tconv cells, CD8 T cells, B cells and NK cells. A statistical validation follows in later figures.

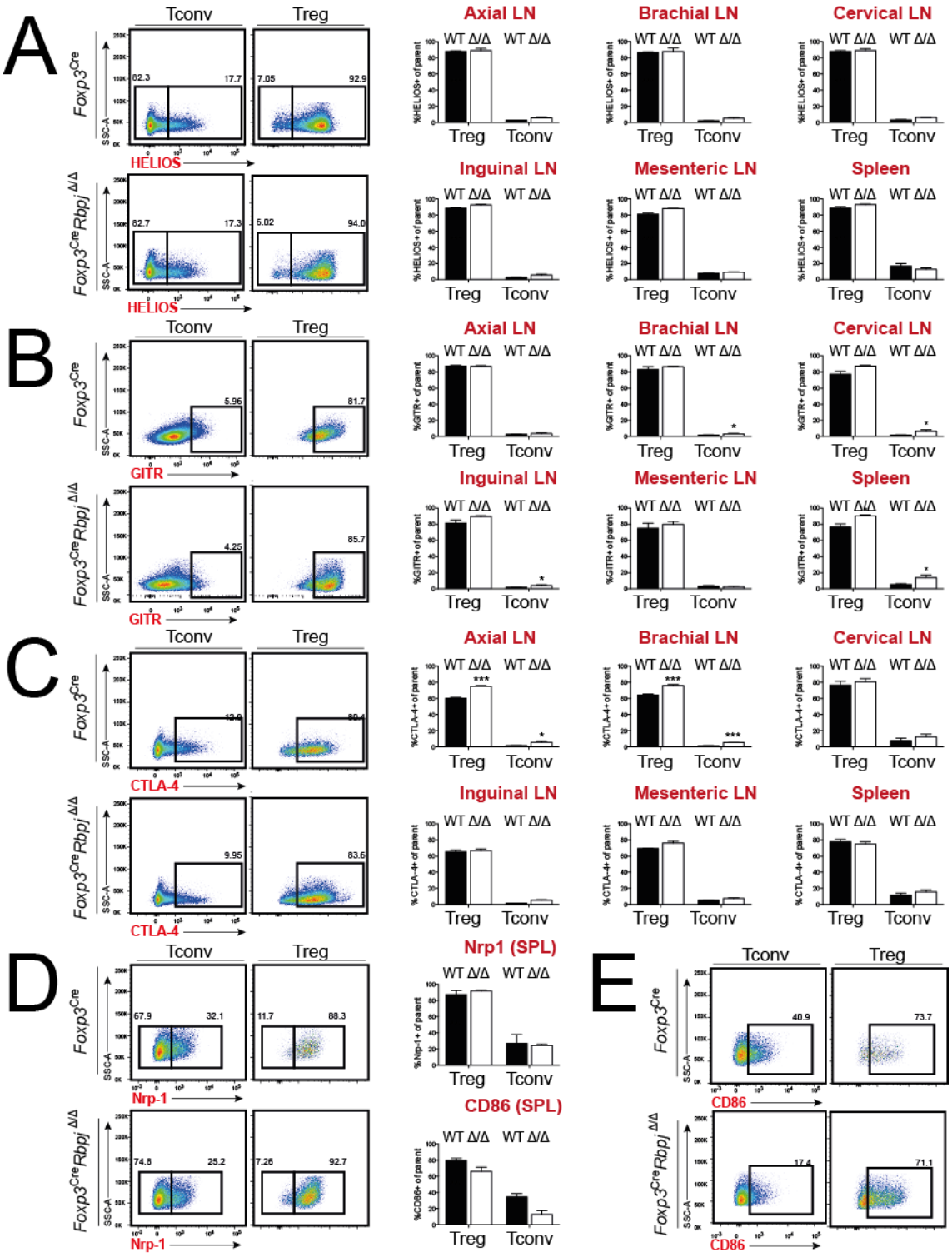

Figure 35: Expression of key Treg proteins in RBPJ KO vs. WT Treg / Tconv cells. We stained for key Treg surface and intracellular proteins. We compared the presence of these specific markers in Treg cells as well as their absence in Tconv cells from sick *Foxp3* ^{Cre}*Rbpj* $^{\Delta/\Delta}$ and *Foxp3* ^{Cre} animals. In part A, we stained for the intracellular protein Helios, in B for the cell surface molecule GITR, in C for the cell surface receptor CTLA-4, in D for Neuropillin-1, and in E for CD86. Statistical significance was determined using unpaired t tests from three to eight biological replicates measured in separate experiments (*p<0.05, **p<0.01, and ***p<0.001). Due to separate measurements with individual machine settings, evaluation of median fluorescence intensity for individual protein stainings is not feasible.

Treg cells from *Foxp3*^{Cre}*Rbpj*$^{\Delta/\Delta}$ mice are suppressive and demethylated at the CNS2

To determine whether Treg cells from sick *Foxp3* ^{Cre}*Rbpj*$^{\Delta/\Delta}$ mice lose their suppressive capacity and thereby promote the pro-inflammatory environment observed in these animals, we performed an *in-vitro* suppression assay with congenically labeled T-responder cells and MHCII-positive APCs (**Figure 36**). Our data demonstrate that both Treg cells from *Foxp3*^{Cre}*Rbpj*$^{\Delta/\Delta}$ and *Foxp3*^{Cre} animals were suppressive *in-vitro*. Furthermore, we analyzed the methylation of the CNS2 / TSDR region, which is important for Treg cell lineage stability [36, 127, 183]. No differences were detected between Rbpj-deficient and -proficient Treg cells, both displaying strong demethylation at the TSDR locus. Tconv cells were hypermethylated at this site, as expected.

Treg cells from *Foxp3*^{Cre}*Rbpj*$^{\Delta/\Delta}$ mice are clonally diverse

To rule out single-clone expansion or malignant transformation of Rbpj-deficient Treg cells, we isolated genomic DNA from Treg cells of sick *Foxp3* ^{Cre}*Rbpj*$^{\Delta/\Delta}$ and *Foxp3* ^{Cre} animals. DNA was subjected to T-cell receptor sequencing and identification of TCR-β chains. In total, we identified 27718 ± 4689 (KO) vs. 39460 ± 6306 (WT) uniquely rearranged loci, indicating a modest decrease in clonality in Treg cells from sick *Foxp3*^{Cre}*Rbpj*$^{\Delta/\Delta}$ mice ($p=0.065$) This translates also in changed productive clonality with 0.1300 ± 0.0176 (KO) vs. 0.0506 ± 0.0091 (WT, $p<0.01$), indicating that Treg samples from sick *Foxp3* ^{Cre}*Rbpj*$^{\Delta/\Delta}$ mice have slightly more pre-dominant clones. Our summary in **Figure 36C** shows the most abundant clones for J01 and J02 chains, with only minor differences observed between Treg cells from sick *Foxp3*^{Cre}*Rbpj*$^{\Delta/\Delta}$ and *Foxp3*^{Cre} animals. From this, we can conclude that Treg cells from sick *Foxp3* ^{Cre}*Rbpj*$^{\Delta/\Delta}$ animals retain their polyclonal TCR repertoire, ruling out malignant conversion or single-clone expansion as reason for the increased Treg frequency.

Treg cells from *Foxp3*^{Cre}*Rbpj*$^{\Delta/\Delta}$ mice do not produce pro-inflammatory cytokines

We stimulated Treg cells from sick *Foxp3*^{Cre}*Rbpj*$^{\Delta/\Delta}$ and *Foxp3*^{Cre} animals with PMA/Ionomycin and measured intracellular expression of pro-inflammatory (IFN-γ, IL-2, TNF-α) and anti-inflammatory (IL-10) cytokines. Again, no differences were observed between Rbpj-deficient and -proficient Treg cells, indicating that the deletion of Rbpj in Treg cells does not mediate a pro-inflammatory conversion of this cell type.

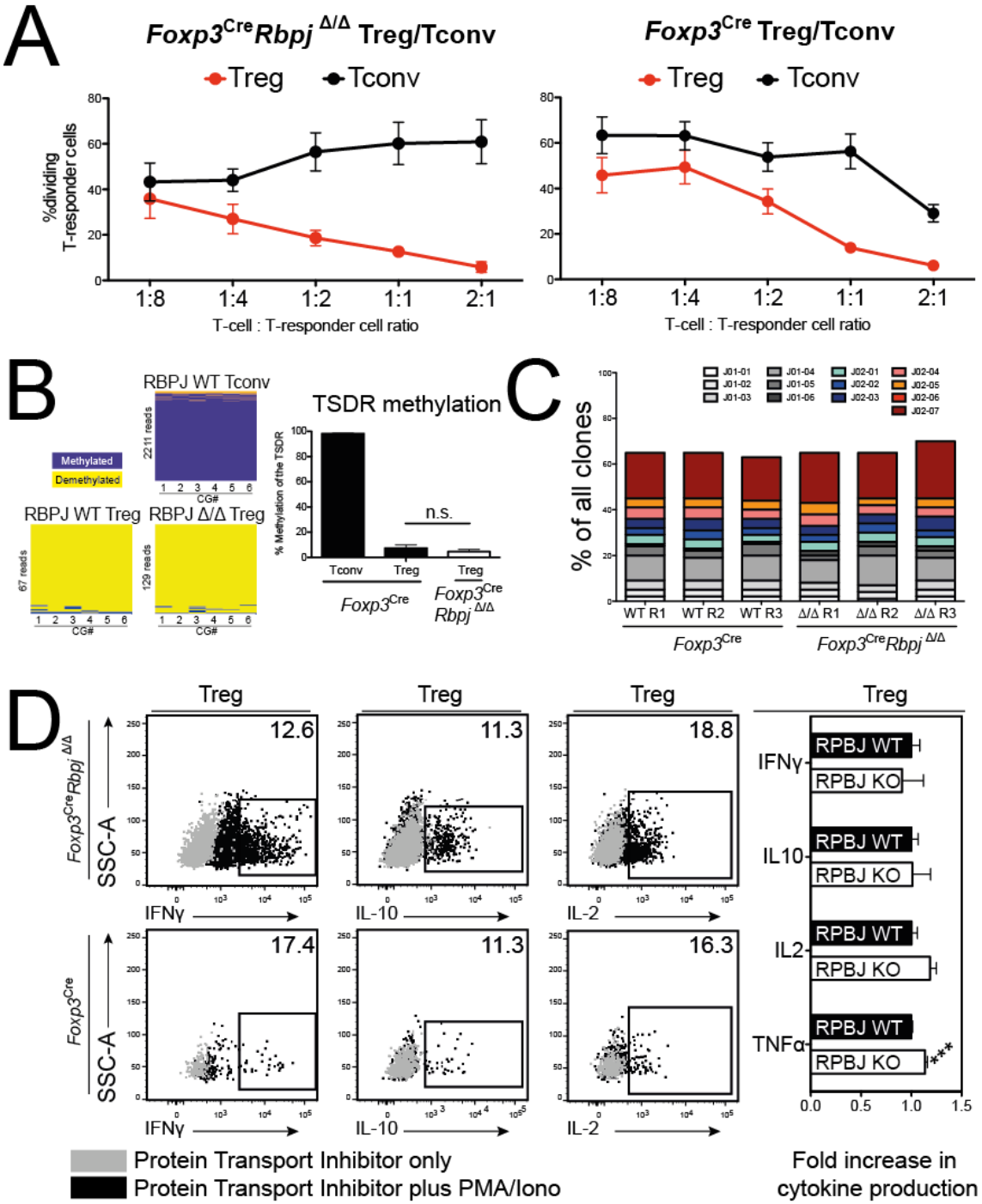

Figure 36: Comparison of Treg footprint and function in Rbpj-deficient Treg cells. We performed an *in-vitro* suppression assay (A) with Treg cells from sick *Foxp3* ^{Cre}*Rbpj*$^{\Delta/\Delta}$ (left) and *Foxp3* ^{Cre} (right) mice. In B, we measured CG methylation at the TSDR in the *Foxp3* gene promoter. The bar graphs are representative of three biological replicates. Furthermore, we assessed clonal diversity via TCR sequencing of Treg cells (C). The graph represents the clonal variety of J01 and J02 chains, respectively. In part D, Treg cells were isolated and incubated with or without PMA/Ionomycin in the presence of transport inhibitors. Intracellular cytokine expression was measured by flow cytometry. The bar graphs represent four biological replicates in two separate experiments. Statistical testing was performed with an unpaired student's t test with ns $p>0.05$ and ***$p<0.001$.

The selective deletion of RBPJ in Treg cells decreases cell death by apoptosis

Animals with a Treg-specific Rbpj deficiency display increased Treg cell number and frequency in spleen and lymph nodes. Since these cells do not express more Nrp-1 or Helios, we can rule out peripheral conversion of Tconv into Treg as source of the largely increased Treg cell compartment. Since increased proliferation or reduced apoptosis of $Rbpj^{\Delta/\Delta}$ Treg cells could be responsible for elevated cell numbers, we stained for Caspase-3 expression in Treg and Tconv cells from healthy, but advanced-age $Foxp3^{Cre}Rbpj^{\Delta/\Delta}$, sick $Foxp3^{Cre}Rbpj^{\Delta/\Delta}$ animals, and $Foxp3^{Cre}$ controls. We observed a strong decrease in Caspase-3 expression, which correlated with an increase in Treg frequency on a per-animal basis (**Figure 37** A-B-C). To validate these data, we measured Annexin-V expression on Treg cells from sick $Foxp3^{Cre}Rbpj^{\Delta/\Delta}$ mice (**Figure 37** D-E). Based on Hoechst cell cycle measurements, we did not detect any differences between WT and KO Treg cells for their cycling behavior (part G) in sick animals, but a strongly significant increase in KI-67 expression indicates recent cell divisions (part F).

B cells increase in number, get activated and produce autoimmune antibodies

Using our extended 12-color immunofluorescence panel described earlier, we investigated the number and activation status of B cells in sick $Foxp3^{Cre}Rbpj^{\Delta/\Delta}$ animals vs. controls (**Figure 38**). First, we stained for the expression of L-selectin (CD62L), a protein usually expressed on naive T cells and required to extravasate into secondary lymphoid tissues. Interestingly, we could observe a significant decrease of L-selectin expression on B cells from lymph nodes and spleen, indicating activation and differentiation into a memory/effector-like phenotype. Also, the overall B-cell number was steadily increased in lymphoid tissues. Next, we analyzed levels of Ig subtype antibodies in the peripheral blood serum of sick $Foxp3^{Cre}Rbpj^{\Delta/\Delta}$ and control mice. We observed a strong increase in IgG1 and IgE antibody secretion, while IgG3 was downregulated, indicating a class switch as classically induced by IL-4 treatment[1]. Finally, we measured the quality of peripheral blood serum to bind SDS-PAGE separated gross protein isolates from various organs of RAG2 KO animals. Our data indicate that, at least for some organs, autoimmune antibodies are present in the peripheral blood serum of sick $Foxp3^{Cre}Rbpj^{\Delta/\Delta}$ animals, again indicating B-cell activation and maturation.

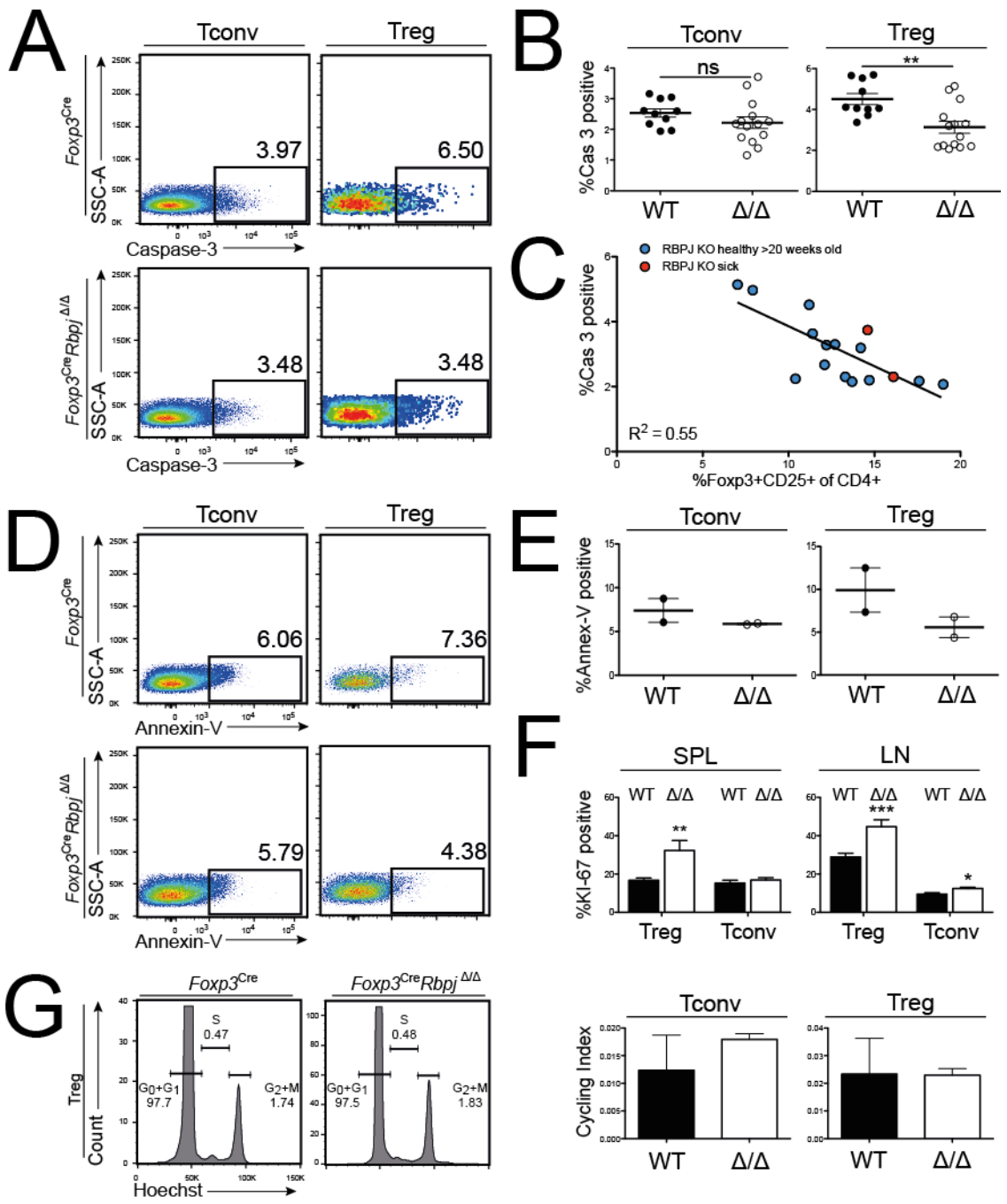

Figure 37: Analysis of apoptosis and cell cycle in T cells from *Foxp3*^{Cre}*Rbpj*$^{Δ/Δ}$ mice.

Graph A shows representative dot plots for Caspase-3 expression in Treg and Tconv cells from sick *Foxp3*^{Cre}*Rbpj*$^{Δ/Δ}$ vs. *Foxp3*^{Cre} cells. In part B, we analyzed the Caspase-3 expression in Treg cells from old, but healthy *Foxp3*^{Cre}*Rbpj*$^{Δ/Δ}$ mice (age > 18 weeks) and compared to age-matched wild type controls. In parallel, we measured the percentage of Treg cells among CD4^{pos} T cells and correlated the Caspase-3 downregulation to an increase in Treg percentage (C). For further validation, we also stained Annexin-V on Treg cells from sick *Foxp3*^{Cre}*Rbpj*$^{Δ/Δ}$ vs. *Foxp3*^{Cre} controls (D and E). Finally, we investigated the cell cycle status of Treg cells (G) and their expression intensity for KI-67 (F). Dot plots are representative of at least three biological replicates. Statistical testing was performed with an unpaired student's t test with ns $p>0.05$ and *$p<0.05$, **$p<0.01$, and ***$p<0.001$.

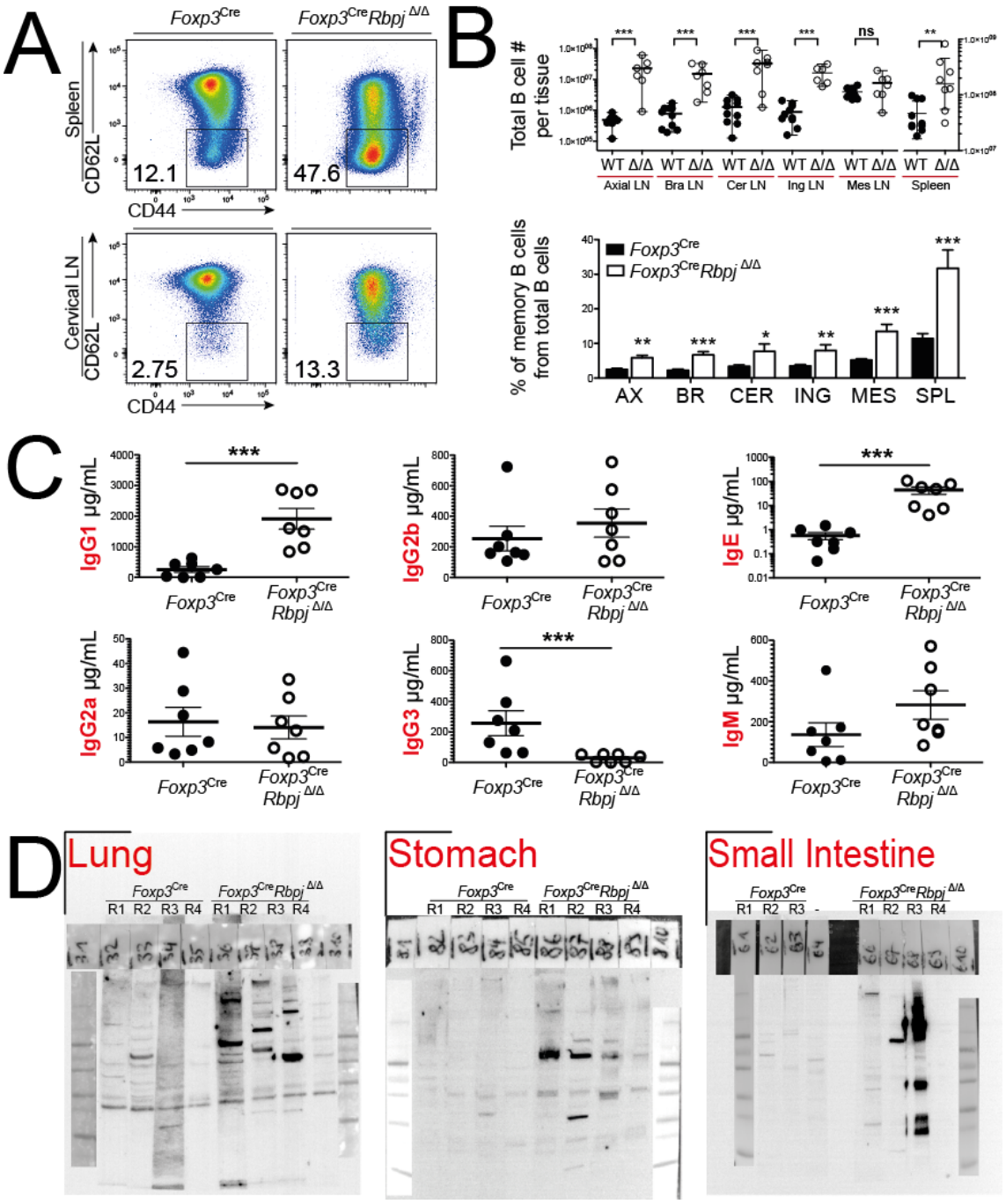

Figure 38: B cell tissue frequency and antibody secretion in *Foxp3*^{Cre}*Rbpj*$^{Δ/Δ}$ mice.
First, we investigated the downregulation of CD62L on B cells from sick *Foxp3*^{Cre}*Rbpj*$^{Δ/Δ}$ vs. *Foxp3*^{Cre} mice isolated from spleen and lymph nodes (representative dot plots in A). In B, we quantified the absolute number of B cells in various tissues including the axial lymph node, brachial LN, cervical LN, inguinal LN, mesenteric LN and spleen. The lower graph depicts the increase of memory-type B cells (CD62 low) in the respective tissues. The visualized data are representative of at least seven biological replicates and at least five independent experiments.
In C, we measured the concentration of Ig subtypes in peripheral blood serum of seven sick *Foxp3*^{Cre}*Rbpj*$^{Δ/Δ}$ mice and respective WT controls with ELISA. Blood serum was also used in D to assess autoantibody presence against specific tissues isolated from RAG KO mice in Western Blots. Statistical significance was determined using the Mann-Whitney t test (*p<0.05, **p<0.01, and ***p<0.001).

CD4^{pos} Tconv cells express memory markers, increase in tissue frequency and produce cytokines

Since B cells showed strong signs of activation and effector function, we stained for the expression of CD44 and CD62L on Tconv cells from sick *Foxp3*^{Cre}*Rbpj*$^{\Delta/\Delta}$ vs. *Foxp3*^{Cre} mice (**Figure 39**). We observed a significant downregulation of L-selectin on Tconv cells from sick mice, along with an upregulation of CD44. This is a strong indicator of antigen-experience and maturation of naive T cells into effector T cells[184]. A strong upregulation of CD44 was also observed in Treg cells, again indicating a pro-inflammatory environment leading to activation of both effector T cells and regulatory T cells. When investigating tissue numbers of Tconv cells, a steady increase in lymph node and spleen tissues was observed, indicating effector T cell proliferation and activation. Finally, we measured the expression of pro-inflammatory cytokines by Tconv cells upon PMA/Ionomycin stimulation. Not surprisingly, we found that Tconv cells from sick *Foxp3*^{Cre}*Rbpj*$^{\Delta/\Delta}$ mice produce significantly more IL-2, IL-4 (data not shown), IL-10, and IFN-γ than their wild type control counterparts. Taken together, these data indicate strong activation of Tconv cells and a likely differentiation into T$_H$ effector subsets.

CD8^{pos} T cells, myeloid-derived cells and NK cells respond to the pro-inflammatory environment

In **Figure 40**, we show strongly increased numbers of CD8^{pos} cytotoxic T cells in sick *Foxp3*^{Cre}*Rbpj*$^{\Delta/\Delta}$ mice (A). Furthermore, CD8^{pos} cytotoxic T cells in these animals express CD44, a marker of antigen experience, at a very high percentage. It can be inferred that CD8^{pos} T cells, just like Treg, Tconv and B cells, develop into effector cells in the pro-inflammatory environment generated in sick *Foxp3*^{Cre}*Rbpj*$^{\Delta/\Delta}$ animals. Also, myeloid-origin cells respond to this environment (B). We can detect a steady increase of CD11b^{pos}Ly6C^{pos} myeloid cells (granulocytes and monocytes) into lymphoid tissues. Being usually a rather scarce population, they now account for up to 20% of CD3^{neg}NK1.1^{neg} cells. Finally, we also measured NK cell numbers and their activation status by CD25 expression (C). A modest, but significant increase in NK cells numbers in sick *Foxp3*^{Cre}*Rbpj*$^{\Delta/\Delta}$ mice was detected, and they express more CD25, which indicates that the innate immune system responds to the pro-inflammatory environment in these mice as well.

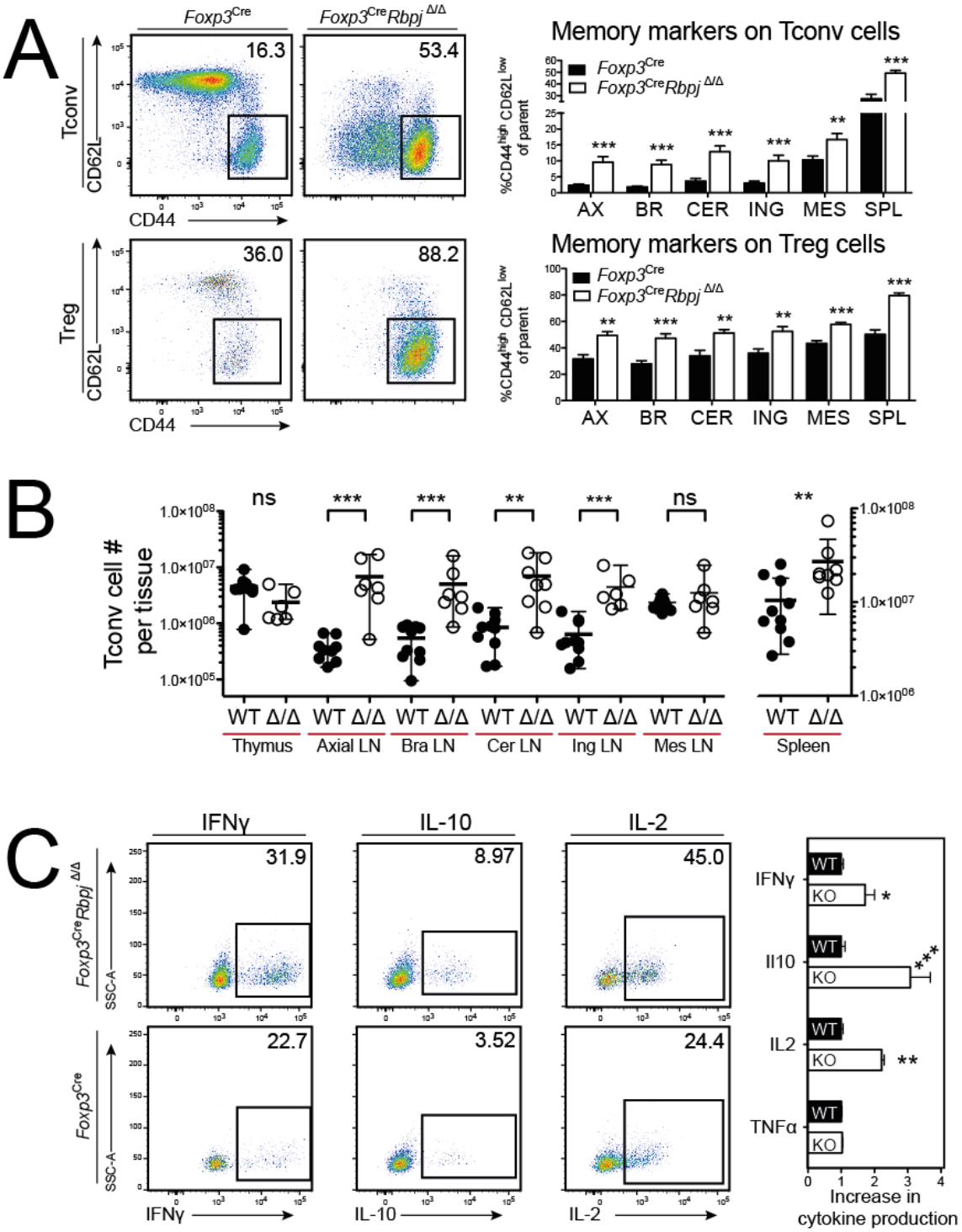

Figure 39: Tconv cell number, memory marker expression and cytokine secretion.
In A, we show representative dot plots illustrating the downregulation of CD62L and upregulation of CD44 on Treg and Tconv cells from sick *Foxp3* ^{Cre}*Rbpj*$^{\Delta/\Delta}$ mice. The bar graphs are representing at least seven biological replicates in at least five separate experiments. From the same dataset, we calculated the absolute number of Tconv cells in various lymphoid tissues in B. Finally, we stimulated Tconv cells with PMA/Ionomycin and checked their cytokine secretion profile in C. Statistical significance was determined using the Mann-Whitney t test (*p<0.05, **p<0.01, and ***p<0.001).

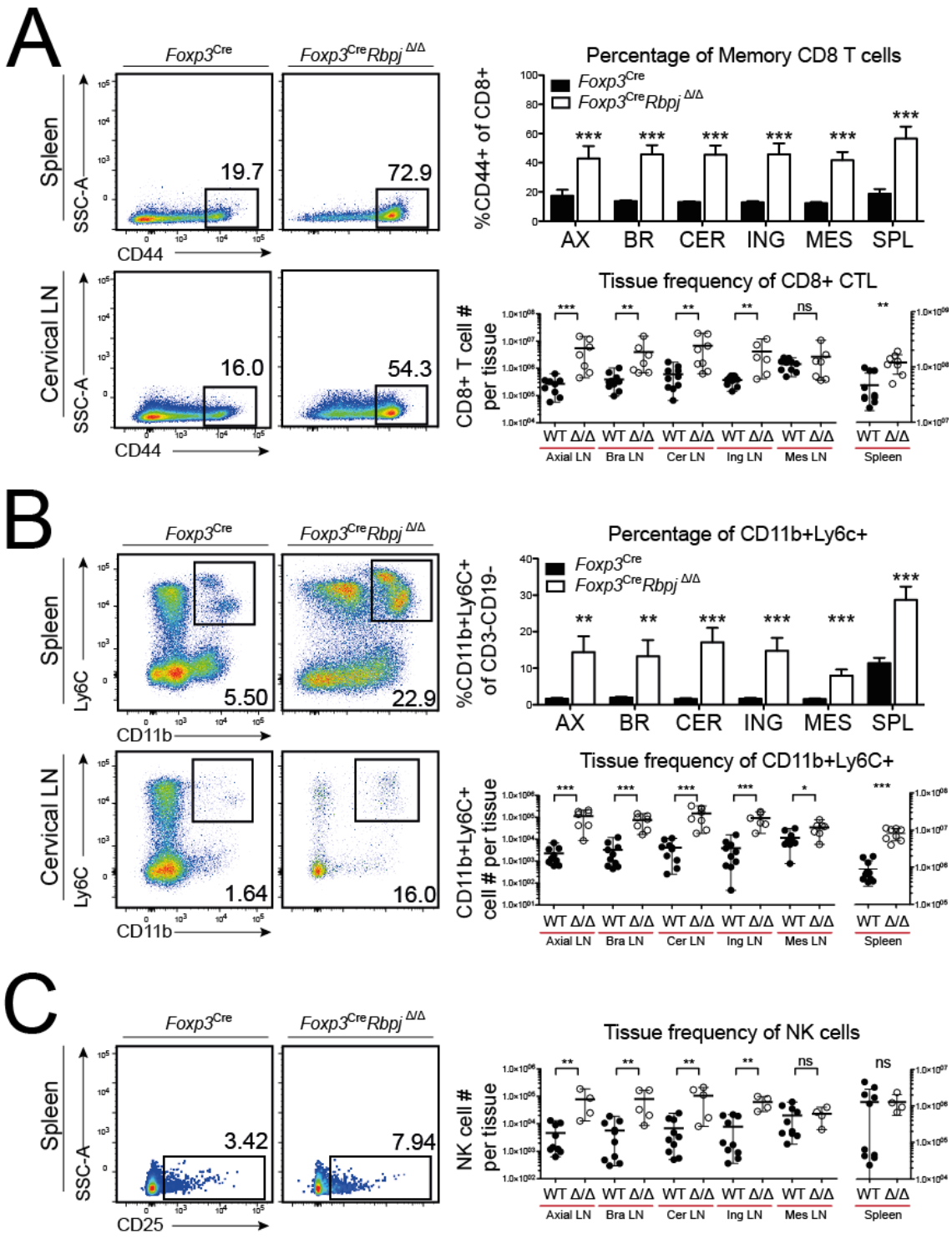

Figure 40: CD8 T cell, CD11b^{pos}Ly6C^{pos} myeloid cell and NK cell analysis.
We measured the absolute tissue frequency of CD8 ^{pos} T cells in sick *Foxp3* ^{Cre}*Rbpj*$^{Δ/Δ}$ vs. *Foxp3*^{Cre} animals (A), and quantified the expression of CD44 as a marker of antigen exposure. In B, we identified CD11b^{pos}Ly6c^{pos} myeloid cells and quantified their increase in both percentage and absolute numbers in several tissues. Finally, we investigated NK-cell numbers in C, and quantified their activation status via CD25 staining as shown in the dot plots. Bar graphs represent at least 7 biological replicates assayed in three or more individual experiments, with significance elucidation by Mann-Whitney t testing (*p<0.05, **p<0.01, and ***p<0.001).

Pathological evaluation of different tissues reveals skin inflammation

We evaluated tissue architecture and signs of autoimmune infiltrations in specimens from sick *Foxp3* ^{Cre}*Rbpj*$^{\Delta/\Delta}$ and *Foxp3* ^{Cre} mice via Haematoxylin and Eosin staining of formalin-fixed tissues (**Figure 41**). In collaboration with a pathologist, we examined specimens from the lymphatic system (axial, brachial, cervical, inguinal lymph nodes; spleen), the cardiovascular system (heart), respiratory system (lung), digestive system (small intestine, large intestine, stomach), endocrine system (pancreas, adrenal gland, salivary gland, kidneys), nervous system (brain, eyes) as well as liver. Furthermore, we embedded skin pieces with obvious inflammation, such as snout, ears or patches of skin, and compared them with non-inflamed tissues. While this in-depth analysis is still ongoing, a general conclusion is that most organs did not show signs of lymphocyte infiltration. The liver, despite being increased in weight about 1.5 fold, had some cellular infiltrates, but would not classify as inflamed (hepatitis). Lymph nodes and spleen were greatly enlarged, but maintained their tissue architecture. We are currently staining for B cells to evaluate the germinal center architecture more closely. The only obvious site of inflammation was skin, where infiltrates were present, and overall tissues architecture was severely compromised. While most organs are untouched, skin is heavily affected and might enhance systemic disease by the re-circulation of cells via the lymph system. We also tested peripheral blood of these mice via standard clinical small panel testing (data not shown).

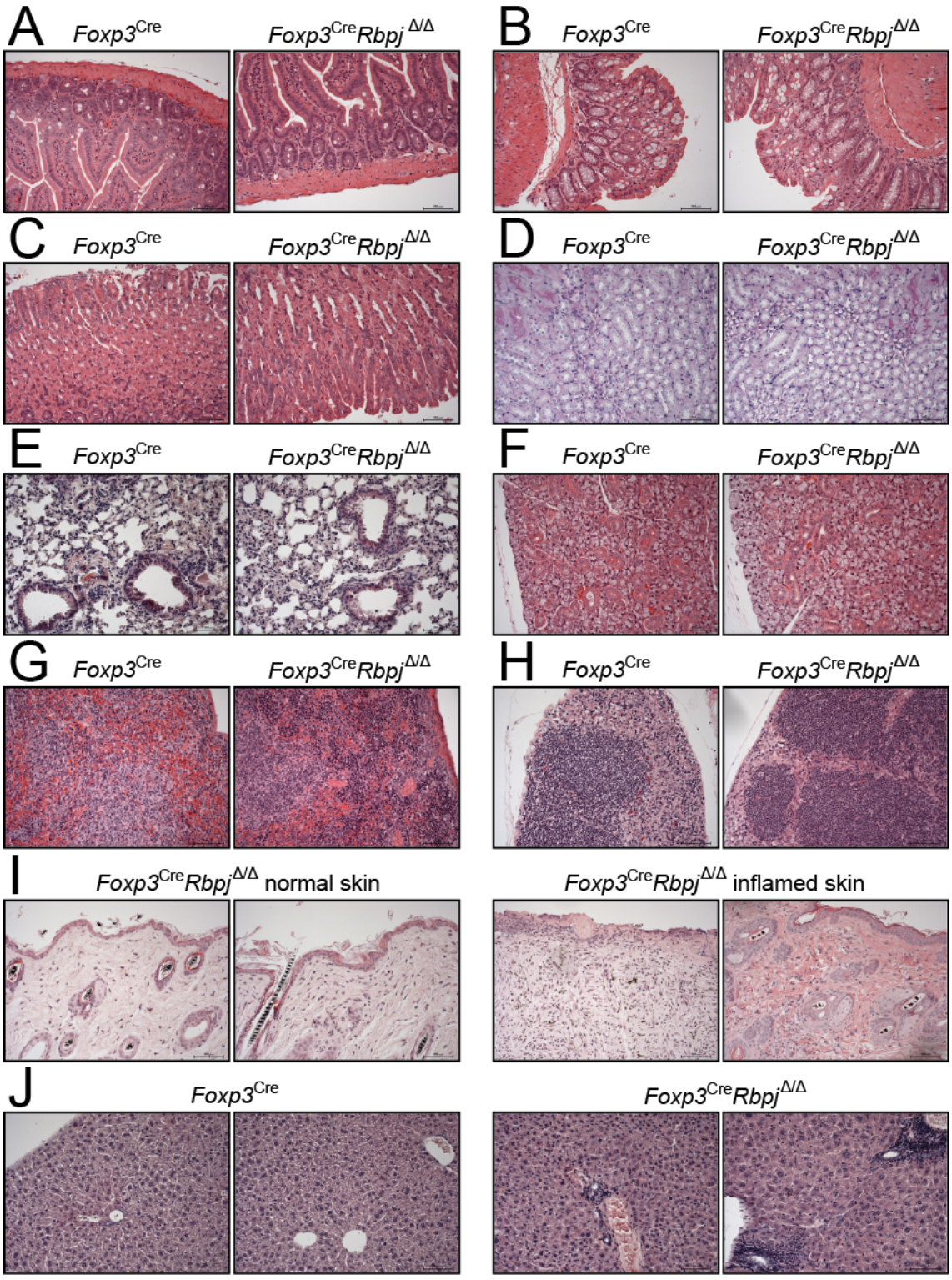

Figure 41: Pathological evaluation of organs and tissues from *Foxp3*^{Cre}*Rbpj*$^{\Delta/\Delta}$ mice.

We isolated organs from sick *Foxp3* ^{Cre}*Rbpj*$^{\Delta/\Delta}$ and *Foxp3* ^{Cre} mice and stored them in formalin. Tissues were then embedded, cut, and H&E stainings were performed. Photographs were taken with a Zeiss AxioPlan microscope. Tissue morphology and architecture was evaluated optically. A: Small intestine; B: Large intestine; C: Stomach; D: Kidneys; E: Lungs; F: Salivary Gland; G: Spleen; H: Cervical LN; I: Skin, with patches of normal (left) and inflamed skin (right) from the same animal; J: Liver, with two images from different samples of the same genetic background.

Treg cells from sick *Foxp3*^{Cre}*Rbpj*$^{\Delta/\Delta}$ mice display a specific gene signature

We isolated Treg and Tconv cells from healthy young *Foxp3*^{Cre}*Rbpj*$^{\Delta/\Delta}$ and *Foxp3*^{Cre} age-matched controls and subjected them to gene expression profiling (**Figure 42A**). We observed only one gene, Deltex-1, to be significantly downregulated in Rbpj-deficient Treg cells. Since the Illumina bead chip array used for gene expression profiling does not contain a probe for Rbpj, its loss cannot be shown in this plot. The strong downregulation of Dtx-1 was confirmed by qPCR (data not shown, $p<0.001$). When comparing Rbpj-deficient or –proficient Treg cells to respective Tconv cells, the typical Treg-specific signature with upregulation of Foxp3 and Nrp1 and downregulation of Pde3b can be appreciated. In contrast to this, Dtx-1 is specifically downregulated in RBPJ-deficient Treg cells, but not Tconv cells. In **Figure 42B**, we now compared the gene expression profile of Treg cells isolated from sick *Foxp3*^{Cre}*Rbpj*$^{\Delta/\Delta}$ animals versus healthy heterozygous control animals. Now, a distinct signature can be identified. While Dtx-1 remains downregulated, more factors such as Bcl-2, CD86 or CCR7 follow this trend. Furthermore, several proteins are upregulated, such as the IL7R, KLRG-1 or ITGAE. Since sick *Foxp3*^{Cre}*Rbpj*$^{\Delta/\Delta}$ mice display an inflamed environment with lymphadenopathy and splenomegaly, we can infer that parts of the specific Treg signature are based on their elevated activation status. This is also true for gene expression in Tconv cells, where we now detect several factors to be up – or downregulated in sick vs. healthy mice. To evaluate whether the discrete signature identified in Treg cells from sick *Foxp3*^{Cre}*Rbpj*$^{\Delta/\Delta}$ mice is already present in young healthy *Foxp3*^{Cre}*Rbpj*$^{\Delta/\Delta}$ mice, we overlaid upregulated genes of the *Foxp3*^{Cre}*Rbpj*$^{\Delta/\Delta}$ sick Treg signature with the gene expression data of young healthy animal Rbpj-deficient Treg cells. We observed that a significant proportion of genes were already upregulated in Treg cells from otherwise healthy *Foxp3*^{Cre}*Rbpj*$^{\Delta/\Delta}$ animals, indicating that the signature and its molecular consequences are already prepared, but have not caused pathological effects yet. The same observation has been made for genes specifically downregulated in Treg cells from sick *Foxp3* ^{Cre}*Rbpj*$^{\Delta/\Delta}$ mice. In **Figure 43**, we confirm part of the Rbpj-deficient Treg signature via flow cytometry. Furthermore, we show top 40 up – and downregulated genes in an unsupervised hierarchical clustering.

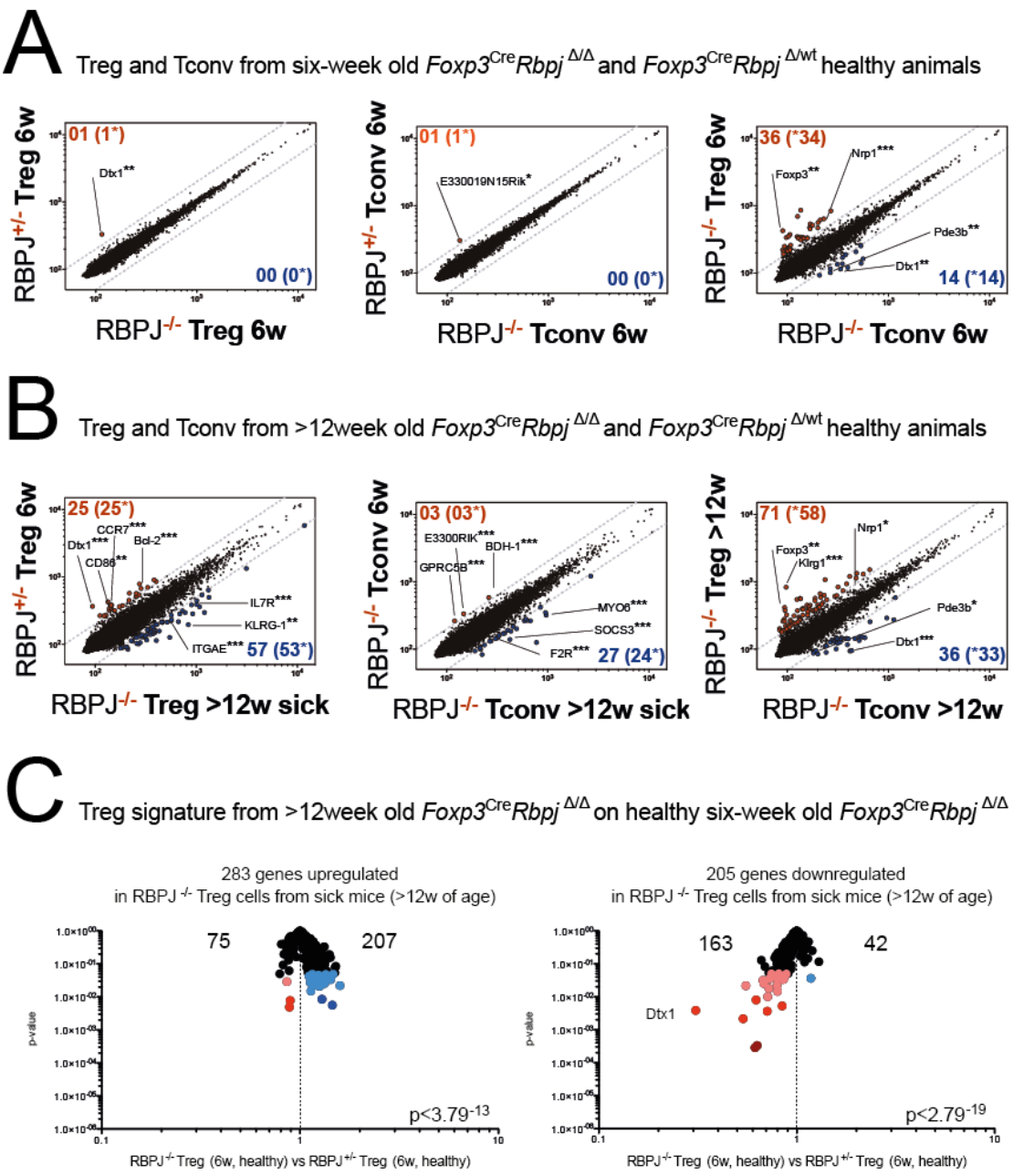

Figure 42: Gene expression comparison of T cells from *Foxp3*^{Cre}*Rbpj*$^{Δ/Δ}$ mice.
Treg and Tconv cells were isolated from spleen using FACS and subjected to gene expression profiling with Illumina Bead Chip technology. In A, we compared gene expression profiles of Treg and Tconv cells isolated from healthy *Foxp3* ^{Cre}*Rbpj*$^{Δ/Δ}$ and *Foxp3* ^{Cre} animals of young age (age < 6 weeks). In B, we cross-compare Treg cells from advanced-age sick *Foxp3*^{Cre}*Rbpj*$^{Δ/Δ}$ mice (age > 12 weeks) and young healthy *Foxp3* ^{Cre} mice (age < 6 weeks). Each plot represents averaged gene expression data from three biological replicates (age < 6 weeks) or four biological replicates (*Foxp3*^{Cre}*Rbpj*$^{Δ/Δ}$ sick mice > 12 weeks), with p-values calculated with a two-tailed student's t test. Numbers indicate genes with >2 or <0.5 fold average differential expression and p<0.05. Next, we overlaid upregulated genes (part C, left side) and downregulated genes (part C, right side) in Treg cells from *Foxp3* ^{Cre}*Rbpj*$^{Δ/Δ}$ sick mice onto the gene signature of young healthy *Foxp3* ^{Cre}*Rbpj*$^{Δ/Δ}$ mice. Numbers indicate the number of genes that are up-or downregulated in the young animal Treg signature, respectively, and p-values are based on chi-square testing.

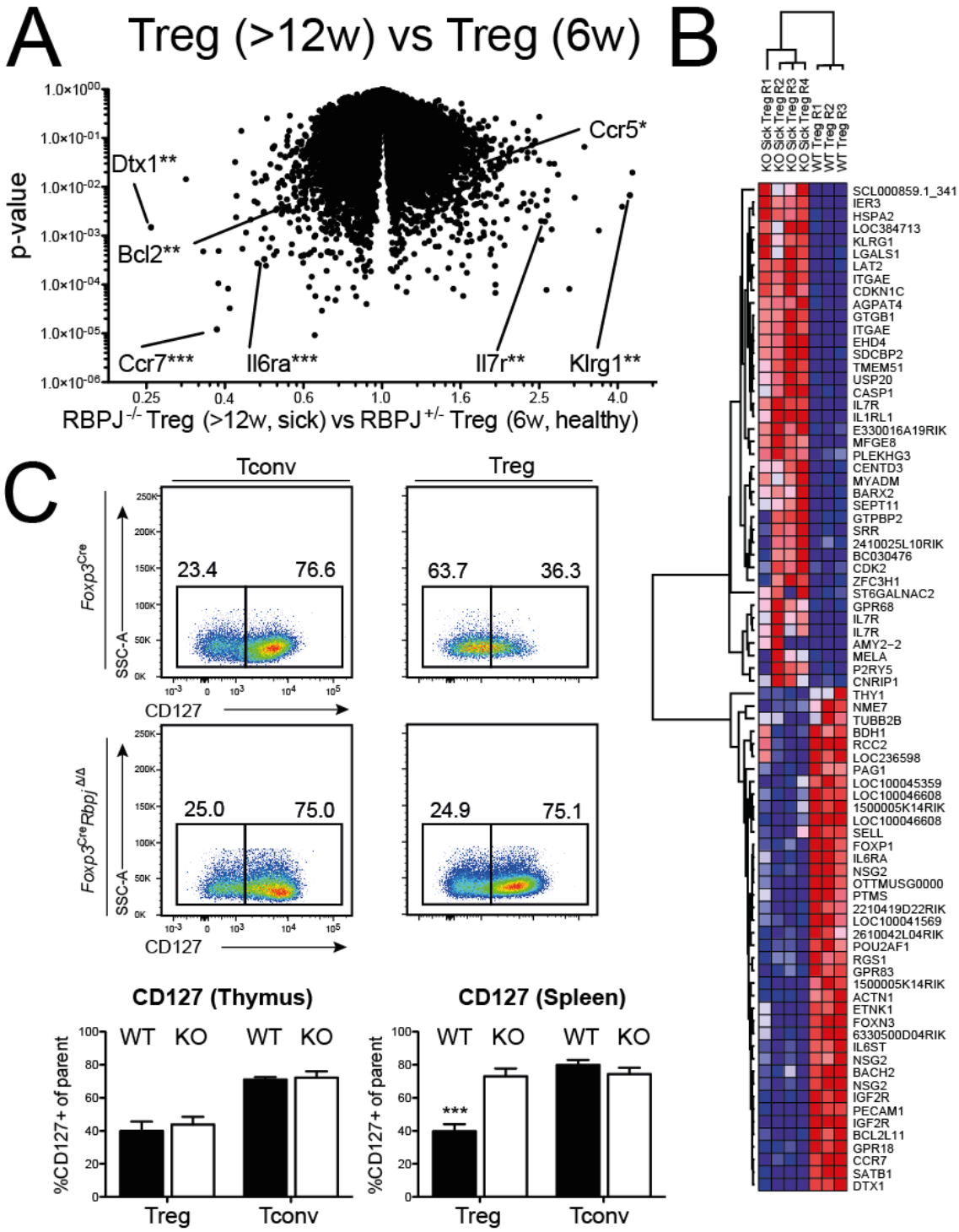

Figure 43: Analysis and verification of the Rbpj-specific Treg gene signature.
Graph A shows a p-value vs. gene expression comparison between Treg cells from advanced-age sick *Foxp3* ^{Cre}*Rbpj*$^{\Delta/\Delta}$ mice (>12 weeks of age) and healthy *Foxp3* ^{Cre} mice (6 weeks of age). In B, we used the top 40 up- and downregulated genes (without p-value correction) and subjected them to unsupervised hierarchical clustering. Red indicates high expression strength. In C, we confirmed gene expression data from A and B via flow cytometry. Treg and Tconv cells from spleens of sick *Foxp3*^{Cre}*Rbpj*$^{\Delta/\Delta}$ mice and *Foxp3*^{Cre} controls were stained for IL7R expression. The bar graphs represent at least 4 (thymus) or 6 (spleen) replicates in several separate experiments. Statistical testing in A and C was performed with a two-tailed unpaired students t test (*p<0.05, **p<0.01, and ***p<0.001).

Treg and Tconv cells from sick *Foxp3*^{Cre}*Rbpj*$^{\Delta/\Delta}$ mice are T_H1, T_H2, and T_H17 prone

We used the microarray data from Treg and Tconv cells isolated from sick *Foxp3*^{Cre}*Rbpj*$^{\Delta/\Delta}$ and *Foxp3*^{Cre} cells and calculated over – and under expressed genes, as described earlier (23948 downregulated, 22288 upregulated). We then overlaid this signature with genes specifically upregulated in T_H1, T_H2, and T_H17 differentiated T cells. Gene expression data for cytokine-induced T_H1, T_H2, and T_H17 cells were published earlier. Then, we calculated genes specifically upregulated in the respective T-cell subset, which yielded between 200 and 400 T-subset specific genes. Next, we looked for T-subset specific upregulated genes in our microarray data. Results are shown in **Figure 44**. Interestingly, we identified that most T_H-subset upregulated genes are also upregulated in Treg cells from *Foxp3*^{Cre}*Rbpj*$^{\Delta/\Delta}$ mice (77% for T_H1, 69% for T_H2, and 75% for T_H17) compared to Treg cells from *Foxp3*^{Cre} mice. Furthermore, this lineage skewing is also present in Tconv cells from sick *Foxp3*^{Cre}*Rbpj*$^{\Delta/\Delta}$ mice. To make sure that our dataset is not biased, we generated *Foxp3*^{Cre}*NICD*^{LSL} mice, which constantly express the Notch intracellular domain, and checked the gene signature in healthy young mice (6 weeks) against *Foxp3*^{Cre} mouse Treg cells. We then overlaid the T_H1, T_H2, and T_H17 specific genes and evaluated bias. Since these mice are healthy, and did not display signs of autoimmunity or T-cell activation, no T_H bias was observed: T_H1-, 2-, or 17- upregulated genes were distributed equally, with 50% for T_H1, 56% for T_H2, and 53% for T_H17. Statistical evaluation by χ^2 testing still displays a significant difference, what is based on the strong upregulation of genes in Treg cells from *Foxp3*^{Cre}*NICD*^{LSL} mice compared to *Foxp3*^{Cre} mice (17105 downregulated, 28986 upregulated). The signature overlays indicate that our T_H-subset bias is specific for the pro-inflammatory scenario in sick *Foxp3*^{Cre}*Rbpj*$^{\Delta/\Delta}$ mice. Furthermore, we also stained for GATA-3 and T-bet, lineage-defining transcription factors for both T_H1 (T-bet) and T_H2 (GATA-3) subsets, in Treg, Tconv and CD8 T cells from sick *Foxp3*^{Cre}*Rbpj*$^{\Delta/\Delta}$ mice. Interestingly, all three T cell types show enriched expression in these factors. This observation runs in concert with previous data, where we showed that Tconv cells from these mice more readily produce IL-10 and IFN-γ, but also IL-4. Taken together, our observations indicate that, in sick *Foxp3*^{Cre}*Rbpj*$^{\Delta/\Delta}$ mice, autoimmune pathology evolves not only due to the expansion of one specific T_H subset, but rather by a systemic, unbiased expansion of pro-inflammatory T cells.

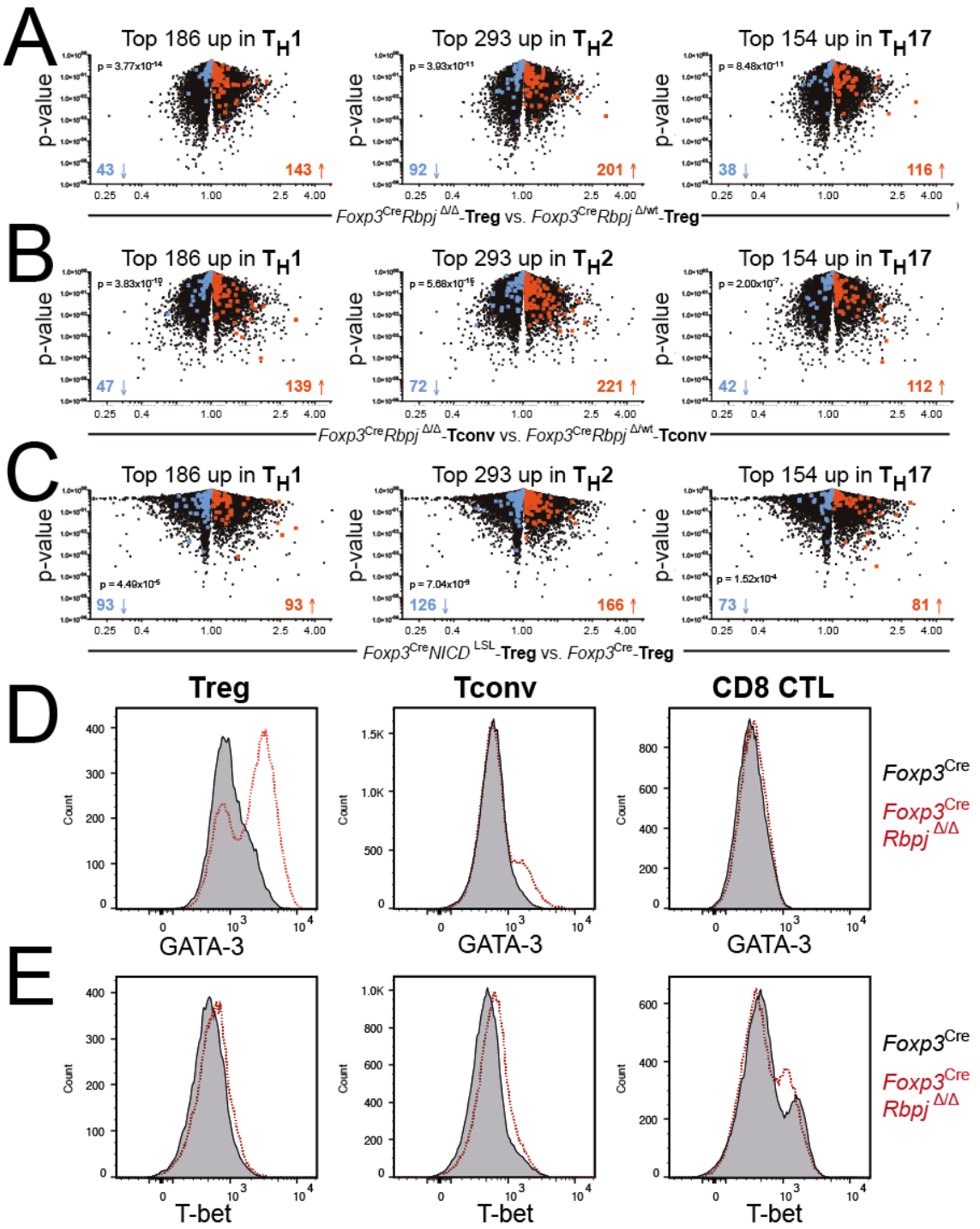

Figure 44: Analysis of T_H1, T_H2, and T_H17 lineage-defining gene expression.
Graph A shows a gene expression comparison between Treg cells from advanced-age sick *Foxp3*^{Cre}*Rbpj*$^{Δ/Δ}$ mice and healthy *Foxp3* ^{Cre} heterozygous mice, as shown already in **Figure 42**. Here, we overlaid it with genes specifically upregulated in T_H1 (left), T_H2 (middle) or T_H17 (right) differentiated cells. Numbers indicate how many T_H-subset regulated genes are upregulated also in Treg cells from sick *Foxp3*^{Cre}*Rbpj*$^{Δ/Δ}$ mice (red) or not (blue). In B, we repeated this approach with the Tconv cell signature from sick *Foxp3*^{Cre}*Rbpj*$^{Δ/Δ}$ and *Foxp3*^{Cre} mice, and in C we performed this comparison with Treg gene signatures from *Foxp3* ^{Cre}*NICD*^{LSL} and *Foxp3* ^{Cre} mice. In D and E, we stained for key T_H1 and T_H2 proteins in Treg, Tconv and CD8 T cells from sick *Foxp3* ^{Cre}*Rbpj*$^{Δ/Δ}$ mice and *Foxp3* ^{Cre} mice.

The IL7R links KLRG-1 expression and proliferation of Rbpj-deficient Treg cells

In our gene expression profiling, we detected KLRG-1 to be overexpressed in RBPJ-deficient Treg cells isolated from sick *Foxp3* ^{Cre}*Rbpj*$^{\Delta/\Delta}$ mice. Therefore, we performed flow cytometric staining for this marker, along with the IL7R (**Figure 45**). Our data clearly indicate that the IL7R^{high} expressing Treg cells are also positive for KLRG-1, which could indicate that this population is indeed responsible for the massive cellular expansion of Treg cells observed in these mice. Co-staining for IL7R and KI-67, which shows that only IL7R ^{high} Treg cells drive the massive proliferation in *Foxp3* ^{Cre}*Rbpj*$^{\Delta/\Delta}$ animals, supports this notion. KI-67 is present during all active cell cycle phases (G1, S, G2, mitosis), but is completely absent in resting cells [185]. Therefore, we sought to determine the molecular link between IL7R expression and Treg cell numbers in **Figure 46**. First, we measured IL7R expression in T-conventional cells of young healthy *Foxp3*^{Cre}*Rbpj*$^{\Delta/\Delta}$ and *Foxp3*^{Cre} animals, older healthy *Foxp3*^{Cre}*Rbpj*$^{\Delta/\Delta}$ and *Foxp3*^{Cre} animals, and sick *Foxp3*^{Cre}*Rbpj*$^{\Delta/\Delta}$ animals with age-matched *Foxp3*^{Cre} controls. We observed no difference in IL7R expression in Tconv cells. We also evaluated CD25^{pos}Foxp3^{YFPpos} Treg cells from all three groups for their IL7R expression. Interestingly, an about two-fold increase in IL7R ^{high} Treg cell frequency can already be observed in otherwise healthy *Foxp3*^{Cre}*Rbpj*$^{\Delta/\Delta}$ animals. Furthermore, in sick *Foxp3*^{Cre}*Rbpj*$^{\Delta/\Delta}$ animals, more than 80% of Treg cells display the IL7R at high levels. When we correlated the frequency of IL7R ^{high} expressing Treg cells with the frequency of Treg cells of CD4 T cells in all three groups of *Foxp3* ^{Cre}*Rbpj*$^{\Delta/\Delta}$ animals, we observe a reasonably good correlation between IL7R expression and increase in Treg frequency (**Figure 46C**, $R^2 = 0.6543$). Therefore, we now sought to investigate the molecular link between the absence of Rbpj in Treg cells from *Foxp3* ^{Cre}*Rbpj*$^{\Delta/\Delta}$ animals and the expression of the IL7R. As already mentioned in the introduction, binding of Rbpj to the IL7R-promoter has been investigated already. To proof this binding, we performed Chromatin IP experiments with an anti-Rbpj antibody followed by real-time PCR based detection putative Rbpj binding sites on the IL7R gene (**Figure 46D**). Therefore, we measured putative IL7R binding-site DNA in Rbpj-antibody based immunoprecipitations with Rbpj-deficient Treg cells (control) and wildtype Treg cells. We then calculated the relative binding of Rbpj to the respective fragment in Treg cells from *Foxp3*^{Cre} mice vs. Treg cells from *Foxp3*^{Cre}*Rbpj*$^{\Delta/\Delta}$ mice. To this end, we could show that Rbpj indeed binds the IL7R gene, probably downmodulating its activity in the absence of active Notch signaling.

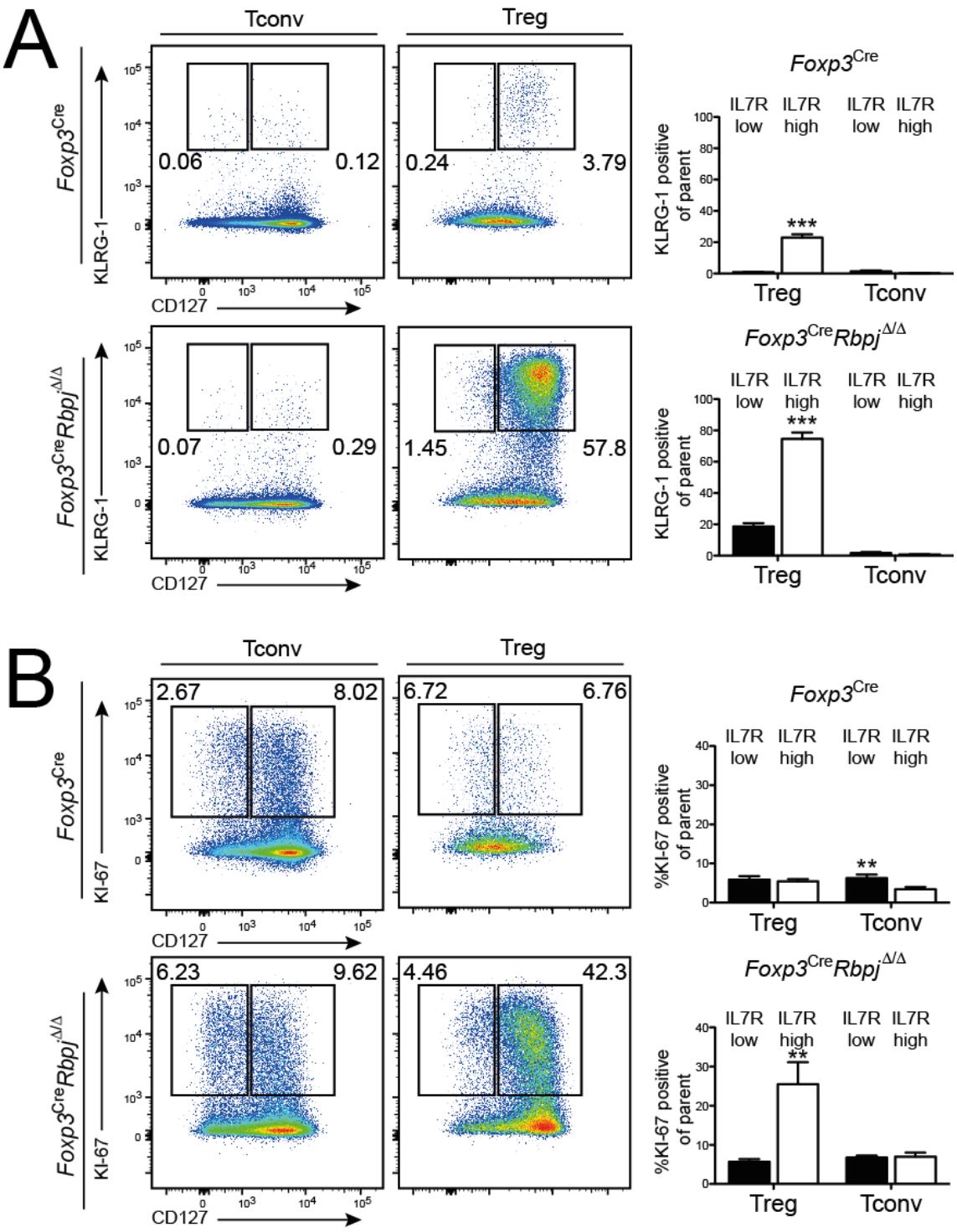

Figure 45: Correlation between IL7R, KLRG-1 and KI-67 expression.
We stained splenic Treg and Tconv cells from sick *Foxp3* ^{Cre}*Rbpj*$^{\Delta/\Delta}$ and *Foxp3*^{Cre} mice for expression of CD127 (IL7R), KLRG-1 and KI-67. In A, we show representative dot plots for KLRG-1 expression vs. CD127 expression. The histograms depict expression of KLRG-1 in pre-gated IL7R^{high} and IL7R^{low} Treg and Tconv cells from six sick *Foxp3*^{Cre}*Rbpj*$^{\Delta/\Delta}$ and eight *Foxp3*^{Cre} controls. In B, we evaluate the expression of KI-67 vs. CD127. The bar graphs represent 4 or more biological replicates in several separate experiments. Statistical testing in was performed using a two-tailed unpaired students t test, with *p<0.05, **p<0.01, and ***p<0.001.

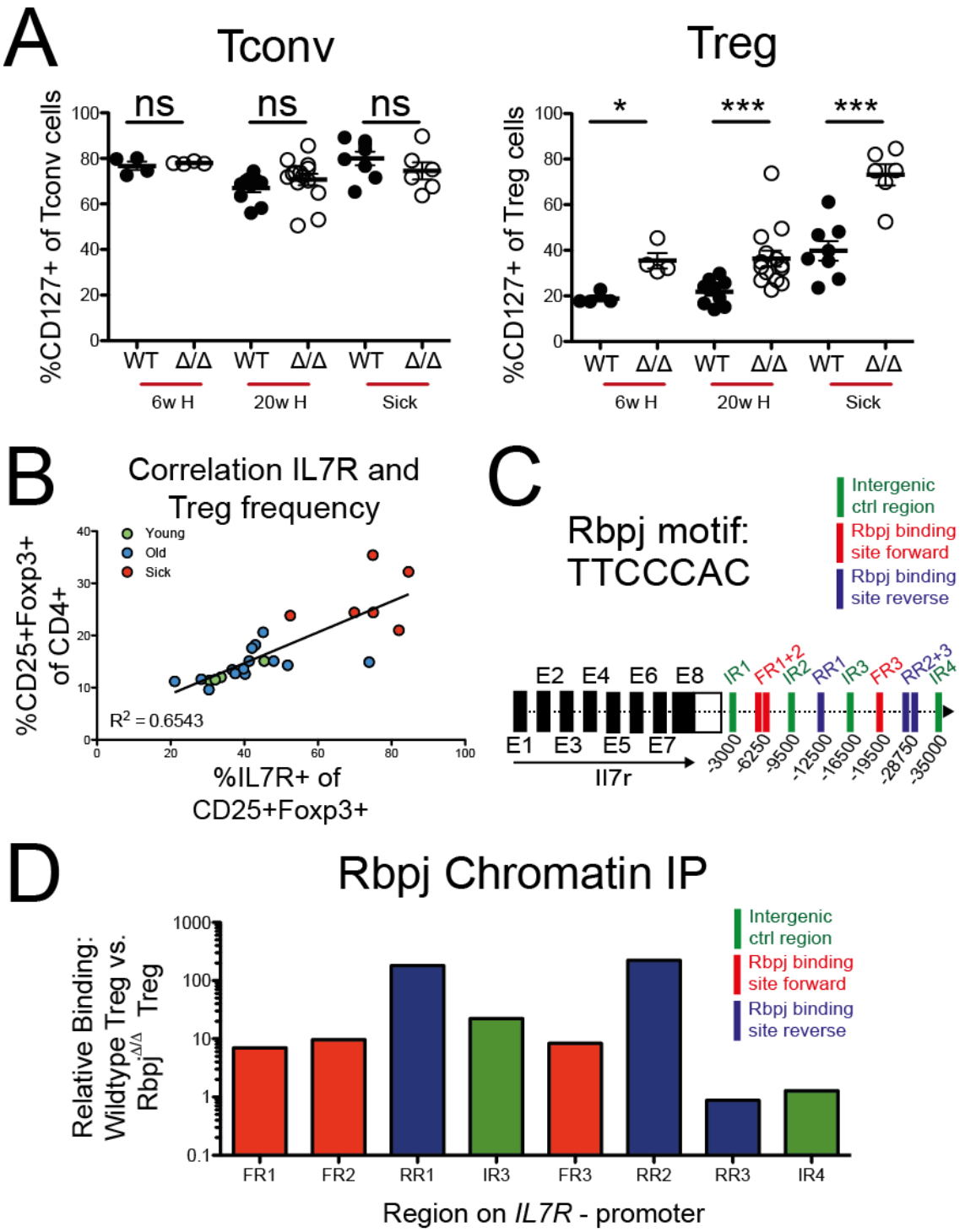

Figure 46: Molecular link between Treg cell proliferation and IL7R expression.
In A, we plot IL7R expression in Treg and Tconv from young healthy *Foxp3*^{Cre}*Rbpj*$^{Δ/Δ}$ and *Foxp3*^{Cre}, advanced-age healthy *Foxp3* ^{Cre}*Rbpj*$^{Δ/Δ}$ and *Foxp3* ^{Cre} mice or sick *Foxp3* ^{Cre}*Rbpj*$^{Δ/Δ}$ and age-matched *Foxp3* ^{Cre} mice. Statistical evaluation was performed using a two-tailed student's t test. The *IL7R* expression data were correlated with Treg frequency in part B, and a linear regression fitting has been performed. R Square and significance values have been calculated using Prism software. In C, we show the RBPJ binding motif and its forward and reverse orientation in the *IL7R* gene. In D, we show results of a Chromatin IP with an anti-Rbpj mAb and Rbpj-deficient Treg cells as well as wild type Treg cells. We plot mean relative binding of wild type Treg over Rbpj-deficient Treg cells for binding sites described in C.

8 Discussion

Whole-genome and amplicon-based sequencing reveals differential methylation of the *Foxp3* gene

In this thesis, we first investigated the molecular control of *Foxp3*, the master regulator of Treg cells, on an epigenetic level. We asked several questions dealing with the CpG methylation status of the *Foxp3* gene, and addressed those with our amplicon- and whole genome-based approaches. First, we wanted to evaluate whether the TSDR/CNS2 is the only region with a Treg-specific demethylation pattern. Our data clearly indicate that there is at least one additional Treg-specific demethylated region, just downstream of the *Foxp3* promoter (Region 3). We confirmed that this region is demethylated specifically once thymic Treg cells express *Foxp3*, but not in thymic Treg cell precursors. Furthermore, its demethylation pattern is stable in antigen-experienced Treg cells, and independent of the *Foxp3* protein expression strength as measured with our Foxp3^{GFP} reporter model. Interestingly, our whole-genome sequencing dataset not only confirms the selective demethylation of region 3 and its blueprint, the TSDR (Region 4), in Treg cells, but also the extent of this region – indeed, the whole first *Foxp3* intron carries a Treg-specific demethylated phenotype, which has not been detected by previous MeDIP-based sequencing approaches [44]. In contrast to this, it was surprising to find the 5' neighboring gene of *Foxp3*, *Ppp1r3f*, completely demethylated at both its promoter and the first exon. Deeper bioinformatical analysis will reveal the complexity of the epigenetic regulation of such genes in combination with gene expression profiling.

Another important question was the analysis of the methylation status of the *Foxp3* promoter and its exons in Treg cells. Our data indicate a dichotomy between both areas: the promoter is demethylated not only in Treg cells, but also Foxp3 non-expressing Tconv cells and CD8^{pos} T cells. This indicates that the promoter per se is open for binding by the transcriptional machinery once proper *Foxp3*-inducing transcription factors are presented, as discussed in the following paragraph. Furthermore, additional epigenetic mechanisms such as histone modifications and nucleosome positioning might add another layer of epigenetic control of the promoter region. A study by Ohkura and co-workers investigated histone modifications at the *Foxp3* Treg-specific demethylated region, and identified a euchromatic histone marker (H3K4me3) at this

region, keeping it in a transcriptionally permissive state [44]. Unfortunately, the promoter was not analyzed in this study. The authors also looked at highly methylated *Foxp3* exons (here: exon 11). They were shown to be both methylated at their CG dinucleotides and to lack H3K4me3 trimethlyation at the histones, indicating a non-permissive state for gene expression induction. Again validating our amplicon-based data with the whole-genome analysis, we identified that almost all exonic regions of the *Foxp3* gene are highly methylated: The Treg-specific demethylation pattern is not only absent in exon 6 and 8 (region 5 and 6), but most of the protein-coding exons and introns of *Foxp3*. As discussed in the introduction, more than 95% of CG dinucleotides in non-regulatory sequences are methylated to increase genetic stability [106]; we can detect the same for *Foxp3* coding regions. This highlights the importance of demethylational events in the *Foxp3* promoter and intron 1.

When is the Treg-specific demethylation pattern established? Our results indicate that T-cell receptor based signals, inducing the cytokine-dependent (late) Treg precursor, are not immediately involved in the demethylation events. Once late Treg precursor cells receive stimulation by common γ-chain cytokines, *Foxp3* expression and Treg-specific demethylation is induced. This would indicate that both programs are initiated in parallel, and that demethylation at specific regions is not a pre-requisite for *Foxp3* induction, but a means of stabilizing gene expression once initiated. This is also confirmed by our findings that Foxp3 expression levels (Foxp3 high-medium-low as measured by the *Foxp3*$^{\mathbf{GFP}}$ reporter) have no influence on epigenetic marks in the *Foxp3* gene. Therefore, the methylation patterns might act as a binary switches, stabilizing *Foxp3* expression when on (=demethylated) or leading to a progressive loss of *Foxp3* expression when off (=methylated). This can be confirmed by looking at *in-vitro* induced Treg cells (iTreg), which gradually lose *Foxp3* expression once TCR and cytokine stimuli are removed [125]. These iTreg cells have no selective demethylation at intron 1. Furthermore, when the CNS2/TSDR region was selectively deleted in mice, loss of *Foxp3* gene expression in Treg cells over time occurred, again validating the role of epigenetic modification in specific regions of *Foxp3* for its long-lasting and stable expression in Treg cells [153]. Sakaguchi and co-workers dissected the establishment of the Treg-specific methylation program and *Foxp3* gene induction with various genetic models on a whole-genome scale [44]: They found that TCR-stimulation induces a Treg cell-specific CpG hypomethylation pattern, which is independent of *Foxp3* induction. Furthermore, they showed that this pattern is, once established in the thymus, also

present in the periphery, even in the absence of *Foxp3* protein expression. Finally, the authors discovered that this epigenetic framework is necessary to complement the Treg-specific gene signature and to promote lineage stability, finally leading to full suppressive capacity. In line with this, the Treg-specific demethylation framework has been shown to regulate many key Treg genes independently of Foxp3 activity. Examples include CD25 (*Il2ra*), CTLA-4 (*Ctla4*), GITR (*Tnfrsf18*), or Eos (*Lkzf4*).
Finally, we looked at the T-cell compartment in Dnmt1-hypomorphic (*Dnmt1* ^{chip}) mice. We detected a decreased Treg frequency to about 50% of normal. This runs in concert with findings from the specific knockout of the TSDR in mice, where Treg cell numbers decrease with increasing age of the animals, but not in young mice [153]. Since *Dnmt1* ^{chip} mice already have particular defects in the generation of precursor cells in the bone marrow, with a particular shift in the myeloid / lymphoid lineage decision, care has to be taken when comparing cell numbers in this mouse with its wild type littermates. Upon the investigation of the epigenetic imprinting of the *Foxp3* gene in circulating Treg cells from *Dnmt1*^{chip} mice, we saw that they maintained their specific demethylation pattern, and, more importantly, conventional T cells also remained methylated at the Treg-specific demethylated regions. This indicates that this epigenetic mark is important even in a Dnmt1-hypomorphic scenario. We also analyzed markers for peripherally induced Treg cells, like Helios or Nrp-1, on Treg cells from *Dnmt1* ^{chip} and WT mice. Since we observed no significant differences, increased peripheral conversion of Tconv cells is very unlikely – this supports the above-mentioned observation that Tconv cells from this mouse have methylated Treg-specific regions 3 and 4, protecting them from unintended *Foxp3* induction.
Taken together, we not only identified a new Treg-specific demethylated region in this study, but we also extended this region to cover the whole *Foxp3* Intron 1. We investigated its induction during Treg development and confirmed its stability in circulating Treg cells. We showed that the Treg-specific demethylation is also present in *Dnmt1*^{chip} mice. Lastly, we could show that this demethylation pattern is independent of tissue localization of Treg cells. In terms of tissue-specific adaptation, we were able to isolate Treg cells from four different tissues (fat, liver, skin, lymph node) with high viability and purity. We subjected them to whole-genome bisulfite sequencing and mapped the data to the mouse genome. We identified the methylation pattern of the *Foxp3* gene in these tissue-derived Treg cell populations and compared it to our patterns observed from splenic and lymph node Treg vs. Tconv cells. We did not observe any

tissue-specific differences in the Treg-specific demethylation of intron 1, the *Foxp3* promoter, or upstream and downstream gene elements. This indicates that Treg-specific demethylation is a reliable and stable marker also for tissue-adapted Treg cells. Furthermore, we already prepared RNA sequencing libraries to link whole-genome methylation data to gene expression profiles. Our next-generation run data indicate homogenous sequencing and data acquisition, which should result in a high quality dataset. Furthermore, we can already detect quite profound differences in the whole-genome methylation level between Treg cells from different tissues, indicating that tissue adaptation might indeed be mediated by epigenetic events. Therefore, it will be most interesting to study differentially methylated regions in more detail, and to link differentially methylated promoter sites or gene regions to the respective gene expression profile.

Specific proteins bind the *Foxp3* gene promoter and downmodulate its activity

Since epigenetics is only one arm of transcriptional control, we surveyed the *Foxp3* gene promoter for transcription factor binding activity as well. We used a quite novel unbiased proteomic approach to decipher the molecular complex binding to the *Foxp3* gene promoter. Since we used Foxp3 non-expressing EL4 T cells for our study, it was feasible that we would detect potential *Foxp3* repressing transcription factors. In order to detect Foxp3 inducing factors, we initially though to repeat this procedure with Foxp3-induced EL4 T cells as well. Unfortunately, we were not able to induce Foxp3 protein expression by TCR-stimulation and TGF-β treatment in these cells to an extent and number suitable for inverted ChIP analysis.

When performing this procedure with nuclear proteins isolated from EL4 T cells, we identified several thousand proteins binding to either the very proximal *Foxp3* promoter ("Fra1) or its more distal parts ("Fra2", "Fra3"). To exclude unspecific protein binding to the bead system, we used stringent criteria to select candidates for luciferase-based validation: First, we disregarded proteins binding to two or more fragments; if proteins bound to all three fragments, it was very likely that these proteins were ligated to biotinylation sites or the bead itself. If proteins bound two regions, they might act co-operatively across our assay junction. These would be disregarded in our selection process and classify as false-negatives. Second, we investigated whether our candidate proteins had been detected across both biological replicates and with a certain peptide recovery rate, which forms the basis of the p-value calculation. Furthermore, a false-discovery rate adjustment was performed to reduce the probability of false-positive results. Third, we analyzed whether our candidate proteins are expressed in T cells, which was the case for most of our factors. Finally, more technical aspects during the molecular cloning procedure (cDNA length, availability of commercially available ORFs) narrowed the list of candidates to its final touch. On this list, we identified and cloned out following putative *Foxp3*-promoter binding partners:

To the very proximal *Foxp3* Fra1 promoter sequence, we identified: THAP Domain Containing 11 (Thap11), a transcriptional repressor important during embryogenesis and maintenance of pluripotency; Single-Stranded DNA-Binding Proteins 1 and 2 (Ssbp1 and Ssbp2), which are involved in the regulation of genomic stability in the nucleus; Replication Protein 1 (Rpa1), playing a role for DNA replication and cellular DNA damage response; Poly(RC) Binding Protein 1 and 2 (Pcbp1 and Pcbp2), which are both multifunctional genes involved in RNA binding and co-activation of pro-virus

RNA replication; Heterogeneous Nuclear Ribonucleoproteins (Hnrnpk, Hnrnpd, Hnrnpab) that bind pre-mRNA and influence its processing; a Y Box Binding Protein 1 (Ybx1), which has been reported to modulate the interaction between mRNA and transcription factors at gene promoters, therefore being a transcriptional regulator; Splicing Factor 1 (Sf1), reported as putative transcription repressor which is required for spliceosome assembly; and a Small Nuclear RNA Activating Complex 1 (Snapc1), important for transcription of RNA-polymerase II and III nuclear RNA genes.

We identified 5 binding partners to the more proximal *Foxp3* promoter Fra 2: three Zinc finger proteins Znf574, Znf691, and Znf692, where involvement in transcriptional regulation is predicted, but no more detailed functions are known; Nuclear Transcription Factor Y α (Nfya), which forms a complex with B and C subunits to bind DNA with high affinity, thereby regulating its expression; Regulatory Factor X 1 (Rfx1), transcriptional activator binding target DNA as monomer or heterodimer with other Rfx family members, essential for MHC II gene expression.

Following binding partners were identified at the most distal *Foxp3* promoter fragment 3: Myb-like, SWIRM and MPN Domains 1 (Mysm1), a metalloprotease that actively de-represses epigenetically silenced genes (H2A histone modification) and thereby promotes initiation and elongation steps for gene induction; TGF-β induced Factor Homeobox 2 (Tgif2), a transcriptional repressor recruiting epigenetic silencing mechanisms to TGF-β responsive genes. It might interact with Smad proteins and recruits histone deacetylase proteins; Transcription Factor CP2 (Tfcp2), reported to bind various cellular promoters and regulating the transcriptional switch; N(α)-Acetyltransferase 38, NatC Auxiliary Subunit (Naa38), a protein involved in the acetylation of methionine residues (all gene ontology information from genecards.com, [186]).

In the introduction, we summarized, in a very detailed manner, the pathways involved in *Foxp3* gene expression control. Interestingly, we did not detect obvious factors in our short list of the TCR/CD28 signaling pathway, the PI3K/Akt pathway or the NFκB pathway with our procedure. Only one protein (Tgif2), involved in silencing TGF-β responsive genes, was identified in our screen as a part of the TGF-β axis. When analyzing the GO terms for our candidate proteins carefully, one can appreciate that these proteins fall into three categories: First, some proteins identified with our procedure are reported to repress gene transcription, therefore taking part in gene silencing. Since we know that the *Foxp3* promoter is demethylated in Foxp3 non-

expressing Tconv cells, the presence of a gene-silencing complex at the *Foxp3* promoter in these cells would be feasible. Second, we identified factors for DNA replication and repair/genomic stability. These could be maintenance factors, binding to DNA without inducing gene expression. Third, we found factors that bind RNA or aid in RNA processing and splicing. These proteins are probably standing by to produce pre-mRNA as soon as activating factors are present, being part of a pre-assembled DNA-dependent RNA processing machinery.

In order to confirm the repressive function of some of those factors, we cloned them into eukaryotic expression vectors and tested them in a *Foxp3*-promoter luciferase system. As expected, some factors significantly downmodulated gene expression once over expressed in 293 cells, whereas no factors strongly upregulated gene expression. Furthermore, we tested all factors against small 500 bp *Foxp3* promoter luciferase vectors. Here, we also detected more downregulating effects of our candidate factors. Since 293 cells are derived from embryonic kidney, we now wanted to test our candidates in a T-cell based system. Therefore, we used Jurkat T cells, stimulated with PMA and Ionomycin to induce *Foxp3* gene expression at the full *Foxp3* promoter luciferase vector. Again, some candidates were able to significantly downmodulate gene expression. There was no overlap in the downregulating activity of factors in 293 cells and Jurkat T cells. This can be explained by the test system differences: in 293 cells, endogenous *Foxp3* promoter activity ("leakage") was downmodulated, whereas in Jurkat T cells, TCR-stimulation inducing *Foxp3* promoter activity was decreased. Finally, we tested our factors in TCR – and TGF-β stimulated primary mouse iTreg cells. In this scenario, no factor was able to overrule this potent stimulus. Since we already know that TGF- β pathway components signal along the CNS1 region, but not the *Foxp3* promoter, our promoter binding partners might be unable to dampen this stimulation. Furthermore, from these results, one could infer a rather recessive mode of action for our factors: once no TCR – or TGF-β based signals are present, they can occupy the *Foxp3* promoter and either actively downmodulate expression or block access of transcription-inducing complexes. Once TCR and TGF-β pathway signals are active, the suppressive effect can be overruled. Since our partners were identified based on their binding patterns to the *Foxp3* promoter, and not the CNS1-3 regions, one can also infer that gene-inducing signals at these sites further overrule *Foxp3*-promoter based repression.

Finally, we compared the gene expression profile of our candidate factors in Foxp3-expressing and non-expressing T cells as well as Foxp3-negative cell lines. It was quite surprising to find differences between mouse and human T cells: whereas our candidate *Foxp3*-promoter binding factors are over expressed in human Tconv cells, no differences in expression on protein or RNA level can be detected in the mouse system. Since *Foxp3* gene expression can be transiently induced in human T cells by activation, which normally does not occur in murine T cells, this system difference might be explained by the special circumstances in both species: murine Tconv cells resist *Foxp3* induction when activated by cognate antigen. But in humans, Tconv cells can upregulate Foxp3 in the presence of pro-inflammatory stimuli without becoming a regulatory T cell, losing *Foxp3* gene expression again once stimulation ceases. Therefore, in the human system, TCR engagement by antigen can induce *Foxp3* to a certain extent. Since our factors are only upregulated in the human system, one could infer that the general "leakiness" of the *Foxp3*-regulating system in human Tconv cells is compensated in part by our candidate factors. In the mouse system, where *Foxp3* is more tightly regulated, these factors can still repress gene expression at the promoter, but don't require such strong upregulation.

Additionally, with all candidate factors expressed in EL4 and Jurkat T cells, these cells generally resist strong means of *Foxp3* induction: we were not able to induce *Foxp3* mRNA or protein in Jurkat or EL4 cells by TGF-β treatment in combination with TCR-stimulation by CD3/CD28 microbeads or plate-bound CD3/CD28 (data not shown).

To summarize, we detected putative *Foxp3* promoter binding proteins in this study. We confirmed the gene-repressive nature of some of our candidate factors, and analyzed their expression signature amongst different cell types. To finally prove their function to downmodulate *Foxp3* promoter activity, a Crispr/Caspase based deletion of candidate proteins in a T-cell line *in-vitro* or the T-cell specific knockout *in-vivo* could validate our dataset.

Rbpj is a Notch-independent regulator of Treg cell homeostasis and function

Foxp3 is the master transcription factor in Treg cells, and has been identified by its specific overexpression in these cells. Another protein, Rbpj, is overexpressed in Treg cells as well, albeit at a much lower Treg/Tconv ratio. Our Notch reporter studies and Notch receptor expression analysis revealed that Notch signaling is not active in steady-state Treg cells. So why is Rbpj upregulated in these cells?

Since RBPJ without Notch signaling can act as a profound repressor of transcription, we wanted to study the specific role of Rbpj in Treg cells. Therefore, we performed a Treg-specific deletion of this protein. In young animals, the deletion had no further consequences, as gene expression analysis of Treg cells from six-week old *Foxp3*^{Cre}*Rbpj*$^{\Delta/\Delta}$ and *Foxp3*^{Cre} animals confirmed: only two genes, *Rbpj* and *Dtx1*, were downregulated on a larger scale, with quite a few genes differentially regulated on a smaller scale. Once animals aged beyond 10 weeks, and probably received certain environmental triggers, strong lymphoproliferation with skin pathology, splenomegaly and lymphadenopathy had been observed. Not only Treg cells, which of course were the only cells to experience the loss of Rbpj, increased strongly in absolute numbers (about 10fold), but also conventional T cells, B cells, myeloid cells, and NK cells. Pathological examination revealed that lymph nodes and spleen, albeit being several times bigger than normal, retained their tissue architecture and compartmentalization. This resembles studies where Nr4a transcription factors, which are normally required for proper *Foxp3* induction at the promoter, had been deleted. Treg cells became less suppressive and accelerated the conversion of T cells into T_H2 or T_{FH} effector cells, causing strong lymphoproliferation and autoimmunity [145, 187]. In contrast to this, Treg cells deficient in Rbpj still express Treg-lineage defining proteins such as Foxp3, CD25, CTLA-4, Helios, Nrp-1, and others. Furthermore, gene expression analysis of Treg cells from sick *Foxp3*^{Cre}*Rbpj*$^{\Delta/\Delta}$ revealed that the Treg-specific gene signature was intact. This was confirmed by *in-vitro* experiments, where Rbpj-deficient Treg cells were still suppressive in a CFSE-based *in-vitro* suppression assay and did not produce pro-inflammatory cytokines such as IFN-γ or IL-2 upon PMA/Ionomycin stimulation. Finally, they showed normal demethylation at the CNS2/TSDR region, indicating strong and persistent *Foxp3* expression in these cells. In addition to this, massive parallel sequencing of the T-cell receptors in Treg cells from sick *Foxp3*^{Cre}*Rbpj*$^{\Delta/\Delta}$ and *Foxp3*^{Cre} revealed no substantial differences in TCR repertoire, indicating that neither clonal outgrowth nor malignant conversion accounted for the strong increase in Treg

cell numbers. Additionally, thymic Treg numbers were not different in sick *Foxp3*^{Cre}*Rbpj*$^{\Delta/\Delta}$ and *Foxp3*^{Cre} mice, ruling out increased thymic output as source of increased Treg cell frequency. So why are there so many Treg cells?

Since we did not detect significant differences in the expression of Neuropillin-1 or Helios, which usually indicate peripheral conversion of Tconv into Treg cells, the strong increase in the Treg compartment could be based on either strong proliferation or decreased apoptosis, or both. Therefore, we next determined expression levels of active Caspase-3: significantly less Treg cells expressed active Caspase-3, a sign of imminent apoptosis, in *Foxp3*^{Cre}*Rbpj*$^{\Delta/\Delta}$ animals, as compared to *Foxp3*^{Cre} animals. No differences were detected in Tconv cells. Furthermore, stainings for KI-67 revealed that Rbpj-deficient Treg cells had a much more profound history of proliferation, although analysis of cell cycle via DNA staining did not reveal any more cycling during late-stage disease. Since both lymph nodes and spleen were increased dramatically at this point, and we ruled out malignant conversion as a means of cellular proliferation, we can expect that programs controlling cellular growth by nutrient deprivation or by measuring the size of the respective niche are still active and prevent runaway proliferation as seen with malignant cell lines or primary tumor cells.

But why do other cells, such as B cells, NK cells, and Tconv cells, also increase in numbers? To determine the activation status of these immune cells, we stained for L-selectin, CD25 and CD44. Tconv cells, B cells, CD8 T cells, and NK cells showed significant signs of activation, indicating mobilization against self-tissues in this mouse. Furthermore, we identified autoantibodies via Western Blot and identified an IL-4 (or T_H2) characteristic Ig-subtype class switch in peripheral blood serum. Therefore, we overlaid *Foxp3*^{Cre}*Rbpj*$^{\Delta/\Delta}$ Treg- or Tconv upregulated genes with upregulated genes identified in T_H1, T_H2, and T_H17 gene expression data [129]: indeed, elements of all three pro-inflammatory effector cell types were also upregulated in both Treg and Tconv cells from the *Foxp3*^{Cre}*Rbpj*$^{\Delta/\Delta}$ mouse, indicating that Rbpj-deficient Treg cells lost their ability to control T_H subset differentiation *in-vivo*. In contrast to this, the signature observed in *Foxp3* ^{Cre}*NICD*^{LSL} mice did not show a bias towards either one of the T_H subsets. The upregulation of both T_H1 and T_H2 signature in Tconv cells from sick *Foxp3*^{Cre}*Rbpj*$^{\Delta/\Delta}$ mice was confirmed by intracellular cytokine stainings, where IFN-γ, IL-2, IL-10, and IL-4 were increased. In addition to this, intracellular proteins staining revealed an increase in the expression of both GATA-3 and T-bet, again indicating that both arms of T_H subsets were expanded in this mouse.

Next, we carefully analyzed our gene expression data and the signature present in sick *Foxp3*^{Cre}*Rbpj*$^{\Delta/\Delta}$ animals. We observed that the cell surface receptor for interleukin 7 (IL7R), which is ubiquitously expressed in Tconv cells and CD8 T cells, but not Treg cells, is suddenly upregulated also on Rbpj-deficient Treg cells. Looking at gene expression data from young, healthy *Foxp3*^{Cre}*Rbpj*$^{\Delta/\Delta}$ animals, we saw that loss of Rbpj, early on, translates into increased IL7R expression. Next, we observed that the overexpression of the IL7R is tightly linked to increased Treg cell numbers, with increased proliferation (based on KI-67 and KLRG-1) and decreased apoptosis in these cells. Therefore, we concluded that Rbpj might regulate expression of the IL7R, and the Treg-specific Rbpj deletion induces a strong cytokine stimulation of this cell type, leading to enhanced proliferation.

Furthermore, our gene expression microarray showed the early-on downregulation of Dtx-1, a factor driving T-cell anergy and resistance towards TCR engagement [188]. This might, in combination with the overexpression of the IL7R, release the brakes for increased Treg cell proliferation. Therefore, we investigated the molecular link between Rbpj and the IL7R by Chromatin IP (ChIP), and validated its specific binding there. To further validate this molecular link, we are now planning overexpression studies in T-cell lines and several *in-vitro* experimental procedures such as luciferase-based gene promoter activity screens with both *Rbpj* and *Dtx1* transgenes. We are also testing an Rbpj-Chromatin-IP in primary Treg cells followed by next-generation sequencing. A Rbpj-ChIP-sequencing approach has already been undertaken in a 2013 study with mammalian myogenic cells in the context of stimulated Notch signaling via the exposure to Dll1 ligand [189]. The authors reported that Rbpj bound 158 gene areas upon Dll1 binding, 78 of which were within or near genes. A common Rbpj binding motif, (CC)GTGGGAA, was identified to be present in about 80% of putative binding sites. Furthermore, the study showed that Rbpj binds 63 sites independent of Notch activity, indicating that it might be involved in Notch-independent gene regulation. Once cells were stimulated, 128 genes were induced, while the Rbpj-NICD complexes repressed 175 genes. The authors correlated the putative Rbpj binding sites to gene expression profiles and determined that, of the genomic regions constantly associated with Rbpj and therefore independent of Notch signaling, only one gene was subsequently upregulated upon Dll1 ligand stimulation. This strongly indicates that Rbpj has a Notch-independent role in the regulation of genes; it is thought that Rbpj acts as a general repressor of gene transcription. If NICD translocates to the nucleus upon active Notch

signaling, it can displace repressors and induce gene transcription in concert with Rbpj, or repress gene transcription, respectively. Importantly, for Notch-regulated genes, a simple deletion of Rbpj did not upregulate their expression, indicating that it does not actively repress at those sites or relies on co-factors for gene induction. In contrast to this, Rbpj deletion released suppression at Notch-independent sites, indicating that Rbpj can act as a Notch-independent suppressor of gene translation. If we are able to confirm the role of Rbpj as a repressor of IL7R expression in the absence of NOTCH signaling, and possibly also Dtx-1 expression, we can link molecular deletion of Rbpj and its effects on Treg cell proliferation and homeostasis.

Since we discussed the role of Rbpj in Treg cells and correlated it with our data, we now want to take a step back and review the role of Notch signaling, dependent or independent of Rbpj, for Treg cell homeostasis. Notch-ligand expression by APCs has a profound impact on T-subset generation. When APCs present antigen in the context of Jag1 overexpression, induction of Treg cells from naive T cells has been observed; these Treg cells were shown to inhibit immune responses and transfer tolerance to recipient mice [190]. In another study, Jag1 was overexpressed in Epstein-Barr virus-positive lymphoblastic B-cell lines. Upon co-cultivation with autologous T cells, they acquired a regulatory behavior with increased IL-10 production and the potential to downmodulate proliferation and cytotoxic function of effector T cells [191]. Furthermore, the *in-vivo* administration of Jag-2 expressing hematopoietic progenitor cells in NOD mice caused an expansion of a peripheral Treg cell pool, mediated by Notch3 activation. In contrast to this, Dll4 downmodulates induction of Treg cells. In a model of EAE, treatment with a Dll4 blocking mAb increased Treg cell numbers and decreased EAE severity by downmodulating the effector T_H1/T_H17 response. It is proposed that Dll4 inhibits the Janus kinase 3 (JAK3)-induced STAT5 phosphorylation, which is important for TGF-β mediated induction of Treg cells [166, 192]. Therefore, we can summarize that Jag-ligands promote Treg cell generation, whereas Dll4 ligand inhibits this process.

The involvement of Notch receptors has also been studied. Global treatment with GSIs *in-vitro* blocks the TGF-β mediated upregulation of *Foxp3* gene expression. In the same study, TGF-β induced Smad3 was shown to interact with Notch1, and blocking of this interaction seems to hinder peripheral Treg cell induction. Once, in the same study, GSIs were applied systemically, downregulation of Foxp3 expression was followed by liver lymphocyte infiltration. *In-vitro* studies showed that Treg cells from GSI-treated animals had reduced suppressive capacity as well as reduced Foxp3 expression, leading

to the escape of autoimmune effector T cells [193]. A third report investigated the binding of Rbpj in combination with Notch1-ICD at the *Foxp3* promoter. The *Foxp3* promoter contains a highly conserved RBPJ-binding site meeting the consensus sequence criteria C(T)GTGGGAA. The authors showed that the N1ICD-Rbpj complex could act as trans-activator at this site, confirmed also by Chromatin-IP experiments [194].

The Notch3 receptor, overexpressed on Treg cells compared to Tconv cells, also has a function for Treg cell induction. When Notch3-ICD was overexpressed in thymocytes and T cells, more Treg cells and enhanced CD25 expression have been reported. Interestingly, it was noted that Notch3-dependent *Foxp3* gene induction relies on NFκB pathway components, and both Rbpj and NFκB have overlapping binding sites at the *Foxp3* gene promoter. It was noted that Protein-kinase Cθ (PKCθ), involved in canonical NFκB activation, serves as downstream target of Notch3- and TCR-based signals. If both Notch3-IC and PKCθ were deleted, less Treg cells were produced. This deletion also impaired peripheral Treg generation and Foxp3 expression levels. On the other hand, the upregulation of Notch3 expression lead to the expansion of the Treg niche while remaining fully suppressive, indicating that Notch3 can influence Treg cell homeostasis and function via cooperative effects with PKCθ and NFκB signaling components [195]. In summary, Notch 1 and 3 might play important roles for the homeostasis and function of Treg cells – Notch1 mediating TGF-β induced peripheral Treg induction, and Notch3 influencing thymic Treg cell induction via the PKCθ- NFκB axis. Since our study misses Notch 3 protein and mRNA expression data in Treg cells from wild type and $Foxp3^{Cre}Rbpj^{\Delta/\Delta}$ mice, we are currently performing these experiments.

Notch signaling has also been studied under disease conditions. Two studies evaluated the influence of Notch in the control of graft versus host disease (GVHD) [196, 197]. Expression of dnMAML1, a Notch pathway downmodulator, in mature $CD4^{pos}$ and $CD8^{pos}$ T cells reduced GvHD severity and organ damage, decreased the pro-inflammatory environment, and lead to increased Treg cell expansion. Furthermore, Notch-defective T cells retained their graft versus tumor activity and were still able to mediate anti-leukemia efficiencies. Once animals were systematically treated with GSIs, GvHD was prevented, but side effects at the intestinal epithelium occurred. These findings lead the authors to investigate more closely how Notch signaling mediates autoimmune effects. When they blocked Notch 1 or 2 and Dll1 or 4 with blocking antibodies, it was shown that these signaling pathways are actively involved in

mediating GvHD, with Notch1 and Dll4 being most potent. A combined blockade of Dll1 and Dll4 lead to prevention of GvHD, without any intestinal pathology. Interestingly, Treg cells continuously expanded following this treatment. Similar results have been obtained in reports studying aplastic anemia [198] and vascular inflammation [199]: GSI treatment or specific Notch1 deletion have been shown to be beneficial in both pathological scenarios, both reporting a potential role of Notch signaling in preventing T_H1 differentiation and in promoting Treg cell induction. Taken together, these studies indicate that Notch signaling mediates multifaceted functions in T cells. Whereas Notch signaling is pivotal for the thymic and peripheral induction of Treg cells, it is also implicated in disease progression and severity of autoimmune disease. Therefore, one can infer that Notch has a strong context-dependent way of action, and detailed studies for its functions in T-cell subpopulations under steady state and disease conditions are required. To put it into context with our results, we stained for the expression of Notch1 and Notch2 in Treg cells from sick *Foxp3*^{Cre}*Rbpj*$^{\Delta/\Delta}$ and *Foxp3*^{Cre} mice (data not shown). Again, we did not detect any changes in Notch receptor expression, indicating that the above-mentioned effects of Notch signaling on T_H subset generation might not be relevant in our model.

But what happens once Notch signaling, in the form of over expression of Notch intracellular domain, is constantly active in Treg cells? A recent 2015 study by Charbonnier and co-workers addressed the impact of Notch signaling in Treg cells with the aid of various genetic models [200]. First, the authors investigated the effects of defective Notch receptor generation in Treg cells. Therefore, they selectively deleted the *Pofut1* gene, encoding an enzyme required for the fucosylation of Notch receptors, in Treg cells. The observed a decrease in peripheral CD3 and CD4 T cell numbers, with an increase in naive Treg cells (relative to other CD4 T cells). The expression intensities of key Treg proteins such as Foxp3, CD25, CTLA-4, Helios, and Nrp-1 were increased in peripheral Treg cells. Thymus-resident Treg cells, which just started to express Foxp3 and its linked transgene, the Cre recombinase, did not experience the consequences of Notch signaling deficiencies yet and were normal in number and frequency. To identify whether the effects of Notch-receptor deletion were canonical, the authors performed a Treg-specific *Rbpj* knockout, yielding pretty much the same results as described above: increased Treg cell numbers and increased expression of key Treg proteins. One can conclude that loss-of-function mutations of all Notch receptors in already-developed Treg cells increase their concomitant expression of CD25, Helios, and Nrp-1, increasing

the fitness of Treg cells under steady state conditions. Our data from young and healthy *Foxp3*^{Cre}*Rbpj*$^{\Delta/\Delta}$ mice also show that Treg cells in these mice are, at least based on key protein expression and *in-vitro* assay performance, equally functional as compared to wild type Treg cells.

To study the effects of defective Notch signaling in Treg cells under disease conditions, the authors induced GvHD by lethal irradiation of donor mice followed by transfer of HLA-mismatched splenocytes. When they co-transferred either Rbpj-deficient or Notch-deficient Treg cells, GvHD was attenuated. This again indicates elevated fitness and potency of Notch-deficient Treg cells. Furthermore, they observed a strongly increased Treg compartment, both in frequency and absolute numbers, alongside a downregulation of apoptosis markers on Treg cells. Therefore, Notch-signaling deficiency protects Treg cells from early apoptosis, and increases their potency to down-modulate GvHD in a transfer model.

To study the effects of Notch overactivity in already-developed Treg cells, the authors overexpressed Notch1-ICD in Treg cells. They observed increased expression of typical Notch target genes such as *Hes1*, *Hey1*, and *Dtx1*. The animals suffered from lymphoproliferative disease with large-vessel vasculitis and organ infiltrations, along an expansion of memory effector T cells with increased IFN-γ expression. The Treg cell compartment was decreased, and markers for apoptosis were increased. Furthermore, Treg cells exhibited less expression of CD25, CTLA-4, OX40, Helios, Nrp-1 and Eos. Treg cells showed defects in suppressive capacity, and were less stable when adoptively transferred, albeit being demethylated at the CNS2 locus. The above-mentioned defects in Treg cells were alleviated once Rbpj was co-deleted while overexpressing Notch1-ICD. This indicates that canonical Notch signaling is responsible, once active, for a competitive disadvantage in Treg cells. This translates into a reduction Treg cell number and suppressive capacity, finally leading to effector cell escape, lymphoproliferation, and autoimmune disease. Notch signaling can mediate this via its direct binding to Foxp3-regulated genes, where it can antagonize Foxp3 binding or revert the epigenetic marks set by Foxp3. Furthermore, Notch is implicated in the ability of Treg cells to abort T_H1 programming of effector T cells.

To summarize, the above-mentioned study investigated the role of Notch signaling for the Treg cell compartment. It showed that a deletion of Notch components increased Treg frequency and fitness, while an overexpression of Notch1-IC caused increased Treg apoptosis with decreased Treg functionality, finally leading to systemic

autoimmunity. It was proposed that Notch1-IC overexpressing Treg cells lose their ability to control T_H1 responses: normally, Treg cell run only a certain part of the T_H1 differentiation program to preserve their potential to suppress T_H1 effector T cell responses. With Notch1-IC overactive, this blockade is bypassed and Treg cells acquire the ability to make pro-inflammatory cytokines while unable to downregulate effector T cells, rendering them unable to control peripheral immune tolerance.

Taking this information into account, we can conclude the following from our study of Rbpj-deficient Treg cells: a deficiency in Rbpj protects Treg cells from early apoptosis, thereby increasing Treg cell numbers. Furthermore, our data link the IL7R and Dtx-1 to this deletion, enabling a molecular understanding of the increased fitness and proliferation of Rbpj-deficient Treg cells. Furthermore, even though Treg cells from *Foxp3*^{Cre}*Rbpj*$^{\Delta/\Delta}$ animals were still suppressive *in-vitro* (based on our data) and protected against GvHD in a transfer model (based on [200]), autoimmune pathology still evoked in this model, not appreciated in the previously-mentioned study. Interestingly, these pathological evaluations mimic observations in human patients suffering from Omenn syndrome: studies report hepatomegaly, splenomegaly, and lymphadenopathy, as well as erythroderma (inflammatory skin disease) and chronic diarrhea. Furthermore, serum IgE levels are elevated, autoantibodies are generated and more IL-4 cytokine is produced. Closer examination revealed that these patients suffer from impaired T-cell development in the thymus [201, 202]. It would be interesting to investigate whether patients have mutations in *Rbpj*, *Dtx1*, or *Il7r* genes in their Treg compartment, probably also leading to increased Treg cell numbers and thereby mimicking our genetic deletion approach. Interestingly, one study already indicated development of this disease in a patient with mutations in the *Il7ra* gene, although care must be taken since this receptor has multifaceted roles in thymic T-cell development and post-thymic T-cell homeostasis [203].

Taken together, we showed that Rbpj, commonly expressed in Treg cells, might be involved in the regulation of homeostasis and function of these cells. Its selective knockout causes a moribund increase in Treg cell frequency, and renders them defective to control autoimmune responses over time. Therefore, manipulations at the Rbpj signaling axis might on the one hand promote Treg proliferation and survival, but might also render them defective for their most important function, the suppression of autoimmune events.

Implications of this work for future studies and research

Initially, we set the goal that our studies presented in this thesis would enhance the knowledge about transcriptional control of Treg cells and thereby provide a benefit for society. Indeed, we investigated the epigenetic status of the *Foxp3* gene and its promoter in detail, providing additional knowledge about CG-dinucleotide methylation-based control at this locus. Since the selected demethylation of the TSDR in Treg cells is being used as clinical marker for Treg cells (Epiontis GmbH, part of the Immune Tolerance Network), our detailed analysis of the *Foxp3* gene can provide additional probes for epigenetic diagnosis of Treg cell characteristics for the clinic. Furthermore, our whole-genome based epigenetic analysis of Treg cells from fat, skin, liver, and lymph nodes will allow the precise detection of tissue-based differences in the CG methylation status. Once we detect and analyze Treg-specific and tissue-specific epigenetic alterations, this knowledge can be used for the development of additional diagnostic tests. Importantly, since we already know that tissue-resident Treg cells take on specific effector functions, our methylation data will provide new insight into tissue-specific adaption of not only Treg cells, but also T cells in general. This could, one day, allow the specific manipulation of tissue-resident Treg cell frequency or function, clinically relevant in many disease such as diabetes (fat-resident Treg cells), psoriasis and other autoimmune skin diseases (skin-resident Treg cells), or hepatitis (liver-resident Treg cells).

Next, we identified a repressive complex at the *Foxp3* gene promoter, which might enhance or even block Foxp3 protein expression. Since many studies search for Foxp3-regulating small molecules or proteins, our data could allow the prediction of such interactions and explain the efficacy of certain drugs identified with these screens. One day, this knowledge might be used for the *in-vivo* manipulation of *Foxp3* promoter occupancy – with the goal to adjust *Foxp3* expression strength therapeutically.

Finally, in our Rbpj study, we identified a novel, Notch-independent axis regulating Treg cell homeostasis and function. We observed that mice with Rbpj-deficient Treg cells develop autoimmune disease over time. Interestingly, these mice have highly elevated Treg cell numbers, and these Treg cells are functional and suppressive *in-vitro*. Still, they lost their *in-vivo* functionality, indicating that Rbpj has a Notch-independent role to maintain proper performance of Treg cells. Understanding the detailed mechanisms of action, these findings could eventually allow the fine-regulation of Treg cell number and function *in-vivo*, becoming a clinically relevant treatment option.

Publications relevant to or originating from this work (published or pending)

- *Richards DM,* ***Delacher M****, Goldfarb Y, Kägebein D, Hofer AC, Abramson J and Feuerer M.* Treg cell differentiation: from thymus to peripheral tissue. Prog Mol Biol Transl Sci. 2015; 136: 175-205.

- *Barra MM, Richards DM, Hofer AC,* ***Delacher M****, Feuerer M*. Premature expression of Foxp3 in double-negative thymocytes. PLoS One. 2015 May 15; 10(5).

- *Barra MM, Richards DM, Hansson J, Hofer AC,* ***Delacher M****, Hettinger J, Krijgsveld J, Feuerer M.* Transcription Factor 7 Limits Regulatory T Cell Generation in the Thymus. J Immunol. 2015 Oct 1; 195(7): 3058-70.

- *Medrikova D, Sijmonsma TP, Sowodniok K, Richards DM,* ***Delacher M****, Sticht C, Gretz N, Schafmeier T, Feuerer M, Herzig S*: Brown adipose tissue harbors a distinct sub-population of regulatory T cells. PLoS One. 2015 Feb 25; 10(2).

- ***Michael Delacher****, Lisa Schreiber, David M Richards, Carla Farah, Markus Feuerer and Jochen Huehn:* Transcriptional Control of Regulatory T cells, Curr Top Microbiol Immunol. 2014; 381:83-124.

- *Seidel P, Remus M,* ***Delacher M,*** *Grigaravicius P, Reuss DE, Frappart L, Von Deimling A, Feuerer M, Abdollahi A, Frappart PO*: Specific epidermal Nbn deletion causes premature hair loss and psoriasiform dermatitis. Re-submitted to Journal of Infectious Diseases 2015, publication pending.

- *Herzig Y, Brezis MR, Katz S, Ben-Hur S, Shkedy A, Eisenberg M, Levi B,* ***Delacher M****, Goldfarb Y, Ben-Dor S, Giraud M, Breiling A, Feuerer M and Abramson J.* What Turns Aire on? – Transcriptional programs controlling the expression of the Autoimmune regulator gene. Under review at Nature Immunology 2015, publication pending.

9 References

1. Ken Murphy, P.T., Mark Walport *Janeway's Immunobiology*, 2007.

2. Sakaguchi, S., Yamaguchi, T., Nomura, T. & Ono, M. Regulatory T cells and immune tolerance. *Cell* **133**, 775-787 (2008).

3. Miller, J.F. The golden anniversary of the thymus. *Nat Rev Immunol* **11**, 489-495 (2011).

4. Kyewski, B. & Klein, L. A central role for central tolerance. *Annu Rev Immunol* **24**, 571-606 (2006).

5. Starr, T.K., Jameson, S.C. & Hogquist, K.A. Positive and negative selection of T cells. *Annu Rev Immunol* **21**, 139-176 (2003).

6. Anderson, M.S. *et al.* The cellular mechanism of Aire control of T cell tolerance. *Immunity* **23**, 227-239 (2005).

7. Anderson, M.S. *et al.* Projection of an immunological self shadow within the thymus by the aire protein. *Science* **298**, 1395-1401 (2002).

8. Nagamine, K. *et al.* Positional cloning of the APECED gene. *Nat Genet* **17**, 393-398 (1997).

9. Bonomo, A. *et al.* Pathogenesis of post-thymectomy autoimmunity. Role of syngeneic MLR-reactive T cells. *J Immunol* **154**, 6602-6611 (1995).

10. Shevach, E.M. Regulatory T cells in autoimmmunity*. *Annu Rev Immunol* **18**, 423-449 (2000).

11. Asano, M., Toda, M., Sakaguchi, N. & Sakaguchi, S. Autoimmune disease as a consequence of developmental abnormality of a T cell subpopulation. *J Exp Med* **184**, 387-396 (1996).

12. Sakaguchi, S., Sakaguchi, N., Asano, M., Itoh, M. & Toda, M. Immunologic self-tolerance maintained by activated T cells expressing IL-2 receptor alpha-chains (CD25). Breakdown of a single mechanism of self-tolerance causes various autoimmune diseases. *J Immunol* **155**, 1151-1164 (1995).

13. Sakaguchi, S. *et al.* T cell-mediated maintenance of natural self-tolerance: its breakdown as a possible cause of various autoimmune diseases. *J Autoimmun* **9**, 211-220 (1996).

14. Khattri, R., Cox, T., Yasayko, S.A. & Ramsdell, F. An essential role for Scurfin in CD4+CD25+ T regulatory cells. *Nat Immunol* **4**, 337-342 (2003).

15. Hori, S., Nomura, T. & Sakaguchi, S. Control of regulatory T cell development by the transcription factor Foxp3. *Science* **299**, 1057-1061 (2003).

16. Fontenot, J.D., Gavin, M.A. & Rudensky, A.Y. Foxp3 programs the development and function of CD4+CD25+ regulatory T cells. *Nat Immunol* **4**, 330-336 (2003).

17. Wildin, R.S., Smyk-Pearson, S. & Filipovich, A.H. Clinical and molecular features of the immunodysregulation, polyendocrinopathy, enteropathy, X linked (IPEX) syndrome. *J Med Genet* **39**, 537-545 (2002).

18. Wildin, R.S. *et al.* X-linked neonatal diabetes mellitus, enteropathy and endocrinopathy syndrome is the human equivalent of mouse scurfy. *Nat Genet* **27**, 18-20 (2001).

19. Lahl, K. *et al.* Selective depletion of Foxp3+ regulatory T cells induces a scurfy-like disease. *J Exp Med* **204**, 57-63 (2007).

20. Abbas, A.K. *et al.* Regulatory T cells: recommendations to simplify the nomenclature. *Nat Immunol* **14**, 307-308 (2013).

21. Fontenot, J.D., Dooley, J.L., Farr, A.G. & Rudensky, A.Y. Developmental regulation of Foxp3 expression during ontogeny. *J Exp Med* **202**, 901-906 (2005).

22. Hsieh, C.S., Lee, H.M. & Lio, C.W. Selection of regulatory T cells in the thymus. *Nat Rev Immunol* **12**, 157-167 (2012).

23. Jordan, M.S. *et al.* Thymic selection of CD4+CD25+ regulatory T cells induced by an agonist self-peptide. *Nat Immunol* **2**, 301-306 (2001).

24. Moran, A.E. *et al.* T cell receptor signal strength in Treg and iNKT cell development demonstrated by a novel fluorescent reporter mouse. *J Exp Med* **208**, 1279-1289 (2011).

25. Lee, H.M., Bautista, J.L. & Hsieh, C.S. Thymic and peripheral differentiation of regulatory T cells. *Adv Immunol* **112**, 25-71 (2011).

26. Bautista, J.L. *et al.* Intraclonal competition limits the fate determination of regulatory T cells in the thymus. *Nat Immunol* **10**, 610-617 (2009).

27. Leung, M.W., Shen, S. & Lafaille, J.J. TCR-dependent differentiation of thymic Foxp3+ cells is limited to small clonal sizes. *J Exp Med* **206**, 2121-2130 (2009).

28. Burchill, M.A. *et al.* Linked T cell receptor and cytokine signaling govern the development of the regulatory T cell repertoire. *Immunity* **28**, 112-121 (2008).

29. Lio, C.W. & Hsieh, C.S. A two-step process for thymic regulatory T cell development. *Immunity* **28**, 100-111 (2008).

30. Yang, S., Fujikado, N., Kolodin, D., Benoist, C. & Mathis, D. Immune tolerance. Regulatory T cells generated early in life play a distinct role in maintaining self-tolerance. *Science* **348**, 589-594 (2015).

31. Atarashi, K. *et al.* Induction of colonic regulatory T cells by indigenous Clostridium species. *Science* **331**, 337-341 (2011).

32. Lathrop, S.K. *et al.* Peripheral education of the immune system by colonic commensal microbiota. *Nature* **478**, 250-254 (2011).

33. Coombes, J.L. *et al.* A functionally specialized population of mucosal CD103+ DCs induces Foxp3+ regulatory T cells via a TGF-beta and retinoic acid-dependent mechanism. *J Exp Med* **204**, 1757-1764 (2007).

34. Chen, W. *et al.* Conversion of peripheral CD4+CD25- naive T cells to CD4+CD25+ regulatory T cells by TGF-beta induction of transcription factor Foxp3. *J Exp Med* **198**, 1875-1886 (2003).

35. Becker, C. *et al.* TGF-beta suppresses tumor progression in colon cancer by inhibition of IL-6 trans-signaling. *Immunity* **21**, 491-501 (2004).

36. Polansky, J.K. *et al.* DNA methylation controls Foxp3 gene expression. *Eur J Immunol* **38**, 1654-1663 (2008).

37. Shevach, E.M. Mechanisms of foxp3+ T regulatory cell-mediated suppression. *Immunity* **30**, 636-645 (2009).

38. Allan, S.E. *et al.* Activation-induced FOXP3 in human T effector cells does not suppress proliferation or cytokine production. *Int Immunol* **19**, 345-354 (2007).

39. Miyara, M. *et al.* Functional delineation and differentiation dynamics of human CD4+ T cells expressing the FoxP3 transcription factor. *Immunity* **30**, 899-911 (2009).

40. Miyao, T. *et al.* Plasticity of Foxp3(+) T cells reflects promiscuous Foxp3 expression in conventional T cells but not reprogramming of regulatory T cells. *Immunity* **36**, 262-275 (2012).

41. Sugimoto, N. *et al.* Foxp3-dependent and -independent molecules specific for CD25+CD4+ natural regulatory T cells revealed by DNA microarray analysis. *Int Immunol* **18**, 1197-1209 (2006).

42. Hill, J.A. *et al.* Foxp3 transcription-factor-dependent and -independent regulation of the regulatory T cell transcriptional signature. *Immunity* **27**, 786-800 (2007).

43. Tran, D.Q., Ramsey, H. & Shevach, E.M. Induction of FOXP3 expression in naive human CD4+FOXP3 T cells by T-cell receptor stimulation is transforming growth factor-beta dependent but does not confer a regulatory phenotype. *Blood* **110**, 2983-2990 (2007).

44. Ohkura, N. *et al.* T cell receptor stimulation-induced epigenetic changes and Foxp3 expression are independent and complementary events required for Treg cell development. *Immunity* **37**, 785-799 (2012).

45. Thornton, A.M. *et al.* Expression of Helios, an Ikaros transcription factor family member, differentiates thymic-derived from peripherally induced Foxp3+ T regulatory cells. *J Immunol* **184**, 3433-3441 (2010).

46. Takatori, H. *et al.* Helios Enhances Treg Cell Function in Cooperation With FoxP3. *Arthritis Rheumatol* **67**, 1491-1502 (2015).

47. Jarvis, A. *et al.* Small molecule inhibitors of the neuropilin-1 vascular endothelial growth factor A (VEGF-A) interaction. *J Med Chem* **53**, 2215-2226 (2010).

48. Bruder, D. *et al.* Neuropilin-1: a surface marker of regulatory T cells. *Eur J Immunol* **34**, 623-630 (2004).

49. Weiss, J.M. *et al.* Neuropilin 1 is expressed on thymus-derived natural regulatory T cells, but not mucosa-generated induced Foxp3+ T reg cells. *J Exp Med* **209**, 1723-1742, S1721 (2012).

50. Yadav, M. *et al.* Neuropilin-1 distinguishes natural and inducible regulatory T cells among regulatory T cell subsets in vivo. *J Exp Med* **209**, 1713-1722, S1711-1719 (2012).

51. Milpied, P. *et al.* Neuropilin-1 is not a marker of human Foxp3+ Treg. *Eur J Immunol* **39**, 1466-1471 (2009).

52. Zhan, Y. *et al.* TCR-mediated activation promotes GITR upregulation in T cells and resistance to glucocorticoid-induced death. *Int Immunol* **16**, 1315-1321 (2004).

53. Shimizu, J., Yamazaki, S., Takahashi, T., Ishida, Y. & Sakaguchi, S. Stimulation of CD25(+)CD4(+) regulatory T cells through GITR breaks immunological self-tolerance. *Nat Immunol* **3**, 135-142 (2002).

54. Stephens, G.L. *et al.* Engagement of glucocorticoid-induced TNFR family-related receptor on effector T cells by its ligand mediates resistance to suppression by CD4+CD25+ T cells. *J Immunol* **173**, 5008-5020 (2004).

55. Ephrem, A. *et al.* Modulation of Treg cells/T effector function by GITR signaling is context-dependent. *Eur J Immunol* **43**, 2421-2429 (2013).

56. Schaer, D.A. *et al.* GITR pathway activation abrogates tumor immune suppression through loss of regulatory T cell lineage stability. *Cancer Immunol Res* **1**, 320-331 (2013).

57. Brunet, J.F. *et al.* A new member of the immunoglobulin superfamily--CTLA-4. *Nature* **328**, 267-270 (1987).

58. Tai, X. *et al.* Basis of CTLA-4 function in regulatory and conventional CD4(+) T cells. *Blood* **119**, 5155-5163 (2012).

59. Barnes, M.J. *et al.* CTLA-4 promotes Foxp3 induction and regulatory T cell accumulation in the intestinal lamina propria. *Mucosal Immunol* **6**, 324-334 (2013).

60. Richards, D.M. *et al.* Treg Cell Differentiation: From Thymus to Peripheral Tissue. *Prog Mol Biol Transl Sci* **136**, 175-205 (2015).

61. Feuerer, M. *et al.* Lean, but not obese, fat is enriched for a unique population of regulatory T cells that affect metabolic parameters. *Nat Med* **15**, 930-939 (2009).

62. Cipolletta, D., Cohen, P., Spiegelman, B.M., Benoist, C. & Mathis, D. Appearance and disappearance of the mRNA signature characteristic of Treg cells in visceral adipose tissue: age, diet, and PPARgamma effects. *Proc Natl Acad Sci U S A* **112**, 482-487 (2015).

63. Cipolletta, D., Kolodin, D., Benoist, C. & Mathis, D. Tissular T(regs): a unique population of adipose-tissue-resident Foxp3+CD4+ T cells that impacts organismal metabolism. *Semin Immunol* **23**, 431-437 (2011).

64. Cipolletta, D. *et al.* PPAR-gamma is a major driver of the accumulation and phenotype of adipose tissue Treg cells. *Nature* **486**, 549-553 (2012).

65. Feuerer, M., Shen, Y., Littman, D.R., Benoist, C. & Mathis, D. How punctual ablation of regulatory T cells unleashes an autoimmune lesion within the pancreatic islets. *Immunity* **31**, 654-664 (2009).

66. Bennett, C.L. *et al.* The immune dysregulation, polyendocrinopathy, enteropathy, X-linked syndrome (IPEX) is caused by mutations of FOXP3. *Nat Genet* **27**, 20-21 (2001).

67. Hiraoka, N., Onozato, K., Kosuge, T. & Hirohashi, S. Prevalence of FOXP3+ regulatory T cells increases during the progression of pancreatic ductal adenocarcinoma and its premalignant lesions. *Clin Cancer Res* **12**, 5423-5434 (2006).

68. Sather, B.D. *et al.* Altering the distribution of Foxp3(+) regulatory T cells results in tissue-specific inflammatory disease. *J Exp Med* **204**, 1335-1347 (2007).

69. Antiga, E. *et al.* Regulatory T cells in the skin lesions and blood of patients with systemic sclerosis and morphoea. *Br J Dermatol* **162**, 1056-1063 (2010).

70. Zhang, K. *et al.* Functional characterization of CD4+CD25+ regulatory T cells differentiated in vitro from bone marrow-derived haematopoietic cells of psoriasis patients with a family history of the disorder. *Br J Dermatol* **158**, 298-305 (2008).

71. Sugiyama, H. *et al.* Dysfunctional blood and target tissue CD4+CD25high regulatory T cells in psoriasis: mechanism underlying unrestrained pathogenic effector T cell proliferation. *J Immunol* **174**, 164-173 (2005).

72. Trujillo, G., Hartigan, A.J. & Hogaboam, C.M. T regulatory cells and attenuated bleomycin-induced fibrosis in lungs of CCR7-/- mice. *Fibrogenesis Tissue Repair* **3**, 18 (2010).

73. Hartl, D. *et al.* Quantitative and functional impairment of pulmonary CD4+CD25hi regulatory T cells in pediatric asthma. *J Allergy Clin Immunol* **119**, 1258-1266 (2007).

74. Pesenacker, A.M., Broady, R. & Levings, M.K. Control of tissue-localized immune responses by human regulatory T cells. *Eur J Immunol* **45**, 333-343 (2015).

75. Ma, X. *et al.* A high-fat diet and regulatory T cells influence susceptibility to endotoxin-induced liver injury. *Hepatology* **46**, 1519-1529 (2007).

76. Breous, E., Somanathan, S., Vandenberghe, L.H. & Wilson, J.M. Hepatic regulatory T cells and Kupffer cells are crucial mediators of systemic T cell tolerance to antigens targeting murine liver. *Hepatology* **50**, 612-621 (2009).

77. Erhardt, A., Biburger, M., Papadopoulos, T. & Tiegs, G. IL-10, regulatory T cells, and Kupffer cells mediate tolerance in concanavalin A-induced liver injury in mice. *Hepatology* **45**, 475-485 (2007).

78. Gao, Q. *et al.* Intratumoral balance of regulatory and cytotoxic T cells is associated with prognosis of hepatocellular carcinoma after resection. *J Clin Oncol* **25**, 2586-2593 (2007).

79. Kobayashi, N. *et al.* FOXP3+ regulatory T cells affect the development and progression of hepatocarcinogenesis. *Clin Cancer Res* **13**, 902-911 (2007).

80. Burzyn, D. *et al.* A special population of regulatory T cells potentiates muscle repair. *Cell* **155**, 1282-1295 (2013).

81. Littman, D.R. & Rudensky, A.Y. Th17 and regulatory T cells in mediating and restraining inflammation. *Cell* **140**, 845-858 (2010).

82. Nishikawa, H. & Sakaguchi, S. Regulatory T cells in tumor immunity. *Int J Cancer* **127**, 759-767 (2010).

83. Nishikawa, H. & Sakaguchi, S. Regulatory T cells in cancer immunotherapy. *Curr Opin Immunol* **27**, 1-7 (2014).

84. Onizuka, S. *et al.* Tumor rejection by in vivo administration of anti-CD25 (interleukin-2 receptor alpha) monoclonal antibody. *Cancer Res* **59**, 3128-3133 (1999).

85. Sutmuller, R.P. *et al.* Synergism of cytotoxic T lymphocyte-associated antigen 4 blockade and depletion of CD25(+) regulatory T cells in antitumor therapy reveals alternative pathways for suppression of autoreactive cytotoxic T lymphocyte responses. *J Exp Med* **194**, 823-832 (2001).

86. Antony, P.A. *et al.* CD8+ T cell immunity against a tumor/self-antigen is augmented by CD4+ T helper cells and hindered by naturally occurring T regulatory cells. *J Immunol* **174**, 2591-2601 (2005).

87. Lutsiak, M.E. *et al.* Inhibition of CD4(+)25+ T regulatory cell function implicated in enhanced immune response by low-dose cyclophosphamide. *Blood* **105**, 2862-2868 (2005).

88. Ercolini, A.M. *et al.* Recruitment of latent pools of high-avidity CD8(+) T cells to the antitumor immune response. *J Exp Med* **201**, 1591-1602 (2005).

89. Nishikawa, H. *et al.* Accelerated chemically induced tumor development mediated by CD4+CD25+ regulatory T cells in wild-type hosts. *Proc Natl Acad Sci U S A* **102**, 9253-9257 (2005).

90. Walter, S. *et al.* Multipeptide immune response to cancer vaccine IMA901 after single-dose cyclophosphamide associates with longer patient survival. *Nat Med* **18**, 1254-1261 (2012).

91. Attia, P., Maker, A.V., Haworth, L.R., Rogers-Freezer, L. & Rosenberg, S.A. Inability of a fusion protein of IL-2 and diphtheria toxin (Denileukin Diftitox, DAB389IL-2, ONTAK) to eliminate regulatory T lymphocytes in patients with melanoma. *J Immunother* **28**, 582-592 (2005).

92. Dannull, J. *et al.* Enhancement of vaccine-mediated antitumor immunity in cancer patients after depletion of regulatory T cells. *J Clin Invest* **115**, 3623-3633 (2005).

93. Jacobs, J.F. *et al.* Dendritic cell vaccination in combination with anti-CD25 monoclonal antibody treatment: a phase I/II study in metastatic melanoma patients. *Clin Cancer Res* **16**, 5067-5078 (2010).

94. Miyara, M., Ito, Y. & Sakaguchi, S. TREG-cell therapies for autoimmune rheumatic diseases. *Nat Rev Rheumatol* **10**, 543-551 (2014).

95. Hodi, F.S. *et al.* Improved survival with ipilimumab in patients with metastatic melanoma. *N Engl J Med* **363**, 711-723 (2010).

96. Robert, C. *et al.* Ipilimumab plus dacarbazine for previously untreated metastatic melanoma. *N Engl J Med* **364**, 2517-2526 (2011).

97. Simpson, T.R. *et al.* Fc-dependent depletion of tumor-infiltrating regulatory T cells co-defines the efficacy of anti-CTLA-4 therapy against melanoma. *J Exp Med* **210**, 1695-1710 (2013).

98. Dolan, D.E. & Gupta, S. PD-1 pathway inhibitors: changing the landscape of cancer immunotherapy. *Cancer Control* **21**, 231-237 (2014).

99. Topalian, S.L. *et al.* Safety, activity, and immune correlates of anti-PD-1 antibody in cancer. *N Engl J Med* **366**, 2443-2454 (2012).

100. Riley, J.L., June, C.H. & Blazar, B.R. Human T regulatory cell therapy: take a billion or so and call me in the morning. *Immunity* **30**, 656-665 (2009).

101. Zhao, D. *et al.* In vivo-activated CD103+CD4+ regulatory T cells ameliorate ongoing chronic graft-versus-host disease. *Blood* **112**, 2129-2138 (2008).

102. Portela, A. & Esteller, M. Epigenetic modifications and human disease. *Nat Biotechnol* **28**, 1057-1068 (2010).

103. Wyatt, G.R. Recognition and estimation of 5-methylcytosine in nucleic acids. *Biochem J* **48**, 581-584 (1951).

104. Li, B., Carey, M. & Workman, J.L. The role of chromatin during transcription. *Cell* **128**, 707-719 (2007).

105. Bird, A.P. & Southern, E.M. Use of restriction enzymes to study eukaryotic DNA methylation: I. The methylation pattern in ribosomal DNA from Xenopus laevis. *J Mol Biol* **118**, 27-47 (1978).

106. Suzuki, M.M. & Bird, A. DNA methylation landscapes: provocative insights from epigenomics. *Nat Rev Genet* **9**, 465-476 (2008).

107. Jones, P.A. & Takai, D. The role of DNA methylation in mammalian epigenetics. *Science* **293**, 1068-1070 (2001).

108. Bird, A.P. CpG-rich islands and the function of DNA methylation. *Nature* **321**, 209-213 (1986).

109. Larsen, F., Gundersen, G., Lopez, R. & Prydz, H. CpG islands as gene markers in the human genome. *Genomics* **13**, 1095-1107 (1992).

110. Vinson, C. & Chatterjee, R. CG methylation. *Epigenomics* **4**, 655-663 (2012).

111. Rozenberg, J.M. *et al.* All and only CpG containing sequences are enriched in promoters abundantly bound by RNA polymerase II in multiple tissues. *BMC Genomics* **9**, 67 (2008).

112. Tate, P.H. & Bird, A.P. Effects of DNA methylation on DNA-binding proteins and gene expression. *Curr Opin Genet Dev* **3**, 226-231 (1993).

113. Weber, M. *et al.* Distribution, silencing potential and evolutionary impact of promoter DNA methylation in the human genome. *Nat Genet* **39**, 457-466 (2007).

114. Rishi, V. *et al.* CpG methylation of half-CRE sequences creates C/EBPalpha binding sites that activate some tissue-specific genes. *Proc Natl Acad Sci U S A* **107**, 20311-20316 (2010).

115. Frommer, M. *et al.* A genomic sequencing protocol that yields a positive display of 5-methylcytosine residues in individual DNA strands. *Proc Natl Acad Sci U S A* **89**, 1827-1831 (1992).

116. Ball, M.P. *et al.* Targeted and genome-scale strategies reveal gene-body methylation signatures in human cells. *Nat Biotechnol* **27**, 361-368 (2009).

117. Weber, M. *et al.* Chromosome-wide and promoter-specific analyses identify sites of differential DNA methylation in normal and transformed human cells. *Nat Genet* **37**, 853-862 (2005).

118. Cokus, S.J. *et al.* Shotgun bisulphite sequencing of the Arabidopsis genome reveals DNA methylation patterning. *Nature* **452**, 215-219 (2008).

119. Wang, Q. *et al.* Tagmentation-based whole-genome bisulfite sequencing. *Nat Protoc* **8**, 2022-2032 (2013).

120. Reik, W., Dean, W. & Walter, J. Epigenetic reprogramming in mammalian development. *Science* **293**, 1089-1093 (2001).

121. Denis, H., Ndlovu, M.N. & Fuks, F. Regulation of mammalian DNA methyltransferases: a route to new mechanisms. *EMBO Rep* **12**, 647-656 (2011).

122. Zorn, E. *et al.* IL-2 regulates FOXP3 expression in human CD4+CD25+ regulatory T cells through a STAT-dependent mechanism and induces the expansion of these cells in vivo. *Blood* **108**, 1571-1579 (2006).

123. Kim, H.P. & Leonard, W.J. CREB/ATF-dependent T cell receptor-induced FoxP3 gene expression: a role for DNA methylation. *J Exp Med* **204**, 1543-1551 (2007).

124. Baron, U. *et al.* DNA demethylation in the human FOXP3 locus discriminates regulatory T cells from activated FOXP3(+) conventional T cells. *Eur J Immunol* **37**, 2378-2389 (2007).

125. Floess, S. *et al.* Epigenetic control of the foxp3 locus in regulatory T cells. *PLoS Biol* **5**, e38 (2007).

126. Huehn, J., Polansky, J.K. & Hamann, A. Epigenetic control of FOXP3 expression: the key to a stable regulatory T-cell lineage? *Nat Rev Immunol* **9**, 83-89 (2009).

127. Schreiber, L. *et al.* The Treg-specific demethylated region stabilizes Foxp3 expression independently of NF-kappaB signaling. *PLoS One* **9**, e88318 (2014).

128. Morikawa, H. & Sakaguchi, S. Genetic and epigenetic basis of Treg cell development and function: from a FoxP3-centered view to an epigenome-defined view of natural Treg cells. *Immunol Rev* **259**, 192-205 (2014).

129. Wei, G. *et al.* Global mapping of H3K4me3 and H3K27me3 reveals specificity and plasticity in lineage fate determination of differentiating CD4+ T cells. *Immunity* **30**, 155-167 (2009).

130. Morikawa, H. *et al.* Differential roles of epigenetic changes and Foxp3 expression in regulatory T cell-specific transcriptional regulation. *Proc Natl Acad Sci U S A* **111**, 5289-5294 (2014).

131. Cabezas-Wallscheid, N. *et al.* Identification of regulatory networks in HSCs and their immediate progeny via integrated proteome, transcriptome, and DNA methylome analysis. *Cell Stem Cell* **15**, 507-522 (2014).

132. Lipka, D.B. *et al.* Identification of DNA methylation changes at cis-regulatory elements during early steps of HSC differentiation using tagmentation-based whole genome bisulfite sequencing. *Cell Cycle* **13**, 3476-3487 (2014).

133. Brunkow, M.E. *et al.* Disruption of a new forkhead/winged-helix protein, scurfin, results in the fatal lymphoproliferative disorder of the scurfy mouse. *Nat Genet* **27**, 68-73 (2001).

134. Vang, K.B. *et al.* IL-2, -7, and -15, but not thymic stromal lymphopoeitin, redundantly govern CD4+Foxp3+ regulatory T cell development. *J Immunol* **181**, 3285-3290 (2008).

135. Battaglia, M. *et al.* Rapamycin promotes expansion of functional CD4+CD25+FOXP3+ regulatory T cells of both healthy subjects and type 1 diabetic patients. *J Immunol* **177**, 8338-8347 (2006).

136. Delacher, M. *et al.* Transcriptional control of regulatory T cells. *Curr Top Microbiol Immunol* **381**, 83-124 (2014).

137. Tone, Y. *et al.* Smad3 and NFAT cooperate to induce Foxp3 expression through its enhancer. *Nat Immunol* **9**, 194-202 (2008).

138. Mantel, P.Y. *et al.* Molecular mechanisms underlying FOXP3 induction in human T cells. *J Immunol* **176**, 3593-3602 (2006).

139. Oh-Hora, M. *et al.* Agonist-selected T cell development requires strong T cell receptor signaling and store-operated calcium entry. *Immunity* **38**, 881-895 (2013).

140. Ouyang, W. *et al.* Foxo proteins cooperatively control the differentiation of Foxp3+ regulatory T cells. *Nat Immunol* **11**, 618-627 (2010).

141. Harada, Y. *et al.* Transcription factors Foxo3a and Foxo1 couple the E3 ligase Cbl-b to the induction of Foxp3 expression in induced regulatory T cells. *J Exp Med* **207**, 1381-1391 (2010).

142. Burchill, M.A., Yang, J., Vogtenhuber, C., Blazar, B.R. & Farrar, M.A. IL-2 receptor beta-dependent STAT5 activation is required for the development of Foxp3+ regulatory T cells. *J Immunol* **178**, 280-290 (2007).

143. Yao, Z. *et al.* Nonredundant roles for Stat5a/b in directly regulating Foxp3. *Blood* **109**, 4368-4375 (2007).

144. Sekiya, T. *et al.* The nuclear orphan receptor Nr4a2 induces Foxp3 and regulates differentiation of CD4+ T cells. *Nat Commun* **2**, 269 (2011).

145. Sekiya, T. *et al.* Nr4a receptors are essential for thymic regulatory T cell development and immune homeostasis. *Nat Immunol* **14**, 230-237 (2013).

146. Ruan, Q. *et al.* Development of Foxp3(+) regulatory t cells is driven by the c-Rel enhanceosome. *Immunity* **31**, 932-940 (2009).

147. Klunker, S. *et al.* Transcription factors RUNX1 and RUNX3 in the induction and suppressive function of Foxp3+ inducible regulatory T cells. *J Exp Med* **206**, 2701-2715 (2009).

148. Bruno, L. *et al.* Runx proteins regulate Foxp3 expression. *J Exp Med* **206**, 2329-2337 (2009).

149. Maruyama, T. *et al.* Control of the differentiation of regulatory T cells and T(H)17 cells by the DNA-binding inhibitor Id3. *Nat Immunol* **12**, 86-95 (2011).

150. Mantel, P.Y. *et al.* GATA3-driven Th2 responses inhibit TGF-beta1-induced FOXP3 expression and the formation of regulatory T cells. *PLoS Biol* **5**, e329 (2007).

151. Wohlfert, E.A. *et al.* GATA3 controls Foxp3(+) regulatory T cell fate during inflammation in mice. *J Clin Invest* **121**, 4503-4515 (2011).

152. Wang, Y., Su, M.A. & Wan, Y.Y. An essential role of the transcription factor GATA-3 for the function of regulatory T cells. *Immunity* **35**, 337-348 (2011).

153. Josefowicz, S.Z. *et al.* Extrathymically generated regulatory T cells control mucosal TH2 inflammation. *Nature* **482**, 395-399 (2012).

154. Schlenner, S.M., Weigmann, B., Ruan, Q., Chen, Y. & von Boehmer, H. Smad3 binding to the foxp3 enhancer is dispensable for the development of regulatory T cells with the exception of the gut. *J Exp Med* **209**, 1529-1535 (2012).

155. Zheng, Y. *et al.* Role of conserved non-coding DNA elements in the Foxp3 gene in regulatory T-cell fate. *Nature* **463**, 808-812 (2010).

156. Mouly, E. *et al.* The Ets-1 transcription factor controls the development and function of natural regulatory T cells. *J Exp Med* **207**, 2113-2125 (2010).

157. Schuster, M. *et al.* IkappaB(NS) protein mediates regulatory T cell development via induction of the Foxp3 transcription factor. *Immunity* **37**, 998-1008 (2012).

158. Shah, D.K. & Zuniga-Pflucker, J.C. Notch receptor-ligand interactions during T cell development, a ligand endocytosis-driven mechanism. *Curr Top Microbiol Immunol* **360**, 19-46 (2012).

159. Kopan, R. & Ilagan, M.X. The canonical Notch signaling pathway: unfolding the activation mechanism. *Cell* **137**, 216-233 (2009).

160. Gonzalez-Garcia, S., Garcia-Peydro, M., Alcain, J. & Toribio, M.L. Notch1 and IL-7 receptor signalling in early T-cell development and leukaemia. *Curr Top Microbiol Immunol* **360**, 47-73 (2012).

161. Bigas, A., D'Altri, T. & Espinosa, L. The Notch pathway in hematopoietic stem cells. *Curr Top Microbiol Immunol* **360**, 1-18 (2012).

162. Peschon, J.J. *et al.* Early lymphocyte expansion is severely impaired in interleukin 7 receptor-deficient mice. *J Exp Med* **180**, 1955-1960 (1994).

163. Puel, A., Ziegler, S.F., Buckley, R.H. & Leonard, W.J. Defective IL7R expression in T(-)B(+)NK(+) severe combined immunodeficiency. *Nat Genet* **20**, 394-397 (1998).

164. Gonzalez-Garcia, S. *et al.* CSL-MAML-dependent Notch1 signaling controls T lineage-specific IL-7R{alpha} gene expression in early human thymopoiesis and leukemia. *J Exp Med* **206**, 779-791 (2009).

165. Minter, L.M. & Osborne, B.A. Canonical and non-canonical Notch signaling in CD4(+) T cells. *Curr Top Microbiol Immunol* **360**, 99-114 (2012).

166. Auderset, F., Coutaz, M. & Tacchini-Cottier, F. The role of Notch in the differentiation of CD4(+) T helper cells. *Curr Top Microbiol Immunol* **360**, 115-134 (2012).

167. Tanigaki, K. *et al.* Regulation of alphabeta/gammadelta T cell lineage commitment and peripheral T cell responses by Notch/RBP-J signaling. *Immunity* **20**, 611-622 (2004).

168. Bhuyan, Z.A. *et al.* Abrogation of Rbpj attenuates experimental autoimmune uveoretinitis by inhibiting IL-22-producing CD4+ T cells. *PLoS One* **9**, e89266 (2014).

169. Amsen, D. *et al.* Instruction of distinct CD4 T helper cell fates by different notch ligands on antigen-presenting cells. *Cell* **117**, 515-526 (2004).

170. Tanaka, S. *et al.* The interleukin-4 enhancer CNS-2 is regulated by Notch signals and controls initial expression in NKT cells and memory-type CD4 T cells. *Immunity* **24**, 689-701 (2006).

171. Kim, J.M., Rasmussen, J.P. & Rudensky, A.Y. Regulatory T cells prevent catastrophic autoimmunity throughout the lifespan of mice. *Nat Immunol* **8**, 191-197 (2007).

172. Broske, A.M. *et al.* DNA methylation protects hematopoietic stem cell multipotency from myeloerythroid restriction. *Nat Genet* **41**, 1207-1215 (2009).

173. Lu, H. *et al.* Improved tagmentation-based whole-genome bisulfite sequencing for input DNA from less than 100 mammalian cells. *Epigenomics* **7**, 47-56 (2015).

174. Hovestadt, V. *et al.* Decoding the regulatory landscape of medulloblastoma using DNA methylation sequencing. *Nature* **510**, 537-541 (2014).

175. Han, H. *et al.* Inducible gene knockout of transcription factor recombination signal binding protein-J reveals its essential role in T versus B lineage decision. *Int Immunol* **14**, 637-645 (2002).

176. Duncan, A.W. *et al.* Integration of Notch and Wnt signaling in hematopoietic stem cell maintenance. *Nat Immunol* **6**, 314-322 (2005).

177. Zheng, Y. *et al.* Genome-wide analysis of Foxp3 target genes in developing and mature regulatory T cells. *Nature* **445**, 936-940 (2007).

178. Kelsall, I.R., Voss, M., Munro, S., Cuthbertson, D.J. & Cohen, P.T. R3F, a novel membrane-associated glycogen targeting subunit of protein phosphatase 1 regulates glycogen synthase in astrocytoma cells in response to glucose and extracellular signals. *J Neurochem* **118**, 596-610 (2011).

179. Mallona, I., Diez-Villanueva, A. & Peinado, M.A. Methylation plotter: a web tool for dynamic visualization of DNA methylation data. *Source Code Biol Med* **9**, 11 (2014).

180. Gays, F. *et al.* The mouse tumor cell lines EL4 and RMA display mosaic expression of NK-related and certain other surface molecules and appear to have a common origin. *J Immunol* **164**, 5094-5102 (2000).

181. Galili, U., Peleg, A., Milner, Y. & Galili, N. Be13, a human T-leukemia cell line highly sensitive to dexamethasone-induced cytolysis. *Cancer Res* **44**, 4594-4601 (1984).

182. Barra, M.M. *et al.* Transcription Factor 7 Limits Regulatory T Cell Generation in the Thymus. *J Immunol* **195**, 3058-3070 (2015).

183. Toker, A. *et al.* Active demethylation of the Foxp3 locus leads to the generation of stable regulatory T cells within the thymus. *J Immunol* **190**, 3180-3188 (2013).

184. Baaten, B.J. *et al.* CD44 regulates survival and memory development in Th1 cells. *Immunity* **32**, 104-115 (2010).

185. Scholzen, T. & Gerdes, J. The Ki-67 protein: from the known and the unknown. *J Cell Physiol* **182**, 311-322 (2000).

186. WIS. GeneCards. 2015 [cited 2015]Available from: http://www.genecards.org/cgi-bin/carddisp.pl?gene=

187. Sekiya, T. *et al.* Suppression of Th2 and Tfh immune reactions by Nr4a receptors in mature T reg cells. *J Exp Med* **212**, 1623-1640 (2015).

188. Hsiao, H.W. *et al.* Deltex1 is a target of the transcription factor NFAT that promotes T cell anergy. *Immunity* **31**, 72-83 (2009).

189. Castel, D. *et al.* Dynamic binding of RBPJ is determined by Notch signaling status. *Genes Dev* **27**, 1059-1071 (2013).

190. Hoyne, G.F. *et al.* Serrate1-induced notch signalling regulates the decision between immunity and tolerance made by peripheral CD4(+) T cells. *Int Immunol* **12**, 177-185 (2000).

191. Vigouroux, S. *et al.* Induction of antigen-specific regulatory T cells following overexpression of a Notch ligand by human B lymphocytes. *J Virol* **77**, 10872-10880 (2003).

192. Bassil, R. *et al.* Notch ligand delta-like 4 blockade alleviates experimental autoimmune encephalomyelitis by promoting regulatory T cell development. *J Immunol* **187**, 2322-2328 (2011).

193. Samon, J.B. *et al.* Notch1 and TGFbeta1 cooperatively regulate Foxp3 expression and the maintenance of peripheral regulatory T cells. *Blood* **112**, 1813-1821 (2008).

194. Ou-Yang, H.F. *et al.* Notch signaling regulates the FOXP3 promoter through RBP-J- and Hes1-dependent mechanisms. *Mol Cell Biochem* **320**, 109-114 (2009).

195. Barbarulo, A. *et al.* Notch3 and canonical NF-kappaB signaling pathways cooperatively regulate Foxp3 transcription. *J Immunol* **186**, 6199-6206 (2011).

196. Sandy, A.R. *et al.* T cell-specific notch inhibition blocks graft-versus-host disease by inducing a hyporesponsive program in alloreactive CD4+ and CD8+ T cells. *J Immunol* **190**, 5818-5828 (2013).

197. Tran, I.T. *et al.* Blockade of individual Notch ligands and receptors controls graft-versus-host disease. *J Clin Invest* **123**, 1590-1604 (2013).

198. Roderick, J.E. *et al.* Therapeutic targeting of NOTCH signaling ameliorates immune-mediated bone marrow failure of aplastic anemia. *J Exp Med* **210**, 1311-1329 (2013).

199. Piggott, K. *et al.* Blocking the NOTCH pathway inhibits vascular inflammation in large-vessel vasculitis. *Circulation* **123**, 309-318 (2011).

200. Charbonnier, L.M., Wang, S., Georgiev, P., Sefik, E. & Chatila, T.A. Control of peripheral tolerance by regulatory T cell-intrinsic Notch signaling. *Nat Immunol* **16**, 1162-1173 (2015).

201. Zhu, J., Yamane, H. & Paul, W.E. Differentiation of effector CD4 T cell populations (*). *Annu Rev Immunol* **28**, 445-489 (2010).

202. Marrella, V., Poliani, P.L., Sobacchi, C., Grassi, F. & Villa, A. Of Omenn and mice. *Trends Immunol* **29**, 133-140 (2008).

203. Giliani, S. *et al.* Omenn syndrome in an infant with IL7RA gene mutation. *J Pediatr* **148**, 272-274 (2006).

10 Appendix

10.1 List of antibodies used for flow cytometry and FACS

Antigen	Label	Clone	Isotype	Supplier	Cat-#
Biotin	APC	NA	Streptavidin	BioLegend	405207
Biotin	APC/Cy7	NA	Streptavidin	BioLegend	405208
Biotin	PE	NA	Streptavidin	BioLegend	405204
Biotin	PE/Cy7	NA	Streptavidin	BioLegend	405206
Biotin	Brilliant UV 737	NA	Streptavidin	BD	564293
Biotin	Horserad. peroxidase	NA	Streptavidin	BioLegend	405210
Viability dye	DAPI	NA	NA	BD	564907
Viability dye	eFluor506	NA	NA	eBioscience	65-0866
Viability dye	7AAD	NA	NA	BioLegend	640934
CD3	Purified	Okt3	Mouse IgG2a κ	BioLegend	317304
CD3ε	Pacific Blue	145-2C11	Arm. Hamster IgG	BioLegend	100334
CD3ε	Purified	145-2C11	Arm. Hamster IgG	BioLegend	100302
CD3ε	Brilliant Violet 711	145-2C11	Arm. Hamster IgG	BioLegend	100241
CD4	APC	RM4-5	Rat IgG2a κ	BioLegend	100516
CD4	APC/Cy7	GK1.5	Rat IgG2b κ	BioLegend	100414
CD4	Biotin	RM4-5	Rat IgG2a κ	BioLegend	100508
CD4	Brilliant Violet 421	GK1.5	Rat IgG2b κ	BioLegend	100437S
CD4	FITC	RM4-5	Rat IgG2a κ	BioLegend	100510
CD4	Pacific Blue	RM4-5	Rat IgG2a κ	BioLegend	100531
CD4	Brilliant Violet 711	RM4-5	Rat IgG2a κ	BioLegend	100550
CD4	Brilliant Violet 605	RM4-5	Rat IgG2a κ	BioLegend	100548
CD4	PE	RM4-5	Rat IgG2a κ	BioLegend	100512
CD4	PE/Cy7	RM4-5	Rat IgG2a κ	BioLegend	100528
CD4	PerCP/Cy5.5	RM4-5	Rat IgG2a κ	BioLegend	100540
CD4	Brilliant UV 395	GK1.5	Rat IgG2b κ	BD	563790
CD4	Biotin	OKT4	Mouse IgG2b κ	BioLegend	317406
CD8a	APC	53-6.7	Rat IgG2a κ	BioLegend	100712
CD8a	Biotin	53-6.7	Rat IgG2a κ	BioLegend	100704
CD8a	FITC	53-6.7	Rat IgG2a κ	BioLegend	100706
CD8a	Pacific Blue	53-6.7	Rat IgG2a κ	BioLegend	100725
CD8a	Brilliant Violet 605	53-6.7	Rat IgG2a κ	BioLegend	100744
CD8a	PE/Cy7	53-6.7	Rat IgG2a κ	BioLegend	100722
CD8a	PerCP/Cy5.5	53-6.7	Rat IgG2a κ	BioLegend	100734
CD11b	PerCP/Cy5.5	M1/70	Rat IgG2b κ	BioLegend	101228
CD19	APC	6D5	Rat IgG2a κ	BioLegend	115512
CD19	APC/Cy7	6D6	Rat IgG2a κ	BioLegend	115530
CD19	Biotin	6D5	Rat IgG2a κ	BioLegend	115504
CD19	FITC	6D5	Rat IgG2a κ	BioLegend	115506
CD19	PE/Cy7	6D5	Rat IgG2a κ	BioLegend	115520
CD19	Pacific Blue	6D5	Rat IgG2a κ	BioLegend	115523
CD25	APC	PC61	Rat IgG1 λ	BioLegend	102012
CD25	Biotin	PC61	Rat IgG1 λ	BioLegend	102004
CD25	PE	PC61	Rat IgG1 λ	BioLegend	102008
CD25	PE/Cy7	PC61	Rat IgG1 λ	BioLegend	102016
CD25	Biotin	BC96	Mouse IgG1 κ	BioLegend	302624
CD28	Purified	37.51	Syr. Hamster IgG	BioLegend	102102
CD44	Pacific Blue	IM7	Rat IgG2b κ	BioLegend	103020
CD44	Brilliant Violet 421	IM7	Rat IgG2b κ	BioLegend	103039
CD45	APC/Cy7	30-F11	Rat IgG2b κ	BioLegend	103116
CD45.1	PerCP/Cy5.5	A20	Mouse (A. SW)IgG2a κ	BioLegend	110728
CD45.1	PE/Cy7	A20	Mouse (A. SW)IgG2a κ	BioLegend	110730
CD45.2	Pacific Blue	104	Mouse (SJL) IgG2a κ	BioLegend	109820
CD45.2	PerCP/Cy5.5	104	Mouse (SJL) IgG2a κ	BioLegend	109828
CD45.2	Alexa Fluor 647	104	Mouse (SJL) IgG2a κ	BioLegend	109818
CD45.2	APC/Cy7	104	Mouse (SJL) IgG2a, κ	BioLegend	109824
CD49b	Biotin	DX5	Rat IgM κ	BioLegend	108904
CD62L	APC	MEL-14	Rat IgG2a κ	BioLegend	104412
CD62L	APC/Cy7	MEL-14	Rat IgG2a κ	BioLegend	104428
CD62L	PerCP/Cy5.5	MEL-14	Rat IgG2a κ	BioLegend	104432

CD69	PerCP/Cy5.5	H1.2F3	Arm. Hamster IgG	BioLegend	104522
CD90.1	FITC	OX-7	Mouse IgG1 κ	BioLegend	202504
CD90.1	Pacific Blue	OX-7	Mouse IgG1 κ	BioLegend	202522
CD90.1	APC/Cy7	OX-7	Mouse IgG1 κ	BioLegend	202520
CD90.1	PE	OX-7	Mouse IgG1 κ	BioLegend	202524
CD90.1	PE/Cy7	OX-7	Mouse IgG1 κ	BioLegend	202518
CD90.2	APC/Cy7	30-H12	Rat IgG2b κ	BioLegend	105328
CD90.2	APC	30-H12	Rat IgG2b κ	BioLegend	105312
CD103	PE	2E7	Arm. Hamster IgG	BioLegend	121406
CD127	Biotin	A7R34	Rat IgG2a κ	BioLegend	135005
CD127	Brilliant Violet 605	A7R34	Rat IgG2a κ	BioLegend	135025
CD127	Brilliant UV 737	SB/199	Rat IgG2b κ	BD	564399
CD127	Brilliant Violet 421	A7R34	Rat IgG2a κ	BioLegend	135024
CD152/CTLA-4)	PE	UC10-4B9	Arm. Hamster IgG	BioLegend	106305
CD304 (Nrp-1)	Alexa Fluor 488	N43-7	Rat IgG2a κ	MBL	M169-A48
CD357 (GITR)	FITC	DTA-1	Rat IgG2b λ	BioLegend	126308
I-A/I-E (MHC II)	Biotin	M5/114.15.2	Rat IgG2b κ	BioLegend	107603
I-A/I-E (MHC II)	PE/Cy7	M5/114.15.2	Rat IgG2b κ	eBioscience	107629
I-A/I-E (MHC II)	Pacific Blue	M5/114.15.2	Rat IgG2b κ	BioLegend	107620
I-A/I-E (MHC II)	PE	M5/114.15.2	Rat IgG2b κ	BioLegend	107607
I-A/I-E (MHC II)	APC/Cy7	M5/114.15.2	Rat IgG2c κ	BioLegend	107627
KLRG1	Biotin	2F1	Syr. Hamster IgG2 κ	BD	550863
KLRG1	PE	2F1	Syr. Hamster IgG	BioLegend	138407
Ly6-C	APC/Cy7	HK1.4	Rat IgG2c κ	BioLegend	128025
Ly6-C	PerCP/Cy5.5	HK1.4	Rat IgG2c κ	BioLegend	128012
NK1.1	Biotin	PK136	Mouse IgG2a κ	BioLegend	108703
Notch1	Brilliant Violet 421	HMN1-12	Arm. Hamster IgG	Biolegend	130615
Notch2	APC	HMN2-35	Arm. Hamster IgG	Biolegend	130713
Annexin-V	PE	NA	NA	BioLegend	640934
FoxP3	Purified	FJK-16s	Rat IgG2a κ	eBioscience	14-5773-82
FoxP3	PE	FJK-16s	Rat IgG2a κ	eBioscience	12-5773-82
FoxP3	APC	FJK-16s	Rat IgG2a κ	eBioscience	17-5773-82
Helios	PE	22F6	Arm. Hamster IgG	BioLegend	137206
Bcl-2	Alexa Fluor 488	BCL/10C4	Mouse IgG1 κ	BioLegend	633506
IFN-γ	PE	XMG1.2	Rat IgG1 κ	BioLegend	505808
IFN-γ	APC	XMG1.2	Rat IgG1 κ	BioLegend	505809
IL-10	PE	JES5-16E3	Rat IgG2b κ	BioLegend	505008
IL-17A	PE	TC11-18H10.1	Rat IgG1 κ	BioLegend	506903
IL-2	PE	JES6-5H4	Rat IgG2b κ	BioLegend	503808
IL-2	APC	MQ1-17H12	Rat IgG2a, κ	BioLegend	500311
IL-4	PE	11B11	Rat IgG1 κ	BioLegend	504103
IL-17A	PE	TC11-18H10.1	Rat IgG1 κ	BioLegend	506903
TNF-α	PE	MP6-XT22	Rat IgG1 κ	BioLegend	506305
pStat5 (pY694)	Alexa Fluor 647	4/P-STAT3	Mouse IgG2a κ	BD	612599
Caspase-3	PE	NA	NA	Abcam	Ab65617
GATA-3	Alexa Fluor 647	16E10A23	Mouse IgG2b κ	Biolegend	653809
T-bet	Alexa Fluor 647	4B10	Mouse IgG1 κ	Biolegend	644803
IRF4	Alexa Fluor 647	IRF4.3E4	Rat IgG1 κ	Biolegend	646407
Ki-67	PE	B56	Mouse IgG1 κ	BD	556027
Isotype control	PE	RTK2071	Rat IgG1 κ	BioLegend	400407
Isotype control	PE	RTK4530	Rat IgG2b κ	BioLegend	400608
Isotype control	PE	HTK888	Arm. Hamster IgG	BioLegend	400907
Isotype control	Alexa Fluor 488	MOPC-21	Mouse IgG1 κ	BioLegend	400129
Isotype control	Alexa Fluor 488	RTK2758	Rat IgG2a κ	BioLegend	400525
Isotype control	Alexa Fluor 647	RTK2758	Rat IgG2a κ	BioLegend	400526
Isotype control	Alexa Fluor 647	MOPC-173	Mouse IgG2a κ	BioLegend	400234
Isotype control	Brilliant Violet 421	RTK2758	Rat IgG2a κ	BioLegend	400535

10.2 List of mouse strains

Name	Official name	Origin
C57BL/6	C57BL/6 **Jackson # 664**	Charles River Breeding or Jackson Laboratories
***Foxp3*$^{\text{YFP, Cre}}$**	B6.129(Cg)-Foxp3 $^{\text{tm4(YFP/cre)Ayr/}}$ J **Jackson #016959**	A. Rudensky, MSKCC, New York, USA
***Foxp3*$^{\text{GFP}}$**	B6.129(Cg)-Foxp3 $^{\text{tm3(DTR/GFP)Ayr/}}$ J **Jackson #016958**	A. Rudensky, MSKCC, New York, USA
***Foxp3*$^{\text{GFP CD45.1}}$**	B6.SJL-Ptprc ^{a}Pepc ^{b}/BoyJ **Jackson #002014**	Jackson Laboratories
***Foxp3*$^{\text{GFP CD90.1}}$**	B6.PL-Thy1 ^{a}CyJ **Jackson #000406**	Jackson Laboratories
***Notch*$^{\text{eGFP}}$**	B6.SJL/J)F2 Tg(Cp-EGFP)25Gaia/ReyaJ **Jackson #018322**	Jackson Laboratories
***RAG2*$^{-/-}$**	B6-Rag2tm1Fwa **Jackson #008449**	Shinkai Y et al., "RAG-2-deficient mice lack mature lymphocytes owing to inability to initiate V(D)J rearrangement." Cell 1992 Mar 6;68(5):855-67 [PMID 15477487]
***Rbpj*$^{\text{flx/flx}}$**	**N/A**	Nakhai H., Siveke J.T., Klein B., et al., Conditional ablation of Notch signaling in pancreatic development. Development. 2008 Aug;135(16):2757-65. Epub 2008 Jul 17 [PMID 18635610]
***NICD*$^{\text{LSL}}$**	**N/A**	Murtaugh LC; Stanger BZ; Kwan KM; Melton DA. 2003. Notch signaling controls multiple steps of pancreatic differentiation. Proc Natl Acad Sci U S A 100(25):14920-5. [PMID 14657333]
***Dnmt1*$^{\text{chip}}$**	**N/A**	Broske AM et al., "DNA methylation protects hematopoietic stem cell multipotency from myeloerythroid restriction." Nat Genet 2009 Nov 41; 1207-1215 [PMID 19801979]

10.3 List of bisuflite primers used for 454 pyrosequencing

#	Region	Direction	Barcode	Primer plus adaptor sequence plus barcode
0	1	ForP	TATATC	CGTATCGCCTCCCTCGCGCCATCAGTATATCAGGATGTTAGGGTATTAAAGGTTGG
0	1	RevP	TATATC	CTATGCGCCTTGCCAGCCCGCTCAGTATATCCCAATTTTCCTAAAACCAACAATAT
0	2	ForP	TATATC	CGTATCGCCTCCCTCGCGCCATCAGTATATCTATATTTTTAGATGATTTGTAAAGGGTAAA
0	2	RevP	TATATC	CTATGCGCCTTGCCAGCCCGCTCAGTATATCACCTAACTTATAAAAAACTACCACATTATC
0	3.1	ForP	TATATC	CGTATCGCCTCCCTCGCGCCATCAGTATATCAGTGTTTAGTTTTTGTTTTTTTTTTTAGGTTTTG
0	3.1	RevP	TATATC	CTATGCGCCTTGCCAGCCCGCTCAGTATATCTCTTACRTAACACAAACAAAAAATCAATTAAATAC
0	3.2	ForP	TATATC	CGTATCGCCTCCCTCGCGCCATCAGTATATCGTTGTGGTATTGTGTTTGGTATATG
0	3.2	RevP	TATATC	CTATGCGCCTTGCCAGCCCGCTCAGTATATCACACTTAATTCAAATAATCAAATTCATAAT
0	4	ForP	TATATC	CGTATCGCCTCCCTCGCGCCATCAGTATATCTGGGTTTTTTTGGTATTTAAGAAAG
0	4	RevP	TATATC	CTATGCGCCTTGCCAGCCCGCTCAGTATATCAAAAAACAAATAATCTACCCCACAA
0	5	ForP	TATATC	CGTATCGCCTCCCTCGCGCCATCAGTATATCTGAAAGGTTATAATGAAATGATAAGTTTAA
0	5	RevP	TATATC	CTATGCGCCTTGCCAGCCCGCTCAGTATATCATTACCATAACTTCCCCAAAAATAC
0	6	ForP	TATATC	CGTATCGCCTCCCTCGCGCCATCAGTATATCTGATTGTTAATTTTGTTTTTGATTG
0	6	RevP	TATATC	CTATGCGCCTTGCCAGCCCGCTCAGTATATCCAACCTCAATCTCATAATTTTAACC
1	1	ForP	CCACGC	CGTATCGCCTCCCTCGCGCCATCAGCCACGCAGGATGTTAGGGTATTAAAGGTTGG
1	1	RevP	CCACGC	CTATGCGCCTTGCCAGCCCGCTCAGCCACGCCCAATTTTCCTAAAACCAACAATAT
1	2	ForP	CCACGC	CGTATCGCCTCCCTCGCGCCATCAGCCACGCTATATTTTTAGATGATTTGTAAAGGGTAAA
1	2	RevP	CCACGC	CTATGCGCCTTGCCAGCCCGCTCAGCCACGCACCTAACTTATAAAAAACTACCACATTATC
1	3.1	ForP	CCACGC	CGTATCGCCTCCCTCGCGCCATCAGCCACGCAGTGTTTAGTTTTTGTTTTTTTTTTAGGTTTTGT
1	3.1	RevP	CCACGC	CTATGCGCCTTGCCAGCCCGCTCAGCCACGCTCTTACRTAACACAAACAAAAAATCAATTAAATAC
1	3.2	ForP	CCACGC	CGTATCGCCTCCCTCGCGCCATCAGCCACGCGTTGTGGTATTGTGTTTGGTATATG
1	3.2	RevP	CCACGC	CTATGCGCCTTGCCAGCCCGCTCAGCCACGCACACTTAATTCAAATAATCAAATTCATAAT
1	4	ForP	CCACGC	CGTATCGCCTCCCTCGCGCCATCAGCCACGCTGGGTTTTTTTGGTATTTAAGAAAG
1	4	RevP	CCACGC	CTATGCGCCTTGCCAGCCCGCTCAGCCACGCAAAAAACAAATAATCTACCCCACAA
1	5	ForP	CCACGC	CGTATCGCCTCCCTCGCGCCATCAGCCACGCTGAAAGGTTATAATGAAATGATAAGTTTAA
1	5	RevP	CCACGC	CTATGCGCCTTGCCAGCCCGCTCAGCCACGCATTACCATAACTTCCCCAAAAATAC
1	6	ForP	CCACGC	CGTATCGCCTCCCTCGCGCCATCAGCCACGCTGATTGTTAATTTTGTTTTTGATTG
1	6	RevP	CCACGC	CTATGCGCCTTGCCAGCCCGCTCAGCCACGCCAACCTCAATCTCATAATTTTAACC
2	1	ForP	GAGAGA	CGTATCGCCTCCCTCGCGCCATCAGGAGAGAAGGATGTTAGGGTATTAAAGGTTGG
2	1	RevP	GAGAGA	CTATGCGCCTTGCCAGCCCGCTCAGGAGAGACCAATTTTCCTAAAACCAACAATAT
2	2	ForP	GAGAGA	CGTATCGCCTCCCTCGCGCCATCAGGAGAGATATATTTTTAGATGATTTGTAAAGGGTAAA
2	2	RevP	GAGAGA	CTATGCGCCTTGCCAGCCCGCTCAGGAGAGAACCTAACTTATAAAAAACTACCACATTATC
2	3.1	ForP	GAGAGA	CGTATCGCCTCCCTCGCGCCATCAGGAGAGAAGTGTTTAGTTTTTGTTTTTTTTTTAGGTTTTGT
2	3.1	RevP	GAGAGA	CGTATCGCCTCCCTCGCGCCATCAGGAGAGATCTTACRTAACACAAACAAAAAATCAATTAAATAC
2	3.2	ForP	GAGAGA	CGTATCGCCTCCCTCGCGCCATCAGGAGAGAGTTGTGGTATTGTGTTTGGTATATG
2	3.2	RevP	GAGAGA	CTATGCGCCTTGCCAGCCCGCTCAGGAGAGAACACTTAATTCAAATAATCAAATTCATAAT
2	4	ForP	GAGAGA	CGTATCGCCTCCCTCGCGCCATCAGGAGAGATGGGTTTTTTTGGTATTTAAGAAAG
2	4	RevP	GAGAGA	CTATGCGCCTTGCCAGCCCGCTCAGGAGAGAAAAAAACAAATAATCTACCCCACAA
2	5	ForP	GAGAGA	CGTATCGCCTCCCTCGCGCCATCAGGAGAGATGAAAGGTTATAATGAAATGATAAGTTTAA
2	5	RevP	GAGAGA	CTATGCGCCTTGCCAGCCCGCTCAGGAGAGAATTACCATAACTTCCCCAAAAATAC
2	6	ForP	GAGAGA	CGTATCGCCTCCCTCGCGCCATCAGGAGAGATGATTGTTAATTTTGTTTTTGATTG
2	6	RevP	GAGAGA	CTATGCGCCTTGCCAGCCCGCTCAGGAGAGACAACCTCAATCTCATAATTTTAACC
3	1	ForP	ATTATA	CGTATCGCCTCCCTCGCGCCATCAGATTATAAGGATGTTAGGGTATTAAAGGTTGG
3	1	RevP	ATTATA	CTATGCGCCTTGCCAGCCCGCTCAGATTATACCAATTTTCCTAAAACCAACAATAT
3	2	ForP	ATTATA	CGTATCGCCTCCCTCGCGCCATCAGATTATATATTTTTAGATGATTTGTAAAGGGTAAA
3	2	RevP	ATTATA	CTATGCGCCTTGCCAGCCCGCTCAGATTATAACCTAACTTATAAAAAACTACCACATTATC
3	3.1	ForP	ATTATA	CGTATCGCCTCCCTCGCGCCATCAGATTATAAGTGTTTAGTTTTTGTTTTTTTTTTAGGTTTTGT
3	3.1	RevP	ATTATA	CTATGCGCCTTGCCAGCCCGCTCAGATTATATCTTACRTAACACAAACAAAAAATCAATTAAATAC
3	3.2	ForP	ATTATA	CGTATCGCCTCCCTCGCGCCATCAGATTATAGTTGTGGTATTGTGTTTGGTATATG
3	3.2	RevP	ATTATA	CTATGCGCCTTGCCAGCCCGCTCAGATTATAACACTTAATTCAAATAATCAAATTCATAAT
3	4	ForP	ATTATA	CGTATCGCCTCCCTCGCGCCATCAGATTATATGGGTTTTTTTGGTATTTAAGAAAG
3	4	RevP	ATTATA	CTATGCGCCTTGCCAGCCCGCTCAGATTATAAAAAACAAATAATCTACCCCACAA
3	5	ForP	ATTATA	CGTATCGCCTCCCTCGCGCCATCAGATTATATGAAAGGTTATAATGAAATGATAAGTTTAA
3	5	RevP	ATTATA	CTATGCGCCTTGCCAGCCCGCTCAGATTATAATTACCATAACTTCCCCAAAAATAC
3	6	ForP	ATTATA	CGTATCGCCTCCCTCGCGCCATCAGATTATATGATTGTTAATTTTGTTTTTGATTG
3	6	RevP	ATTATA	CTATGCGCCTTGCCAGCCCGCTCAGATTATACAACCTCAATCTCATAATTTTAACC
4	1	ForP	TCCGTC	CGTATCGCCTCCCTCGCGCCATCAGTCCGTCAGGATGTTAGGGTATTAAAGGTTGG
4	1	RevP	TCCGTC	CTATGCGCCTTGCCAGCCCGCTCAGTCCGTCCCAATTTTCCTAAAACCAACAATAT
4	2	ForP	TCCGTC	CGTATCGCCTCCCTCGCGCCATCAGTCCGTCTATATTTTTAGATGATTTGTAAAGGGTAAA
4	2	RevP	TCCGTC	CTATGCGCCTTGCCAGCCCGCTCAGTCCGTCACCTAACTTATAAAAAACTACCACATTATC
4	3.1	ForP	TCCGTC	CGTATCGCCTCCCTCGCGCCATCAGTCCGTCAGTGTTTAGTTTTTGTTTTTTTTTTAGGTTTTGT
4	3.1	RevP	TCCGTC	CTATGCGCCTTGCCAGCCCGCTCAGTCCGTCTCTTACRTAACACAAACAAAAAATCAATTAAATAC
4	3.2	ForP	TCCGTC	CGTATCGCCTCCCTCGCGCCATCAGTCCGTCGTTGTGGTATTGTGTTTGGTATATG
4	3.2	RevP	TCCGTC	CTATGCGCCTTGCCAGCCCGCTCAGTCCGTCACACTTAATTCAAATAATCAAATTCATAAT
4	4	ForP	TCCGTC	CGTATCGCCTCCCTCGCGCCATCAGTCCGTCTGGGTTTTTTTGGTATTTAAGAAAG
4	4	RevP	TCCGTC	CTATGCGCCTTGCCAGCCCGCTCAGTCCGTCAAAAAACAAATAATCTACCCCACAA
4	5	ForP	TCCGTC	CGTATCGCCTCCCTCGCGCCATCAGTCCGTCTGAAAGGTTATAATGAAATGATAAGTTTAA
4	5	RevP	TCCGTC	CTATGCGCCTTGCCAGCCCGCTCAGTCCGTCATTACCATAACTTCCCCAAAAATAC
4	6	ForP	TCCGTC	CGTATCGCCTCCCTCGCGCCATCAGTCCGTCTGATTGTTAATTTTGTTTTTGATTG
4	6	RevP	TCCGTC	CTATGCGCCTTGCCAGCCCGCTCAGTCCGTCCAACCTCAATCTCATAATTTTAACC
5	1	ForP	ATGTCA	CGTATCGCCTCCCTCGCGCCATCAGATGTCAAGGATGTTAGGGTATTAAAGGTTGG
5	1	RevP	ATGTCA	CTATGCGCCTTGCCAGCCCGCTCAGATGTCACCAATTTTCCTAAAACCAACAATAT
5	2	ForP	ATGTCA	CGTATCGCCTCCCTCGCGCCATCAGATGTCATATATTTTTAGATGATTTGTAAAGGGTAAA
5	2	RevP	ATGTCA	CTATGCGCCTTGCCAGCCCGCTCAGATGTCAACCTAACTTATAAAAAACTACCACATTATC
5	3.1	ForP	ATGTCA	CGTATCGCCTCCCTCGCGCCATCAGATGTCAAGTGTTTAGTTTTTGTTTTTTTTTTAGGTTTTGT
5	3.1	RevP	ATGTCA	CTATGCGCCTTGCCAGCCCGCTCAGATGTCATCTTACRTAACACAAACAAAAAATCAATTAAATAC
5	3.2	ForP	ATGTCA	CGTATCGCCTCCCTCGCGCCATCAGATGTCAGTTGTGGTATTGTGTTTGGTATATG
5	3.2	RevP	ATGTCA	CTATGCGCCTTGCCAGCCCGCTCAGATGTCAACACTTAATTCAAATAATCAAATTCATAAT
5	4	ForP	ATGTCA	CGTATCGCCTCCCTCGCGCCATCAGATGTCATGGGTTTTTTTGGTATTTAAGAAAG
5	4	RevP	ATGTCA	CTATGCGCCTTGCCAGCCCGCTCAGATGTCAAAAAACAAATAATCTACCCCACAA
5	5	ForP	ATGTCA	CGTATCGCCTCCCTCGCGCCATCAGATGTCATGAAAGGTTATAATGAAATGATAAGTTTAA
5	5	RevP	ATGTCA	CTATGCGCCTTGCCAGCCCGCTCAGATGTCAATTACCATAACTTCCCCAAAAATAC

5	6	ForP	ATGTCA	CGTATCGCCTCCCTCGCGCCATCAGATGTCATGATTGTTAATTTTGTTTTTGATTG
5	6	RevP	ATGTCA	CTATGCGCCTTGCCAGCCCGCTCAGATGTCACAACCTCAATCTCATAATTTTAACC

6	1	ForP	TGTTGT	CGTATCGCCTCCCTCGCGCCATCAGTGTTGTAGGATGTTAGGGTATTAAAGGTTGG
6	1	RevP	TGTTGT	CTATGCGCCTTGCCAGCCCGCTCAGTGTTGTCCAATTTTCCTAAAACCAACAATAT
6	2	ForP	TGTTGT	CGTATCGCCTCCCTCGCGCCATCAGTGTTGTTATATTTTTAGATGATTTGTAAAGGGTAAA
6	2	RevP	TGTTGT	CTATGCGCCTTGCCAGCCCGCTCAGTGTTGTACCTAACTTATAAAAAACTACCACATTATC
6	3.1	ForP	TGTTGT	CGTATCGCCTCCCTCGCGCCATCAGTGTTGTAGTGTTTAGTTTTTGTTTTTTTTTTTAGGTTTTGT
6	3.1	RevP	TGTTGT	CTATGCGCCTTGCCAGCCCGCTCAGTGTTGTTCTTACRTAACACAAACAAAAAATCAATTAAATAC
6	3.2	ForP	TGTTGT	CGTATCGCCTCCCTCGCGCCATCAGTGTTGTGTTGTGGTATTGTGTTTGGTATATG
6	3.2	RevP	TGTTGT	CTATGCGCCTTGCCAGCCCGCTCAGTGTTGTACACTTAATTCAAATAATCAAATTCATAAT
6	4	ForP	TGTTGT	CGTATCGCCTCCCTCGCGCCATCAGTGTTGTTGGGTTTTTTTGGTATTTAAGAAAG
6	4	RevP	TGTTGT	CTATGCGCCTTGCCAGCCCGCTCAGTGTTGTAAAAAACAAATAATCTACCCCACAA
6	5	ForP	TCCGTC	CGTATCGCCTCCCTCGCGCCATCAGTGTTGTTGAAAGGTTATAATGAAATGATAAGTTTAA
6	5	RevP	TCCGTC	CTATGCGCCTTGCCAGCCCGCTCAGTGTTGTATTACCATAACTTCCCCAAAAATAC
6	6	ForP	TCCGTC	CGTATCGCCTCCCTCGCGCCATCAGTGTTGTTGATTGTTAATTTTGTTTTTGATTG
6	6	RevP	TCCGTC	CTATGCGCCTTGCCAGCCCGCTCAGTGTTGTCAACCTCAATCTCATAATTTTAACC

7	1	ForP	CAATAA	CGTATCGCCTCCCTCGCGCCATCAGCAATAAAGGATGTTAGGGTATTAAAGGTTGG
7	1	RevP	CAATAA	CTATGCGCCTTGCCAGCCCGCTCAGCAATAACCAATTTTCCTAAAACCAACAATAT
7	2	ForP	CAATAA	CGTATCGCCTCCCTCGCGCCATCAGCAATAATATATTTTTAGATGATTTGTAAAGGGTAAA
7	2	RevP	CAATAA	CTATGCGCCTTGCCAGCCCGCTCAGCAATAAACCTAACTTATAAAAAACTACCACATTATC
7	3.1	ForP	CAATAA	CGTATCGCCTCCCTCGCGCCATCAGCAATAAAGTGTTTAGTTTTTGTTTTTTTTTTTAGGTTTTGT
7	3.1	RevP	CAATAA	CTATGCGCCTTGCCAGCCCGCTCAGCAATAATCTTACRTAACACAAACAAAAAATCAATTAAATAC
7	3.2	ForP	CAATAA	CGTATCGCCTCCCTCGCGCCATCAGCAATAAGTTGTGGTATTGTGTTTGGTATATG
7	3.2	RevP	CAATAA	CTATGCGCCTTGCCAGCCCGCTCAGCAATAAACACTTAATTCAAATAATCAAATTCATAAT
7	4	ForP	CAATAA	CGTATCGCCTCCCTCGCGCCATCAGCAATAATGGGTTTTTTTGGTATTTAAGAAAG
7	4	RevP	CAATAA	CTATGCGCCTTGCCAGCCCGCTCAGCAATAAAAAAACAAATAATCTACCCCACAA
7	5	ForP	CAATAA	CGTATCGCCTCCCTCGCGCCATCAGCAATAATGAAAGGTTATAATGAAATGATAAGTTTAA
7	5	RevP	CAATAA	CTATGCGCCTTGCCAGCCCGCTCAGCAATAAATTACCATAACTTCCCCAAAAATAC
7	6	ForP	CAATAA	CGTATCGCCTCCCTCGCGCCATCAGCAATAATGATTGTTAATTTTGTTTTTGATTG
7	6	RevP	CAATAA	CTATGCGCCTTGCCAGCCCGCTCAGCAATAACAACCTCAATCTCATAATTTTAACC

8	1	ForP	GCTACC	CGTATCGCCTCCCTCGCGCCATCAGGCTACCAGGATGTTAGGGTATTAAAGGTTGG
8	1	RevP	GCTACC	CTATGCGCCTTGCCAGCCCGCTCAGGCTACCCCAATTTTCCTAAAACCAACAATAT
8	2	ForP	GCTACC	CGTATCGCCTCCCTCGCGCCATCAGGCTACCTATATTTTTAGATGATTTGTAAAGGGTAAA
8	2	RevP	GCTACC	CTATGCGCCTTGCCAGCCCGCTCAGGCTACCACCTAACTTATAAAAAACTACCACATTATC
8	3.1	ForP	GCTACC	CGTATCGCCTCCCTCGCGCCATCAGGCTACCAGTGTTTAGTTTTTGTTTTTTTTTTTAGGTTTTGT
8	3.1	RevP	GCTACC	CTATGCGCCTTGCCAGCCCGCTCAGGCTACCTCTTACRTAACACAAACAAAAAATCAATTAAATAC
8	3.2	ForP	GCTACC	CGTATCGCCTCCCTCGCGCCATCAGGCTACCGTTGTGGTATTGTGTTTGGTATATG
8	3.2	RevP	GCTACC	CTATGCGCCTTGCCAGCCCGCTCAGGCTACCACACTTAATTCAAATAATCAAATTCATAAT
8	4	ForP	GCTACC	CGTATCGCCTCCCTCGCGCCATCAGGCTACCTGGGTTTTTTTGGTATTTAAGAAAG
8	4	RevP	GCTACC	CTATGCGCCTTGCCAGCCCGCTCAGGCTACCAAAAAACAAATAATCTACCCCACAA
8	5	ForP	GCTACC	CGTATCGCCTCCCTCGCGCCATCAGGCTACCTGAAAGGTTATAATGAAATGATAAGTTTAA
8	5	RevP	GCTACC	CTATGCGCCTTGCCAGCCCGCTCAGGCTACCATTACCATAACTTCCCCAAAAATAC
8	6	ForP	GCTACC	CGTATCGCCTCCCTCGCGCCATCAGGCTACCTGATTGTTAATTTTGTTTTTGATTG
8	6	RevP	GCTACC	CTATGCGCCTTGCCAGCCCGCTCAGGCTACCCAACCTCAATCTCATAATTTTAACC

9	1	ForP	CGTACG	CGTATCGCCTCCCTCGCGCCATCAGCGTACGAGGATGTTAGGGTATTAAAGGTTGG
9	1	RevP	CGTACG	CTATGCGCCTTGCCAGCCCGCTCAGCGTACGCCAATTTTCCTAAAACCAACAATAT
9	2	ForP	CGTACG	CGTATCGCCTCCCTCGCGCCATCAGCGTACGTATATTTTTAGATGATTTGTAAAGGGTAAA
9	2	RevP	CGTACG	CTATGCGCCTTGCCAGCCCGCTCAGCGTACGACCTAACTTATAAAAAACTACCACATTATC
9	3.1	ForP	CGTACG	CGTATCGCCTCCCTCGCGCCATCAGCGTACGAGTGTTTAGTTTTTGTTTTTTTTTTTAGGTTTTGT
9	3.1	RevP	CGTACG	CTATGCGCCTTGCCAGCCCGCTCAGCGTACGTCTTACRTAACACAAACAAAAAATCAATTAAATAC
9	3.2	ForP	CGTACG	CGTATCGCCTCCCTCGCGCCATCAGCGTACGGTTGTGGTATTGTGTTTGGTATATG
9	3.2	RevP	CGTACG	CTATGCGCCTTGCCAGCCCGCTCAGCGTACGACACTTAATTCAAATAATCAAATTCATAAT
9	4	ForP	CGTACG	CGTATCGCCTCCCTCGCGCCATCAGCGTACGTGGGTTTTTTTGGTATTTAAGAAAG
9	4	RevP	CGTACG	CTATGCGCCTTGCCAGCCCGCTCAGCGTACGAAAAAACAAATAATCTACCCCACAA
9	5	ForP	CGTACG	CGTATCGCCTCCCTCGCGCCATCAGCGTACGTGAAAGGTTATAATGAAATGATAAGTTTAA
9	5	RevP	CGTACG	CTATGCGCCTTGCCAGCCCGCTCAGCGTACGATTACCATAACTTCCCCAAAAATAC
9	6	ForP	CGTACG	CGTATCGCCTCCCTCGCGCCATCAGCGTACGTGATTGTTAATTTTGTTTTTGATTG
9	6	RevP	CGTACG	CTATGCGCCTTGCCAGCCCGCTCAGCGTACGCAACCTCAATCTCATAATTTTAACC

10	1	ForP	ACTCTC	CGTATCGCCTCCCTCGCGCCATCAGACTCTCAGGATGTTAGGGTATTAAAGGTTGG
10	1	RevP	ACTCTC	CTATGCGCCTTGCCAGCCCGCTCAGACTCTCCCAATTTTCCTAAAACCAACAATAT
10	2	ForP	ACTCTC	CGTATCGCCTCCCTCGCGCCATCAGACTCTCTATATTTTTAGATGATTTGTAAAGGGTAAA
10	2	RevP	ACTCTC	CTATGCGCCTTGCCAGCCCGCTCAGACTCTCACCTAACTTATAAAAAACTACCACATTATC
10	3.1	ForP	ACTCTC	CGTATCGCCTCCCTCGCGCCATCAGACTCTCAGTGTTTAGTTTTTGTTTTTTTTTTTAGGTTTTGT
10	3.1	RevP	ACTCTC	CTATGCGCCTTGCCAGCCCGCTCAGACTCTCTCTTACRTAACACAAACAAAAAATCAATTAAATAC
10	3.2	ForP	ACTCTC	CGTATCGCCTCCCTCGCGCCATCAGACTCTCGTTGTGGTATTGTGTTTGGTATATG
10	3.2	RevP	ACTCTC	CTATGCGCCTTGCCAGCCCGCTCAGACTCTCACACTTAATTCAAATAATCAAATTCATAAT
10	4	ForP	ACTCTC	CGTATCGCCTCCCTCGCGCCATCAGACTCTCTGGGTTTTTTTGGTATTTAAGAAAG
10	4	RevP	ACTCTC	CTATGCGCCTTGCCAGCCCGCTCAGACTCTCAAAAAACAAATAATCTACCCCACAA
10	5	ForP	ACTCTC	CGTATCGCCTCCCTCGCGCCATCAGACTCTCTGAAAGGTTATAATGAAATGATAAGTTTAA
10	5	RevP	ACTCTC	CTATGCGCCTTGCCAGCCCGCTCAGACTCTCATTACCATAACTTCCCCAAAAATAC
10	6	ForP	ACTCTC	CGTATCGCCTCCCTCGCGCCATCAGACTCTCTGATTGTTAATTTTGTTTTTGATTG
10	6	RevP	ACTCTC	CTATGCGCCTTGCCAGCCCGCTCAGACTCTCCAACCTCAATCTCATAATTTTAACC

10.4 List of Sybr primers and Taqman probes used for qPCR

Taqman Probes for qPCR with Taqman Master Mix		
Gene name	Primer name / Order number	Conjugate
Mouse Dtx-1	Mm00492297_m1	FAM
Mouse Dtx-2	Mm00470116_m1	FAM
Mouse Foxp3	Mm00475162_m1	FAM
Mouse Hes1	Mm01342805_m1	FAM
Mouse Hey1	Mm00468865_m1	FAM
Mouse HPRT	Mm01318746_g1	FAM
Mouse HPRT	Mm03024075_m1	FAM
Mouse Il2ra	Mm01340213_m1	FAM
Mouse Il7r	Mm00434295_m1	FAM
Mouse Notch1	Mm00435249_m1	FAM
Mouse Notch2	Mm00803072_m1	FAM
Mouse Notch3	Mm01345646_m1	FAM
Mouse Notch4	Mm00440525_m1	FAM
Mouse GATA-3	Mm00484683_m1	FAM
Mouse Tbx21	Mm00450960_m1	FAM
Mouse IRF4	Mm00516431_m1	FAM
Mouse Rbpj	Mm0070450_m1	FAM
Mouse Rbpj	Mm01217627_g1	FAM

Sybr Primers for the detection of common Treg / Tconv genes and general immunophenotyping		
Gene name	Primer name	Sequence
Mouse Atf3	Atf3_Syb_ForP1	GAGGATTTTGCTAACCTGACACC
Mouse Atf3	Atf3_Syb_RevP1	TTGACGGTAACTGACTCCAGC
Mouse cActin	cActin_for	GTTTGAGACCTTCAACACCCCA
Mouse cActin	cActin_rev	GACCAGAGGCATACAGGGACA
Mouse CCL2	CCL2_Syb_ForP2	AGGTCCCTGTCATGCTTCTG
Mouse CCL2	CCL2_Syb_RevP2	GCTGCTGGTGATCCTCTTGT
Mouse Ccl4 (MiP-1)	Ccl4_Syb_ForP1	ATGAAGCTCTGCGTGTCTG
Mouse Ccl4 (MiP-1)	Ccl4_Syb_RevP1	GAAACAGCAGGAAGTGGGAG
Mouse CCL5 (Rantes)	CCL5_Syb_ForP2	CTGCTGCTTTGCCTACCTCT
Mouse CCL5 (Rantes)	CCL5_Syb_RevP2	CCCACTTCTTCTCTGGGTTG
Mouse Cd200r1	CD200R1_ForP1	AGGCATTTCCAGTATCACAAGG
Mouse Cd200r1	CD200R1_RevP1	CCAATGGCCGACAAAGTAAGG
Mouse Cd4	CD4_ForP1	TCCTAGCTGTCACTCAAGGGA
Mouse Cd4	CD4_RevP1	TCAGAGAACTTCCAGGTGAAGA
Mouse Cd8a	CD8a_ForP1	CCGTTGACCCGCTTTCTGT
Mouse Cd8a	CD8a_RevP1	CGGCGTCCATTTTCTTTGGAA
Mouse Cd8b	CD8b_ForP1	CTCTGGCTGGTCTTCAGTATGA
Mouse Cd8b	CD8b_RevP1	TCTTTGCCGTATGGTTGGTTT
Mouse Crp	Crp_Syb_ForP1	GCTACTCTGGTGCCTTCTGAT
Mouse Crp	Crp_Syb_RevP1	CAGTAAAGGTGTTCAGTGGCTTC
Mouse Ctla4	CTLA4_ForP1	GCTTCCTAGATTACCCCTTCTGC
Mouse Ctla4	CTLA_RevP1	CGGGCATGGTTCTGGATCA
Mouse Cxcl1	CXCL1 ForP1	CTGGGATTCACCTCAAGAACATC
Mouse Cxcl1	CXCL1 RevP1	CAGGGTCAAGGCAAGCCTC
Mouse CXCL1	CXCL1_Syb_ForP1	CTGGGATTCACCTCAAGAACATC
Mouse CXCL1	CXCL1_Syb_RevP1	CAGGGTCAAGGCAAGCCTC
Mouse Cxcl10	Cxcl10_Syb_ForP1	CTCATCCTGCTGGGTCTGAG
Mouse Cxcl10	Cxcl10_Syb_RevP1	CCTATGGCCCTCATTCTCAC
Mouse Dapl1	Dapl1_ForP1	ATGGCAAACGAAGTACAAGTTCT
Mouse Dapl1	Dapl1_RevP1	TCTTTCCAAAACGCCCATCTC
Mouse Foxp3	mFoxp3_Syb_ForP1	AGAAGCTGGGAGCTATGCAG
Mouse Foxp3	mFoxp3_Syb_RevP1	TACTGGTGGCTACGATGCAG

Mouse Gata3	Gata3 ForP	CTCGGCCATTCGTACATGGAA
Mouse Gata3	Gata3 RevP	GGATACCTCTGCACCGTAGC
Mouse HPRT	HPRT SYB forP2	CTTTGCTGACCTGCTGGATT
Mouse HPRT	HPRT SYB revP2	TATGTCCCCCGTTGACTGAT
Mouse Ifng	Ifng_Syb_ForP1	CAGCAACAGCAAGGCGAAA
Mouse Ifng	Ifng_Syb_RevP1	CTGGACCTGTGGGTTGTTGAC
Mouse Il10	IL-10_Syb_ForP1	ATCGATTTCTCCCCTGTGAA
Mouse Il10	IL-10_Syb_RevP1	TGTCAAATTCATTCATGGCCT
Mouse Il17a	IL17A ForP	TTTAACTCCCTTGGCGCAAAA
Mouse Il17a	IL17A RevP	CTTTCCCTCCGCATTGACAC
Mouse IL1b	IL1b_Syb_ForP1	AGTTGACGGACCCCAAAAG
Mouse IL1b	IL1b_Syb_RevP1	CTTCTCCACAGCCACAATGA
Mouse Il2	IL2_ForP	TGAGCAGGATGGAGAATTACAGG
Mouse Il2	IL2_RevP	GTCCAAGTTCATCTTCTAGGCAC
Mouse Il2ra	IL2ra_ForP1	AACCATAGTACCCAGTTGTCGG
Mouse Il2ra	IL2ra_RevP1	TCCTAAGCAACGCATATAGACCA
Mouse Il2rb	IL2rb_ForP1	TGGAGCCTGTCCCTCTACG
Mouse Il2rb	IL2rb_RevP1	TCCACATGCAAGAGACATTGG
Mouse Il4	IL4 ForP	GGTCTCAACCCCCAGCTAGT
Mouse Il4	IL4 RevP	GCCGATGATCTCTCTCAAGTGAT
Mouse Il6	Il6_Syb_ForP1	GATGGATGCTACCAAACTGGA
Mouse Il6	Il6_Syb_RevP1	TCTGAAGGACTCTGGCTTTG
Mouse Il7	IL7_ForP	TTCCTCCACTGATCCTTGTTCT
Mouse Il7	IL7_RevP	AGCAGCTTCCTTTGTATCATCAC
Mouse Itgam (CD11b)	Itgam_Syb_ForP1	ATTCGGTGATCCCTTGGATT
Mouse Itgam (CD11b)	Itgam_Syb_RevP1	GTTTGTTGAAGGCATTTCCC
Mouse Lrcc32	Lrcc32_ForP1_MD	TCAGCGTCGAGAGCAAGTG
Mouse Lrcc32	Lrcc32_RevP1_MD	GTAGAGAGCTTGGATGTCCAGT
Mouse Lrcc32	Lrcc32_ForP2_MD	GGACATCCAAGCTCTCTACTTGT
Mouse Lrcc32	Lrcc32_RevP2_MD	GAGGAAGCTAATCTGGTTGTCAC
Mouse LT alpha	LT alpha ForP	CCACCTCTTGAGGGTGCTTG
Mouse LT alpha	LT alpha RevP	CATGTCGGAGAAAGGCACGAT
Mouse NKg7	Nkg7_ForP1	TCAAGTCCAGACATTCTTCTCCT
Mouse NKg7	Nkg7_RevP1	CACAAGGTTTCATACTCAGCCC
Mouse Plac8	Plac8_ForP1	GCTCAGGCACCAACAGTTATC
Mouse Plac8	Plac8_RevP1	GCTGCCACTTGACATCCAAGA
Mouse RBPJ	RBPJ_Sybr_E5-6_ForP	AACAGCGATGACATTGGTGTG
Mouse RBPJ	RBPJ_Sybr_E5-6_RevP	ACCGAAGGCGATTGAACAGTG
Mouse RBPJ	RBPJ_Sybr_E6-7_ForP	TTTCCACGCCAGTTCACAACA
Mouse RBPJ	RBPJ_Sybr_E6-7_RevP	TCTGCCCGTAATGGATGTAGC
Mouse RBPJ	RBPJ_Sybr_E2-3_ForP	CTCCACCCAAACGACTCACTA
Mouse RBPJ	RBPJ_Sybr_E2-3_RevP	TCCAACCACTGCCCATAAGATA
Mouse RBPJ	RBPJ_Sybr_E1_ForP	ATGCCCTCCGGTTTTCCTC
Mouse RBPJ	RBPJ_Sybr_E1_RevP	GGACAAGCCCTCCGAGTAGT
Mouse RORgT	RORgT ForP	GACCCACACCTCACAAATTGA
Mouse RORgT	RORgT RevP	AGTAGGCCACATTACACTGCT
Mouse Saa1	Saa1_Syb_ForP1	AGTCTGCCATGGAGGGTTTT
Mouse Saa1	Saa1_Syb_RevP1	CCCGAGCATGGAAGTATTTG
Mouse St8Sia6	St8Sia6_ForP1	TCCTGCGTATGCTCTGGTG
Mouse St8Sia6	St8Sia6_RevP1	CTGTTCCTGGTGCGTGGTA
Mouse T-bet	T-bet ForP	AGCAAGGACGGCGAATGTT
Mouse T-bet	T-bet RevP	GGGTGGACATATAAGCGGTTC
Mouse Tgfb1	Tgfb1_Syb_ForP1	GGAGAGCCCTGGATACCAA
Mouse Tgfb1	Tgfb1_Syb_RevP1	AGGGTCCCAGACAGAAGTTG
Mouse Tnf	Tnf_Syb_ForP1	CCACCACGCTCTTCTGTCTAC
Mouse Tnf	Tnf_Syb_RevP1	AGGGTCTGGGCCATAGAACT

Sybr Primers for Chromatin IP target binding verification		
Gene name	Primer name	Sequence
Mouse Dtx1	Dtx1_RBPJ-BS1_Sybr_ForP1	CCTCCCTGGGAAGCTGAG
Mouse Dtx1	Dtx1_RBPJ-BS1_Sybr_RevP1	GCTCTGATGAAGCCCAGGT
Mouse Dtx1	Dtx1_RBPJ-BS2_Sybr_ForP1	AAAAGGGAGTTCTTGTGAAGCA
Mouse Dtx1	Dtx1_RBPJ-BS2_Sybr_RevP1	ATTTCCCAGCCTTCCCTGT
Mouse Hes1	Hes1_RBPJ-BS1_Sybr_ForP1	CATTTCCTTTCTGCCCAGTAG
Mouse Hes1	Hes1_RBPJ-BS1_Sybr_RevP1	GCCCATTCATTCCTCTCTTG
Mouse Hes1	Hes1_RBPJ-BS2_Sybr_ForP1	GCGTGTCTCTTCCTCCCATT
Mouse Hes1	Hes1_RBPJ-BS2_Sybr_RevP1	GGCCTCTATATATATCTGGGACTGC
Mouse Hes1	Hes1_RBPJ-BS3_Sybr_ForP1	CACAGCGGGACTCCTTTTAC
Mouse Hes1	Hes1_RBPJ-BS3_Sybr_RevP1	CTTCGCCTCTTCTCCATGAT
Mouse IL7R	RBPJ FR1 FORP1	TGCCCTGAATTTCATCCAGAA
Mouse IL7R	RBPJ FR1 FORP2	TTTCAGCCCTGCCTTAACTG
Mouse IL7R	RBPJ FR1 REVP1	ACGTCTGGCCTTGAACTTTC
Mouse IL7R	RBPJ FR1 REVP2	TTACAAGGTACGTCTGGCCT
Mouse IL7R	RBPJ FR2 FORP1	GAAAGTTCAAGGCCAGACGT
Mouse IL7R	RBPJ FR2 FORP2	AGGCCAGACGTACCTTGTAA
Mouse IL7R	RBPJ FR2 REVP1	TGAGAAGGATTCAACTGCGTG
Mouse IL7R	RBPJ FR2 REVP2	CTGGGGAACGGTGGTAATGA
Mouse IL7R	RBPJ RR1 FORP1	ACCCAAGTTGTCATTTCCGTG
Mouse IL7R	RBPJ RR1 FORP2	TGTCATTTCCGTGAAGATACCAC
Mouse IL7R	RBPJ RR1 REVP1	CAGGTACACTCAGATGTCCAGA
Mouse IL7R	RBPJ RR1 REVP2	AGGTTTTCACTAGGTTTTCAGGT
Mouse IL7R	RBPJ FR3 FORP1	GGAGAGAGTGAAAATTCCCAACT
Mouse IL7R	RBPJ FR3 REVP1	TGGAGTTCTGTAGGCCTTTTG
Mouse IL7R	RBPJ FR3 REVP2	TCTATTTGGAGTTCTGTAGGCCT
Mouse IL7R	RBPJ RR2 FORP1	ATAGCTGGTCAGTGGCCA
Mouse IL7R	RBPJ RR2 FORP2	TTAGCAACAACTGATATGAGCAC
Mouse IL7R	RBPJ RR2 REVP1	ACAATGTCACAAAAGCATGGG
Mouse IL7R	RBPJ RR2 REVP2	CTGCTGTGTTACCTCTCTTTCC
Mouse IL7R	RBPJ RR3 FORP1	CCCATGCTTTTGTGACATTGT
Mouse IL7R	RBPJ RR3 FORP2	GGAAAGAGAGGTAACACAGCAG
Mouse IL7R	RBPJ RR3 REVP1	AGGCTGGTGTGTCTTTTGGT
Mouse IL7R	RBPJ RR3 REVP2	TGTGGGCCTTTTATAGCAGAG
Mouse IL7R	RBPJ IR1 FORP1	CAGCAGAGACAACAGGATGG
Mouse IL7R	RBPJ IR1 REVP	CTGTGGTGGGAGAACTGAGT
Mouse IL7R	RBPJ IR2 FORP1	TGTGGAAGCTGAACAACACTC
Mouse IL7R	RBPJ IR2 REVP	TTGGGTATGTTGTGGCTTCA
Mouse IL7R	RBPJ IR3 FORP1	TGCAGATGTCCATGGTCTGT
Mouse IL7R	RBPJ IR3 REVP	TAGCAGTACAGGCCACTCAC
Mouse IL7R	RBPJ IR4 FORP1	AAGGCTGCTAATTCCACCCT
Mouse IL7R	RBPJ IR4 REVP	AAGTACTTGGGTCAGGAGGC

Sybr Primers for Foxp3-promoter binding protein – gene expression verification in murine cells		
Gene name	Primer name	Sequence
Mouse Cux1	mCux1_Sybr_ForP1	TGACCTGAGCGGTCCTTACA
Mouse Cux1	mCux1_Sybr_RevP1	TGGGGCCATGCCATTTACATC
Mouse Hnrnpab	mHnrnpab_Sybr_ForP1	ATGGCGGCTACGACTACTC
Mouse Hnrnpab	mHnrnpab_Sybr_RevP1	GCTGGCTCTTTCCGTAATTTGT
Mouse Hnrnpd	mHnrnpd_Sybr_ForP1	GTGAAGTTGTAGACTGCACTCTG
Mouse Hnrnpd	mHnrnpd_Sybr_RevP1	CCAAAACCCCTTGATCGCC
Mouse Hnrnpk	mHnrnpk_SybrP_ForP1	CAGCTCCCGCTCGAATCTG
Mouse Hnrnpk	mHnrnpk_SybrP_RevP1	ACCCTATCAGGTTTTCCTCCAA
Mouse Naa38	mNaa38_Sybr_ForP1	GGCTGTTATTACTTCTGATGGCA
Mouse Naa38	mNaa38_Sybr_RevP1	ACACCACTTGTTCTACTCCCT
Mouse Nfya	mNfya_Sybr_ForP1	GTTAATGGTGCAAGTCAGTGGA

Mouse Nfya	mNfya_Sybr_RevP1	TCTGCTGTAAACCTTGTGTTCC
Mouse Pcbp1	mPcbp1_SybrP_ForP1	GACGCCGGTGTGACTGAAA
Mouse Pcbp1	mPcbp1_SybrP_RevP1	GTCAGCGTGATGATCCTCTCC
Mouse Pcbp2	mPcbp2_SybrP_ForP1	GCCAGATTTGACCAAGCTGC
Mouse Pcbp2	mPcbp2_SybrP_RevP1	GAGCTGGATTCAATGCCACTG
Mouse Rfx1	mRfx1_Sybr_ForP1	GTTCACGTTGCTCAAGAGGTA
Mouse Rfx1	mRfx1_Sybr_RevP1	TACTGGTAGGTGCTAGAGCGG
Mouse Rfx1	mRfx1_Sybr_ForP2	AGTACCCGGAGACGCCTATC
Mouse Rfx1	mRfx1_Sybr_RevP2	CTGCCGGACACATACATGG
Mouse Rpa1	mRpa1_SybrP_ForP1	ACATCCGTCCCATTTCTACAGG
Mouse Rpa1	mRpa1_Sybr_RevP1	CTCCCTCGACCAGGGTGTT
Mouse Sf1	mSf1_Sybr_ForP1	AGCCGATGGAACCAAGACAC
Mouse Sf1	mSf1_Sybr_RevP1	GCACTATGTAAGCTCTTTCCTGT
Mouse Sf1	mSf1_Sybr_ForP2	AGAAGACCTGACTCGTAAACTGC
Mouse Sf1	mSf1_Sybr_RevP2	CCCTCGCTGTTGTAGATTGGT
Mouse Snapc1	mSnapc1_Sybr_ForP1	CGCTTCCAAGAGATGGACAG
Mouse Snapc1	mSnapc1_Sybr_RevP1	CGTGTGTGGAGGCAAAAAGTAG
Mouse Ssbp1	mSsbp1_Sybr_ForP1	CAACAAATGAGATGTGGCGATCA
Mouse Ssbp1	mSsbp1_Sybr_RevP1	ACGAGCTTCTTACCAGCTATGA
Mouse Tfcp2	mTfcp2_Sybr_ForP1	TGAGTGATGTCCTCGCATTGC
Mouse Tfcp2	mTfcp2_Sybr_RevP1	TCGTTCTCATTATCGGGAGGC
Mouse Tgif2	mTgif2_Sybr_ForP1	ATGTCGGACAGCGATCTAGG
Mouse Tgif2	mTgif2_Sybr_RevP1	TCCCGGAGGATCTTTACTGAC
Mouse Thap11	mThap11_Sybr_ForP1	ATGCCTGGCTTTACGTGCT
Mouse Thap11	mThap11_Sybr_RevP1	GGTGGGTTGGAAGGTGGAG
Mouse Ybx1	mYbx1_Sybr_ForP1	CAGACCGTAACCATTATAGACGC
Mouse Ybx1	mYbx1_Sybr_RevP1	ATCCCTCGTTCTTTTCCCCAC
Mouse Zfp574	mZfp574_Sybr_ForP1	ACATTGAGCACCGCTATGTCT
Mouse Zfp574	mZfp574_Sybr_RevP1	CTCTCTTGGATGAGGGTCTGATA
Mouse Zfp691	mZnf691_Sybr_ForP1	GGAGAAGGGGCTAAACCTTGG
Mouse Zfp691	mZnf691_Sybr_RevP1	GCAGTGACTTTCTGCCTTGTCT
Mouse Zfp691	mZnf691_Sybr_ForP2	GGAGAGTGGATGGCTCAAAGG
Mouse Zfp691	mZnf691_Sybr_RevP2	CGTTCTCAGGTTGGAGGTATTGT
Mouse Zfp691	mZnf691_Sybr_ForP3	ATACCTCCAACCTGAGAACGC
Mouse Zfp691	mZnf691_Sybr_RevP3	GGCGCATTGGTAGTGCTTC
Mouse Zfp692	mZfp692_Sybr_ForP1	GGTGCTCCTGTCTCACACAC
Mouse Zfp692	mZfp692_Sybr_RevP1	CTGCTTAGGTACATCTGAAGGTG

Sybr Primers for Foxp3-promoter binding protein – gene expression verification in human cells		
Gene name	Primer name	Sequence
Human Cux1	Human Cux1_Sybr_ForP1	GAAGAACCAAGCCGAAACCAT
Human Cux1	Human Cux1_Sybr_RevP1	AGGCTCTGAACCTTATGCTCA
Human Foxp3	hFoxp3_Sybr_ForP1	GTGGCCCGGATGTGAGAAG
Human Foxp3	hFoxp3_Sybr_RevP1	GGAGCCCTTGTCGGATGATG
Human Hnrnpab	Human Hnrnpab_Sybr_ForP1	ACCGAGAACGGACATGAGG
Human Hnrnpab	Human Hnrnpab_Sybr_RevP1	GCCACCAACGAACATTTTTCC
Human Hnrnpd	Human Hnrnpd_Sybr_ForP1	GCGTGGGTTCTGCTTTATTACC
Human Hnrnpd	Human Hnrnpd_Sybr_RevP1	TTGCTGATATTGTTCCTTCGACA
Human Hnrnpk	Human Hnrnpk_SybrP_ForP1	CAATGGTGAATTTGGTAAACGCC
Human Hnrnpk	Human Hnrnpk_SybrP_RevP1	GTAGTCTGTACGGAGAGCCTTA
Human Hnrnpk	Human Hnrnpk_SybrP_ForP2	GCAGGAGGAATTATTGGGGTC
Human Hnrnpk	Human Hnrnpk_SybrP_RevP2	TGCACTCTACAACCCTATCGG
Human Naa38	Human Naa38_Sybr_ForP1	GCATTCGCATGACAGATGGAC
Human Naa38	Human Naa38_Sybr_RevP1	CGACGGCTTGAGGAACTCC
Human Nfya	Human Nfya_Sybr_ForP1	CAGTGGAGGCCAGCTAATCAC
Human Nfya	Human Nfya_Sybr_RevP1	CCAGGTGGGACCAACTGTATT
Human Nfya	Human Nfya_Sybr_ForP2	TGAAGGGCAGACCATCGTCTA
Human Nfya	Human Nfya_Sybr_RevP2	TCCTGTTTGAACAATCTGTGCT
Human Pcbp1	Human Pcbp1_SybrP_ForP1	GCCGGTGTGACTGAAAGTG

Human Pcbp1	Human Pcbp1_SybrP_RevP1	CCCAATGATGCTTCCTACTTCC
Human Pcbp1	Human Pcbp1_SybrP_ForP2	AAGAAAGGGGAGTCGGTTAAGA
Human Pcbp1	Human Pcbp1_SybrP_RevP2	GCCGGTCAGAGTGATGATTCTC
Human Pcbp2	Human Pcbp2_SybrP_ForP1	ACTCTCACCATCCGGCTACTT
Human Pcbp2	Human Pcbp2_SybrP_RevP1	TCGCGCATCTTCTTAACTGATTC
Human Pcbp2	Human Pcbp2_SybrP_ForP2	GCGCAGATCAAAATTGCGAAC
Human Pcbp2	Human Pcbp2_SybrP_RevP2	ATATTGAGCCAGGCTAATGCTG
Human Rfx1	Human Rfx1_Sybr_ForP1	CGTGGCTCAAGAGGTGCAG
Human Rfx1	Human Rfx1_Sybr_RevP1	TCTCGGGATAGGAGTAGGTGC
Human Rfx1	Human Rfx1_Sybr_ForP2	CGGCAAGCACCAGCTACTAC
Human Rfx1	Human Rfx1_Sybr_RevP2	GGACACGTACATGGGCATGG
Human Rpa1	Human Rpa1_SybrP_ForP1	GGGGATACAAACATAAAGCCCA
Human Rpa1	Human Rpa1_Sybr_RevP1	CGATAACGCGGCGGACTATT
Human Rpa1	Human Rpa1_SybrP_ForP2	CGGGAATGGGTTCTACTGTTTC
Human Rpa1	Human Rpa1_Sybr_RevP2	CGAGCACAAATGGTCCACTTG
Human Sf1	Human Sf1_Sybr_ForP1	GAAGACCTGACTCGTAAACTGC
Human Sf1	Human Sf1_Sybr_RevP1	CCTCGCTATTGTAGATGGGCT
Human Sf1	Human Sf1_Sybr_ForP2	GGAGCGGCACAACCTCATC
Human Sf1	Human Sf1_Sybr_RevP2	CCGGATCATAATCTTGGCATTGC
Human Snapc1	Human Snapc1_Sybr_ForP1	CGGACAGTGTACGCTTCGAG
Human Snapc1	Human Snapc1_Sybr_RevP1	ATCGCCAAGCCAAAGCTAAAG
Human Snapc1	Human Snapc1_Sybr_ForP2	AGAGTTGGTGCTTTGTATCTGC
Human Snapc1	Human Snapc1_Sybr_RevP2	GCTCTGTCTAGTCGTAGCTTCC
Human Ssbp1	Human Ssbp1_Sybr_ForP1	TGAGTCCGAAACAACTACCAGT
Human Ssbp1	Human Ssbp1_Sybr_RevP1	CCTGATCGCCACATCTCATTAG
Human Ssbp1	Human Ssbp1_Sybr_ForP2	ACTGGGTGATGTCAGTCAAAAG
Human Ssbp1	Human Ssbp1_Sybr_RevP2	TGCTTGTCGCCTCACATTATT
Human Tfcp2	Human Tfcp2_Sybr_ForP1	TCTGGCCGACGAAGTGATTG
Human Tfcp2	Human Tfcp2_Sybr_RevP1	ATCAGGAGGCAAACTCGACTC
Human Tfcp2	Human Tfcp2_Sybr_ForP1	GTGTTCCATGACAGAAGGCTT
Human Tfcp2	Human Tfcp2_Sybr_RevP1	TTATACCCACAGACATCGGGAT
Human Tgif2	Human Tgif2_Sybr_ForP1	TGACCCCTGGTAGCACACTTA
Human Tgif2	Human Tgif2_Sybr_RevP1	GTGGTGGCGTGTTGAAGAGT
Human Thap11	Human Thap11_Sybr_ForP1	ATGCCTGGCTTTACGTGCT
Human Thap11	Human Thap11_Sybr_RevP1	GCGTCCTTTGGAAACGTGTAG
Human Thap11	Human Thap11_Sybr_ForP2	ATACTGGCTCCGACCATTCG
Human Thap11	Human Thap11_Sybr_RevP2	CTTGGCCTCAGTGAGACGC
Human Ybx1	Human Ybx1_Sybr_ForP1	GGGGACAAGAAGGTCATCGC
Human Ybx1	Human Ybx1_Sybr_RevP1	CGAAGGTACTTCCTGGGGTTA
Human Ybx1	Human Ybx1_Sybr_ForP2	CCCCAGGAAGTACCTTCGC
Human Ybx1	Human Ybx1_Sybr_RevP2	AGCGTCTATAATGGTTACGGTCT
Human Zfp574	Human Zfp574_Sybr_ForP1	ACATTGAGCACCGCTATGTCT
Human Zfp574	Human Zfp574_Sybr_RevP1	CCTGCACAAGGGTCTGATAGA
Human Zfp574	Human Zfp574_Sybr_ForP1	AGACCCTTGTGCAGGAGAG
Human Zfp574	Human Zfp574_Sybr_RevP1	GTGGTGCCTTAGGTGATGGC
Human Zfp691	Human Znf691_Sybr_ForP1	GAGCAGAGTCCAGAACCACAC
Human Zfp691	Human Znf691_Sybr_RevP1	GCAGTTCATCCGACAGGCT
Human Zfp691	Human Znf691_Sybr_ForP2	TCGGATGAACTGCAAGAAACTC
Human Zfp691	Human Znf691_Sybr_RevP2	TGTGTTCTCAGGTTGGAGGTA
Human Zfp692	Human Zfp692_Sybr_ForP1	TTCCGCACTAGCAGCAACC
Human Zfp692	Human Zfp692_Sybr_RevP1	AAACCCGCATATCTCACACTG
Human Zfp692	Human Zfp692_Sybr_ForP2	TGTGAGATATGCGGGTTTACCT
Human Zfp692	Human Zfp692_Sybr_RevP2	TGACTCTTGAGGGGCTAGAAG

TOPO Cloning Primers for inverted ChIP candidate proteins and *Foxp3* promoter luciferase cloning		
Gene name	Primer name	Sequence
Human Cux1	Human Cux1_Sybr_ForP1	GAAGAACCAAGCCGAAACCAT
Human Cux1	Human Cux1_Sybr_RevP1	AGGCTCTGAACCTTATGCTCA
Cux1	Cux1_TOPO_ForP1	CACCATGGCGGCCAATGTG
Cux1	Cux1_TOPO_RevP1	TCAGAACTCCCATTCGATGGGC
Cux1	Cux1_TOPO_ForP2	CACCATGGCGGCCAATGTGGGAT
Cux1	Cux1_TOPO_RevP2	TCAGAACTCCCATTCGA
Cux1	Cux1_TOPO_ForP3	CACCATGGCGGCCAATGT
Foxp3 promoter 0-500	FoxpP3_1_500_RevP1	ACTGCTAGAGGGGGATCAGC
Foxp3 promoter 0-500	FoxpP3_1_500_ForP1_Bio	**BIO**-CAAAACTGCAGGCAGGCTTCAGATCCCTTCT
Foxp3 promoter 0-500	FoxpP3_1_500_RevP1_XhoI	CTAGCTCGAGACTGCTAGAGGGGGATCAGC
Foxp3 promoter 0-500	FoxpP3_1_500_ForP1_SbfI	GATCCCTGCAGGGCAGGCTTCAGATCCCTTCT
Foxp3 promoter 1000-1500	FoxpP3_1000_1500_RevP1	CCAGGGTCCTAGTCCTGTCA
Foxp3 promoter 1000-1500	FoxpP3_1000_1500_ForP1_Bio	**BIO**-CAAAACTGCAGGTTGGCTTCAGGAAAACTGG
Foxp3 promoter 1000-1500	FoxpP3_1000_1500_XhoI	CTAGCTCGAGCCAGGGTCCTAGTCCTGTCA
Foxp3 promoter 1000-1500	FoxpP3_1000_1500_ForP1_SbfI	GATCCCTGCAGGGTTGGCTTCAGGAAAACTGG
Foxp3 promoter 500-1000	FoxpP3_500_1000_RevP1	CTGCCATGTGAATGGGAAG
Foxp3 promoter 500-1000	FoxpP3_500_1000_ForP1_Bio	**BIO**-CAAAACTGCAGCCTGGGCCGCTATGTGTAT
Foxp3 promoter 500-1000	FoxpP3_500_1000_XhoI	CTAGCTCGAGCTGCCATGTGAATGGGAAG
Foxp3 promoter 500-1000	FoxpP3_500_1000_ForP1_SbfI	GATCCCTGCAGGCCTGGGCCGCTATGTGTAT
HnrnpAB	Hnrnpab_TOPO_ForP1	CACCATGTCGGACGCGG
HnrnpAB	Hnrnpab_TOPO_RevP1	TCAGTATGGCTTGTAGTTATTCTG
Hnrnpab	Hnrnpab_TOPO_ForP2	CACCATGTCGGACGCGGCTGA
HnrnpAB	Hnrnpab_TOPO_RevP2	TCAGTATGGCTTGTAGTTAT
Hnrnpab	Hnrnpab_TOPO_ForP3	CACCATGTCGGACGCG
Hnrnpd	Hnrnpd_TOPO_ForP1	ATGTCGGAGGAGCAGTTC
Hnrnpd	Hnrnpd_TOPO_RevP1	TTAGTATGGTTTGTAGCTATTTTG
Hnrnpd	Hnrnpd_TOPO_ForP2	CACCATGTCGGAGGAGCAGTTC
Hnrnpd	Hnrnpd_TOPO_ForP3	CACCATGTCGGAGGAGCAGTTCGGA
Hnrnpd	Hnrnpd_TOPO_RevP2	TTAGTATGGTTTGTAGCTA
Hnrnpd	Hnrnpd_TOPO_ForP4	CACCATGTCGGAGGAGCAG
Hnrnpdl	Hnrnpdl_TOPO_ForP1	CACCATGGAGGTCCCGCC
Hnrnpdl	Hnrnpdl_TOPO_RevP1	TTAGTAGGGCTGGTAATTGTTCT
Hnrnpdl	Hnrnpdl_TOPO_RevP2	TTAGTAGGGCTGGTAATT
HnrnpK	Hnrnpk_TOPO_ForP1	CACCATGGAGACCGAACAGC
HnrnpK	Hnrnpk_TOPO_RevP1	TTAGAAAAACTTTCCAGAATACTGC
Mysm1	Mysm1_TOPO_ForP1	CACCATGGAGGCGGAGGAG
Mysm1	Mysm1_TOPO_RevP1	TTACATGAACAATTCCTTTGTACTAT
Naa38	Naa38_TOPO_ForP1	CACCATGACGTCTGCTTTGGAG
Naa38	Naa38_TOPO_RevP1	TCAGTGTGCTACGGAGTTCAGA
Nfya	Nfya_TOPO_ForP1	CACCATGGAGCAGTATACGACAAA
Nfya	Nfya_TOPO_RevP1	TTAGGAAACTCGGATGATCTGTGTCA
Pcbp1	Pcbp1_TOPO_Forp1	CACCATGGACGCCGGTGT
Pcbp1	Pcbp1_TOPO_RevP1	CTAGCTGCACCCCATCCCCT
Pcbp2	Pcbp2_TOPO_ForP1	CACCATGGACACCGGTGTGATT
Pcbp2	Pcbp2_TOPO_RevP1	CTAGCTGCTCCCCATGCCA
Plac8	Plac8_RevP1	GCTGCCACTTGACATCCAAGA
Rfx1	Rfx1_TOPO_ForP1	CACCATGGCAACACAGTCCTATGT
Rfx1	Rfx1_TOPO_RevP1	TTAGCTGGAGGGCAGGG
Rpa1	Rpa1_TOPO_ForP1	CACCATGGTGGGACACCTGAG
Rpa1	Rpa1_TOPO_RevP1	TCACATGTTCTTCCTGATGTTCGC
Sf1	Sf1_TOPO_ForP1	CACCATGGCGACCGGAG
Sf1	Sf1_TOPO_RevP1	CTAGTTCTGTGGTGGAGGCGG
Snapc1	Snapc1_TOPO_ForP1	CACCATGGGGACTCCTGCG
Snapc1	Snapc1_TOPO_RevP1	TCAGCATTTTCTCTTCCTCTTGGG
Ssbp1	Sspb1_TOPO_ForP1	CACCATGTTTCGAAGACCTGTGTT
Ssbp1	Sspb1_TOPO_RevP1	CTACGCCAACCCTTCCAATGAA
Tfcp2	Tfcp2_TOPO_ForP1	CACCATGGCCTGGGCTCTG
Tfcp2	Tfcp2_TOPO_RevP1	CTACTTGAGAATGACATGATAGCT

Tgif2	Tgif2_TOPO_ForP1	CACCATGTCGGACAGCGATCTAG
Tgif2	Tgif2_TOPO_RevP1	CTACTTGGCGTTTTCTGAGACG
Thap11	Thap11_TOPO_ForP1	CACCATGCCTGGCTTTACGT
Thap11	Thap11_TOPO_RevP1	TCACATGCCGTGCTTCTTACG
Ybx1	Ybx1_TOPO_ForP1	CACCATGAGCAGCGAGGCC
Ybx1	Ybx1_TOPO_RevP1	TTACTCAGCCCCGCCCTGC
Zfp574	Zfp574_TOPO_ForP1	CACCATGACTGAGGAGAGTGAAGAGA
Zfp574	Zfp574_TOPO_RevP1	TCAGCCACTGATCTGGACCCC
Zfp691	Zfp691_TOPO_ForP1	CACCATGGGCAGCGAGAAGG
Zfp691	Zfp691_TOPO_RevP1	TTAGCTAAAATCCTTCTCATCTTG
Zfp692	Zfp692_TOPO_ForP1	CACCATGGCCTCTCCGGT
Zfp692	Zfp692_TOPO_RevP1	CTAACTTTTCTCTCTGTTCCTGG

10.5 List of commercial kits used for RNA/DNA purification and chemical modifications

Kit name	Supplier	Order number
AllPrep DNA/RNA Mini Kit	Quiagen	80204
BCA Protein Assay Kit	Pierce	23225
Dual-Light Luciferase and Beta-Gal Reporter Gene Assay System	ThermoFisher	T1003
Epi tec Bisulfite Kit	QIAGEN	59104
NxTRACT-1KT	Sigma	031 M 4035
PureLink PCR purification kit	Life Technologies	K3100-01
PureLink HiPure Plasmid Midiprep Kit	Life Technologies	K2100-05
PureLink Quick Plasmid Miniprep Kit	Life Technologies	K2100-11
QIA amp DNA Micro Kit	QIAGEN	56304
Quick g DNA Micro Prep	Zymo Research	D3020
RNeasy Microarray Tissue Mini Kit	Quiagen	73304
RNeasy Mini Kit	Quiagen	74104

10.6 List of cytokines used for cell culture

Kit name	Supplier	Order number
Human IL-2	PeproTech	212-12-B
Mouse IL-6	PeproTech	216-16
Mouse IL7	R&D	407-ML
Mouse IL-10	PeproTech	210-10
Mouse IFNy	PeproTech	315-05
Human TGF ß1	PeproTech	100-21

10.7 List of chemicals and products used for experiments

Kit name	Supplier	Order number
Accucheck counting Beads	Invitrogen	PCB 100
Acetic acid 100%	Merck	100063.25
Acetone	VWR	20,066,296
ACK Lysing Buffer	Lonza	10-548E
Agar Agar	Roth	5210.3
Agarose NEEO Ultra	Roth	2267.4
Albumin Fraction V	Roth	8076.1
Ammonium bicarbonate	Fulka	9830
Ammonium chloride	Roth	K298.2
Ammonium hydroxide	MB Biomedical	193854
Ammonium peroxysulfate	Serva	13375
Ammonium sulfate	Roth	3746.1
Ampicillin So salt	Roth	K029.1
autoMACS Running Buffer	Miltenyi Biotec	130-091-221
Betaine	Sigma	B2629
Bovine Serum Albumin	Sigma	A4503
Brefeldin A Solution (1000x)	BioLegend	420601
Bromphenol blue sodium salt	AppliChem	A1120
Calcium chloride dihydrate	AppliChem	A 3587
Casein Hydrolysate	Fluka	22090
CFSE	Life Technologies	C34554
Chloramphenicol	Roth	3886.2
Chloroform	Sigma	24216
Click:T EdU buffer additive	Life Technologies	C10425
Coelenterazine	Promega	S2001
Collagenase D	Roche	11088 866 001
Collagenase from Clostridium histolyticum Type IV	Sigma	C5138
Collagenase II	Sigma	C6885
Collagenase IV	Gibco	17104-019
Collagenase VIII	Sigma	C2139
dNTPs	Life Technologies	10297-018
D-Luciferin	Pierce	88293
DPBS	Life Technologies	14190-094
Diphtheria Toxin From Corynebacterium	Sigma	D0564
Dithiothreitol	Biorad	161-0611
Dithiothreitol high purity	GERBU	1008
DMEM	Life Technologies	41965
DMEM	Life Technologies	21063-029
DMSO (Dimethylsulfoxid) 100%	BioLabs	B0515A
DMSO molecular biology grade	Genaxxon Bio	M6324.0100
DNA Marker 2-log Ladder	BioLabs	N3200L
DNA Marker Gen Ladder 100bp	BioLabs	M3094
Dnase I	Roche	REF11284 932 001
DNase I,Lyo.	Roche	11284932001
DT	Sigma	D0564
DTT	Life Technologies	R0861
Dulbecco`s Modified Eagle Med. wo Arginine Lysine	Life Technologies	ME100073L1
Ethanol 70%	Roth	T913-3
Ethanol 99,8%	Roth	9065.1
Ethidiumbromide 1%	Roth	2218.1
Ethylenediamine tetraacetic acid	Sigma	E 9884
Fast 96 well "ROI" Plates	AB	4432426
Fast 96 well Calibration Plate	AB	4432414
Ficoll-Paque Plus	GE Healthcare	17-1440-03

Formalin solution 10% (v/v)	T.J.Baker	
Foxp3 Staining Buffer Set	eBiosciences	REF 00-5523-00
Foxp3 Staining Buffer Set => 10x Perm Buffer	eBiosciences	REF 00-8333-56
Foxp3 Staining Buffer Set => Fixation Perm Diluent	eBiosciences	REF 00-5223-56
Foxp3 Staining Buffer Set => Fixation Perm conc.	eBiosciences	REF 00-5123-43
Freund`s Adjuvant	Gerbu	1842
Gelatine Solution 0,1% in PBS	PAN	P06-20410
Glucose	AppliChem	A1422
Glycerol bidistilled 99,5%	VWR	24,388,295
Glycine	Gerbu	10,231,000
Glyo Blue	Ambion	AM 9516
Goat IGG	MP	#55397
Heparin 5000U/ml	Biochrom	L6510
Hepes 1M	Biowest	L0180-100
Hepes ultrapure	Biomol	5,288,100
Hexadimethrine bromide	Sigma	H9268
Histopaque 1077	Sigma	10771
Hoechst 33342 trihydrochlorid trihydrate	Life Technologies	REF H3570
Hoechst 33342, Trihydrochloride, trihydrat	Life Technologies	H3570
home made Taq Polymerase	NA	NA
Hy Clone HyPure Molecular Biology Grade Water	Thermo Scientific	SH 30538.03
Hyaloronidase	Sigma	H3884
Hydrochlorid acid 37%	VWR	20,252,290
Hydrochlorid acid 1M	VWR	30,024,290
Hygromycin B	Roth	CP13.1
IGEPAL CA-630	MP	198596
Incidin Foam	Ecolab	YFS 16
Ingenio Solution	Mirus	MIR 50111
Ionomycin calcium salt	Cayman	10004974
IPTG	Roth	2316.4
Isopentan e	Lager	13090
Kanamycin sulfate	Roth	T832.2
LB Medium (Luria /Miller)	Roth	x968.1
Lipofectamine 2000 1mg/ml	Life Technologies	11668-027
Lipopolysaccharides f. Escherichia coli 055B5	Sigma	L2880
Lysozyme	Sigma	L6876
Magnesium chloride hex hydrate	Roth	2189.1
May Grünwald´s azur eosine-methylene blue solution	Merck	109,204
MEM Alpha Medium	Life Technologies	22561-021
MEM NEAA	Life Technologies	11140-35
Mercaptoethanol	Sigma	M6250
Methanol Ph Eur	VWR	
MicroBeads anti Biotin	Miltenyi Biotec	120-000-900
Milk powder	Roth	T145.2
Mouse Serum	Biowest	S2160-010
Sodium carbonate	Roth	A 135.1
Sodium dihydrogen carbonate	AppliChem	A1940
Neomycin sulfate	Roth	8668.1
Nonidet P40	AppliChem	A1694
Opti MEM	Life Technologies	31985-047
Passive Lysis Buffer 5X	Promega	E1941
Paraformaldehyde	Roth	0335.3
PBS Dialysed	Life Technologies	26400-036
Phenol	Roth	A156.1
PMA	Biomol	AG-CN2-0010-M001
Polybrene in PBS	Sigma	#107689
Polyethylenglycol 4000	Merck	109,727
Ponceau S Solution	AppliChem	A2935

Potassium chloride	Roth	6781.1
Potassium Phosphate 1M	Sigma	P8709
Potassiumdihydrogenphosphate 98%	Roth	P018.2
Potassiumhydrogencarbonate 99%	Roth	X 887.2
Propanol	Roth	6752.2
Propidium iodine	MP Biomedicals	195458
Protease Inhibitor cocktail complete EDTA-free	Roche	11873580 001
Proteinase K from Engyodontium albumin	Sigma	P6556
Puromycin	Roth	#0240.1
Puromycin Dihydrochlorid	Roth	0240.1
Rnase Inhibitor	AB	100021540
SDS, 20% Solution	BioRad	161-0418
SDS, ultrapure	Roth	2326.1
Sodium azide	AppliChem	A1430
Sodium bisulfide	Sigma	243973
Sodium chloride 99,8%	Roth	9265.1
Sodium deoxycholate	AppliChem	A1531
Sodium hydroxid 99% p.A.	Roth	677.1
Sodium hydroxid 1N	VWR	31,627,290
Sodium hydroxid 1N	VWR	31,627,290
Sodium ortho vanadate	AppliChem	A2196
Sodium Pyruvate Solution 100mM	PAA	S11-003
Sodium acetate	Roth	6773.2
Superscript 2	Life Technologies	18064-14
SYBR Green Master mix	AB	4367659
T cell stimulation Dynabeads mouse T Activator CD3/CD28	Life Technologies	11456D
T cell stimulation Dynabeads mouse T Activator CD3/CD28	Life Technologies	11452D
Taq Man Gene Expression Master Mix	AB	4369016
Th DNA Ligase	BioLabs	M0202
Thioglycollate Broth	Fluka	70157
Tissue- Tek	Sakura	4566
Trans T 293 Reagent	Mirus	MIR 2700
TRIS Pufferan	Roth	4855.1
Tris ultrapure	AppliChem	SAP 12681
TRIS- hydrochloride 99%	Roth	9090.3
Triton X 100	Roth	3051.3
Trizma acetat	Sigma	T1258
Trizol Reagent	Life Technologies	15596018
Tropix Accelerator II	AB	T2182
Tropix Galacton-Plus	AB	T2189
Tropix Lysis Sol.	AB	T2071
Trypsin / EDTA	Life Technologies	25300-054
Tryptone/Peptone ex casein	Roth	8952.3
TSA Cyanine 3 System	Perkim Elmer	NEL 704A001KT
Tween 20	MP	Tween201
Urea	Sigma	U5378
Water sterile, Nuclease free	US Biological	W0900
Western Blot Stripping Buffer	Thermo Scientific	46428
Western Lightning Plus ECL	Perkin Elmer	NEL 105001EA

10.8 List of buffers

Buffer name	Recipe
ACK lysis buffer	1X PBS 0.15M NH_4Cl 10mM $KHCO_3$ 0.1mM Na_2-EDTA
Complete medium for cell culture	1X DMEM 10% (v/v) FCS 10mM HEPES 100U/mL Penicillin 100µg/mL Streptomycin 1mM sodium pyruvate
FACS buffer	1X PBS 1% (v/v) FCS 0.1 % (v/v) NaN_3
LB medium	Distilled water 0.5% (w/v) yeast extract 1.0% (w/v) tryptone 0.5 % (w/v) NaCl
PBS 1X	Distilled water 0.27mM KCl 13.7mM NaCk 10mM Na_2HPO_4 0.2mM KH_2PO_4
PBS-T	1X PBS 0.1% (v/v) Tween 20
Renilla Buffer	80mM K_2HPO_4 20mM KH_2PO_4 100mM NaCL 1mM EDTA
Luciferase Buffer	10mM TRIS-acetate 10mM Mg-acetate 1mM EDTA
Renilla Measurement Buffer	10 mL Renilla Buffer plus 10 µL Renilla substrate (Coelenterazine)
Luciferase Measurement Buffer	15 mL Luciferase Buffer plus 1 aliquot luciferin (5 mg) and 1 aliquot ATP (200mM)

10.9 Equipment and software

Equipment	Manufacturer
AutoMACS Separator	Miltenyi Biotec
Bacterial Incubator	GFL technologies
Cell Culture Hood	Thermo Fisher
Cell Culture Incubator	Eppendorf
Centrifuges	Eppendorf
Electrophoresis	Neolab
FACS ARIA II and III cell sorter	BD Biosciences
LSR Fortessa II and LSR II flow cytometer	BD Biosciences
Canto II and BD Accuri flow cytometer	BD Biosciences
Ultra-deep freezer, freezer, fridge	Liebherr and Thermo Fisher
PCR master cycler	Eppendorf
Nanodrop 2000	Thermo Fisher
UV gel documentation	Neolab
Viia 7 Real time PCR system	Life technologies
Western Blot detection system	Life technologies
Sonication bath	Diagenode
454 pyrosequencing machine	Roche
Illumina Beadchip machine	Illumina
Next generation sequencing	Illumina
Electroporation machine	BioRad
Luminometer	Berthold Technologies
Software	**Developer**
Adobe Illustrator and Photoshop	Adobe Systems
Endnote	Thomson Reuters
FACS DIVA	BD Biosciences
FlowJo	Treestar / Thermo Fisher
ImageJ 64	ImageJ freeware
Microsoft Office	Microsoft
Graphpad Prism	Graphpad
Viia 7 software	Applied Biosystems